laser technology

MICROWAVES

JULY
1976

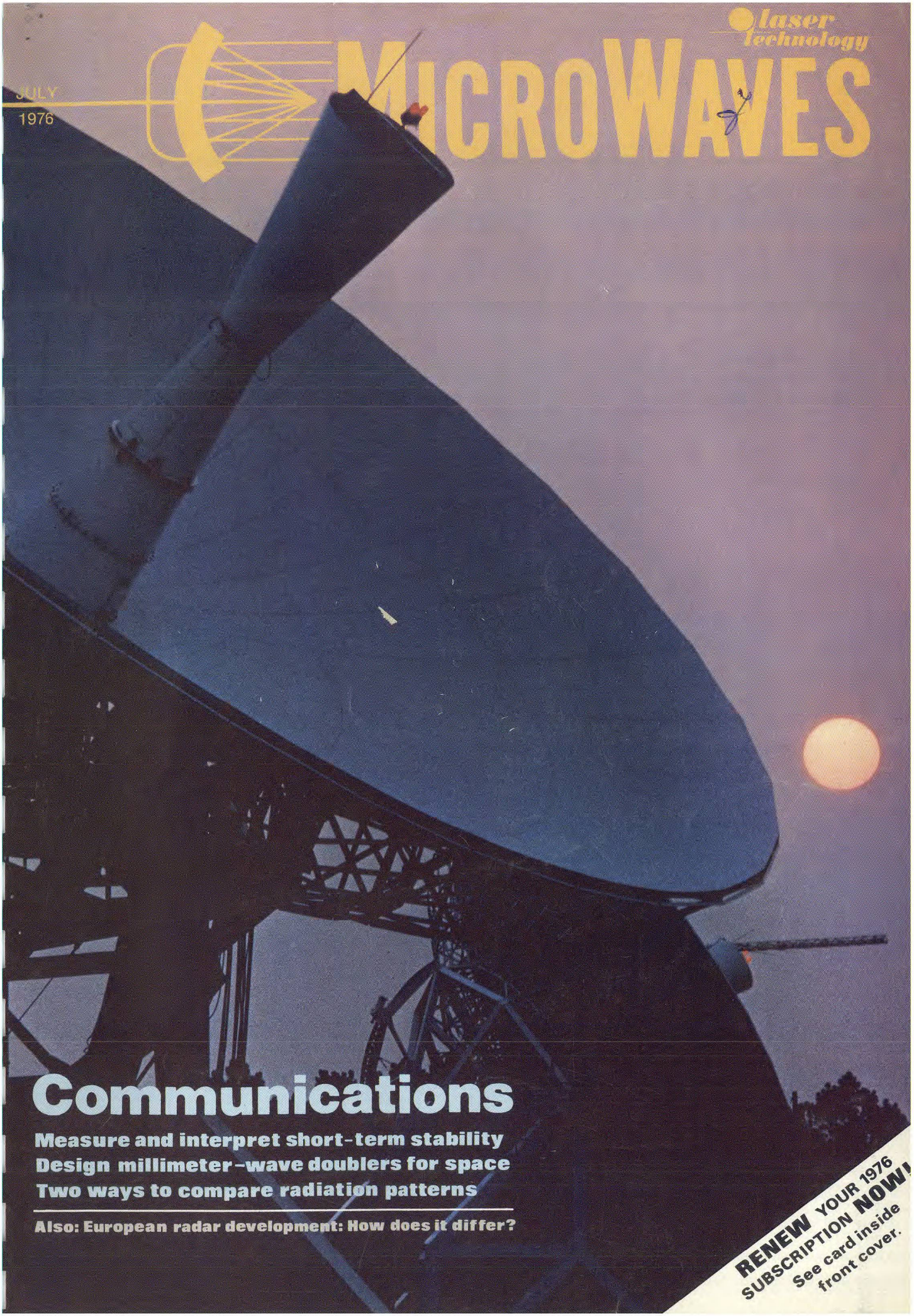

Communications

Measure and interpret short-term stability
Design millimeter-wave doublers for space
Two ways to compare radiation patterns

Also: European radar development: How does it differ?

MICROWAVES
July 1976
Vol. 15, No. 7

news

editorial

technical

Communications

products and departments

About the cover: Silently probing a twilight sky, these giant dishes keep tabs on orbiting weather satellites of the National Oceanic and Atmospheric Administration at Wallops Island, VA. Photo courtesy of the Harris Corporation.

coming next month: Solid-State Sources

Combine Varactor Control with Dielectric Tuning. Carl Klein and Lawrence Korta of Johnson Controls combine mechanical and electric tuning in an inexpensive Gunn oscillator with broad frequency coverage.

Combat Cold Starting Problems. Bernard Sigmon of Theta-Com explores the reasons why sources often fail to oscillate at the design frequency immediately after turn-on.

How Group Delay Relates To Oscillator Stability. Ron Rippy of NASA's Goddard Space Flight Center presents a clear view of exactly what influences oscillator stability by thinking in terms of loop delay.

Publisher/Editor
Howard Bierman

Managing Editor
Stacy V. Bearse

Associate Editor
George R. Davis

Contributing Editor
Harvey J. Hindin

Washington Editor
Paul Harris
Snyder Associates
1050 Potomac St., NW
Washington, DC 20007
(202) 965-3700

Editorial Assistant
Gail Murphy

Production Editor
Sherry Lynne Karpen

Art Director
Robert Meehan

Production
Dollie S. Viebig, Mgr.
Dan Coakley

Circulation
Barbara Freundlich, Dir.
Trish Edelmann
Gene M. Corrado
Sherry Karpen,
Reader Service

Directory Coordinator
Janice Tapp

Editorial Office
50 Essex St.,
Rochelle Park, NJ 07662
Phone (201) 843-0550
TWX 710-990-5071

A Hayden Publication
James S. Mulholland, Jr., President

MICROWAVES is sent free to individuals actively engaged in microwave work. Subscription prices for non-qualified copies:

	1 Yr.	2 Yr.	3 Yr.	Single Copy
U.S.	$15	$25	$35	$2.50
FOREIGN	$20	$35	$50	$2.50

Additional Product Data Directory reference issue, $10.00 each (U.S.), $18.00 (Foreign). POSTMASTER, please send Form 3579 to Fulfillment Manager, MicroWaves, P.O. Box 13801, Philadelphia, PA. 19101.

Back Issues of MicroWaves are available on microfilm, microfiche, 16mm or 35mm roll film. They can be ordered from Xerox University Microfilms, 300 North Zeeb Road, Ann Arbor, MI 48106. For immediate information, call (313) 761-4700.

Hayden Publishing Co., Inc., James S. Mulholland, President, printed at Brown Printing Co., Inc., Waseca, MN.

editorial
AT&T asks Congress to play monopoly

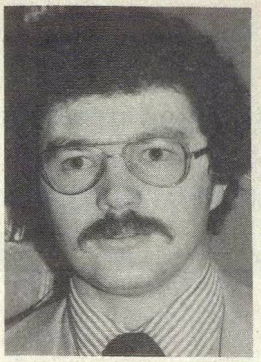

Caught in a squeeze between the FCC's commitment to promote competition in the telecommunications industry and the Justice Department's intensive antitrust efforts, AT&T has spearheaded an all-out drive on Capitol Hill to stake an exclusive claim to long distance telephone services. Heavy election-year lobbying by AT&T and major independents, such as General Telephone and Electronics, United Telecommunications and Continental Telephone, has resulted in the introduction of more than 90 bills in the House and Senate with the goal of making AT&T's Long Lines Department a de jure (legally sanctioned) monopoly.

Basically, the bills would bar competition in long distance services, and permit AT&T or other traditional carriers to acquire all companies that would be forced out of the business, which would certainly include Microwave Communications, Inc. (MCI), Datran and Southern Pacific Communications. The legislation would also bar competitive services by satellite carriers such as RCA Global Communications and American Satellite. Furthermore, the bills would strip the FCC of its jurisdiction over technical and operating standards that affect terminal and accessory equipment attached to local telephone company facilities, and place these responsibilities in the hands of already over-burdened state public utility commissions.

Backers of the "Bell bills" cite the telephone industry's argument that revenues from long distance calling and accessory equipment, such as extensions and switchboards, help to pay for basic, residential telephone services. John D. deButts, chairman of AT&T, has said that if competition were to make significant inroads into long distance services, the average residential telephone bill might increase by up to 75 per cent as a result. Telephone independents (some of which depend on AT&T long lines for up to half of their total revenues) have sponsored studies which back deButts in principle. But neither AT&T nor the independents have been able to supply hard data on the extent to which competition influences rates or service.

Opponents of the Bell bills call attention to other studies which appear to refute the telephone industry's claims. For example, a study by the New York State Public Service Commission concludes that basic telephone service actually subsidizes accessory equipment. And, a 50-man FCC task force assigned to a long-term evaluation of the Bell System reports that competition has been beneficial for consumers, since it has led to improved performance. "There is simply no reliable evidence of any adverse impact from competition on local exchange rates, either now or in the future," sums up John Eger, acting director of the White House Office of Telecommunications Policy.

In spite of the complexity of the issues at hand, Congress must act fast and decisively, before competition with AT&T becomes a moot point. Telecommunications is a capital-intensive industry, and the very possibility that common-carriers might be legislated out of the business has tightened the purse strings at many leading institutions. If Congress drags its heels too long on the issue, money simply won't be there to sustain competition.

Congress must also bear in mind that although the Bell System has done a masterful job of providing basic telephone service to nearly every business and household in the country, this task is virtually complete. We are now entering a new era of telecommunication characterized by innovative and specialized services—areas where Bell's competition has sparkled. Although most competitors have yet to show a profit, they have introduced the consumer to an abundance of new services, and have stimulated established carriers into offering products which were heretofore held off the market due to inordinately slow technological development or for rate-making purposes.

Taken to the bone, the real question facing Congress is how to best serve the changing needs of tomorrow's customers.

Stacy Bearse *Associate Editor*

Measure And Interpret Short-Term Stability

Short-term instabilities in the signal source at the heart of a communications system can be devastating. Be prepared to evaluate this noise using frequency or phase information.

A MICROWAVE signal source can be given excellent long-term frequency stability by phase-locking its output to a low-drift, temperature-stabilized crystal reference, or to an atomic frequency standard. But the *short-term* stability of the source is not as easily controlled, and constitutes a principal source of error in many microwave systems.

Unfortunately, short-term stability is not only hard to optimize, it is also hard to measure. The rather complex methods by which short-term stability must be measured cause us to express the measurement results in unusual terms, which are often subject to misinterpretation and confusion. These difficulties are compounded by the fact that various classes of applications require different methods of measurement, leading to different ways of expressing the short-term stability of a signal source.

Short-term instability is a random phenomenon—small, relatively slow, non-systematic changes in the long-term-average frequency (the carrier frequency). One way of thinking about this random variation is to consider that it is the result of *frequency-modulating the carrier by a complex signal having a limited spectrum signature.* In other words, the spectral content of the modulating signal is not infinite in bandwidth with the same amplitude at all frequencies, like that of white noise, but has most of its energy concentrated at low frequencies, with the amplitude of its frequency components falling off rapidly at higher frequencies. Figure 1(a) shows the spectrum of a signal that would, if it frequency modulated a carrier, result in typical short-term frequency instability. Figure 1(b) shows the resultant spectral distribution of energy around the carrier.

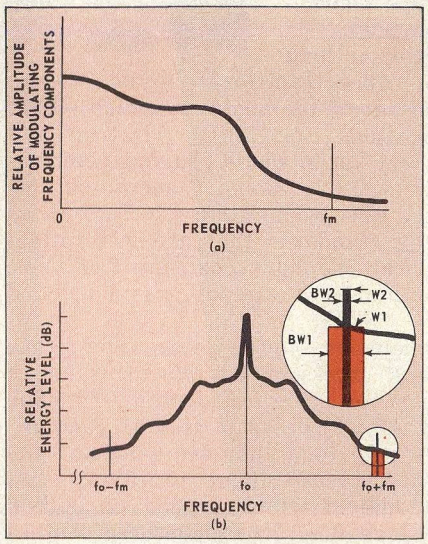

1. Short-term frequency instability can be induced by modulating a single carrier by the spectrum shown in (a). The resultant spectral distribution (b) can be analyzed by considering the spectral power density in a narrow bandwidth.

If we recall that there is a physical correspondence between frequency modulation and phase modulation (i.e., that frequency deviation is equal to the rate of change of phase deviation), then it is possible to express a particular short-term instability in terms of either fm noise or phase noise. As we shall see, the measurement of phase noise, either above or below the carrier (single-sideband phase noise), is preferable to measuring frequency deviations as a means of evaluating signal-source performance when the deviations are small.

Another way of thinking about the short-term instability of the signal source is simply to say that the small, random frequency changes cause phase jitter in the carrier. For some very critical applications, such as in MTI and Doppler radars, the measurement and interpretation of phase jitter is the *only practical way of evaluating* the short-term stability of a signal source.

Measuring and calculating instantaneous "phase jitter" is an extremely complex task, however, involving long-term sampling and computer processing of the data acquired, using very elaborate algorithms drawn from probability theory. All of that is beyond the scope of this article, but the reader should be aware that the simplifying assumptions implicit in the conventional measurements discussed herein render the techniques useless for certain radar applications.

For all other classes of application, be confident of measurements made in terms of either one of two parameters:

- Residual fm noise
- SSB phase noise

Modulation theory key

Fundamental modulation theory is essential to understanding the measurement and specification of short-term stability; a quick review appears on the opposite page in "Modulation Theory: Back To Basics." However, note that the effect of short-term instability cannot be calculated in terms of frequency (or phase) modulation of the carrier by a single modulation frequency, f_m, because the effective modulation spectrum contains many frequency components, and it produces not merely the single output spectrum with two sidebands, but a complex spectrum with many frequency components, which results in a power spectral density curve like that of Fig. 1(b). All of the energy surrounding the carrier is called *residual fm noise* because it represents the short-term instability and can be interpreted in terms of frequency modulation by a random, or noise signal of limited spectrum.

Dr. John B. Payne, III, President, Communication Techniques, Inc., 1279 Route 46, Parsippany, NJ 07054.

Modulation Theory: Back To Basics

A brief review of frequency-moduation theory is useful to establish quantitative relationships between the output spectrum of a signal source and its short-term stability. If a sinusoidal carrier has a constant amplitude, E, and a center frequency f_o, and is not frequency modulated, then its instantaneous magnitude, V, at any time, t, is given by:

$$V = E \sin (2\pi f_o t + \Theta) \quad (1)$$

where Θ is a constant giving the phase of the sine wave at $t = 0$.

If we introduce a sinusoidal frequency modulation, then the phase of the wave will be sinusoidally advanced and retarded from that given in Eq. (1). We can allow for that variation by rewriting Eq. (1) in terms of a phase component, $\Theta(t)$, that is a function of time:

$$V = E \sin [2\pi f_o t + A \sin 2\pi f_m t] \quad (2)$$

where: $\Theta(t) = A \sin 2\pi f_m t$

This is a wave having an instantaneous total phase, β, in radians of:

$$\beta = 2\pi f_o t + A \sin 2\pi f_m t \quad (3)$$

The first term of this expression is the linearly progressing phase of the (unmodulated) carrier, f_o, while the second term is the phase variation (sinsoidal, at the modulating frequency) from the linearly progressing phase, as a function of time.

Differentiating Eq. (3) with respect to time, and dividing by 2π to convert radians to Hertz, we get the instantaneous frequency, f:

$$f = \frac{1}{2\pi}\frac{d\beta}{dt} = f_o + A f_m (\cos 2\pi f_m t) \quad (4)$$

Recalling that A, the peak amplitude of the second term, is really the peak phase deviation caused by the moduation, we can replace A by $\Delta\phi$ in both Eq. (4) and back in Eq. (2):

$$f = f_o + \Delta\phi f_m (\cos 2\pi f_m t) \quad (5)$$

$$V = E \sin [2\pi f_o t + \Delta\phi \sin 2\pi f_m t] \quad (6)$$

Thus, we can express effect of the modulation in either of two ways:

- As "residual fm noise" using Eq. (5), in which the peak frequency deviation is the product $\Delta\phi f_m$; or
- As "single-sideband phase noise" using Eq. (6), in which the peak phase deviation is $\Delta\phi$.

For modulation by a single, sinusoidal signal, there is no distinction between the two methods of expression. If we call the peak frequency deviation Δf, then, from Eq. (5), we know that

$$\Delta f = \Delta\phi f_m \quad (7)$$

$$\text{or that } \Delta\phi = \frac{\Delta f}{f_m} \quad (8)$$

This ratio of peak frequency deviation to modulation frequency is called the fm modulation index, m, so that

$$m = \frac{\Delta f}{f_m} \quad (9)$$

$$\text{and } m = \Delta\phi \quad (10)$$

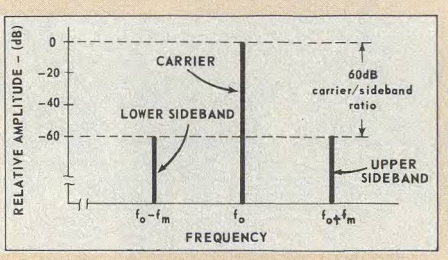

Simple, single-frequency modulation produces upper and lower sidebands.

When a wave is frequency modulated, its spectrum contains frequency components other than the carrier frequency. These occur at $f = f_m$, $f - f_m$, $f + 2f_m$, $f - 2f_m$, $f + 3f_m$, $f - 3f_m$ . . . etc. Fortunately, it can be shown by examining a Bessel-function series expansion of Eq. (5), that for the small values of modulation index associated with random phase noise ($m << 1$), only three components of the wave are significantly high in energy:

- f_o, the carrier,
- $f_o + f_m$, the first upper sideband, and
- $f_o - f_m$, the first lower sideband.

Furthermore, the same analysis shows that the ratio of the amplitude of either sideband to the amplitude of the carrier is:

$$\frac{E_{SB}}{E_C} = \frac{m}{2}$$

Expressing this ratio in decibels, we get:

$$\left.\frac{E_{SB}}{E_C}\right|_{dB} = 20 \log \left(\frac{m}{2}\right) dB \quad (12)$$

or, substituting for m, from Eq. (9):

$$\left.\frac{E_{SB}}{E_C}\right|_{dB} = 20 \log \left(\frac{\Delta f}{2f_m}\right) dB \quad (13)$$

The figure shows the spectrum surrounding a carrier, f_o, modulated by a sine wave, f_m, with a peak deviation small enough so that $m << 1$, thereby rendering negligible all but the first upper and lower sidebands.

Let us consider the case in which a high degree of spectral purity has been achieved—i.e., where the sideband-to-carrier amplitude ratio is −60 dB. From Eq. (13):

$$-60 \text{ dB} = 20 \log \left(\frac{\Delta f}{2f_m}\right)$$

$$\text{or } \frac{\Delta f}{2f_m} = 0.001$$

$$m = 0.002 = \frac{\Delta f}{f_m}$$

$$\text{and } \Delta f = 0.002 f_m$$

From Eq. (10):

$\Delta\phi = m = 0.002$ radians (0.115 degrees)

Sometimes, the frequency deviation is given in terms of its RMS value, rather than its peak value:

$$\Delta f_{RMS} = \frac{\Delta f}{\sqrt{2}} \quad (14)$$

Equation (14) is only true for sine-wave frequency deviation. If RMS frequency deviation is used, then Eq. (13) becomes:

$$\left.\frac{E_{SB}}{E_C}\right|_{dB} = 20 \log \left(\frac{\Delta f_{RMS}}{\sqrt{2} f_m}\right) \quad (15)$$

Equations (8) and (15) are the two expressions used most often in measuring and calculating short-term stability, either in terms of residual fm or in terms of phase noise. ●●

If we could analyze the modulating spectrum of Fig. 1(a) (assuming we knew it), breaking it down into its frequency components, it would be possible to compute the resultant (very complex) output spectrum . . . but the computation would be very difficult indeed. Instead, it is much more to the point to measure certain characteristics of the output spectrum, and express the measurements in terms of equivalent signal-to-noise (carrier-to-sideband) ratios. These measurements, and their interpretations, are the main concerns of this article.

Assume that a frequency-selective, deliberately narrowband detector has been used to measure the energy level in the region of f_m. If that detector has a bandwidth BW, (Hertz), then the product of the energy level measured at f_m and the bandwidth BW has the dimensions of power. This is illustrated in the inset of Fig. 1(b) by the shaded area surrounding the power-level line W_1. Note that this area represents the *energy per unit time of the output spectrum.* In the theory of stochastic (random) processes, it is readily shown that this power may be converted to the power level that would be measured in any other bandwidth (also centered on f_m) by the expression:

$$\frac{W_1}{W_2} = \frac{BW_2}{BW_1}$$

(continued on p. 38)

SHORT-TERM STABILITY

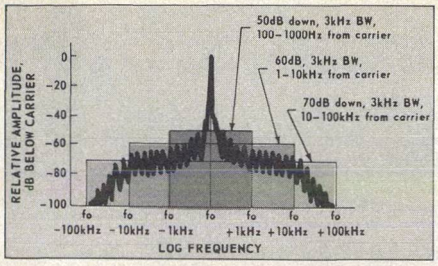

2. Residual fm noise specifications have three components: power level, bandwidth and frequency region.

or

$$\left.\frac{W_1}{W_2}\right|_{dB} = 10 \log \left[\frac{BW_2}{BW_1}\right] \qquad (16)$$

The plot of power level per unit bandwidth versus frequency is called the *power spectral density* characteristic of the signal source. To convert any such measurement to RMS *signal* (voltage or current) level, it is necessary to take the square root of the power or energy level. Hence, in terms of signal level, Eq. (16) becomes:

$$\frac{E_1}{E_2} = \sqrt{\frac{BW_2}{BW_1}} \qquad (17)$$

To see how this expression is used, consider this example: The energy level at 10 kHz above the carrier (f_m = 10 kHz), measured in a 3 kHz bandwidth (BW) is 60 dB below carrier. Calculate the RMS frequency deviation and the equivalent peak and RMS phase deviation.

First, let us calculate the factor by which we can convert the energy level measured to an equivalent per-Hertz value, using Eq. (17):

$$\frac{E_{1\,Hz}}{E_{3\,kHz}} = \sqrt{\frac{1}{3000}} = 0.0183$$

or, $E_{1\,Hz} = 0.0183\ E_{3\,kHz}$

or

$$\left.\frac{E_{1\,Hz}}{E_{3\,kHz}}\right|_{dB} = -34.7\ dB$$

Therefore, the Δf_{RMS} we calculate from the 3 kHz-bandwidth measurement (−60 dB), must be reduced to −94.7 dB, for per-Hertz correlation.

From Eq. (15):

$$\left.\frac{E_{SB}}{E_C}\right|_{dB} = -60 = 20 \log \left[\frac{\Delta f_{RMS\ (3\,kHz)}}{\sqrt{2}\ f_m}\right]$$

or $\Delta f_{RMS(3\,kHz)} = \sqrt{2}\ f_m\ (0.001)$

or $\Delta f_{RMS(3\,kHz)} = 141$ Hertz

Converting this to a per-Hertz bandwidth:

$\Delta f_{RMS\ (1\,HZ)} = 0.0183\ (141)$
$= 2.58$ Hz

The equivalent phase deviation $\Delta\phi$ is obtained from Eq. (8)

$$\Delta\phi = \frac{\Delta f}{f_m} = \frac{\sqrt{2}\ (2.58)}{100{,}000}$$
$$= 3.64 \times 10^{-5} \text{ radians}$$

or $\Delta\phi = 0.00208$ degrees

and $\Delta\phi_{RMS} = \dfrac{0.00208}{\sqrt{2}}$
$= 0.00148$ degrees

Generally, residual fm noise measurements are made in a 3 kHz bandwidth, and both frequency deviation (Δ f) and phase deviation ($\Delta\phi$) are expressed in terms of per-Hertz bandwidth figures.

Making the fm measurement

Before proceeding to actual measurement techniques, consider how the power spectral density curve of a signal is normally evaluated. Figure 2 shows a typical specification, and an output power density spectrum that satisfies the specification. Note that each specification for the residual fm noise has three components:

1. The allowable maximum *power level* relative to the carrier.
2. The *bandwidth* over which the measurement is made.
3. The *frequency region* around the carrier over which the measurement is made.

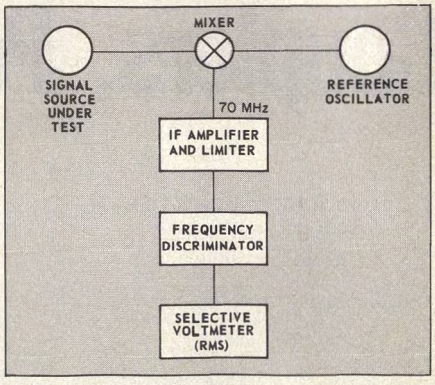

3. Residual fm noise measurements can be made as close as 500 Hz to the carrier with this test setup.

One practical test setup for measuring residual fm noise is shown in Fig. 3. In this scheme, the signal from the source under test is mixed with a reference oscillator having a known noise characteristic. The i-f frequency is not critical; a practical value is 70 MHz. The i-f output from the mixer is filtered and passed through an i-f amplifier. The i-f bandwidth should be at least twice the spectral bandwidth to be measured. For accurate measurements, the i-f response should be relatively flat (±0.5 dB) across this band, since

(continued on p. 41)

SHORT-TERM STABILITY

This is a first order error source. The i-f amplifier is followed by a hard limiter to remove all am noise. This limiter should be driven well into saturation.

Since all am noise has been removed from the carrier by the limiter, frequency jitter or fm noise of the oscillator under test will appear as video baseband noise at the output of the discriminator. Note that this spectrum is the sum of both sidebands; therefore, the single sideband noise level will be 3 dB lower. For best results, the discriminator should be a low-noise design with high sensitivity (5 to 10 V/MHz), and must have adequate bandwidth to handle all desired sideband components.

A plot of the frequency distribution of this noise is obtained by use of a selective voltmeter, tunable low-frequency receiver, or spectrum or wave analyzer. The desired bandwidth is selected, and the selective voltmeter tuned over the appropriate baseband frequencies. A plot of residual fm noise for a high-performance 2 GHz low-noise free-running oscillator is shown in Fig. 4, along with a plot expressing the data in terms of phase noise.

Noise levels down to about 1 or 2 Hz in a 3 kHz bandwidth can be accurately measured with this technique. It is recommended for noise measurements where f_m falls into the range of 500 Hz to 10 MHz away from the carrier. But since

(continued on p. 43)

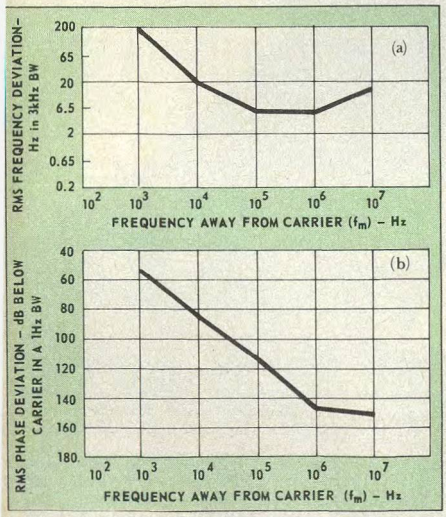

4. RMS frequency deviation data for a 2 GHz free-running oscillator (a) was measured with the setup shown in Fig. 3. RMS phase deviation of the same oscillator (b) was measured with the equipment shown in Fig. 5(a). One curve can be computed from the other using a simple nomograph available from the author by circling **Reader Service Number 297.**

SHORT-TERM STABILITY

the frequency discriminator's output is proportional to deviation (Δ f) rather than modulation index ($\Delta f/f_m$), sensitivity to modulation index makes this discriminator-based method difficult to use for "close-in" ultra-low noise measurements—e.g., for f_m less than 500 Hz.

It should be noted that residual fm noise of a microwave source can also be measured by feeding its output directly to a microwave discriminator, and channeling the discriminator output to a wave analyzer. The limitation of this technique is that it is, of course, essentially a fixed-carrier frequency method, since the microwave discriminator is not tunable over a wide frequency range.

Phase measurements more complex

For ultra-low noise measurements—e.g. within 500 Hz of the carrier—a phase noise measurement is far more sensitive than measurement of residual fm. Phase noise measurements require high relative stability (excellent tracking) between the reference and the source under test. For this reason, they are applicable primarily to crystal-controlled or synthesizer-driven sources. Fortunately, these are about the only sources that *have* ultra-low noise below 500 Hz separation from the carrier. Free-running sources, particularly those operating at microwave frequencies, have relatively high noise below 500 Hz, and therefore, may be evaluated with the previously described fm technique.

Figure 5 shows three test setups recommended for making phase noise measureemnts on phase-locked sources. They differ in their applicability: Figure 5(a) is suitable for measuring very low noise levels at close-in frequencies (near to the carrier, within the phase-lock loop bandwidth); Figure 5(b) is recommended for phase noise measurements outside the phase-lock loop bandwidth, further away from the carrier; Figure 5(c) is the simplest setup, but is limited to a very narrow range of carrier frequencies.

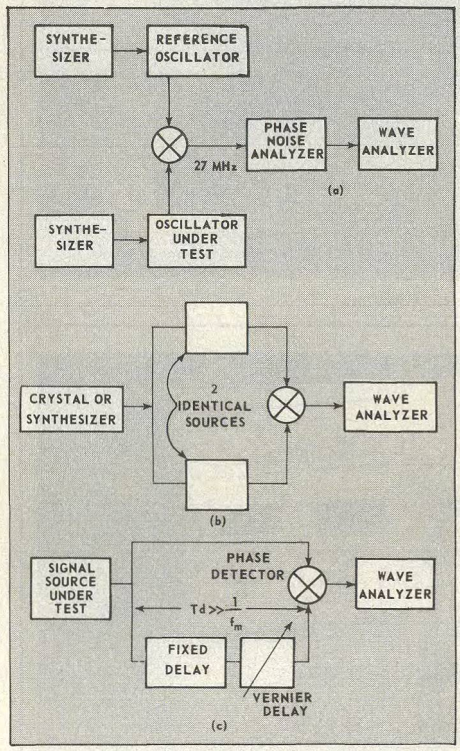

5. Phase noise may be measured using either of these methods. Each claims its own advantages.

The heart of the first measurement scheme is Frequency Engineering Laboratories' Model 800B phase noise analyzer. Because of the extremely narrow bandwidth of the instrument, the difference between the frequencies of the reference and the source under test must be maintained to within 500 Hz in the analyzer's wideband mode, and within 5 Hz in the narrow-band mode. To maintain the 5 Hz tracking, two frequency synthesizers are required to control the source and reference frequencies. (In earlier experiments, a 100 MHz crystal-controlled reference tended to drift too much).

A simple technique that can be used for making phase noise measurements of phase-locked sources is shown in Fig. 5(b). Two identical sources are phase locked to the same crystal or synthesizer to insure that their outputs are at exactly the same frequency. Within the phase-lock loop bandwidth, the noise from the source is that of the crystal or synthesizer. Note, however, that this noise will be cancelled in the phase detector, and no noise output will occur except for second-order effects caused by: (1) the fact that the phase-lock loop does not have infinite gain and (2) some noise introduced by components of the phase-locking mechanism itself.

Outside the loop bandwidth, each source will exhibit its own phase noise characteristics. The noise from the two sources at frequencies above the loop cutoff will be uncorrelated. The noise reading observed, assuming both sources

(continued on p. 44)

are essentially identical, will be 3 dB higher than the actual noise output of either source taken alone. This technique is not recommended for close-in measurements, but does have some limited application where microphonic or loop-noise reduction effects are to be studied.

The scheme depicted in Fig. 5(c) relies on an adjustable delay line (usually, a waveguide to which a "line stretcher" has been added) to perform phase-noise measurements. If the delay introduced is much longer than $1/f_m$, then the two signals arriving at the phase detector will be completely uncorrelated for that frequency. (When two signals are uncorrelated, their phase and amplitude values have different time distributions, so that they will not cancel out in a phase detector). The output of the phase detector is, then, the phase noise spectrum for f_m and all frequencies above it. There are two major limitations to this method. First, it is difficult to introduce sufficient delay to make measurements of close-in noise (at which f_m is low, calling for long delays), and second, it is difficult to adjust the delay over wide ranges.

Take care with calibration

Whether frequency or phase measurements are being made, the test setup must first be calibrated by establishing the scale factor of the discriminator. There are several ways to do this, but probably the easiest way is by signal substitution. If one is fortunate enough to have a signal generator with built-in frequency modulation of a known deviation, then the resultant modulated signal can be inserted, either at the rf or i-f frequency, to establish a reference or calibration factor at the discriminator output.

If such a generator is not available, an alternate approach can be taken using equipment common to most laboratories (see Fig. 6). An ordinary generator, operating at either i-f or rf will work, but it must have an fm modulation input.

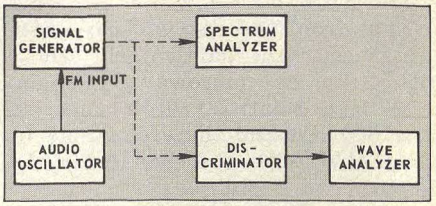

6. This calibration setup requires equipment found in most labs.

The object is to frequency modulate the carrier with a known deviation, then to drive the discriminator with this known deviation in order to determine the system's calibration factor.

The fm deviation level is established by the well-known fm carrier-null technique; that is, first modulate the signal generator using the audio oscillator, which is set to f_m. Observe the signal generator's output on a spectrum analyzer. Slowly increase the level of modulation of the signal generator. As this drive level is increased from zero, the modulation sidebands will increase in amplitude and the carrier will decrease. A point will be reached at which the carrier will approach zero. At the corresponding modulation level, the following relationship between the modulation frequency (f_m) and the peak frequency deviation (Δf) exists:

$$\frac{\Delta f}{f_m} = 2.404$$

In other words, the modulation index at the first carrier null is 2.404. For example, if $f_m = 17.65$ kHz, and the modulation level is set to the first carrier null, the resultant peak fm deviation is 42.4 kHz. Since most measuring setups read the RMS deviation of the input signal, the peak deviation should be converted to 30 kHz RMS deviation.

This modulated signal is now connected to the fm or phase discriminator and the wave analyzer is tuned to the modulation frequency, f_m. The resultant level is the double-sideband reference level. Since this sideband signal at f_m is a single-frequency sideband signal, its level will be independent of the wave analyzer bandwidth. Therefore, when measuring noise, a consistent bandwidth must be used.

When the oscillator under test is now connected and the double sideband RMS noise level at a given f_m from the carrier, reads (say) 80 dB below the reference calibration level, the resultant single-sideband fm noise, as measured in the bandwidth of the wave analyzer at f_m from the carrier, will be 3 dB lower.

If a phase noise setup is being calibrated, then the known deviation is converted to an equivalent phase noise level by Eq. (8). Additionally, either fm or phase systems may be calibrated by means of an accurately known signal added to the carrier. This results in an RMS phase deviation of:

$$\text{RMS} = \frac{E_{SB}}{2E_c} \text{ radians}$$

The accuracy of any measurement cannot be better than the calibration accuracy; the substitution methods described above are preferred to direct calibration techniques. With these methods, calibration and measurement accuracies of the order of 1 dB RMS are realizable.

All of the measurements and calculations discussed in the foregoing text have assumed that the random phenomenon we call short-term frequency or phase change can be *averaged over a bandwidth, weighted and expressed as an equivalent time-invariant quantity.* In fact, *instantaneous* values of random functions may be much larger than such averages and, in microwave systems requiring the highest order of stability, even these brief and/or very-seldom occurring excursions are significant. ••

Design Space Qualified Millimeter-Wave Doublers

Optimize doubler designs by computer before machining to save money and time. Here, the authors demonstrate the circuit modeling procedure using 19 and 28 GHz examples.

SPACE communications activity in the 20 and 30 GHz bands has created a need for stable, low-cost signal sources. Fundamental frequency sources are fine for many applications, but where very high stability is required, such as in propagation experiments, these sources are inadequate.

Millimeter-wave frequency multipliers are the answer whenever ultra-high stability is required. Beginning with a temperature-controlled 132.222-MHz crystal oscillator, it is possible to apply a chain of multipliers and achieve 1 part in 10^6 frequency stability at 30 GHz, with 90 per cent of the power contained in a ±150 Hz bandwidth centered on that frequency.

Millimeter-wave multipliers are typically designed by first mounting the diode in a circuit, then using an iterative synthesis process of cutting and measuring to arrive at the final design. The technique discussed here eliminates the laborious, expensive task of measuring and cutting by first characterizing the diode, its package and mounting parasitics, and then building a circuit model suitable for analysis with a microwave circuit analysis computer program. The computer model is then optimized to match the diode, stabilize the circuit and filter the input and output frequencies.

The circuit is "cut" from the resulting computer model, but can only be expected to exhibit near optimum performance. Final optimization is obtained from small-signal measurements on the actual circuit using bias sweeping techniques. [1-3]

Raymond L. Sicotte, Staff Engineer, Aiken Industries, 9125 Gaither Road, Gaithersburg, MD 20760, and **Richard C. Mott,** Member of the Technical Staff, Comsat Laboratories, Box 115, Clarksburg, MD 20734.

One popular, accessible microwave circuit analysis program is MICAP, available through Tymeshare, Inc., Cupertino, CA. Another is GCP, which was used in this work, and developed originally at M. I. T. Lincoln Laboratory as described in LL Technical Note 1969-34, "Automatic Microwave Circuit Analysis with GCP-MOD2."

To illustrate this design process, we will describe two doublers which were included as part of the transmitter section of the AT&T propagation experiment aboard the recently launched Comstar domestic communications satellite. The doubler circuit layout is shown in Fig. 1. The input signal is coupled via a capacitive probe from the input waveguide to the input coaxial transformer and low-pass filter. The characteristic impedance of the filter is equal to the real part of the diode impedance at the input frequency. The diode is tuned at the input frequency by the inductance of the output waveguide below its cutoff frequency and at the output frequency by a combination of the output waveguide inductance and the stopband reactance of the low-pass filter. The output waveguide transformer steps are designed so that the waveguide presents the optimum load impedance to the diode. The bias low-pass filter stabilizes the circuit against potential parametric oscillations while providing decoupling to an adjustable external bias resistor. Both doubler circuits were built around GaAs varactors supplied by Alpha Industries.

Matching is the key

The key to successful doubler design is tuning and matching the varactor at the input and output frequencies. Figure 2 shows the equivalent circuit of the mounted diode at the input frequency. The elements are identified as follows:

Z_{ji} = varactor junction operating impedance at the input frequency
L_D = diode package lead inductance
C_l = diode package shunt capacitance
L_{li} = inductance external to diode package
L_2, L_3 = inductances of output waveguide below its cutoff frequency
R_{si} = series resistance of diode and circuitry at the input frequency.
R_{in} (ext) = real part of the packaged and mounted diode input impedance.

The elements of the internal package are obtained from the manufacturer or may be measured according to the IEEE standard specification.[4] The external inductance, L_{li}, is obtained using the standard method suggested by Getsinger.[5]

Inductances L_2 and L_3 are introduced by the output waveguide operating below its cutoff frequency at the input frequency. They are calculated from output waveguide reactances X_2 and X_3, shown in Fig. 3. The output waveguide characteristic impedance for frequencies below cutoff is given by:

$$Z_o = j\left(\frac{2b}{a}\right)\sqrt{\mu/\epsilon}\left(\frac{1}{\sqrt{(f_c/f)^2 - 1}}\right) \qquad f < f_c \qquad (1)$$

where b and a are the waveguide height and width, respectively, and Z_0 is imaginary for a waveguide below cutoff. Reactance X_2 is obtained by successive application of the impedance transformation equation for a transmission line below the cutoff frequency:

$$jX_i = Z_{0i}\left(\frac{Z_{Li} + Z_{0i}\tanh\gamma\ell_i}{Z_{0i} + Z_{Li}\tanh\gamma\ell_i}\right), \quad i = 1, 2$$

where

X_i = input reactance
Z_{Li} = load impedance (imagi-

(continued on p. 48)

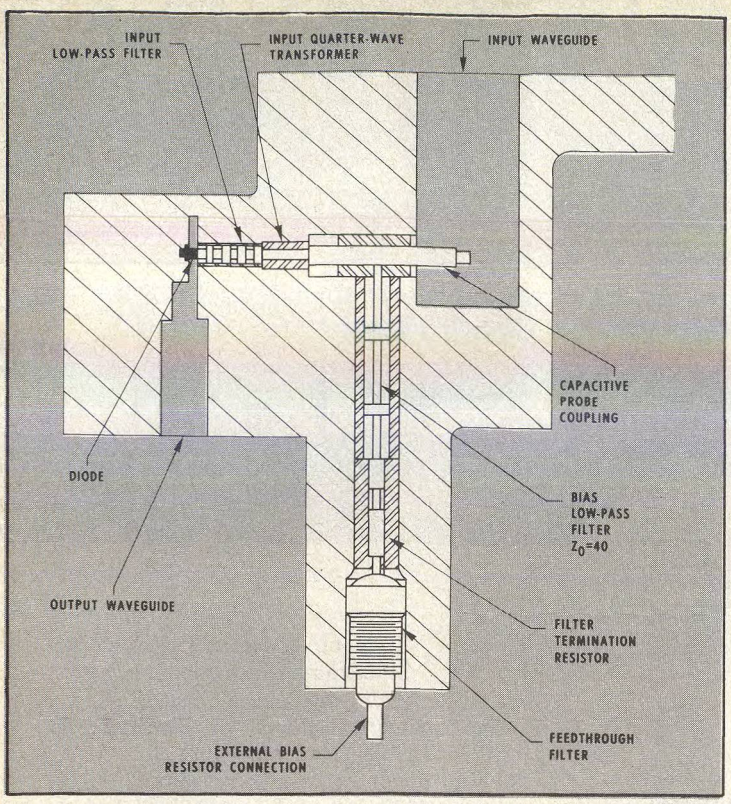

1. A capacitive probe couples energy from the input waveguide to the varactor. A quarter-wave transformer matches the 50-ohm probe transition to the low-pass filter.

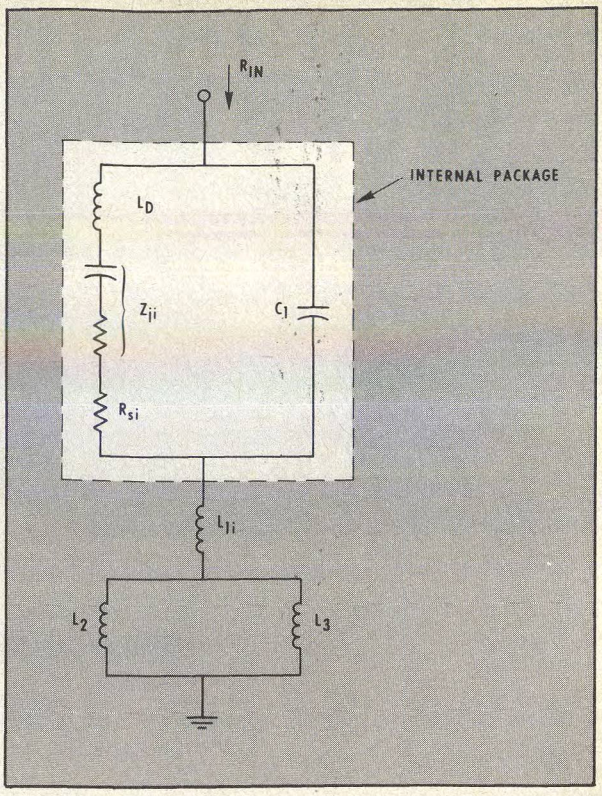

2. The equivalent circuit of the mounted diode at the input frequency includes elements attributed to the package and the waveguide.

nary) of the ith line
Z_{0i} = characteristic impedance of the ith line
γ = propagation constant (real for waveguide below cutoff)
ℓ_i = length of the ith line

Reactance X_3 is given by

$$jX_3 = Z_{02} \tanh \gamma \ell_i \qquad (3)$$

Using these parameters, computer-aided circuit analysis is used to optimize the input reactance, principally by adjusting the waveguide height (changing Z_{02}). The input real part match is achieved by designing the low-pass filter with a characteristic impedance equal to $R_{in(ext)}$.

The equivalent circuit for the mounted diode at the output frequency is shown in Fig. 4. Internal package parameters L_D and C_1 are the same for the input and output frequencies, while R_{so} is the series loss resistance at the output frequency. External inductance L_{1o} is calculated at the output frequency

(continued on p. 51)

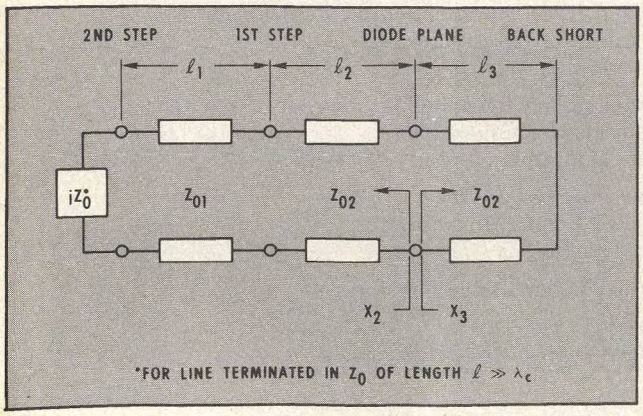

3. Output waveguide reactances, X_2 and X_3, can be used to calculate L_2 and L_3 in Figure 2.

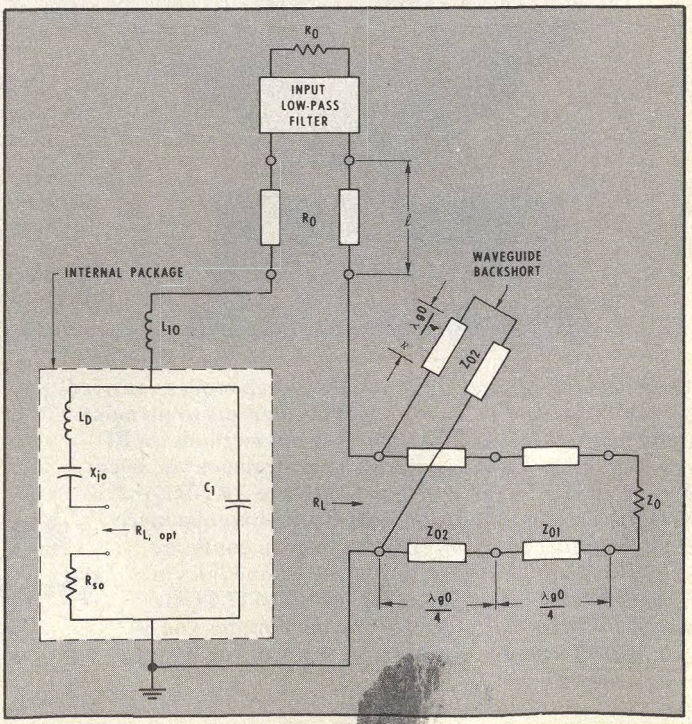

4. The equivalent circuit of the mounted diode at the output frequency includes the low-pass filter.

by using the same technique employed to obtain the input circuit inductance, L_{1i}. The characteristic impedance of the coaxial line connecting the low-pass filter to the diode circuit is equal to the low-pass filter characteristic impedance, R_o. The length, ℓ, of this line, together with the filter design, is adjusted to obtain the reactance required to resonate the diode at the output frequency. The optimum diode load resistance, R_L, is achieved by adjusting Z_{01} to transform the full height output waveguide characteristic impedance to R_L. Again, the circuit is optimized using computer-aided design techniques before it is fabricated.

It should be noted that the cutoff frequencies of both the input and bias low-pass filter are important in terminating the diode in a real impedance out-of-band to prevent the excitation of parametric instabilities. The bias filter and the input waveguide form a diplexer network with a crossover frequency equal to the cutoff frequency of the input waveguide. Similarly, the input low-pass filter and output waveguide form a diplexer with a crossover frequency equal to the cutoff frequency of

(continued on p. 53)

Table 1: Design Parameters For Two Frequency Ranges

Parameter	9.5 to 19 GHz	14.8 to 28.56 GHz
Diode		
$C_{j\ min}$	0.16 pF	0.11 pF
V_B	20 V	15 V
f_c (−6)	400 GHz	500 GHz
Package Style	Micro-Pill	Min-Dot
L_D	0.16 nH	0.12 nH
C_i	0.2 pF	0.12 pF
Input Circuit		
Diode Junction[6-8] Impedance	10 Ω-j33 Ω*	10 Ω-j33 Ω*
L_{1i}	0.07 nH	0.04 nH
L_2	0.856 nH	0.445 nH
L_3	0.440 nH	0.225 nH
Signal LPF, R_o	6 Ω	10 Ω
Bias LPF, R_o	40 Ω	40 Ω
R_{si} (assumed)	2.2 Ω	3.5 Ω
Output Circuit		
Diode Junction[6-8] Impedance	16.5 Ω-j16.5 Ω*	16.5 Ω-j16.5 Ω*
External Inductance, L_{1o}	0.08 nH	0.043 nH
Input LPF Reactance	−j2.9 Ω	−j3.7 Ω
R_L, OPT	13 Ω	15.4 Ω
R_{so} (assumed)	2.0 Ω	3.0 Ω

*Drive level, M = 2.

the output waveguide. This technique terminates the varactor in a real impedance at all frequencies out of band, which effectively inhibits the excitation of parametric instabilities.

"Cold tests" improve match

A complete list of the parameters involved in the computer optimization of the Comstar doublers is shown in Table 1. Initial hardware fabricated to these specifications did not perform up to par, however, because of the approximations used to calculate the parasitic reactances and the assumptions for the parasitic loss resistances. Preliminary measurements of the doubler return loss showed that the circuits were close, but not optimally matched. Each doubler was "cold tested" to determine the input and output impedance presented to the diode, and the associated coupling ciruit elements which relate these impedances to their respective measurement planes. The improvement in doubler performance as a result of fine tuning matching circuitry is shown in Table 2.

A full discussion of the varactor circuit cold test theory and procedure is given in Reference 9. A practical application of the theory is presented here. The value of the bias sweeping measurement technique is that it makes possible the decoupling of the input and the output circuits so that the matching and tuning can be evaluated separately. Measurements of return loss on an operating multiplier simply indicate that a matching problem exists; cold testing reveals its location as well as the nature of the problem, i.e., input tuning, input real-part match, output tuning or output real-part match.

Figure 5 is an equivalent circuit which describes the coupling between the input or output waveguide flange and the diode junction. The elements are as follows:

Z_{input} = impedance presented to the varactor junction
R_c = series resistance representing circuit losses
R_s = diode junction series loss resistance
L_s = series inductance which resonates the average varactor capacitance
$S(V)$ = elastance (reciprocal of lossless non-linear capacitance) as a function of junction voltage (V)

(continued on p. 56)

Table 2: Measured Doubler Performance

	19-GHz Doubler Performance (P_{in} = +17.0 dBm)			28-GHz Doubler Performance (P_{in} = +14.5 dBm)		
	Measured Initial	Measured Final	Predicted*	Measured Initial	Measured Final	Predicted*
Conversion Loss (dB)	3.0	2.2	2.1	4.1	3.2	3.3
Return Loss (dB)	9.5	27.1		17.8	22.0	
1-dB Output		500		1200	1700	
Bandwidth (MHz)						
Efficiency %	50	60	62	39	48	47

*Diode theoretical loss + 0.5-dB circuit loss estimate [see Eq. 11].

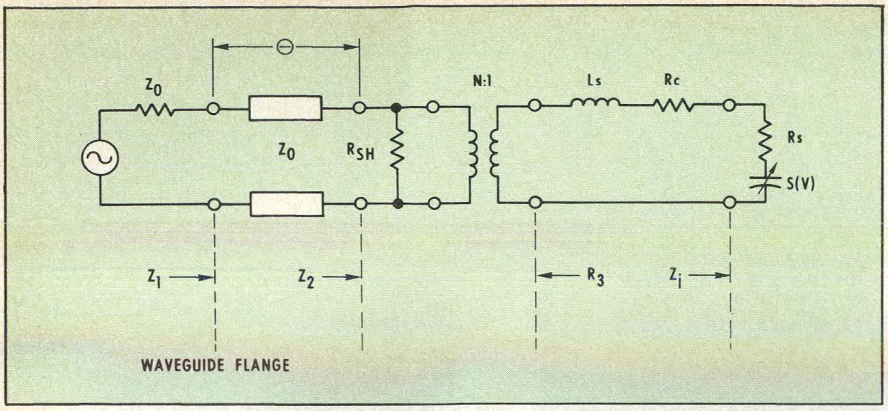

5. Coupling between the input or output waveguide flange and the diode junction is described by this circuit.

R_{SH} = shunt loss resistance.

The circuit is correctly designed when the diode is resonant and the real-part impedance match is achieved at both input and output ports. The condition for resonance is given by

$$L_s = \frac{S_{01}}{(\omega_0)^2} \qquad (5a)$$

$$L_s = \frac{S_{02}}{(2\omega_0)^2} \qquad (5b)$$

at the input and output ports, where S_{01} and S_{02} are the average diode elastances at the input and output frequencies, respectively.

A real-part match is achieved at the input when

$$R_3 = R_c + R_s + R_{in} \qquad (6a)^*$$

and at the output when

$$R_3 = R_L - R_c - R_s \qquad (6b)$$

*The effect of R_{SH} was found to be negligible; hence, it has been omitted here.

where under full power conditions, R_{in} is the real part of the pumped, lossless varactor junction impedance at the input frequency and R_L is the optimum load resistance for the lossless varactor. These values are obtained from the analyses given in References 6-8.

Note the difference between Eqs. 6(a) and 6(b). When diode and circuit losses are nontrivial, it is important to consider them correctly to arrive at the proper value of R_3 for matching.

Determining the matching elements

The elements of the coupling circuit are derived from slotted-line, small-signal impedance measurements of the doubler as a function bias voltage. The resulting impedance points lie on a circle when plotted on a Smith Chart. The angle through which the circle is rotated until it is coincident with a constant resistance circle is the electrical distance (Θ) that corresponds to shifting the reference plane of measurement from the waveguide flange to the Z_2 measurement plane of Fig. 5. Figure 6 is the resulting Smith Chart plot. The points A, B and C in Fig. 6 refer to Z_2, and are identified with respect to the notation in Fig. 5 as follows: For point A, $V_0 = V_B$, and:

$$Z_A = n^2\left[R_c + R_s - j\frac{S_{MAX}}{\omega_0} + j(\omega_0 L_s)\right] \qquad (7)$$

where n is the transformer ratio as shown in Fig. 5 and $S_{MAX} = S(V_B)$. For point B, $V_0 = V_R$ (tuned condition).

$$\frac{S(V_R)}{\omega_0} = \omega_0 L_s \qquad (8)$$

and $Z_B = n^2(R_c + R_s)$

For point C, $V_0 = V_F$, and:

$$Z_c = n^2\left(R_c + R_s - j\frac{S_{MIN}}{\omega_0} + j\omega_0 L_s\right) \qquad (9)$$

where $S_{MIN} = S(V_F)$.

Because $S(V_0)$ is found by separately measuring the varactor's elastance voltage characteristics, L_s is now determined. From Fig. 6, it is clear that

$$X_2(V_B) - X_2(V_F) = -\frac{n^3}{\omega_0}\left[S(V_B) - S(V_F)\right] \qquad (10)$$

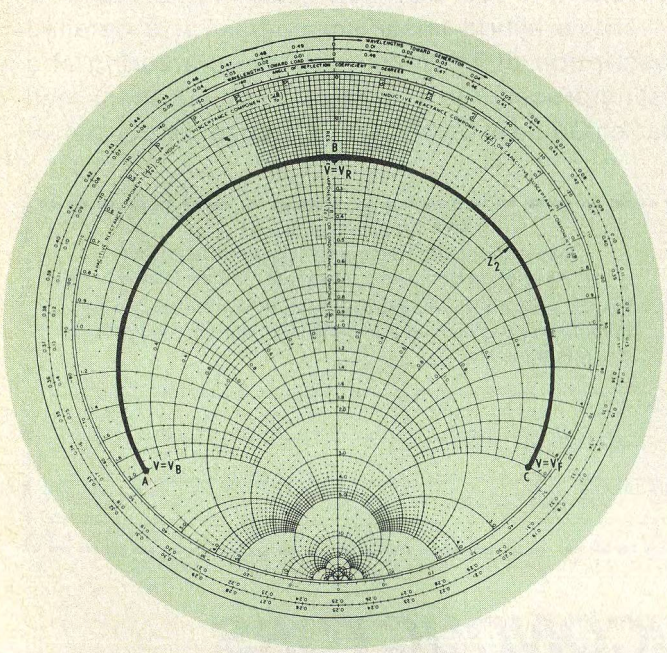

6. Swept bias measurement techniques provide impedance points which lie on a circle on the Smith Chart.

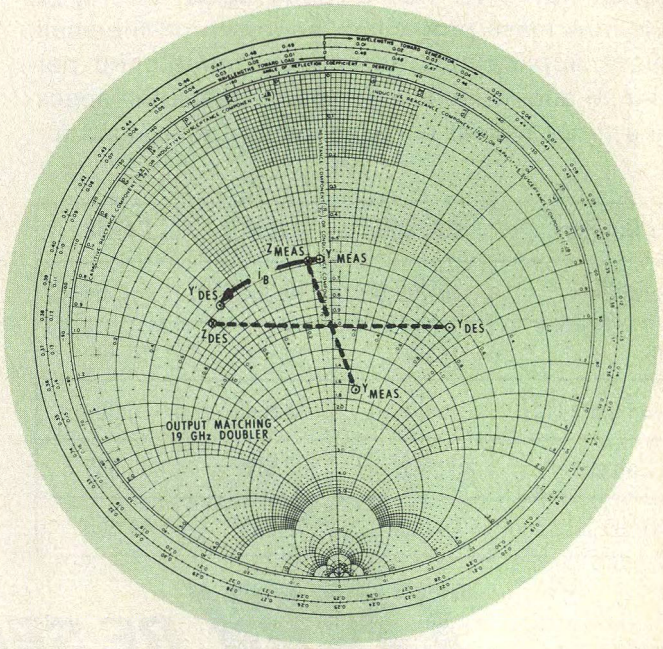

7. Measured and desired input impedance points are rotated to form a new reference plane.

The left side of Eq. (10) is taken from the Smith Chart, and n^2 can now be determined because S is shown as a function of voltage. It is possible to determine $R_s + R_c$ from Eq. (7) or (9) and calculate circuit losses. Input and output circuit efficiencies can be approximated using the following equations:

$$\eta_{c,\,in} = \frac{1}{1 + \dfrac{(R_c + R_s)}{R_{in}}}$$

$$\eta_{c,\,out} = \frac{1}{1 + \left(\dfrac{(R_c + R_s)}{R_L}\right)}$$

High-frequency, low-capacitance varactors contain a significant voltage-variable resistive term, and small-signal impedance is more accurately represented by:

$$Z_j = R_s' - R_s''(V_o) - j\frac{S(V_o)}{\omega_o} \quad (12)$$

The voltage variable resistive term, $R_s''(V_o)$, is small, and can be neglected when deembedding the varactor on a 9.5 to 19-GHz doubler. However, this term is significant and must be included when dealing with the 14 to 28 GHz design due to lower capacitance and hence, smaller junction area of the diode. The resistive term is larger, thus the voltage-variable part more prominent. Special techniques developed by Atia[10] which consider the voltage-variable resistance were employed to perform the deembedding of the Comstar multipliers.

Match for optimum performance

The matching technique involves

(continued on p. 58)

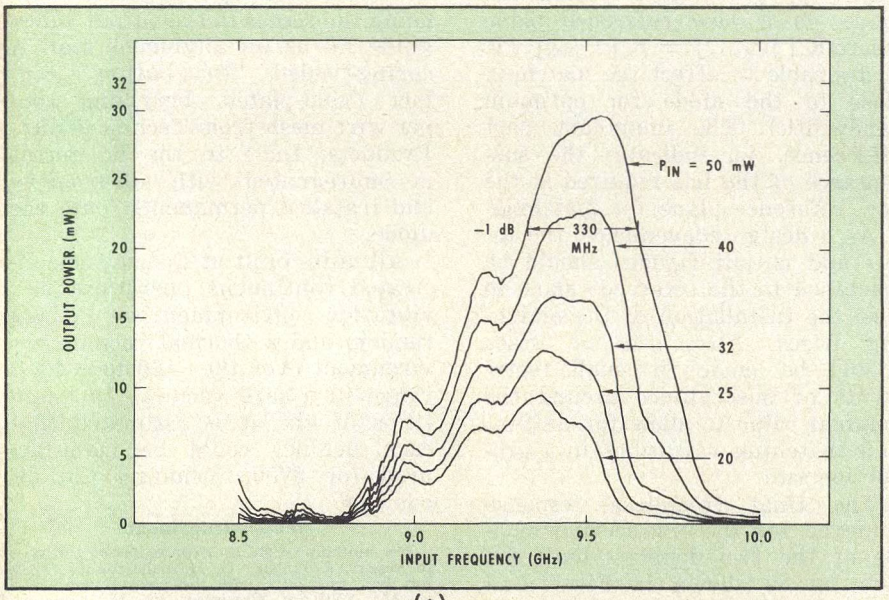

(a)

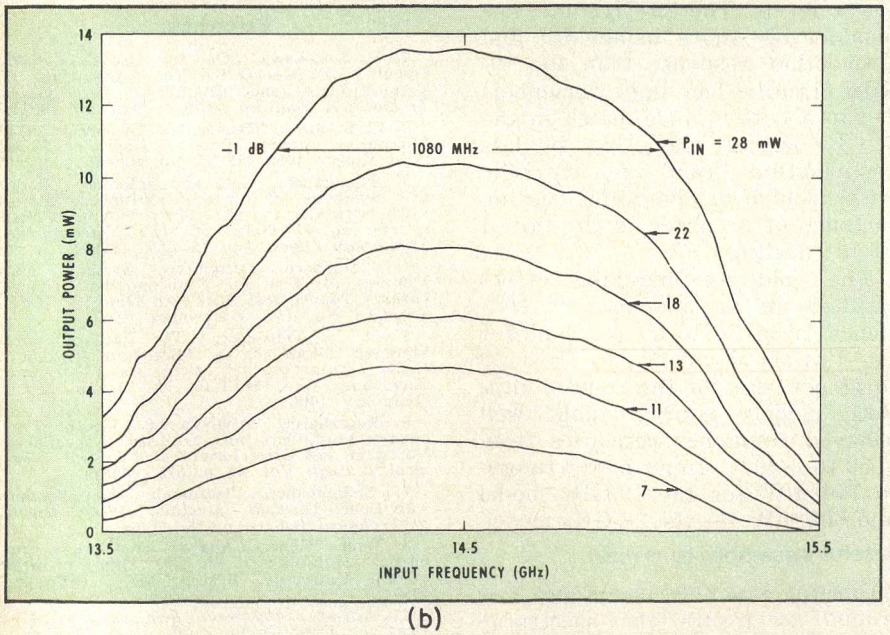

(b)

8. Measured frequency response is smoother for the 28-GHz unit due to better diode matching.

changing the impedance presented to the diode junction by the initial circuit design into that required for optimum performance. This is accomplished by using the measured elements of the coupling circuit of Fig. 5 to calculate the impedance of Z_{input} presented to the diode junction. Both the measured and desired values of Z_{input} are transformed through the coupling network into the waveguide of characteristic impedance Z_0 where the initial cold test measurements were performed. Two points, Z_{MEAS} and Z_{DES}, plotted on a Smith Chart in Fig. 7, are shown at the waveguide flange for convenience. The corresponding admittance points are shown as Y_{MEAS} and Y_{DES}. The two points are rotated through an angle, ϕ, preferably toward the diode, to a new reference plane where $R_e[Y'_{MEAS}] = R_e[Y'_{DES}]$. (It is desirable to effect the matching close to the diode for optimum bandwidth). The imaginary part difference, j_B, indicates the susceptance of the iris required at the new reference plane for matching.

As a design convenience, the input and output flanges should be machined to the reference plane to ease the installation of the matching irises. Also, sets of irises should be made in small increments of susceptance around the nominal value to allow for unit-to-unit matching variations in a production run.

The final frequency response achieved for the engineering models of the two doublers built for Comstar is shown in Figs. 8(a) and 8(b) at a number of input power levels. The 28-GHz unit has considerably more bandwidth and a smoother response than the 19-GHz circuit. The improvement is due to a better diode match in the 28-GHz circuit resulting in less perturbation from the matching irises, which demonstrates the importance of accuracy in the initial circuit design.

The cold-test matching effort resulted in an increase in efficiency from 50 to 60 per cent for the 19-GHz doubler, and from 39 to 48 per cent for the 28-GHz unit. Both models exhibit stable, well behaved frequency responses from −60 to +40°C. Input power ranges to 740 mW for the 19-GHz model and 603 mW for the 28-GHz model.

Careful assembly is critical

Careful assembly techniques are crucial to insure the successful operation of space-qualified units. Precision-soldering of the bias-line low-pass filter to the main center conductor is accomplished using a split-block alignment jig to achieve the correct line length of the filter's first section. The press-fit of the input low-pass filter's center-conductor section and dielectric into the surrounding coaxial ground shield is achieved using a pre-formed metal guide and tool. Most of the doubler's dimensions in this region are toleranced to one-half of one mil ($\pm 0.005''$) and dimensioned for a line-to-line fit. The press-fit is essential to the proper transfer characteristics of the input low-pass filter. All teflon dielectric sleeves are cross-pinned to the doubler body.

Finally, the diode is silver-epoxied to the input low-pass filter using the recess in the output waveguide lid as an alignment tool. A spring-loaded "fuzz-button" contact (gold-plated, beryllium copper wire mesh from Technical Wire Products, Inc.) in the lid recess is impregnated with silver-epoxy and installed permanently onto the diode.

All units built at Comsat demonstrated continuous operation in a vibration environment of 7 G's random and a thermal vacuum environment over the −60 to +40°C range in a hard vacuum. In quantities of six, it is estimated that each doubler could be manufactured for $700, including the diode. ••

Acknowledgement

The authors wish to express their gratitude to Messrs. J. Jerome, G. Hawisher and J. Molz for their assistance with the measurements and to Mr. William Getsinger for his technical guidance throughout the project.

References

1. L. Kurokawa, "On The Use of Passive Circuit Measurements For The Adjustments Of Variable Capacitance Amplifiers," *Bell System Technical Journal*, pp. 361-381, (January, 1962).

2. C. B. Swan, "Design and Evaluation of a Microwave Varactor Tripler," *Digest of Technical Papers*, 1965 ISSCC, pp. 106-107.

3. Steinbrecher, Goff and Solomon, "Iterative Synthesis of Varactor-Multiplier Microwave Networks and a Doubler with 0.17 Watt Output at 47 GHz," *G-MTT International Symposium Digest*, pp. 157-159, (1967).

4. "Standard Definitions, Symbols and Methods of Test for Semiconductor Tunnel (Esaki) Diodes and Backward Diodes," *IEEE Standard No. 253*, (December, 1963).

5. W. J. Getsinger, "The Packaged and Mounted Diode as a Microwave Circuit," *IEEE Transactions on Microwave Theory and Techniques*, Vol. MTT-14, No. 2, pp. 58-69, (February, 1966).

6. Burckhardt, "Analysis of Varactor Frequency Multipliers for Arbitrary Capacitance Variation and Drive Level," *Bell System Technical Journal*, Vol. 44 p. 675, (1965).

7. Steinbrecher, "Harmonic Multiplication with Punch-Through Varactors," *ISSCC Digest of Technical Papers*, p. 68, (1966).

8. Tang, "General Analysis of Idlerless Frequency Multipliers," Ph. D. Thesis, Northeastern University, Boston, MA, (February, 1969).

9. Watson, *Microwave Semiconductor Devices and Their Circuit Applications*, Mc-Graw-Hill, Inc., New York, pp. 245-248, (1969).

10. A. E. Atia, "Diode De-Imbedding Procedure," to be published.

Two Ways To Plot Sidelobe Patterns

Two methods for analyzing antenna sidelobe power-gain data are compared. One is best for EMC studies, while the second is well suited for determining frequency sharing criteria.

A knowledge of antenna sidelobe characteristics is as important as a knowledge of the performance characteristics represented by maximum power gain and mainlobe beamwidth for studies of electromagnetic compatibility of terrestrial and satellite communication stations, susceptibility of electronic countermeasure antennas to jamming, and susceptibility of search radars to interference. For terrestrial stations, sidelobe characteristics of on-site antennas over the entire hemisphere are required for determining coordination procedures and criteria for frequency sharing.

Two formats have been used to present measured and calculated sidelobe power-gain characteristics. Both formats are used to display what may be called statistical radiation patterns—patterns which will become more common as spectrum utilization becomes more important.

The oldest format, the probability plot[1-3], is most useful for electromagnetic compatibility studies for which antenna pointing is arbitrary. Probability plots consist of cumulative proportions of amplitude data expressed in decibels, normalized with respect to the pattern maximum or relative to the gain of an isotropic radiator, plotted against a linear or non-linear scale of proportions—often percentages.

Figure 1 is an example of a probability plot with a linear amplitude scale for power gain and a non-linear probability scale. The data curve is obtained by plotting each data point, in order of decreasing amplitude, against the inner boundaries of (n + 1) equal intervals on the probability scale. The number of data points, n, is equal to 42760 for this particular set of data and the inner boundaries are located on the per cent scale at

$$100\left(\frac{1}{42761}, \frac{2}{42761}, \cdots \frac{42760}{4276}\right)$$

The second format, briefly described in a recent C.C.I.R. report[4], is most useful for determining coordination procedures and criteria for frequency sharing among terrestrial and satellite communication stations. Data consists of power gain plotted against the angle measured from the antenna's electrical boresight. Figure 2 shows a typical power-gain angular distribution plot with a logarithmic

R. G. FitzGerrell, Group Leader, Antenna Performance, **Leroy L. Haidle,** Electromagnetic Engineer, Institute for Telecommunication Sciences, US Department of Commerce, Boulder, CO 80302.

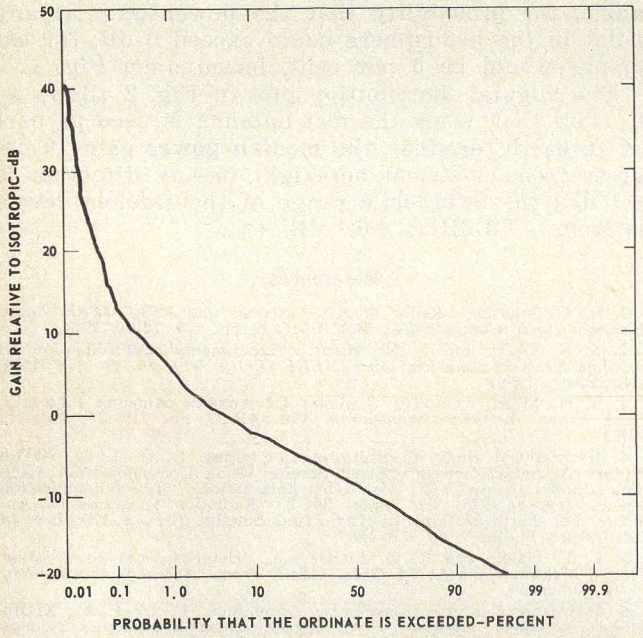

1. This probability plot of a statistical radiation pattern is composed of all data measured over the hemisphere centered on the test antenna—a 2.44-meter dish mounted atop a mobile, earth terminal operating at 7.5 GHz.

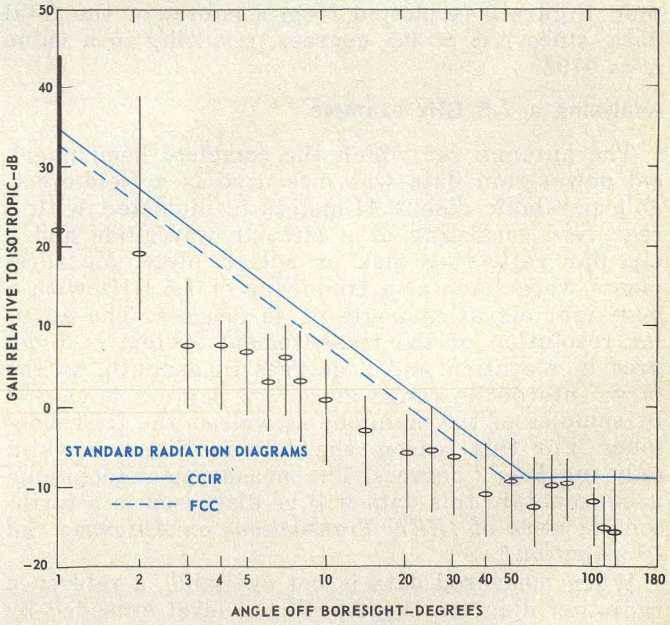

2. Angular distribution of a subset of the data used for Fig. 1 includes median values of data in 1 degree wide intervals. These are shown as circles on vertical lines representing the interdecile ranges.

scale for the angles and a linear scale for the power gain expressed in decibels. The median values of all data lying in the ranges $\phi_A \pm \Delta\phi$ are shown as circles on the vertical lines representing the interdecile range of data where the ϕ_A are specified angles off boresight and $2\Delta\phi$ is the angular range of the data used to characterize the pattern behavior at the locations of ϕ_A. This format is of interest because the angular distribution of the sidelobe levels is preserved in contrast to the probability plot. Figure 2 is plotted from a subset of the total data, since $\Delta\phi = 0.5$ degrees, resulting in a value $n = 4794$.

Analyzing a 7.5 GHz example

The antenna for which the complete hemispherical power-gain data was measured is a field-erectable parabolic dish, 2.44-meters in diameter, with a rear feed consisting of a circular waveguide and a circular reflecting disk or splash plate. Measurements were made at a frequency of 7.5 GHz with a boresight elevation angle of 45 degrees. The angular resolution of the measurement system is 1 degree in elevation and 2 degrees in azimuth, so the large interdecile range at $\phi = 2$ degrees is caused by samples of the mainlobe as well as the first sidelobes. For this reason, the data in Fig. 2 is valid only for $\phi > 2$ degrees. The measurement technique used to obtain this data will be discussed in a forthcoming issue of *IEEE Transactions on Antennas and Propagation*.[5]

When measured data is not available, a reference radiation diagram representing a level exceeded by a small fraction of the sidelobes may be used for compatibility and susceptibility studies. The solid line in Fig. 2 from ($\phi = 1°$, G = 34 dB) to ($\phi = 58°$, G = −10 dB) to ($\phi = 180°$, G = −10 dB) represents the C. C. I. R. standard radiation diagram[6] for circular antennas defined by

$$G = 52 - 10\log_{10}(D/\lambda) - 25\log_{10}\phi, \text{ dB} \quad (1)$$

where G is the power gain, D and λ are the antenna diameter and the wavelength expressed in the same units, and ϕ again is the angle in degrees measured from electrical boresight. This equation, based upon work reported by Boithias and Behe,[7] is assumed to be valid for

$$\phi_1 \leq \phi \leq \phi|_G = -10 \text{ dB}$$

where the angle ϕ_1 is the position of the first sidelobe given by $\phi_1 \approx 100/(D/\lambda)$ degrees.

Plotting an FCC standard

The dashed line in Fig. 2 represents a standard diagram given in the FCC Rules and Regulations 25.209, Antenna Performance Standards, which states:

"(a) Any antenna to be employed in transmission at an earth station in Communication-Satellite Service shall conform to the following standard:
Outside the main beam, the gain of the antenna shall lie below the envelope defined by:

$$32 - 25\log_{10}(\Theta) \text{ dBi} \quad 1° \leq \Theta \leq 48°$$
$$-10 \text{ dBi} \quad 48° < \Theta \leq 180°$$

where Θ is the angle in degrees from the axis of the main lobe, and dBi refers to dB relative to an isotropic radiator. For the purposes of this section, the peak gain of an individual sidelobe may be reduced by averaging peak level with the peaks of the nearest sidelobes on either side, or with the peaks of two nearest sidelobes on either side, provided that the level of no individual sidelobe exceeds the gain envelope given above by more than 6 dB."

The FCC standard is simply Eqn. (1) for $D/\lambda = 100$. Data in Fig. 2 was not "smoothed" according to the procedures described by the FCC.

The probability plot characterizes the statistical antenna power-gain performance, for a specified site geometry, regardless of where an interested observer is located in the hemisphere around it. If our test antenna was used as part of a search radar, with its boresight axis at a 45-degree elevation angle, the probability that the power gain at any point in the hemisphere could exceed 0 dB, for example, would be 5 per cent, based upon Fig. 1.

The angular distribution plot of Fig. 2 allows us to state that, when the test antenna is used as part of an earth terminal, the median power gain 10 degrees from electrical boresight in any direction is +1 dB; the interdecile range of the sidelobe levels is from −7.6 dB to +6.1 dB. ••

References

1. R. C. Johnson, "Radar Search Antennas and RFI," *IEEE Trans. Electromagnetic Compatibility*, Vol. EMC 6, pp. 1-8, (July, 1964).

2. S. K. Grace and S. N. Miller, "Experimental Determination Of Antenna Sidelobe Statistics," *Proc. IEEE (Lett.)*, Vol. 54, pp. 1593-1594, (November, 1966).

3. S. N. Miller, "On The Statistics Of Analytic Antenna Patterns," *IEEE Trans. Antennas Propagation*, Vol. AP-21, pp. 219-224, (March, 1973).

4. **International Radio Consultative Committee, C. C. I. R., XIIIth** Plenary Assembly, Geneva, "Fixed Service Using Communication Satellites (Study Group 4)," Vol. IV, International Telecommunication Union, Geneva, 1975. See Report 391-2, "Radiation Diagrams Of Antennae For Earth Stations In The Fixed Satellite Service For Use In Interference Studies," pp. 176-180.

5. L. L. Haidle and R. G. FitzGerrell, "Hemispherical Power Gain Pattern Measurements At 7.5 GHz," *IEEE Trans. Antennas Propagation*, to be published.

6. International Radio Consultative Committee, C. C. I. R., XIIIth Plenary Assembly, Geneva, "Fixed Service Using Radio-Relay Systems (Study Group 9)," Vol. IX, International Telecommunications Union, Geneva, 1975. See Report 614, "Reference Radiation Patterns For Radio Relay System Antennae," pp. 234-237.

7. L. Boithias and R. Behe, "Directivite Maximale En Dehors De L'Axe Des Ouvertures Rayonnantes Equiphases," Ann. Des Tele Comm., pp. 325-340, (September-October, 1971).

laser technology

AUGUST
1976

MICROWAVES

Also in this issue:

Metal-detecting radar rejects clutter naturally
Highlights from the European Microwave Conference

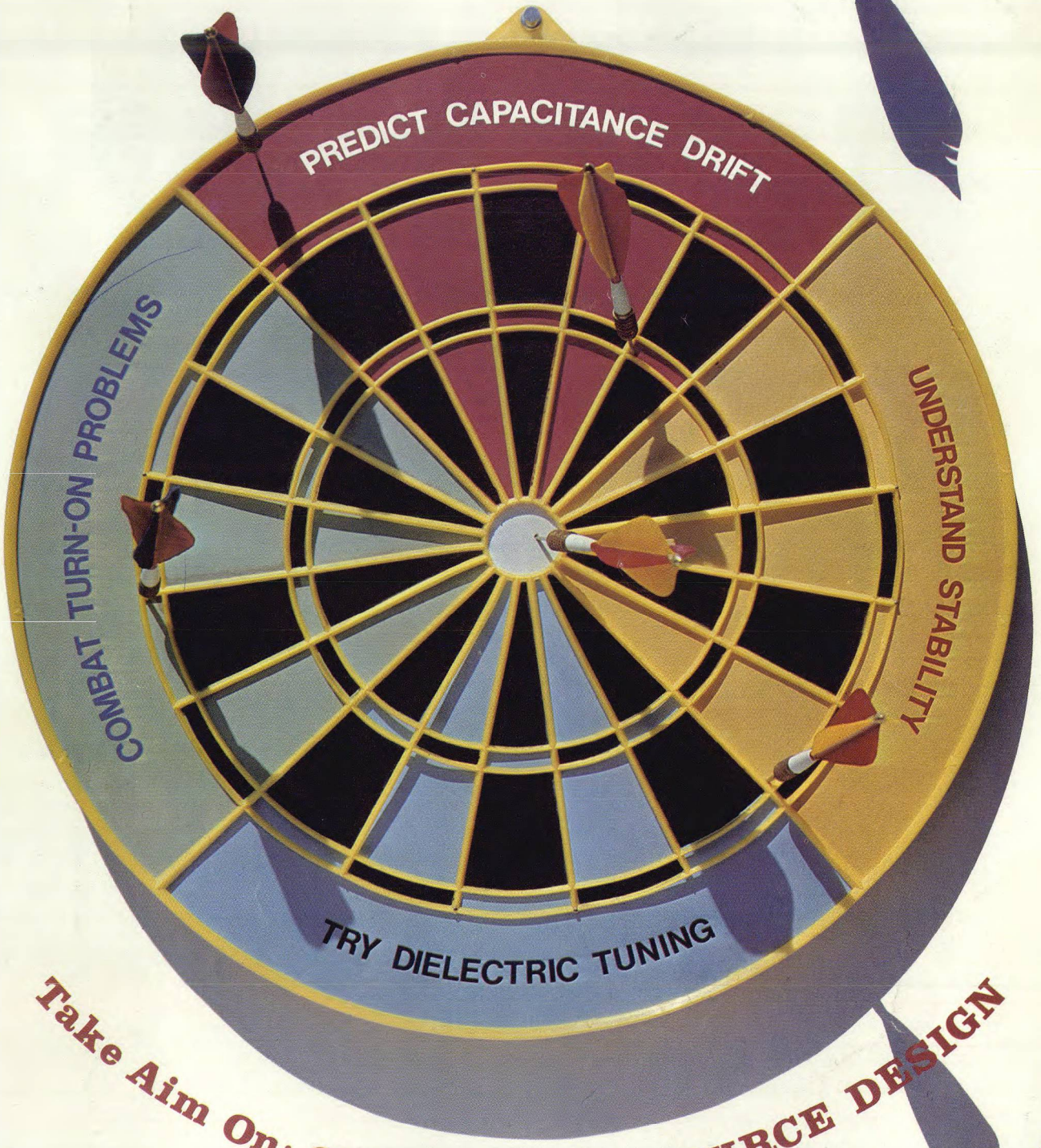

Take Aim On: SOLID-STATE SOURCE DESIGN

SPECIAL SECTION: Your guide to
EUROPEAN MICROWAVE CONFERENCE
See co
tar

MICROWAVES

August 1976
Vol. 15, No. 8

news

editorial

technical

Sources

departments

About the cover: This month, four authors demonstrate how your next source design can be right on target. Cover composition and photo by Art Director Robert Meehan.

coming next month: Electronic Warfare

Design Large Dynamic Range PIN Diode Modulators. Authors from General Dynamics provide all the information necessary to build PIN diode modulators for precise control of power over a 100 dB dynamic range.

Linearize Microwave VCO Tuning. Build your own linearizers using digital-to-analog converters for computer-control of microwave VCOs at the ultra-fast tuning rates required for EW receivers.

What's the Future for Gigabit Logic? The next major thrust in radar system design might well hinge on increasing the speed of analog-to-digital converters . . . a task which will require logic functions at gigabit rates. Semiconductor designers are turning toward the MESFET, Gunn and hybrid structures to attain the ultra-high switching speeds (about 20 ps) required.

Publisher/Editor
Howard Bierman

Managing Editor
Stacy V. Bearse

Associate Editor
George R. Davis

Contributing Editor
Harvey J. Hindin

Washington Editor
Paul Harris
Snyder Associates
1050 Potomac St., NW
Washington, DC 20007
(202) 965-3700

Editorial Assistant
Gail Murphy

Production Editor
Sherry Lynne Karpen

Art Director
Robert Meehan

Production
Dollie S. Viebig, Mgr.

Circulation
Barbara Freundlich, Dir.
Trish Edelmann
Gene M. Corrado
Sherry Karpen,
Reader Service

Directory Coordinator
Janice Tapp

Editorial Office
50 Essex St.,
Rochelle Park, NJ 07662
Phone (201) 843-0550
TWX 710-990-5071

A Hayden Publication
James S. Mulholland, Jr.,
President

MICROWAVES is sent free to individuals actively engaged in microwave work. Subscription prices for non-qualified copies:

	1 Yr.	2 Yr.	3 Yr.	Single Copy
U.S.	$15	$25	$35	$2.50
FOREIGN	$20	$35	$50	$2.50

Additional Product Data Directory reference issue, $10.00 each (U.S.), $18.00 (Foreign). POSTMASTER, please send Form 3579 to Fulfillment Manager, MicroWaves, P.O. Box 13801, Philadelphia, PA. 19101.

Back Issues of MicroWaves are available on microfilm, microfiche, 16mm or 35mm roll film. They can be ordered from Xerox University Microfilms, 300 North Zeeb Road, Ann Arbor, MI 48106. For immediate information, call (313) 761-4700.

Hayden Publishing Co., Inc., James S. Mulholland, President, printed at Brown Printing Co., Inc., Waseca, MN.

news/meetings

9-11. Government Microcircuit Applications Conference. Dutch Inn, Lake Buena Vista, Orlando, FL. Contact: Konrad H. Fischer, US Army Electronics Command, Attn: AMSEL-TL-IC, Fort Monmouth, NJ 07703 (201) 544-4547.

9-11. IEEE International Pulsed Power Conference. Hilton Inn, Lubbock, TX. Contact: Dr. T. R. Burkes, Dept. of Electrical Engineering, Texas Tech University, Lubbock, TX 79409 (806) 742-1251.

9-12. Millimetric Waveguide Systems. IEE, London, England. Contact: IEE, Savoy Place, London, WC2R, OBL, England.

29-December 1. National Telecommunications Conference. Fairmont Hotel, Dallas, TX. Contact: Gerald D. Haynie, Chairman, Technical Program Committee, NTC-76, Room 3E-231, Bell Telephone Labs, Holmdel, NJ 07733.

December

6-8. IEEE International Electron Devices Meeting. Washington Hilton Hotel, Washington, DC. Contact: Dr. Josef Berger, 1976 IEDM Technical Program Chairman, Hewlett-Packard Co., 1501 Page Mill Rd., Bldg. 1U, Palo Alto, CA 94304 (415) 493-1501.

February

16-18. International Solid-State Circuits Conference. Sheraton Hotel, Philadelphia, PA. Contact: SSC Council, Philadelphia Section, University of PA, Philadelphia, PA.

Call For Papers

Deadline: October 1. IEEE International Symposium on Circuits and Systems. Phoenix, AZ. Covers all aspects of the theory, design and application of circuits and systems. The meeting will be held on April 25-27, 1977. Contact: T. N. Trick, Dept. EE, University of Illinois, Urbana, IL 61801 (217) 333-0943.

Deadline: January 15. International Microwave Symposium. Sheraton Harbor Island Hotel, San Diego, CA. Areas of interest: optical techniques, submillimeter waves, high power, biological effects and medical applications, digital systems. The meeting will be held on June 21-23, 1977. Contact: Dr. Gerald Schaffner, TPC 1977 MTT-S Symposium, Teledyne Ryan Aeronautical, 2701 Harbor Drive, San Diego, CA 92112.

Cross The Barrier Of Varactor Drift

Predict a capacitance-temperature coefficient (CTC) for PN junction varactors and apply it for better source design. Use simple curve-tracer tests to weed out diodes prone to drift.

THE few "puffs" of capacitance presented by a varactor diode is the prime parameter controlling the frequency of many voltage-controlled oscillators. The fact that the diode's depletion layer capacitance changes with bias voltage is well recognized, and is, of course, the basis of VCO tuning. The fact that this capacitance also varies with temperature fluctuations, either ambient or those due to dissipated power in the diode, is not as well recognized, and consequently is the source of many stability problems.

Fortunately, this capacitance temperature variation is predictable, which distinguishes the phenomenon from so-called "post-tuning drift" effects, which relate to the relatively immature state of the diode material and fabrication techniques used in the production of microwave semiconductors. Understanding the intrinsic behavior of a varactor diode will enable the circuit designer to calculate a capacitance-temperature coefficient (CTC) for each device, use this parameter to design better-performing circuits and screen out devices prone to excessive drift problems.

Tuning varactors are normally reverse biased. In this mode of operation, capacitance per unit area is given by:*

$$C = \left[\frac{\epsilon q N}{2(\phi - V)}\right]^{\gamma} \qquad (1)$$

where ϵ is the semiconductor dielectric constant,
q is the "built in" or contact potential,
V is the applied bias, and
$1/N = 1/N_A^- + N_D^+$.

N_A^- and N_D^+ are the ionized impurity densities in the p- and n-type material, respectively. For typical diodes, N can be assumed constant over a common operating temperature range of 20 to 80°C. The exponent, γ, is related to the carrier density profile existing on each side of the PN junction, and is equal to 0.5 for an abrupt junction and 0.333 for a linearly graded junction. Abrupt junctions are generally associated with epitaxial growth, as in the case of GaAs, while linearly graded junctions are obtained with diffusion technologies. The case $\gamma = 0.5$ is usually preferred, as it gives a larger tuning range, although in practice, intermediate values can be observed.

Differentiating Eq. (1) with respect to temperature and normalizing for the case of $\gamma = 0.5$ results in a basic expression for CTC:

$$CTC = \frac{1}{C}\frac{dC}{dT} = \frac{1}{2}\left[\frac{1}{\epsilon}\frac{d\epsilon}{dT} - \frac{1}{(\phi - V)}\frac{d\phi}{dT}\right] \qquad (2)$$

Anthony A. Immorlica, Member of Technical Staff, Microwave Device Group, Rockwell International Science Center, 1049 Camino Dos Rios, Thousand Oaks, CA 91360.

The first term on the hight-hand side of Eq. (2) describes changes in the semiconductor's dielectric constant with temperature. This term has been measured for GaAs and Si, as shown in Table I. It is relatively invariant over wide temperature ranges and determines the ultimate lower bound of a diode's CTC. The second term, $(\phi - V)^{-1}$, is directly proportional to the temperature dependence of the contact potential and is a more complicated function of the semiconductor's properties. The contact potential, ϕ, for a nondegenerately doped semiconductor for which $N_A \approx N_A^-$ and $N_D \approx N_D^+$ is given by†

$$\phi = \frac{kT}{q} \ln \frac{N_A N_D}{n_i^2} \qquad (3)$$

where the intrinsic carrier concentration, n_i, is given by

$$n_i^2 = N_{co} N_{vo} \left(\frac{T}{300}\right)^3 e^{-E_g/kT}, \qquad (4)$$

and k is the Boltzman constant. In Eq. (4), N_{co} and N_{vo} are the conduction and valence band densities of states at 200°K and E_g is the energy gap. The bracketed term accounts for the temperature dependence of N_c and N_v.

Differentiating Eq. (3) with respect to temperature and combining with Eq. (2) yields the full expression for the capacitance-temperature coefficient

$$CTC = \frac{1}{2}\left\{\frac{1}{\epsilon}\frac{d\epsilon}{dT} - \frac{1}{\phi - V}\left[\frac{dE_g}{dT} + k \ln\left(\frac{N_A N_D}{N_{co} N_{vo}}\right) - 3k\left(1 + \ln\left(\frac{T}{300}\right)\right)\right]\right\} \qquad (5)$$

Equation (5) demonstrates that a diode's CTC is actually a function of three sets of variables:

- The intrinsic material properties of the semiconductor, including the dielectric constant (ϵ), energy gap (E_g) and density of states (N_{co}, N_{vo}).
- Extrinsic material properties, including the donor and acceptor impurity concentrations (N_D and N_A). These quantities determine the diode's breakdown voltage.
- The operating conditions, that is, the applied bias (V) and ambient temperature (T).

*It is assumed that charge density (Q) is either constant or varying with distance (x) from the PN junction, as $Q = ax + b$, where $a > 0$. A more general treatment is given in Reference 1, which assumes a Q of the form ax^m. This is pertinent to the case of the hyperbrupt junction which is not considered here.

The implications of Eq. (5) can be seen more easily by plotting CTC as a function of $(\phi - V)^{-1}$, with the breakdown voltage as a parameter and ϕ fixed at

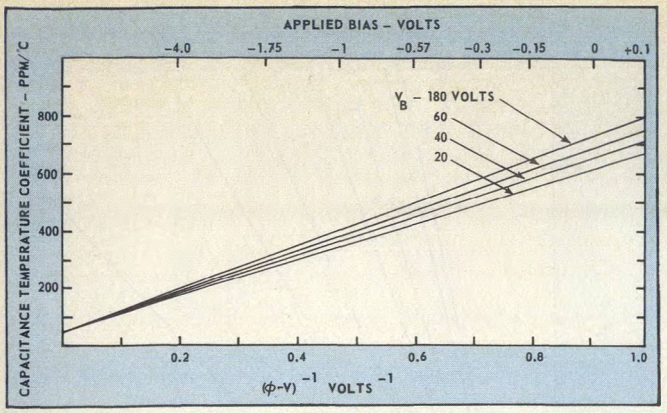

1. CTC falls rapidly as negative bias is increased in this plot of Eq. (5). Note the influence of breakdown voltage.

1.1 volts. From Fig. 1, it can be seen that the capacitance-temperature coefficient is greater for diodes with higher breakdown voltages. This fact should be borne in mind when specifying the breakdown voltage for a particular application. Although the effect is small, this is one instance where overdesigning one parameter (higher than necessary V_B) adversely affects another.

†In practice, GaAs varactors are often fabricated with p^+ n junctions, and thus, have one degenerately doped region (i.e., $N_A \neq N_A^-$). In such a case, ϕ can be approximated graphically by first solving the equation:

$$N_{VO}\, e^{\eta_F} = \frac{N_A}{1 + 2e^{\eta_F}}$$

where η_F is a Fermi factor. The solution of this equation gives N_A^- which is then used in place of N_A in Eq (3). Device manufacturers, however, do not normally supply data on N_A and N_D. In this event, it is reasonable to assume that $N_A^+ = 0.1\ N_{vo}$ and to estimate N_D from the measured breakdown voltage.[6] (Similar arguments apply to Si n^+p junctions). With the above approximations, the capacitance-temperature coefficient can usually be estimated in sufficient accuracy for engineering purposes.

Choose bias voltage carefully

By far the largest factor determining CTC is reverse bias voltage. As shown in Fig. 1, CTC drops very rapidly with a small reverse bias. In fact, as a general rule of thumb, CTC falls by a factor of two, as bias voltage falls from zero to a value equal to the contact potential. However, although the capacitance-temperature coefficient can be maintained at a low value by having $|V| \geq \phi$ this benefit is obtained by forfeiting a portion of the capacitance tuning ratio given by

$$\frac{C(V)}{C(V_B)} = \left[\frac{\phi - V_B}{\phi - V}\right]^{1/2} \qquad (6)$$

For example, a 40-volt breakdown GaAs diode, used over its full range of reverse bias voltages (i.e., 0-40 volts), has a capacitance tuning ratio of 6.1:1 and a maximum CTC of 650 ppm/°C. The same diode biased from $\phi < |V| < 40$ has a 30 per cent smaller tuning ratio but a maximum CTC of only 350 ppm/°C. These tradeoffs can be reduced or eliminated by tailoring the semiconductor doping profile such that the derivative of the capacitance versus voltage characteristic is maximized at bias voltages in excess of $|V| = \phi$ rather than at $V = 0$. This behavior is normally found for "step-abrupt" or "hyperabrupt" junction devices.

A brief example will help crystallize the designers' approach to varactor selection. Assume a varactor diode with a 4:1 capacitance ratio is required for tuning an X-band voltage-controlled oscillator which must be stable within 100 MHz over an ambient temperature range of 20 to 80°C. From Eq. (6), it is apparent that a diode with a 20-volt breakdown will satisfy the tuning ratio requirements. (For simplicity, the package parasitic capacitance is neglected in this example). Let's examine the VCO's frequency shift resulting from this diode's intrinsic CTC.

The frequency behavior of the VCO can be approximated by

$$f_o \propto \frac{1}{\sqrt{LC}}$$

where L is an inductance. Thus, it can be shown that the fractional frequency shift is related to CTC by

$$\frac{\Delta f}{f_o} = -\frac{1}{2}\,(CTC)\Delta T, \qquad (7)$$

where ΔT is the temperature change. The worst case shift will occur at the lower end of the band where the CTC is highest, by virtue of the fact that the varactor bias is low. From Fig. 1 for the 20-volt varactor at zero bias, CTC = 620 ppm/°C. Thus, $\Delta f = -1/2\ f_o\ (CTC)\ \Delta T = -153$ MHz for $f_o = 8.2$ GHz, the bottom of X-band. Clearly, the 20-volt breakdown varactor cannot meet both the capacitance ratio and Δf_{max} specifications.

Next, consider a 40-volt breakdown diode. To keep $|\Delta_F| < 100$ MHz requires CTC $\leq$ 400 ppm/°C, as is seen from Eq. (7). This requires that the diode be maintained at a minimum reverse bias, V_{min}, at the low end of the band. The tuning ratio is calculated from

$$\frac{C(_{min})}{C(V_B)} = \left(\frac{\phi - V_B}{\phi - V_{min}}\right)^{1/2} \qquad (8)$$

where $\phi \approx 1.1$ volts. From this equation, we see that a tuning ratio nearly indentical to that of the 20-volt diode can be obtained for the 40-volt device with $V_{min} = -\phi = -1.1$ volts. At this bias, CTC = 350 ppm/°C, $\Delta f = 86$ MHz and both the tuning and Δf_{max} specifications are met!

The salient points of this example can be summarized as follows. To minimize frequency shift due to ambient temperature changes, the minimum varactor voltage should be kept as far into reverse bias as possible, consistent with the tuning requirements. Tuning ratio may be maintained by using higher voltage breakdown diodes, although the package parasitic capacitance, typically 0.1 to 0.2 pF, places on upper bound on the tuning ratio. Another constraint on higher breakdown voltage diodes arises from the degradation of Q with increasing V_B. In summary, there is a tradeoff between CTC and tuning ratio in abrupt-junction devices when it is desired to minimize the effects of ambient temperature changes.

It is interesting at this point to compare the predicted performance of Si and GaAs. Although the parameters appearing in Eq. 5, vary substantially for the two semiconductors (see Table 1), the CTC vs. $(\phi - V)^{-1}$ characteristic do not differ significantly, as illustrated in Table 2. Thus, one is free to choose the semiconductor based on other considerations. At the higher frequencies (C-band and above), GaAs is usually preferred in tuning applications due to its inherently higher mobility, and, therefore, lower loss. On the other hand, Si devices are, at present, less expensive and benefit from a more mature technology.

Measure CTC with bridge and thermocouple

Capacitance versus temperature measurements have been made on a number of abrupt PN junction GaAs

(continued on p. 38)

varactors over a temperature range of 20 to 80°C for various values of reverse bias. The diodes were placed in a shielded brass fixture and heated at a rate varying from 1 to 3°C/min. The differential capacitance was measured at 1 MHz using a capacitance meter, whose output was displayed on an X-Y recorder. A change in diode capacitance to a resolution of 0.001 pF can be obtained by offsetting the diode's room temperature junction capacitance with an external capacitor on the differental input to the meter. A chromel-alumel thermocouple was used to monitor the temperature of the diode's metal-ceramic case.

Typical results are shown in Fig. 2, which is a plot of the change of the device capacitance as a function of temperature with the bias voltage as parameter. As predicted, there is a strong correlation between the rate of change of capacitance and the bias voltage.

The rate of change of the data presented in Fig. 2, normalized to the room temperature junction capacitance at the respective bias voltage, is plotted as a function of $(\phi - V)^{-1}$ in Fig. 3. The value of ϕ, 1.1 volts, was determined from measured capacitance-voltage data at room temperature. The intercept in Fig. 3, given by $1/2\epsilon\ d\epsilon/dT$, agrees remarkably well with that expected from published data on the rate of change of dielectric constant with temperature for GaAs[2]. Estimating the value of N_A and N_D from the measured breakdown voltage, the calculated slope, given by $1/2\ d\phi/dT$, is also in excellent agreement with that measured, as can be seen by comparison with Fig. 1.

Table 1: Some properties of GaAs and Si

	GaAs	Si	
$\frac{1}{\varepsilon}\frac{d\varepsilon}{dT}$	100[2]	78[3]	ppm/°C
$\frac{dE_g}{dT}$[4]	−500	−230	ppm/°C
N_{co}[5]	4.7×10^{17}	2.8×10^{19}	cm^{-3}
N_{vo}[5]	7.0×10^{18}	1.0×10^{19}	cm^{-3}

Table 2: A comparison of the intercept and slope of CTC vs. $(\phi - V)^{-1}$ for GaAs and Si PN junctions

V_B	GaAs (assumes $N_A^- = 0.1\ N_{vo}$)		Si (assumes $N_D^+ = 0.1\ N_{co}$)	
	INTERCEPT $\frac{1}{2\varepsilon}\frac{d\varepsilon}{dT}$ (ppm/°C)	SLOPE $\frac{1}{2}\frac{d\phi}{dT}\left(\frac{ppm-V}{°C}\right)$	INTERCEPT $\frac{1}{2\varepsilon}\frac{d\varepsilon}{dT}$ (ppm/°C)	SLOPE $\frac{1}{2}\frac{d\phi}{dT}\left(\frac{ppm-V}{°C}\right)$
20	50	625	39	610
40	50	664	39	654
80	50	703	39	699
160	50	741	39	744

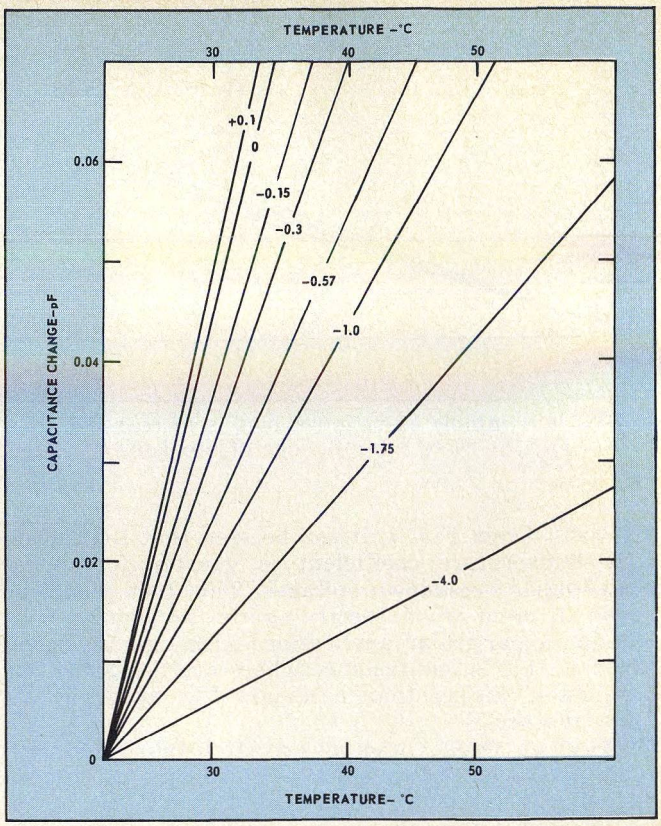

2. Measurements show linear change in capacitance over a range of 30 to 50°C. Data was taken for a 70 V breakdown GaAs PN junction varactor, over a +0.1 to −4 VDC bias range.

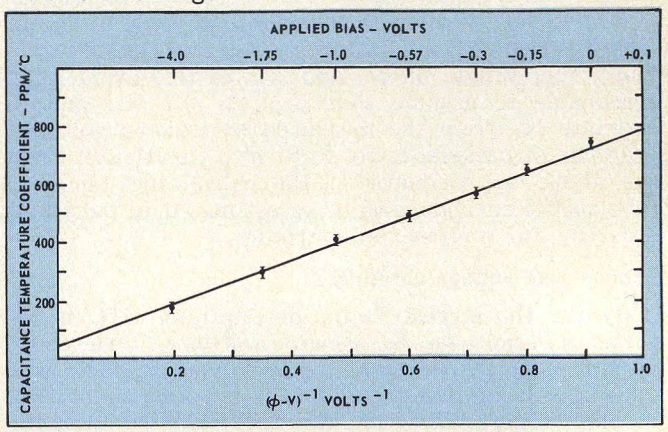

3. CTC is calculated from measured data shown in Fig. 2, normalized with respect to room temperature junction capacitance. Note agreement with curve in Fig. 1 for 70 V device.

Departure from ideal behavior is often indicative of problems in the material or device fabrication technologies. Deep "traps" lying in the forbidden band of the semiconductor, which can have time constants ranging from milliseconds to days, and mobile surface states due to contamination or poor junction passivation are chiefly responsible for non-conforming results. These problems, often common in an immature semiconductor technology, are manifested by capacitance characteristics which are not repeatable, being influenced by such factors as previous bias history and heating rate.

Use a curve tracer to screen diodes

It is not an easy task to determine with simple electrical measurements the exact nature of the problems leading to departures from near ideal behavior.

(continued on p. 40)

VARACTOR DRIFT

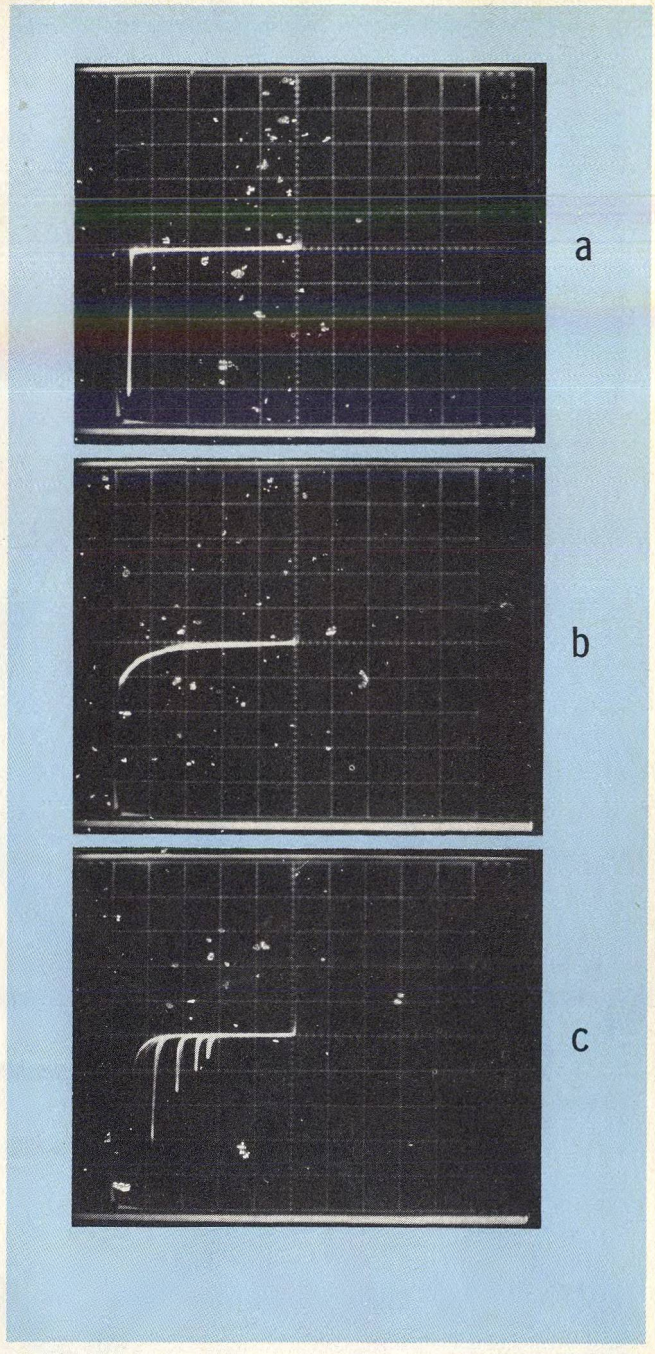

4. Simple curve tracer tests can be used to screen out diodes with potential drift problems.

High surface electric fields, mobile surface states and deep traps as well as multiple shallow donor and acceptor levels may all contribute to the problem. Nevertheless, whatever the cause, there are simple tests to single out diodes which can be expected to vary substantially from ideal behavior.

Surface passivation problems are normally reflected in the reverse leakage current properties of a diode. The theoretical bulk leakage for a typical GaAs varactor is well under 1 nA at room temperature and, thus, is not resolved on a curve tracer with a sensitivity of 10 μA/cm (Fig. 4(a)). Thus, if a current-voltage characteristic was examined on a curve tracer having a sensitivity of 10 μA/cm, any reverse current could be attributable to surface effects. Furthermore, on this scale, the leakage would be more than some three orders of magnitude higher than the theoretical bulk leakage, casting some suspicion on the

quality of the device! Leakage, *per se*, does not affect the performance of a varactor provided the resulting conductance is well below the device susceptance. However, a *change* of surface leakage with bias or temperature is deleterious. Such a change is indicative of mobile ionic contamination which can cause a distortion of the depletion region near the surface of a mesa diode, affecting the capacitance in an unpredictable manner. This is especially true for the smaller capacitance devices which have a large perimeter to area ratio.

Device users can screen diodes for potential problems by simple curve tracer tests. Diodes with gross leakage characteristics like those illustrated in Fig. 4(b) should be eliminated, even if the intended operating range lies below the point where leakage becomes prevalent. A more subtle indication of device problems is illustrated by V_B "walkout" shown in Fig. 4(c). Although a similar condition can be caused by bulk current filaments, it is more often associated with surface effects. In this phenomenon, the apparent breakdown voltage increases, often by many volts, as the bias drive to the diode is slowly increased. This condition is caused by a redistribution of the surface ionic contamination under the influence of the electric field. (In testing for this effect, care should be taken to keep the avalanche current at a low value to avoid thermal heating effects which result in an increased V_B). The above phenomena have been correlated in this study with anomalous capacitance-temperature characteristics, and should serve as a rejection criterion.

Properly fabricated mesa diodes are physically contoured to keep the surface electric field lower than the bulk value, partially alleviating surface leakage problems. In addition, some manufacturers pre-screen all diodes by conducting "burn-in" tests under reverse bias at elevated temperatures. In such cases the more drift/prone varactors are presumably eliminated and it is unlikely that surface problems will be detected in the remaining lot by simple curve tracer tests.

Capacitance drift problems can also be caused by bulk phenomena. For severe cases, the capacitance drift with time after the application of an abrupt change of the reverse bias voltage can easily be observed on an oscilloscope coupled to the output of a capacitance meter. This effect is enhanced if the device is initially forward biased. It is important to note that these tests do not guarantee immunity to long term "post-tuning drift" but will help in screening the more troublesome diodes. An understanding of the intrinsic behavior of the varactor diode is a suitable departure point for analyzing tuning drift phenomena. ••

References

1. M. H. Norwood and E. Shatz, "Voltage Variable Capacitor Tuning: A Review," *Proc. IEEE*, 56, pp. 788-798, (May, 1968).
2. T. Lu, G. H. Glover and K. S. Champlin, "Microwave Permittivity of the GaAs Lattice at Temperatures Between 100° and 600°K, *Appl. Phys. Lett.*, 13, p. 404 (December, 1968).
3. M. Cardona, W. Paul and H. Brooks, "Dielectric Constant of Ge and Si as a Function of Volume," *J. Phys. Chem. Solids*, 8, pp. 204-206, (August, 1959).
4. J. I. Pankove, *Optical Processes In Semiconductors*, Prentice-Hall, p. 412, (1971).
5. S. Sze, *Physics of Semiconductor Devices*, John Wiley & Sons, p. 57, (1969).
6. H. J. Kuno, J. R. Collard and A. R. Gobat, "Avalanche Breakdown Voltage of GaAs p^+-n-n^+ Diode Structures," *Appl. Phys. Lett.*, 14, pp. 343-345, (June, 1969).

Think Group Delay For . . .

A New Look At Source Stability

By thinking in terms of group delay, one can consider the contributions of all components to oscillator stability. This analysis shows why specifying Q alone is not sufficient.

PHASE slope is traditionally regarded as the key parameter that determines an oscillator's frequency stability.[1] What appears to go unnoticed, however, is that phase slope is nothing more than group delay in the loop. Thinking in terms of group delay can lead to a general explanation of how all component parts of an oscillator affect its frequency stability.

Phase slope, if constant, can be defined as the ratio of the change in loop phase to the resulting change in oscillator frequency ($\Delta\theta/\Delta f$), and is related to the loaded Q_L of a single cavity or LC resonator by:

$$\frac{\Delta\theta}{\Delta f} = \frac{2Q_L}{f_o} \qquad (1)$$

Rearranging, stability can be expressed in terms of Q_L as:[2]

$$\frac{\Delta f}{\Delta f_o} = \frac{\Delta\theta}{2Q_L} \qquad (2)$$

where,

Δf is the change in oscillator frequency
f_o is the frequency of oscillation
$\Delta\theta$ is the phase shift in radians responsible for the frequency change
Q_L is the loaded or in-circuit Q of the resonator

This expression has some limitations, however. For example, one might think that doubling the Q_L of the resonator would improve frequency stability by a factor of two. But, if the instability is caused by temperature sensitivity or aging of the resonator, doubling the Q_L will not improve stability, since $\Delta\theta$ also doubles, and nothing is gained. The only way to improve stability is to use a more stable resonator.

On the other hand, if the instability is caused by any circuit element other than the resonator, the expected improvement will occur.

Note that Eq. (2), which is written in terms of Q_L, does not make this distinction clear. Also, the expression is only indirectly applicable to oscillators that must be described in terms of their "equivalent Q," such as Wein bridge[3] and Surface Acoustic Wave (SAW)[4]. This "equivalent Q" is the Q that a single LC resonator would have if it had the same phase slope as the circuit in question. The translation of the phase slope to equivalent Q is quite useful for comparing different types of frequency determining elements, such as SAW delay lines and cavity resonators, but it is more desirable to work with group delay when analyzing the effects of all components on overall frequency stability. To illustrate this, we shall express Eq. (2) in terms of group delay by using the relationship,[4] $Q = \pi f_o \tau_R$, which holds for a single LC resonator or cavity near the resonant frequency:

$$\frac{\Delta f}{f_o} = \frac{\Delta\theta}{2\pi f_o \tau_R} \qquad (3)$$

where:

τ_R = delay time of resonator

Note that Eq. (3) only considers the contribution of the resonator to the oscillator's stability. Now, let us consider the effects on stability of all the major components in an oscillator, such as the resonator having delay τ_R, an amplifier having delay τ_A, and a matching network having delay τ_M. If, over a given temperature range, each component undergoes an independent phase shift, $\Delta\theta_R$, $\Delta\theta_A$ and $\Delta\theta_M$, how will the frequency stability of the oscillator be influenced? Since we are now working directly with group delay, this problem is easy to handle. The overall stability will be:

$$\frac{\Delta f}{f_o} = \frac{\Delta\theta_R + \theta_A + \Delta\theta_M}{2\pi f_o (\tau_R + \tau_A + \tau_M)} \qquad (4a)$$

or in terms of radians:

$$\frac{\Delta\omega}{\omega_o} = \frac{\Delta\theta_R + \Delta\theta_A + \Delta\theta_M}{\omega_o (\tau_R + \tau_A + \tau_M)} \qquad (4b)$$

What follows is a derivation of this result with supporting experimental data, and a practical example of how group delay can be used to calculate oscillator stability.

1. An oscillator may be represented by an amplifier in series with a phase modulator.

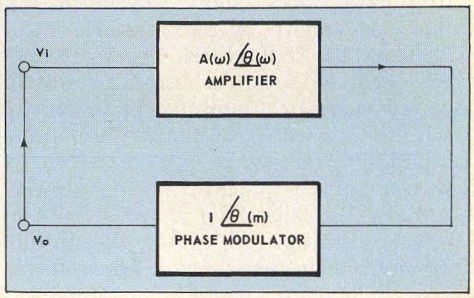

Loop delays are equal

Consider the oscillator in Fig. 1, represented by an amplifier and phase modulator having transfer functions as indicated. The phase modulator is assumed to have negligible group delay in comparison to the amplifier. It is evident that:

$$V_o = V_i \qquad (5)$$

The transfer function of the amplifier/phase modulator is:

$$V_i [(A(\omega) \angle\theta(\omega))(1 \angle\theta(m))] = V_o \qquad (6)$$

Ron Rippy, Electronic Engineer, National Aeronautics And Space Administration, R. F. Technology Branch Code 715, Goddard Space Flight Center, Greenbelt, MD 20771.

Substituting Eq. (5) into Eq. (6) yields:

$$V_i [(A(\omega)/\theta(\omega))(1/\theta(m))] = V_i \quad (7)$$

Dividing both sides by V_i gives:

$$[(A(\omega)/\theta(\omega))(1/\theta(m))] = 1 \quad (8)$$

Separating the magnitude and angular components of Eq. (8):

$$A(\omega) = 1 \quad (9)$$

$\theta(\omega) + \theta(m) = 2\pi n$, where n is an integer. (10)

Equations (9) and (10) state the conditions necessary for steady-state oscillations. Namely, that the closed loop gain be one (the open loop gain can be and usually is greater than one), and the phase shift around the loop be zero or a multiple of 2π radians. The loop bandwidth is assumed sufficiently narrow to allow oscillation at only one multiple of 2π.

By differentiating Eq. (10) with respect to ω, it is possible to show that the closed loop group delay is equal to the open loop group delay meaning that closed loop data can be obtained from open loop measurements. Differentiating (10) with respect to ω:

$$\frac{d\theta(\omega)}{d\omega} + \frac{d\theta(m)}{d\omega} = 0 \quad (11)$$

or

$$\frac{d\theta(m)}{d\omega} = -\frac{d\theta(\omega)}{d\omega} \quad (12)$$

but $-d\theta\omega/d\omega$ is the closed loop group delay of the amplifier which, since the modulator delay was stipulated as being negligible, is the total closed loop delay of the oscillator (τ_{CL}). Thus

$$\frac{d\theta(m)}{d\omega} = \tau_{CL}(\omega) \quad (13)$$

Since $-d\theta(\omega)/d\omega$ is also the open loop delay of the amplifier and modulator (τ_{OL}), it follows that $\tau_{OL} = \tau_{CL}$.

Figure 2 shows the results of open and closed loop measurements of the relationship between phase and frequency changes of a single stage amplifier having a 12.510900 MHz series resonant crystal in the emitter circuit. The input impedance is matched to achieve a maximum VSWR of 1.2:1 measured with a dual directional coupler inserted into the loop at the input of the amplifier. The open loop measurements were made at a power output of +9.3 dBm, the same level developed by the oscillator. Phase shift in the τ_{CL} measurement can be obtained by inserting small segments of RG58 coax cable into the loop, and measured on a vector voltmeter (VVM). As can be seen, the slopes of the two curves are almost identical, indicating that $\tau_{OL} \cong \tau_{CL}$.

If we now assume that τ_{CL} in Eq. (13) is constant in the frequency region of interest, (as demonstrated by the constant slope in Fig. 2), Eq. (13) can be rewritten as:

$$d\omega = \frac{d\theta(m)}{\tau_{CL}} \quad (14)$$

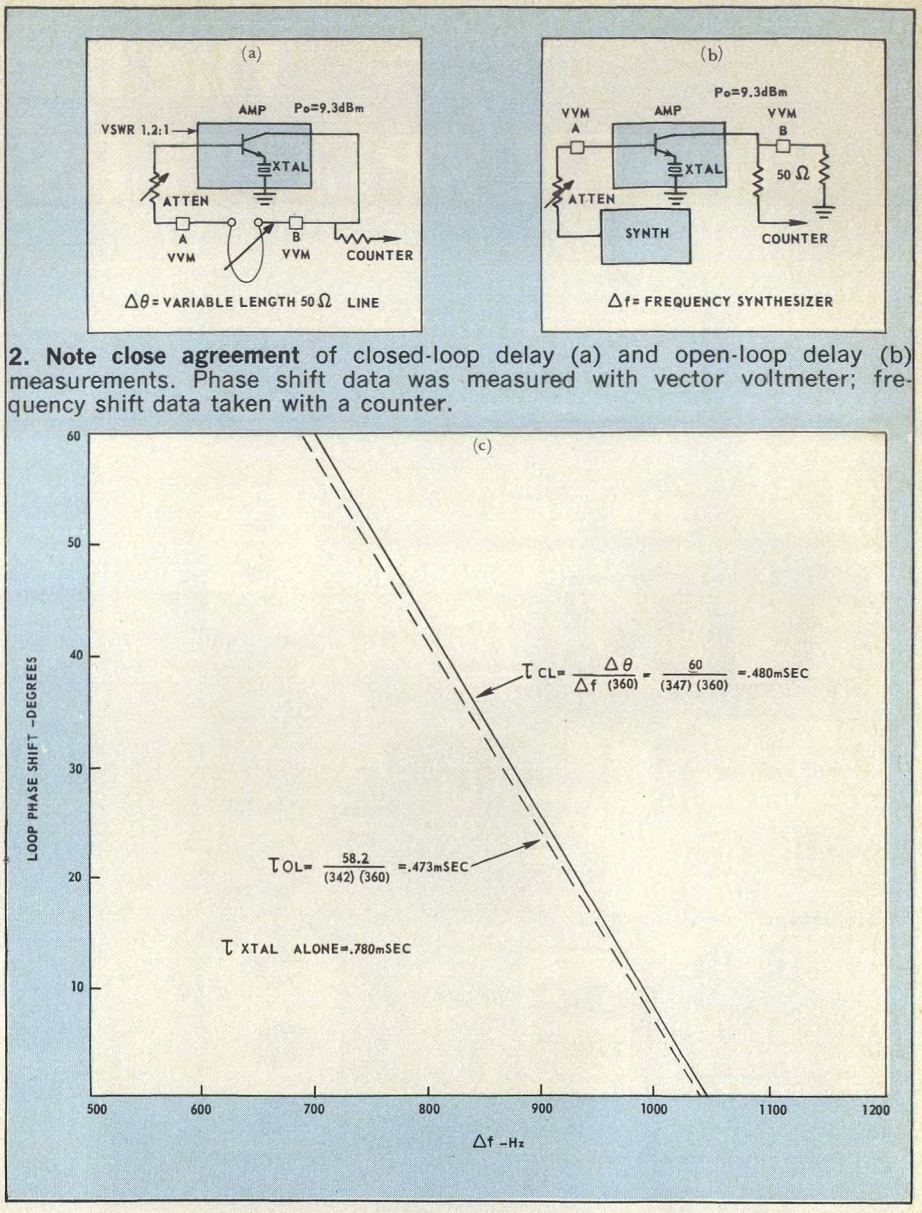

2. Note close agreement of closed-loop delay (a) and open-loop delay (b) measurements. Phase shift data was measured with vector voltmeter; frequency shift data taken with a counter.

The simple and evidently fundamental nature of (14) should be noted. It is nothing more than the equation, $\theta = \omega t$ expressed in differential form for the special case where t, which is group delay, is a constant. Integrating Eq. (14):

$$\omega = \frac{\theta(m) - \theta_o}{\tau_{CL}} + \omega_o \quad (15)$$

Where ω is the frequency of oscillation during a phase shift $\theta(m)$ in the modulator, θ_o is the phase shift in the modulator and ω_o is the frequency of oscillation before the phase shift occurs. If only the incremental change in frequency is of interest, Eq. (14) may be rewritten:

$$\Delta\omega = \frac{\Delta\theta(m)}{\tau_{CL}} \quad (16)$$

Since $\theta(m)$ may be a complex time varying function (15) applies under dynamic as well as static conditions. For example, assume $\theta(m) = \Delta\theta \sin \omega_m t$, where $\Delta\theta$ is the peak phase excursion of the modulator and ω_m is the modulating frequency. Substituting into Eq. (15) and assuming $\theta_o = 0$:

$$\omega = \frac{\Delta\theta}{\tau_{CL}} \sin \omega_m t + \omega_o$$

(continued on p. 46)

And since $\Delta\omega = \Delta\theta/\tau_{CL}$:

$$\omega = \Delta\omega \sin \omega_m t + \omega_o$$

which will be recognized as the equation for the instantaneous frequency of an FM wave with sinusoidal modulation.

This analysis indicates that if group delay in an oscillator is constant, the frequency of oscillation can be described by two simple expressions, Eqs. (14) and (15). The derivation applies to any oscillator that can be represented as a two-port amplifier with output-input feedback. Implicit in Eqs. (14) and (15) is the condition that only phase shift in the loop causes a frequency change. Amplitude disturbances will not affect frequency unless amplitude to phase conversion occurs in the loop.

Some limitations of these equations are: 1) They do not apply during oscillator turn on, i.e., before Eq. (9) is satisfied; 2) They do not apply if for any reason τ becomes a function of ω (in this case, Eq. (13) must be used); and 3) They do not describe frequency disturbances caused by phase disturbances, $\theta(m)$, which occur in a time interval less than τ, or so quickly as to fall outside the loop bandwidth.[5]

Q isn't the whole story

Note that Q, which is often considered essential in specifying stability is conspicuously absent from Eqs. (14) and (15). The results indicate only two parameters determine stability inside the loop bandwidth, the amount of phase jitter, $\theta(m)$, and group delay, τ, in the loop. If stability is to be improved, $\theta(m)$ must be reduced or τ must be increased, *but care must be taken not to optimize one parameter while degrading the other.*

For example, if the stability of an oscillator depends entirely on a single resonant circuit, the relation, $\tau = 2Q/\omega_0$, may be substituted into Eq. (16) to obtain an expression containing Q:

$$\Delta\omega = \frac{\omega_o \Delta\theta(m)}{2Q} \qquad (17)$$

It should be noted, however, that Eq. (17) is less general than Eq. (16) since it applies only to oscillators that contain a single resonant circuit as the frequency determining element. Thus, it can be seen that high Q alone does not insure stability. Stability will be poor regardless of how high Q is, if the circuit elements are unstable and produce a correspondingly high $\Delta\theta(m)$.

A good example of this is an oscillator which uses an active circuit to reduce losses or increase the Q of the resonant circuit. Any increase in Q causes at least an equal increase in phase jitter ($\Delta\theta_m$) and, therefore, no improvement in stability.

Interestingly, the group delay concept explains how self-sustaining oscillators can have infinite Q and yet have imperfect stability. As has been shown, frequency stability is determined by group delay which does not become infinite when the loop is closed. The fact that Q is infinite seems to mean only that the waveform is undamped.

Is loop filtering effective?

The group delay concept contradicts the idea that narrow band filtering in the loop is responsible for oscillator stability. Measurements suggest that phase noise outside the loop bandwidth can cause at least as much frequency jitter as phase noise inside the loop bandwidth. This is illustrated by Fig. 3, which was obtained by modulating a varactor placed across the collector circuit of the one-stage amplifier shown in Fig. 2. This induces a small phase disturbance in the loop at a rate which varies from low frequencies inside the loop (i.e., crystal) bandwidth to higher frequencies well outside the loop bandwidth. The resultant oscillator frequency jitter, Δf, was measured on a discriminator. As can be seen, higher frequencies (above 340 Hz) outside the loop bandwidth produce a jitter that increases at 6 dB per octave. This is a characteristic of frequency jitter caused by phase modulation and indicates no filtering by the oscillator.

If the varactor is placed in series with the crystal, or if the oscillator output is taken across a small resistor in series with the crystal, some filtering of the higher frequency PM jitter does occur.[7] However, the conclusion reached from these measurements is that narrowband filtering by the loop is not responsible for stability. The real value of narrow loop bandwidth appears to be the side benefit of large group delay. If phase noise outside the loop bandwidth must be suppressed, the oscillator output should be passed through a very narrow crystal filter.

3. Group delay can be calculated by finding the point at which FM and PM asymptotes intersect.

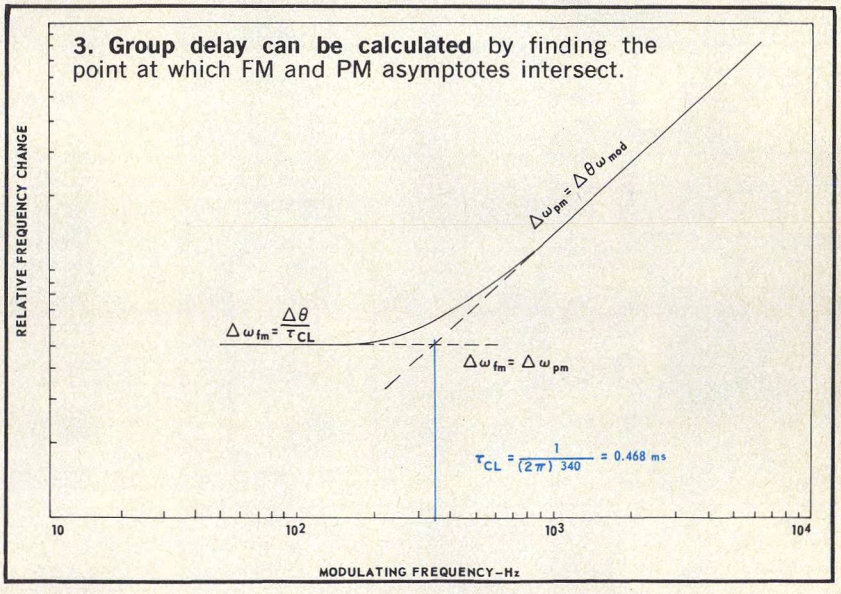

The intersection of the asymptotes in Fig. 3 occurs where Δf due to pure PM equals Δf due to pure FM and provides an easy means of measuring the value of τ_{CL} or the actual Q of the oscillator. The equations for the FM and PM asymptotes, respectively, are:

$$\Delta\omega_{FM} = \frac{\Delta\theta}{\tau_{CL}} \text{ and } \Delta\omega_{PM} = \Delta\theta\omega_{mod}$$

Setting these two expressions equal to each other, yields

$$\tau_{CL} = \frac{1}{\omega_{mod}}$$

The modulating frequency at the intersection is 340 Hz which gives a value of $\tau_{CL} = 1/2\pi(340) = 0.468$ ms, corresponding to a $Q = \omega_o\ \tau_{CL}/2$ of 18.4×10^3. This is in reasonable agreement with the value of

(continued on p. 48)

0.480 ms ($Q = 18.9 \times 10^3$) obtained from Fig. 2. Although the data for Fig. 3 was obtained using simulated noise (external noise was added to the loop) similar results have been obtained by others[7,8] in measuring intrinsic oscillator noise.

Designing with group delay

As an example, let's use the group delay concept to calculate the expected temperature stability of a 2.3 GHz oscillator whose stability is primarily derived from a silver-plated brass cavity having an unloaded Q of 1300 and a loaded or in-circuit Q of 540 (see Fig. 4).

The parameters listed for each component were measured on a network analyzer. Values of $\Delta\theta$ were obtained by measuring (at the frequency of oscillation) the phase change in each component caused by a temperature change, ΔT, from 25 to 60°C. In addition to the measured value of $\Delta\theta$ for the cavity resonator, a calculated value was also obtained based on the assumtion that $\Delta\theta/\omega_0\tau\,\Delta T$ = coefficient of linear expansion for brass (1.9×10^{-5}cm/cm°C). The agreement between the measured and calculated values is within 4.6 per cent.

To calculate the expected temperature stability of the oscillator, we can use an expanded version of Eq. (16). Note that the group delay concept allows us to consider the individual contributions of all oscillator components, not just the influence of the resonator

$$\frac{\Delta\omega}{\omega_0\,^\circ C} = \frac{\Delta\theta_A+\Delta\theta_P+\Delta\theta_R+\Delta\theta_C+\Delta\theta_S}{\omega_0(\tau_A+\tau_P+\tau_R+\tau_C+\tau_S)} \qquad (19)$$

where

$\Delta\theta$ = the phase shift in radians °C of each component
τ = the group delay of each component
ω_0 = oscillator frequency
$\Delta\omega$ = frequency change

Substituting the data from Fig. 4 into Eq. (19)

$$\frac{\Delta\omega}{\omega_0\,^\circ C} = \frac{(-1.71-1.11-21.5+.20+.98)\times10^{-3}}{14.57\times10^9[(1.6+2.23+74+.46+.38)\times10^{-9}]} \qquad (20)$$

$$= -2.02\times10^{-5}/^\circ C \text{ or } -0.202 \text{ ppm}/^\circ C$$

Experiments demonstrate good agreement between calculated and measured stability for a 50°C change in temperature, as shown in Fig. 5. One source of error in the calculated stability is the assumption that $\Delta\theta/^\circ C$ is constant over the entire temperature range. Another source of error is the variation of the insertion loss (or gain in the case of the amplifier) of each component due to a change in temperature. This affects frequency due to amplitude to phase conversion in the loop. This effect can be minimized by placing a variable attenuator in the loop and adjusting it so that the frequency change per dB change in attenuation is minimum. But this approach is useful only if the loop has enough excess gain to permit it. Designing the loop amplifier to be an ideal symmetrical limiter would probably accomplish the same result. The effect of either approach on oscillator stability is easily predicted by expanding Eq. (19) to include additional group delays (τ) and phase changes ($\Delta\theta$).

It is perhaps worth noting that in order to make a stable oscillator, one must first start with a stable amplifier. Any spurious positive feedback in the amplifier increases τ_A and causes the amplifier to have an overly large influence on stability.

Equation (19) shows that adding a perfect delay line ($\Delta\theta = 0$) to the oscillator loop will improve stability by making the denominator larger without increasing the size of the numerator. It is probably feasible to double the loop delay, and hence, the effective oscillator Q by this approach. But if too much delay is added without adding additional selectivity, the circuit will oscillate at two or more frequencies separated by $(\tau_{CL})^{-1}$.

The example illustrates the utility of using group delay to analyze stability directly. But the group delay analysis also provides an interesting perspective on the traditional Q specification. For example, note that an oscillator will have essentially the same temperature stability as the resonator itself if the other loop components: 1) Have the same phase stability $\Delta\theta/\omega_0\,\tau\,^\circ C$ as the resonator; or 2) Have a very low τ compared to the resonator. In terms of Q, the latter condition implies that the Q of the resonator should be as high as possible and the "effective Q" of the other components should be as low as possible. In a good oscillator, the Q or τ of all circuitry other than the resonator should not be more than 1 or 2 per cent of the resonator's Q or τ. Thus, although it might at first seem like "overkill" to use an amplifier having 500 MHz bandwidth in an oscillator having only 5 MHz bandwidth, it may, in fact, be necessary to avoid degrading the stability of the resonator. ••

Acknowledgement The author is grateful to Dennis Zimmerman, Dave Hepler and Ken Liedy.

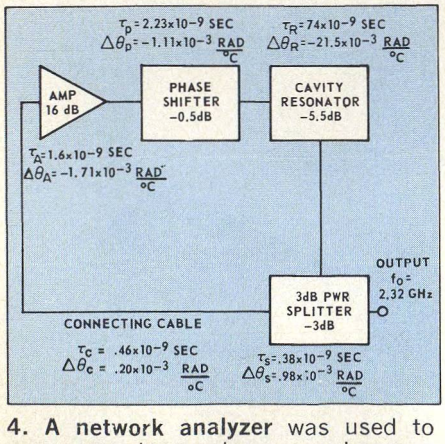

4. A network analyzer was used to measure phase change and group delay for each component in this oscillator circuit.

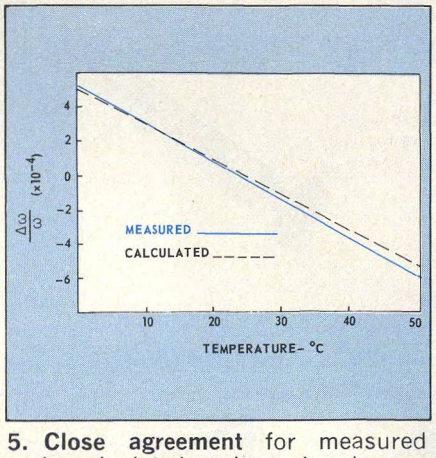

5. Close agreement for measured and calculated values is demonstrated over a 50°C temperature range.

References

1. Jacob Millman, "Vacuum-Tube and Semiconductor Electronics," McGraw-Hill Book Company, New York, p. 488 (1958).

2. D. J. Healy III, "Flicker of Frequency and Phase and White Frequency and Phase Fluctuations in Frequency Sources," *Proc. of the 26th Annual Symposium on Frequency Control*, p. 30, (1972).

3. *Electronic Measurements and Instrumentation*, edited by Bernard M. Oliver and John M. Cage, McGraw-Hill, New York, p. 331 (1971).

4. H. G. Vollers and L. T. Claiborne, "RF Oscillator Control Utilizing Surface Wave Delay Lines," *Proc. of the 28th Annual Symposium on Frequency Control*, p. 256, (1974).

5. R. R. Rippy, "Group Delay Versus Oscillator Stability," unpublished paper.

6. Ulrich L. Rohde, "Crystal Oscillator Provides Low Noise," *Electronic Design*, pp. 98-99, (Oct. 11, 1975).

7. D. B. Leeson, "A Simple Model of Feedback Oscillator Noise Spectrum," *Proc. IEEE*, Vol. 54, No. 2, pp. 329-330, (February, 1966).

8. Elie J. Baghdady and Southard Lippincott, "Characterization of Causes of Signal Phase and Frequency Instability," prepared under NASA Contract No. NAS 2-5337, Report No. NASA CR 73, 442, p. 45, (Jan. 8, 1970).

For Broadband, Tunable Sources . . .

Combine Varactor Control With Dielectric Tuning

This diode oscillator design combines mechanical and electrical tuning in an inexpensive package. Advantages include broad frequency coverage with little power variation.

MANY modern solid-state microwave power sources built around Gunn and Impatt diodes are unnecessarily expensive to manufacture. Conventional designs often change frequency with variations in load impedance, and may not provide broadband frequency tuning with constant output power.

These problems can be economically overcome by employing a blend of varactor diode and dielectric tuning, and by only loosely coupling the cavity to both the diode and the output coupling aperture. This design approach is suitable for either Gunn or Impatt diodes, since a broad range of reactive impedance values can be easily obtained by varying the length of the oscillator's open coaxial transmission line, or by changing the capacitive fringing impedance at the open end of the oscillator cavity.

The oscillator shown in Fig. 1 is constructed by coupling a Gunn or Impatt diode to an open-ended coaxial transmission line through an impedance network that contains diode-to-cavity and cavity-to-load coupling. Note that the net impedance of the diode plus the cavity must be equal to zero for oscillations to occur. The diode's packaging impedance cannot be neglected at X-band frequencies, but it can be exploited in the design of an oscillator. The packaging impedance forms a current divider network around the diode by means of series and shunt impedances, as shown in Fig. 2. The diode packaging impedance can be effectively utilized to couple the diode chip to an open coaxial transmission line oscillator cavity.

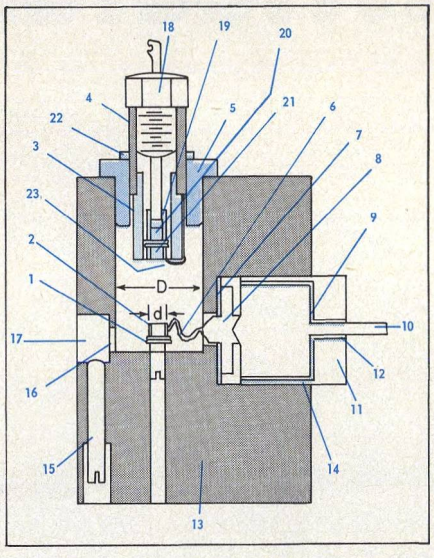

1. Gunn or Impatt diode
2. Diode hat, or open ended coaxial transmission line
3. Rexolite rod
4. Threaded Rexolite tuning screw
5. Open cavity plug
6. Bias wire and rf choke
7. Bypass capacitance dielectric washer
8. Bias disc
9. Bypass capacitance dielectric washer
10. Bias connector
11. Bias plug
12. Insulating sleeve
13. Cavity block
14. Bypass capacitance dielectric sleeve
15. Aperture tuning screw
16. Coupling iris
17. Coupling impedance transformer
18. Modulator feedthru bypass capacitance
19. Varactor diode hat
20. Varactor diode
21. Varactor diode hat
22. Locking nut
23. Ground wire

1. The varactor diode is located at the end of a dielectric tuning rod in this X-band oscillator design.

The frequency of the oscillator is determined by the impedances of the Gunn or Impatt diode and the conjugate impedance match provided by the cavity. The cavity's impedance and resonant frequency are determined by the ratio of its diameter to the diameter of the center conductor (D/d), the length of the diode hat or open coaxial transmission line, and its fringing capacitance.

An equivalent circuit for the oscillator is shown in Fig. 3. For a typical 50 mW, X-band silicon avalanche diode, the parameters shown in the equivalent circuit are: $C_{pk} = 0.3$ pF, $C_c = 0$, $C_j = 0.3$ pF, $L_{pk} = 0.4$ nH, $R_s = 1.5\ \Omega$, $R_d = -1000\ \Omega$. Using these numbers, the overall diode impedance turns out to be $Z_d = -6.431 + j28.4$. The input impedance of a lossless, open-ended coaxial transmission line is:

$$Z_c = jZ_0 \cot \beta L \qquad (1)$$

where Z_0 is the characteristic impedance of the transmission line, $\beta = 2\pi/\lambda$ is the phase constant and L is the length of the line. The equivalent circuit representation of the radiating iris is shown in Fig. 3 as an inductive pi network. The shunt elements, X_a, approximate an infinite impedance, while the series element, X_b, has a small value.

Power transfer is optimized when the combined cavity and load losses are matched to the generator's impedance. The output coupling can be adjusted with the reduced height waveguide impedance transformer's tuning screw, as shown in Fig. 1. Here, power is maximized while the oscillator's frequency is held relatively constant.

Oscillation requires the sum of the coaxial transmission line impedance, the output coupling impedance and the packaged diode impedance equal zero:

$$Z_{diode} + Z_{coax} + Z_{out} = 0 \qquad (2)$$

Equating the reactive part of Eqn. (2) to zero establishes the frequency of operation. Setting the real part equal to zero yields information on the oscillator's output power capability. Since one is presently unable to obtain definite data on chip negative resistance, an analysis of the real portion of the impedance will be omitted. We will assume that the negative resistance of the diode is sufficient to com-

Carl F. Klein, Senior Research Engineer and **Lawrence B. Korta,** Engineering Administration Manager, Johnson Controls, Inc., 507 East Michigan Street, P.O. Box 423, Milwaukee, WI 53202.

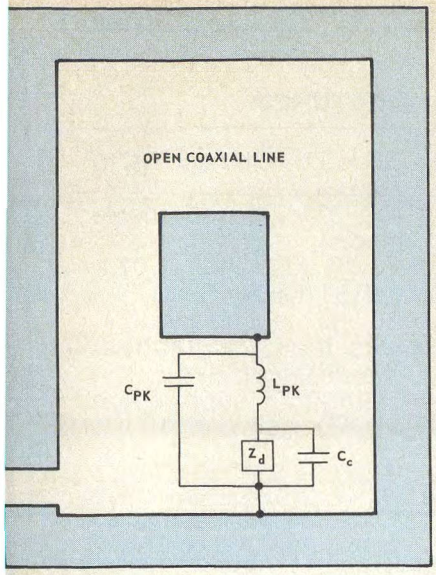

2. Series and shunt packaging impedances form a current divider network around the diode chip, coupling it to the open coaxial line.

pensate for resistive losses in the cavity.

Neglecting the real impedance components in Eqn. (2), we obtain:

$$X_{diode} + X_{coax} + X_{out} = 0 \quad (3)$$

The reactive coupling impedance introduced by the coupling iris in series with the open-ended transmission line impedance is quite small and can be neglected. The shunt impedance introduced by the iris is extremely large, and can also be neglected.

The length of the open-coaxial transmission line can be determined by equating it to the conjugate impedance at the diode terminals. Thus, one can easily match an oscillator diode's impedance to that of the oscillator cavity.

Course and fine tuning provided

Solid-state, fundamental frequency cavity oscillators are frequency tunable by mechanically changing some physical dimension, typically length, of the cavity. This often results in unnecessary mechanical complexity and can lead to undesirable power losses. The cavity used in this design, however, permits simple, low-loss mechanical frequency tuning without mechanical hang-ups.

Basically, this technique works by influencing the fringing capacitance at the open end of the cavity by a change in dielectric constant through the insertion of a dielectric center conductor. The dielectric used to perform this function should have a low dissipation factor and a reasonably high dielectric constant relative to that of air. Rexolite, with a typical dissipation factor and dielectric constant of 5 $\times$ 10^{-4} and 2.5, respectively, is a good choice. Other materials which might be considered are Teflon, which has a lower dissipation factor but also lower dielectric constant, or any one of several specialized materials such as Stycast and Eccostock, which have attractive electrical characteristics, but higher cost. By inserting a Rexolite rod into the open end of the oscillator's cavity, one obtains the frequency tuning capability shown in Fig. 4.

Additional tuning or frequency modulation capabilities can be introduced by further loading the cavity with a varactor diode. The varactor diode's DC bias and AC modulation are applied through a feed-through capacitor. A detailed view of the diode's tuning and modulation assembly is shown in Fig. 5. The novelty of this tuning scheme lies in the placement of the varactor diode directly within the dielectric tuning element. Course frequency adjustments can be achieved by varying the length of dielectric center conductor projecting into the cavity. Fine tuning, on the other hand, is accomplished by controlling the varactor diode's bias, thus presenting a variable capacitive load to the cavity.

(continued on p. 52)

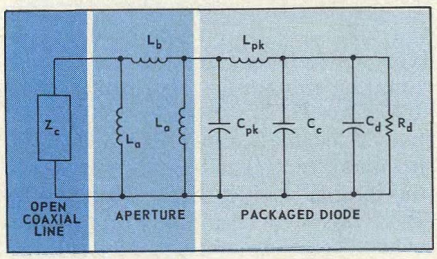

3. The oscillator's equivalent circuit includes chip package and coupling iris impedances.

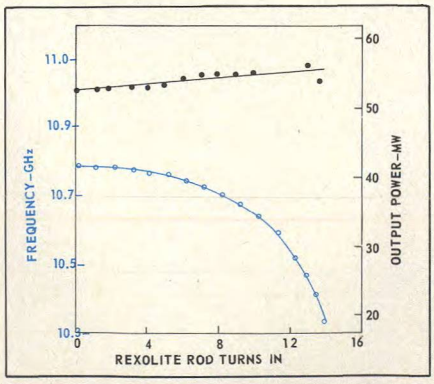

4. A mechanical tuning range of about 500 MHz corresponds to a power variation of about 3 dB. This source uses a Hughes' 93D-12 Impatt diode.

5. The tuning assembly includes a Rexolite rod and varactor diode. See Fig. 1 for key.

A plot of the oscillator's frequency and power as a function of varactor diode bias is shown in Fig. 6(a). The amount of capacitive loading is determined by the voltage or modulation across the diode and its insertion depth into the coaxial cavity. Changing the voltage applied to the varactor diode changes its capacitance, as shown in the plot of diode capacitance as a function of applied voltage in Fig. 6(b).

Loop coupling is symmetric

The varactor diode's novel placement has several other advantages. By locating the varactor within the dielectric center conductor, the diode's electronically controlled variable impedance is easily coupled into the oscillator cavity. As the dielectric center conductor is threaded to permit center conductor length adjustment, this same adjustment mechanism is available to easily control varactor coupling. Note that the varactor loop is magnetically coupled to the coaxial cavity. As the cavity fields are axially symmetric, rotation of the center conductor and hence the varactor loop, does not significantly affect coupling between varactor and cavity. Note that for loop coupling, the loop must enclose lines of magnetic flux which, in this case, are circles concentric about the center conductor. Flux linkage using the center conductor varactor mount is seen to be independent of rotational position. Contrast this situation with the more commonly used side wall loop coupling, where the coupling goes to zero every 90° of loop rotation when the plane of the coupling loop lies in the plane of the magnetic flux lines.

Another useful feature of this coaxial varactor tuning element approach is its flexibility. A mechanically-tunable oscillator can be readily converted to one with electronic tuning and modulation capability with the simple replacement of a center conductor assembly.

As in any circuit design, certain tradeoffs must be considered in the use of the varactor/dielectric center conductor cavity approach. Higher costs must be compared to benefits in increased microwave diode yield. The placement of the varactor loop in the dielectric center conductor is more complicated, and presumably more costly, than a simple side wall mounting. This complication must be evaluated relative to the improved tuning characteristics. Not all things to all people, the varactor/dielectric center conductor concept does offer an attractive option in microwave oscillator design. ••

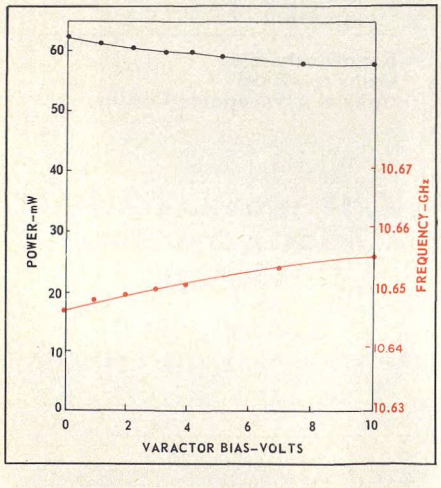

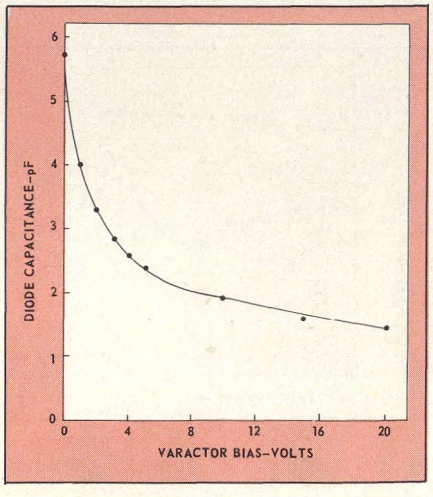

6. An electrical tuning range of about 10 MHz is achieved by varying varactor bias from 0 to 10 V (a). Diode capacitance change is shown in (b).

MOBILE

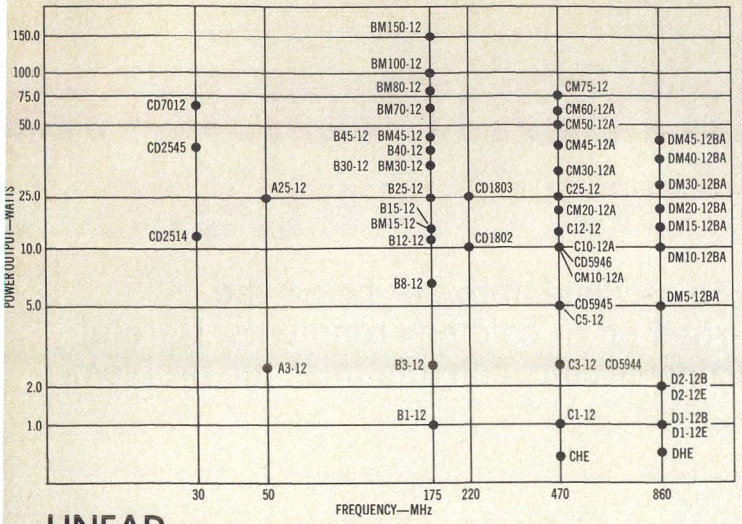

MICROWAVE

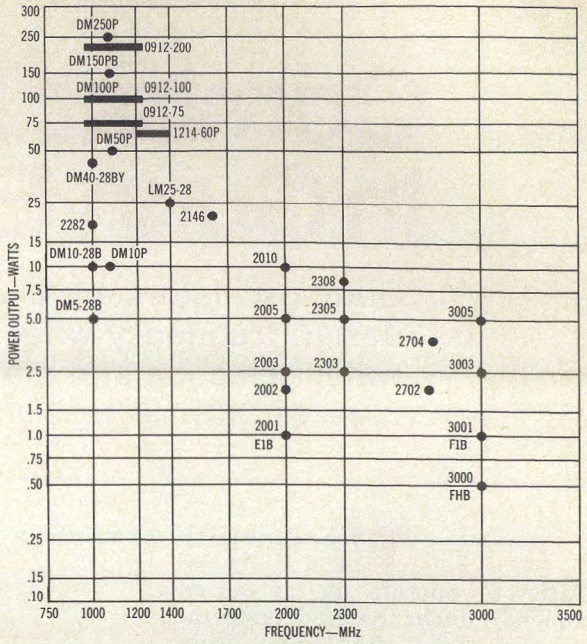

LINEAR

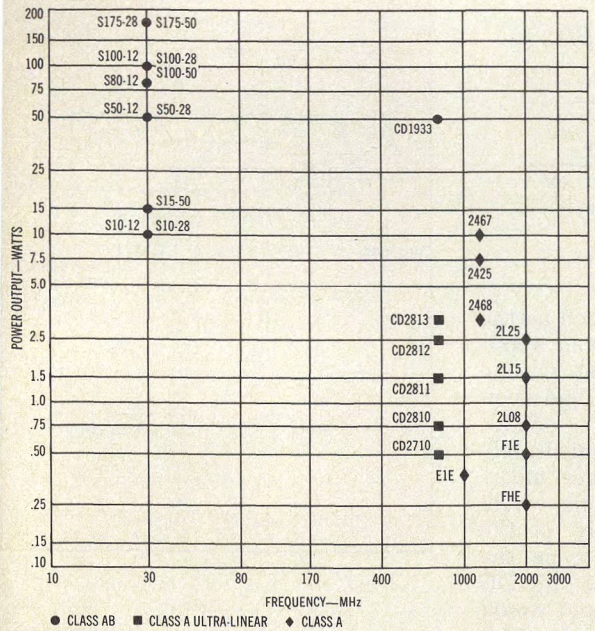

MILITARY

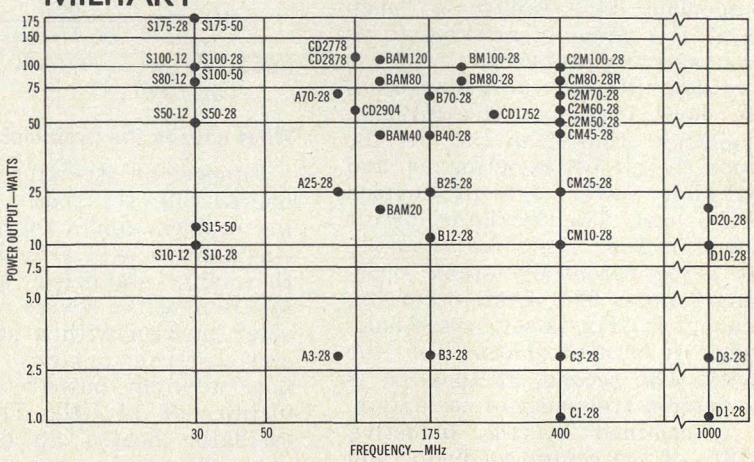

Combat Turn-On Problems In Gunn-Effect Sourcers

Gunn oscillators are likely to oscillate above or below the design frequency when turned on in cold environments. Careful wafer selection and stabilizing circuits can minimize the problem.

THE inability of a Gunn oscillator to operate at its design frequency under reduced temperature conditions often spells doom for an otherwise well-designed component. This failure to "snap start" is commonly referred to as a cold starting problem.

In actuality, the unit does oscillate; however, it is oscillating at a frequency other than the one for which the circuit is optimized, and negligible power is being coupled to the load. The oscillator circuit shown in Fig. 1(a), for example, has three potentially stable operating points. The first, occurring at about 8 GHz, is set by the half-wave, re-entrant nature of the cavity. The second, at 10 GHz, is the desired frequency of oscillation, as determined by the inductive nature of the center conductor and the gap capacitance (C_g) formed by the end of the center conductor and the top of the Gunn diode package. A third point occurs at about 14 GHz, due to the full-wave nature of the oscillator cavity. The full-wave condition occurs at a frequency somewhat lower than twice the half-wave frequency due to the increased role played by fringing capacitances at higher frequencies.*

A more exact picture of the desired frequency of oscillation can be developed by considering the lumped equivalent circuit shown in Fig. 1(b):

$$\omega = (L(\omega) \cdot C(\omega))^{-1/2} \qquad (1)$$

where:

$$L(\omega) \triangleq \frac{Z_o}{\omega} \cdot \tan(\beta\ell)$$

$$C(\omega) \triangleq \frac{C_p C_g}{C_p + C_g K(\omega)}$$

$$K(\omega) \triangleq \frac{\omega'^2_d - \omega^2}{\omega'^2_d + \omega_p^2 - \omega^2}$$

and: $\omega'^2_d \triangleq (L_d (C_d + C_m))^{-1}$

$\omega_p^2 \triangleq (L_d C_p)^{-1}$

What causes the problem?

Suppose an oscillator such as the one in Fig. 1(a) had a cold starting problem, and a DC bias voltage was applied to it after it had been thermally stabilized at −55°C. Monitoring the source immediately after turn-on with a power meter and spectrum analyzer, one would note a slight output only in the vicinity of 14 GHz. Then, as the oscillator heated up due to DC power dissipation, the output would suddenly increase to normal as the frequency jumped to 10 GHz.

In order for the cold starting problem to exist, four criteria have to be satisfied. They are:

1. A potentially stable operating point must exist at a higher frequency.
2. The Gunn diode must have a negative resistance bandwidth wide enough to sustain oscillations at the higher frequency.
3. An increase in the transit frequency of the Gunn diode must occur at the colder temperature.
4. The Gunn diode bias must traverse a value upon turn-on such that the higher frequency operating point and transit frequency coincide.

The first criterion is automatically satisfied by the full-wave characteristic of the cavity at this higher frequency. The second is satisfied by the Gunn diode, which by nature is a broadband negative resistance device. The third and fourth criteria are satisfied by the diode physics and the fact that the application of DC bias automatically insures that the Gunn bias will cross a point for transit frequency/circuit frequency coincidence.

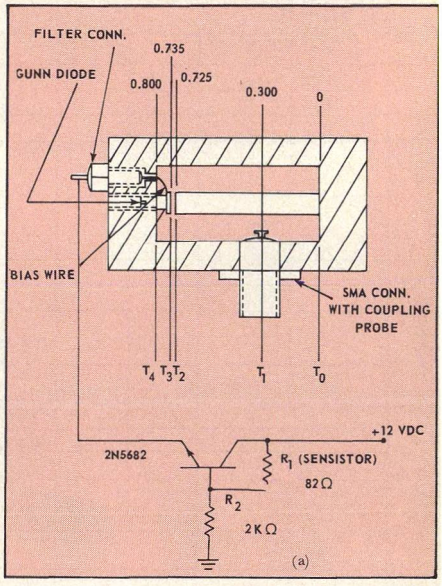

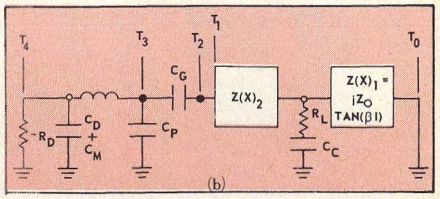

1. A simplified Gunn oscillator (a), designed to operate at 10 GHz, will also oscillate at 8 and 14 GHz due to half and full-wave characteristics. Lumped element equivalent circuit is shown in (b).

(continued on p. 58)

*The dominant TEM mode becomes a radial mode in the volume surrounding the packaged Gunn diode.

Bernie Sigmon, Microwave Engineering Manager, Theta-Com, 2216 W. Peoria Avenue, P. O. Box 9728, Phoenix, AZ 85068.

COMBAT TURN-ON PROBLEMS

Figure 2 clarifies the last two prerequisites by showing the Gunn diode transit frequency dependence on temperature and voltage. As temperature decreases, the mobility of charge carriers increases, causing an increase in the diode's transit frequency (for a fixed bias voltage). Since the diode bias has to traverse this voltage point in going from 0 to steady state (higher transit frequencies are associated with lower diode bias voltages), a stable operating point at a near full-wave frequency can be obtained.

Choose diodes carefully

If the Gunn diode was a relatively narrow-band device, such as an Impatt diode, one could simply select diodes whose transit frequency and range of oscillation were at the desired operating frequency. Since this is not the case, diode wafer selection is in order. This, along with stabilizing and bias circuits, will give the designer an edge in conquering the cold starting problem.

Perhaps the best method for wafer selection is to try sample diodes from various wafers in the oscillator while monitoring the output spectrum on a broadband spectrum analyzer. With each sample diode, the Gunn bias should be manually brought from zero volts to the optimum voltage level for the diode/circuit performance. Careful visual monitoring of the output spectrum from 3 GHz to 18 GHz will reveal any oscillations. An optimum device for the circuit will begin oscillating at the desired frequency once threshold voltage is reached, and will maintain this frequency even past the point of power degradation due to too high a Gunn bias. Once a diode sample is found that performs satisfactorily, that diode and wafer should be characterized for its construction, threshold voltage and doping characteristics.

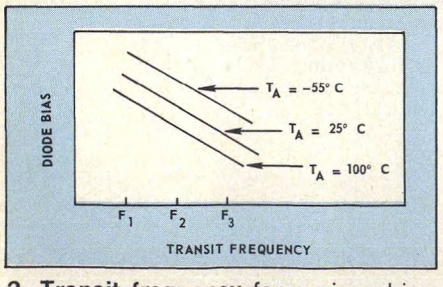

2. Transit frequency for a given bias voltage rises as temperature falls.

For the oscillator depicted in Fig. 1, a diode was selected which had an optimum transit frequency between 10 and 14 GHz, such that the 8 GHz resonance could not be satisfied. This particular source, developed for an ECM program, operates over a range of −55 to +110°C without the aid of heater power.

Damp out undesired modes

If the circuit still exhibits cold starting problems once the best choice of Gunn diodes has been made, circuit stabilization may be in order. Resistances and conductances, properly located within the cavity, can be used to damp out undesired frequencies, without disturbing the specified point of operation. For example, the oscillator shown in Fig. 1 was designed with a shunt conductance placed at the 10 GHz E-field minimum point, which also was the plane of the 14 GHz E-field maximum point. Thus, the undesired higher frequency operating point was overcoupled, or damped out, without affecting the desired frequency of operation. Since the selected Gunn diode could not sustain oscillation at 8 GHz, 10 GHz became the only stable point at which the source could operate.

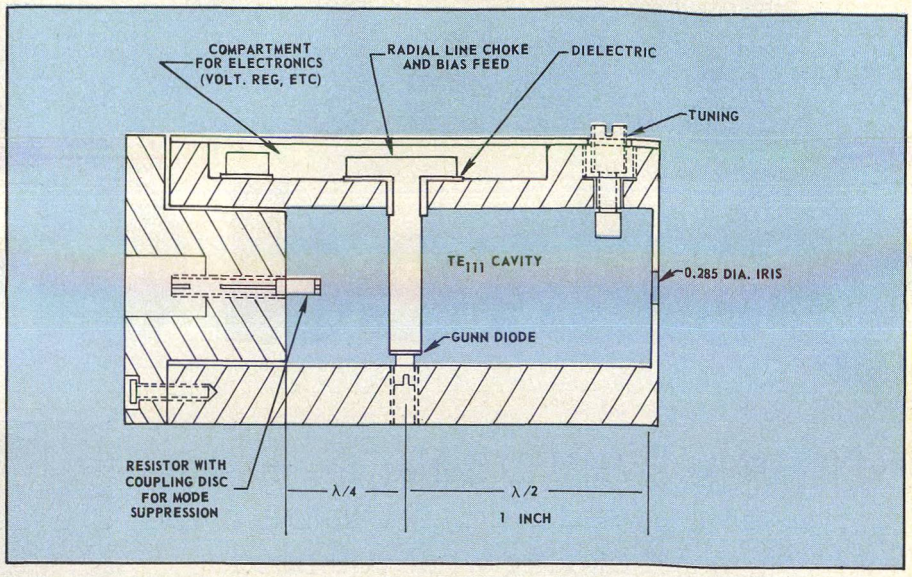

3. A simple resistor damps out undesired modes. In the case of this 9 GHz, TE_{111} oscillator, the resistor suppresses two TEM modes along the bias rod at 6 and 12 GHz, plus a TM_{010} mode at about 9.5 GHz.

To better understand how failure to cold start may be thwarted by the use of a resistance or conductance to damp out unwanted modes of resonance, consider the 9 GHz Gunn oscillator presented in Fig. 3. This particular design had an optimally coupled effective Q of 2,000 and a power output of 0.25 watts at a frequency of 9.0 GHz. However, due to propagation of an extraneous TM_{010} mode and two TEM modes in the bias rod, cold starting was a problem. By adding a resistor attached to a brass tuning rod in a plane tangential to the undesired E-fields, these three modes were successfully damped out without disturbing the TE_{111} mode of the cavity. In this case, a 100-ohm, carbon composition resistor was used with a metal coupling disc soldered to one lead.

Further stabilization of frequency and power is easily accomplished by programming the Gunn bias voltage over temperature, using the emitter-follower circuit shown in Fig. 1. With this scheme, frequency pushing helps to maintain frequency-temperature stability. The change in bias voltage also helps to correct for the diode's active impedance change with temperature, thereby aiding in cold starting and power optimization. ••

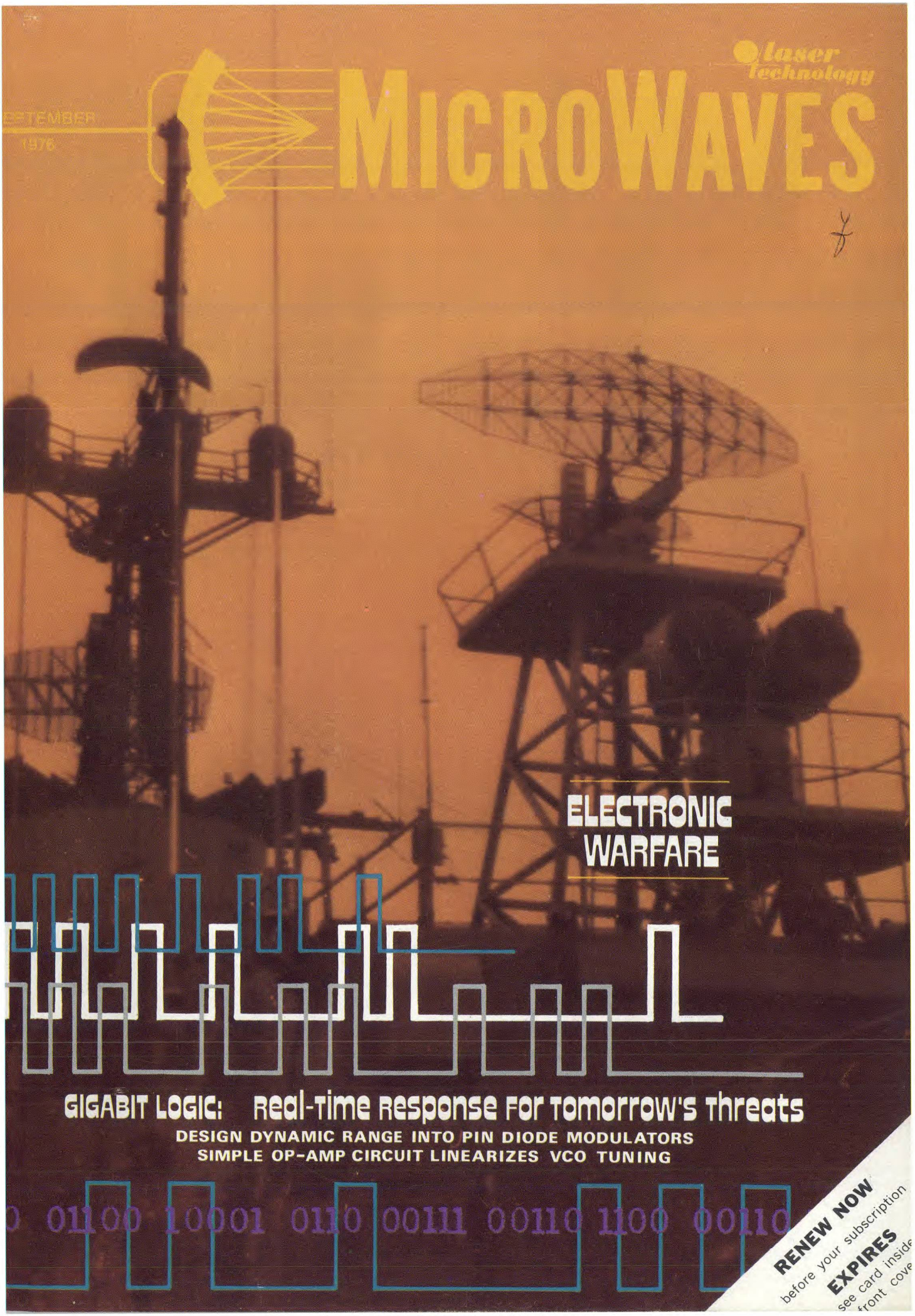
laser technology
MICROWAVES
SEPTEMBER
1976
ELECTRONIC WARFARE
GIGABIT LOGIC: Real-time Response for Tomorrow's Threats
DESIGN DYNAMIC RANGE INTO PIN DIODE MODULATORS
SIMPLE OP-AMP CIRCUIT LINEARIZES VCO TUNING
0 01100 10001 0110 00111 00110 1100 00110
RENEW NOW
before your subscription
EXPIRES
see card inside
front cove

MICROWAVES

September 1976
Vol. 15, No. 9

news

editorial

technical

ELECTRONIC WARFARE

departments

About the cover: Today's fundamental research into gigabit-rate logic circuits may well result in faster-working radars to cope with tomorrow's threats. Photo of Navy's SPS-58 search radar courtesy of Westinghouse. Composition by Art Director Robert Meehan.

coming next month: Amplifiers

Try Serial-Feed Amplifier Arrays. Don't restrict amplifier designs to binary tiers linked by hybrid couplers! Serial feeds allow any number of amplifiers—odd or even—to be arrayed for greater flexibility and appreciable cost savings.

Phase Match TWTs for More Efficient Combining. Here's a proven method of phase matching TWTs using a simple length of cable at the input. It's based on a test set-up that can be assembled from instruments found in most labs.

Thick Film: A Low-Cost Alternative for MICs? New conductor compounds and clever design techniques are drastically changing thick-film/thin film trade offs. New developments here and abroad are examined in this news story.

Publisher/Editor
Howard Bierman

Managing Editor
Stacy V. Bearse

Associate Editor
George R. Davis

West Coast Editor
Jose C. De León
Hayden Publishing Co.
744-R Coleman Avenue
Menlo Park, CA 94025
(415) 325-8280

Washington Editor
Paul Harris
Snyder Associates
1050 Potomac St. NW
Washington, DC 20007
(202) 965-3700

Contributing Editor
Harvey J. Hindin

Editorial Assistant
Gail Murphy

Production Editor
Sherry Lynne Karpen

Art Director
Robert Meehan

Production
Dollie S. Viebig, Mgr.

Circulation
Barbara Freundlich, Dir.
Trish Edelmann
Sherry Karpen,
Reader Service

Directory Coordinator
Janice Tapp

Editorial Office
50 Essex St.,
Rochelle Park, NJ 07662
Phone (201) 843-0550
TWX 710-990-5071

A Hayden Publication
James S. Mulholland, Jr.,
President

MICROWAVES is sent free to individuals actively engaged in microwave work. Subscription prices for non-qualified copies:

	1 Yr.	2 Yr.	3 Yr.	Single Copy
U.S.	$15	$25	$35	$2.50
FOREIGN	$20	$35	$50	$2.50

Additional Product Data Directory reference issue, $10.00 each (U.S.), $18.00, (Foreign). POSTMASTER, please send Form 3579 to Fulfillment Manager, MicroWaves, P.O. Box 13801, Philadelphia, PA. 19101.

Back Issues of MicroWaves are available on microfilm, microfiche, 16mm or 35mm roll film. They can be ordered from Xerox University Microfilms, 300 North Zeeb Road, Ann Arbor, MI 48106. For immediate information, call (313) 761-4700.

Hayden Publishing Co., Inc., James S. Mulholland, President, printed at Brown Printing Co., Inc., Waseca, MN.

Behind The Design Of VCO Linearizers

Transform the VCO's exponential tuning characteristic to a linear function for better EW performance. Build the linearizer as a hybrid circuit for small size and minimum post-tuning drift.

HOW does one gain that slight advantage necessary in the deadly game of electronic warfare? In a receiver, it might be a matter of identifying threat frequencies without delay. In a transmitter, it might be the ability to modulate at a number of different RF frequencies in either a time-shared or frequency-multiplex mode. In either case, an easily tuned, voltage-controlled oscillator is the key.

A local oscillator with linear tuning permits EW receivers to respond to direct computer commands through a simple digital to analog converter, without complex and costly non-linear conversion circuitry. A linearly tuned VCO upgrades the EW transmitter from a wideband noise source to a smart jammer—frequency hopping over many bands to cover multiple threats.

Clearly, the VCO is the heart of either system. But the oscillator could not provide the fine edge in performance without another component —the tuning linearizer.

Varactor-tuned VCOs inherently have a non-linear tuning voltage versus RF frequency characteristic, as shown in Fig. 1. The unlinearized RF output frequency increases monotonically with varactor input voltage, which ranges from typically 0.3 to 40 volts for an 8 to 12 GHz oscillator. Only one frequency exists for each value of tuning input across the entire frequency range.

However, the addition of a linearizer to the VCO input transforms the high-voltage non-linear varactor tuning characteristic into a lower voltage linear function at the linearizer input. Therefore, a constant input voltage range (typically 0 to 10 volts) may be applied to the linearizer to achieve the same RF frequency range. In addition, the linearizer stabilizes the VCO's varactor input, which exhibits a wide variation in input impedance, by providing a fixed input impedance of 1 to 10 kilohms for VCO input bandwidths up to 1 MHz.

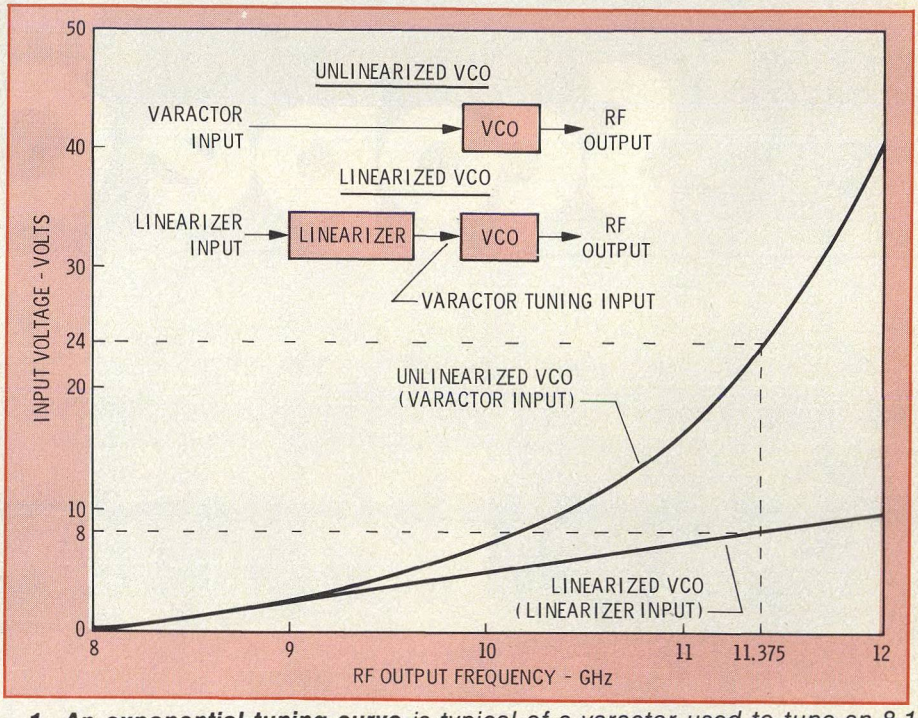

***1. An exponential tuning curve** is typical of a varactor used to tune an 8-12 GHz source.*

Take a piecewise approach

In order to match the VCO's unlinearized tuning characteristic, the linearizer makes a piecewise linear approximation to the tuning characteristic, as shown in Fig. 2. The approximation curve is often divided into equal frequency divisions, as illustrated by the ten equal straight-line frequency segments. The actual tuning curve of the linearized VCO will fall within some small deviation (nonlinearity) about a straight line drawn between two points on the linearized VCO tuning characteristic. By increasing the number of frequency segments, the nonlinearity may be significantly reduced. For octave bandwidth units, a nonlinearity of ±0.5 per cent is readily achieved. For narrowband VCOs (10-15 per cent bandwidth), the nonlinearity may be improved to ±0.1 per cent. The linearizer is composed of two circuits: a high-voltage operational amplifier, used to accommodate the voltage requirements of the VCO, and a "breakpoint" generator, used to change the gain of the operational amplifier at successive predetermined voltages, or breakpoints. In effect, the breakpoint generator adjusts the operational amplifier gain for the closest possible match to the VCO's tuning characteristic.

Since most VCO tuning characteristics are offset from zero volts at the low-end frequency, F_1, the linearizer must provide a voltage at the VCO input when the input voltage to the linearizer is zero. In the circuit of Fig. 3, this offset is obtained from the voltage V_1 applied to the inverting

Ronald N. Buswell, Head of Design Engineering Section, Watkins-Johnson Company, 440 Mt. Herman Road, Scotts Valley, CA 95065.

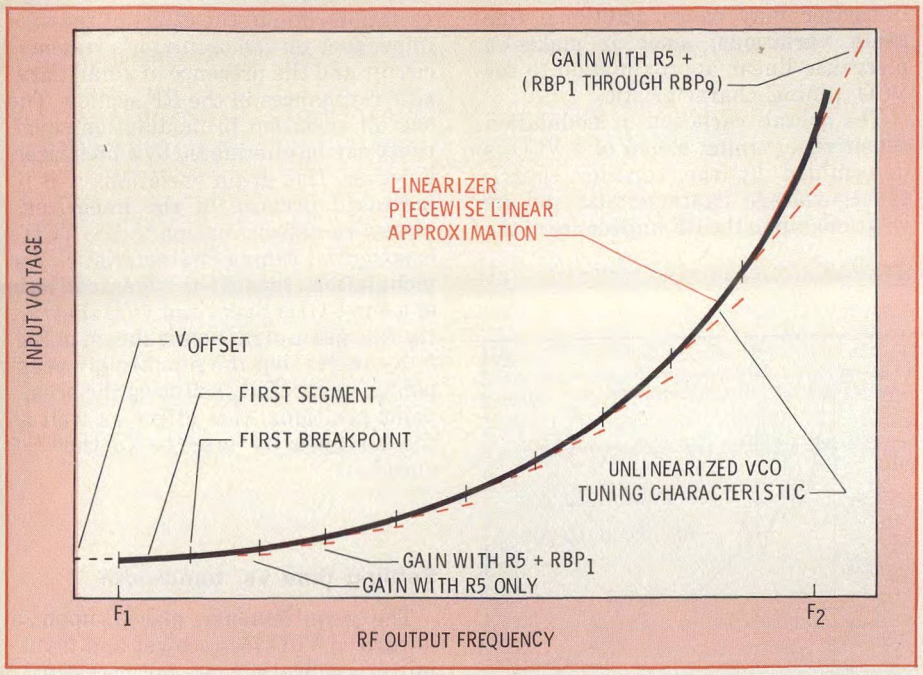

2. *A piecewise linear approximation* *includes many "breakpoints."*

amplifier input through resistor R_5, and is given by the equation:

$$V_{offset} = -V_1 \times \frac{R_6}{R_5}$$

In order to match the slope of the VCO's tuning characteristic, the operational amplifier gain is adjusted over successive frequency segments. During the first frequency segment, the operational amplifier gain is given by the equation:

$$G = \left(\frac{R_2}{R_1 + R_2}\right)\left(1 + \frac{R_6}{R_5}\right)$$

where R_5 is the same resistance value used to establish the voltage offset.

To match the VCO's tuning characteristic for the second and successive frequency segments, the gain of the operational amplifier is increased at each breakpoint by decreasing the inverting input resistance to the operational amplifier. As the input voltage is increased from zero volts, the voltage at V_2 is also increased. Voltages at the bases of the breakpoint transistors are adjusted so these transistors turn on within the range of V_2. Therefore, as the tuning voltage increases, successive breakpoint transistors turn on the shunt R_5 with breakpoint resistors RBP_1—RBP_n. As a result, the gain of the operational amplifier is increased in proportion to the ratio R_6/R'_5 where R'_5 is an equivalent input resistance. In effect, the inverting input resistance R'_5 to the operational amplifier is decreased by shunting R_5 with an additional breakpoint resistor for each additional frequency segment. All the breakpoint resistors shunt R_5 at high-end frequency, F_2.

The breakpoint resistors, RBP_1 through RBP_n, are selected to match the tuning characteristic of each varactor-tuned VCO driven by the linearizer. Resistors, RP_1 through RP_n, position the points along the tuning characteristic at which the breakpoint transistors turn on.

Use two amplifier stages

Since the VCO may require a varactor tuning input voltage as large as 60 volts to tune across an octave frequency range, the linearizer operational amplifier must be capable of supplying this voltage as an output. In order to achieve this high voltage requirement and a video bandwidth on the order of 1 MHz, and to minimize settling time and post-tuning drift, the operational amplifier contains a low-voltage, high-gain stage (A1) followed by a high-voltage, low-gain stage (A2).

The high-voltage stage has an open-loop gain on the order of 400 and a closed loop gain of 10. Its modulation bandwidth exceeds 1 MHz. The low-voltage stage has an open-loop gain of 10,000, and its modulation bandwidth in this application is in excess of 2 MHz. The combined amplifier has an open-loop gain greater than 100,000 which achieves the desired stability, and a modulation bandwidth greater than 1 MHz for a 50-volt output.

(Continued on p. 38)

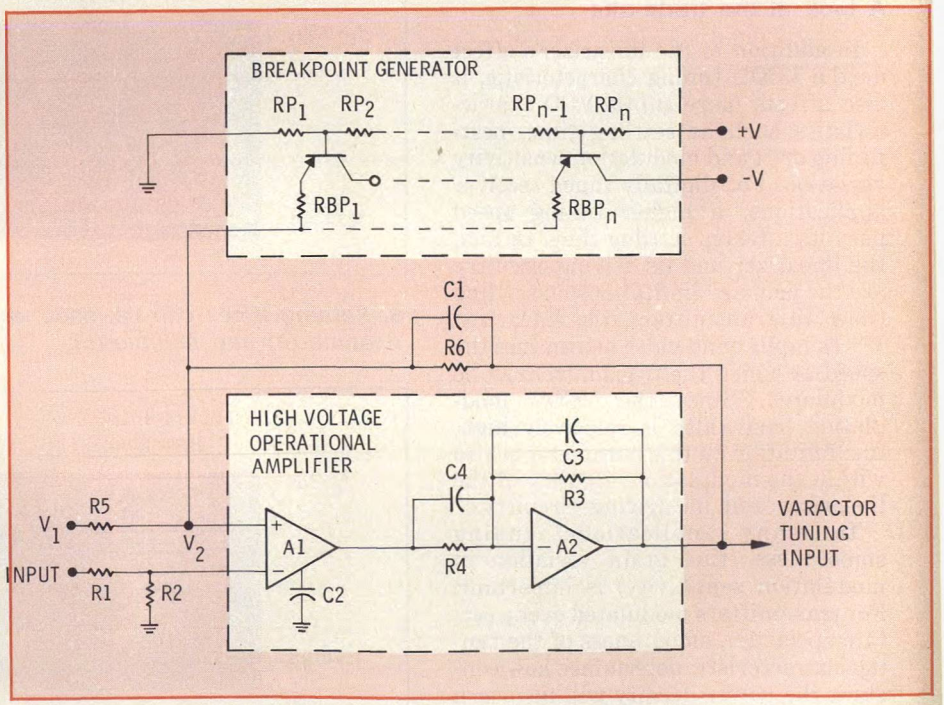

3. *A breakpoint generator* *biasing a high-voltage op-amp provides the linearization function.*

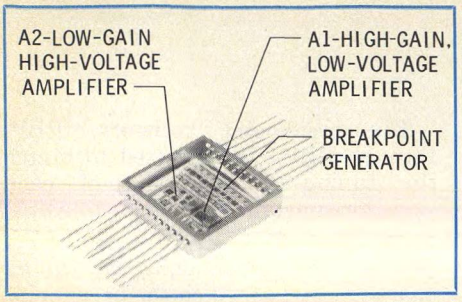

***4. Hybrid packaging** keeps lead lengths short. Package measures 0.625-inches square.*

To accommodate the requirements for small size in EW applications, and to effectively heat sink and temperature stabilize the linearizer circuit, a hybrid linearizer design (Fig. 4) can be mounted within the VCO package. The hybrid contains the high gain and high-voltage stages of the operational amplifier, and breakpoint generator. In this case, the hybrid circuit is fabricated on a 0.025-inch alumina substrate and mounted in a 20-lead flatpack. Voltage polarity in or out of the hybrid can be of two versions—one having a positive input and output, and the other having a negative input and output. Since the common interface voltage range is 0 to +10 volts, and optimum varactor-tuned VCO performance is achieved with a negative varactor input voltage, an input inverter amplifier is incorporated into the PC board to drive a negative output linearizer.

A look at the trade-offs

In addition to the linearizer's effect on the VCO's tuning characteristic, it also affects more subtle VCO characteristics such as settling time, post-tuning drift and modulation sensitivity variation. For digitally tuned receiver applications, a higher tuning speed permits a faster settling time. In fact, the linearizer and its driving circuitry are the primary limitations on settling time. In transmitters, the linearized VCO's input bandwidth determines the speed at which the transmitter can be modulated. Since the VCO's modulation bandwidth is relatively high, the limitation on this parameter is also within the modulation circuitry of the linearizer and its driving circuitry.

In many applications, tuning smoothness (fine grain variation in modulation sensitivity) is important. For transmitters modulated over a certain spectrum, smoothness of the tuning characteristic determines how constant the power density will be over a given band. In digitally tuned receivers, the variation in the frequency step size for a given input voltage step will be governed by the modulation sensitivity variation. Fine grain variations in modulation sensitivity are present in the VCO itself; however, the linearizer may cause additional fine grain variations, since it makes a piecewise linear approximation to the VCO tuning characteristic.

The overall variation in modulation sensitivity (tuning slope) of a VCO is determined by the varactor capacitance—voltage characteristic and its relationship to the RF impedance of the VCO's transistor or bulk-effect diode. This may be as high as 20:1 for an octave bandwidth unit. In addition, the VCO tuning curve exhibits fine grain variations due to the effect of the load impedance on the oscillator's resonant circuit and the presence of small parasitic resonances in the RF section. The overall variation in modulation sensitivity can be eliminated by a linearizer, however, fine grain variations will be increased because of the linearizer's piecewise approximation to the VCO's exponential tuning characteristic. The modulation sensitivity characteristic of a 4 to 8 GHz linearized VCO showing the fine grain structure is shown in Fig. 5. By increasing the number of breakpoints, or carefully selecting the breakpoint positions, this effect as well as the nonlinearity may be further reduced.

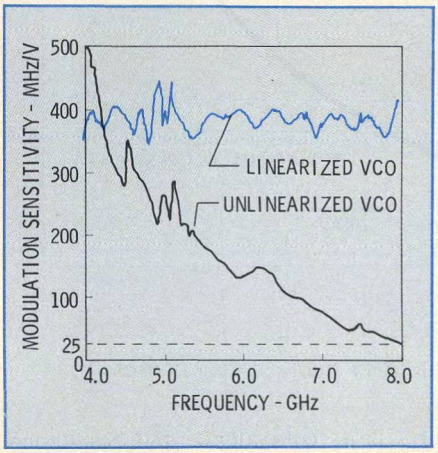

***5. The overall variation** in modulation sensitivity is eliminated by the linearizer. Fine grain variations remain in this 4 to 8 GHz source.*

Settling time vs. bandwidth

The requirements placed upon a linearized VCO for receiver and transmitter applications are not necessarily compatible. A linearized VCO optimized for maximum modulation bandwidth will not necessarily settle as fast as the same optimized for minimum settling time.

A linearizer may be aligned for either minimum settling time or max-

(continued on p. 46)

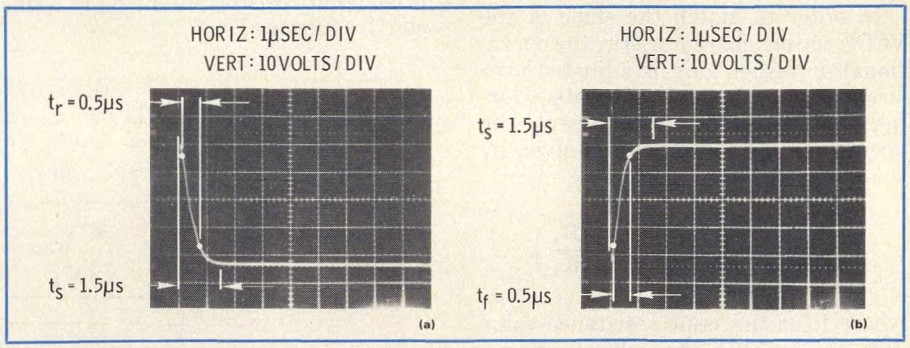

***6. Settling times** can be made very small by optimizing the linearizer. Note risetime (a) and falltime (b).*

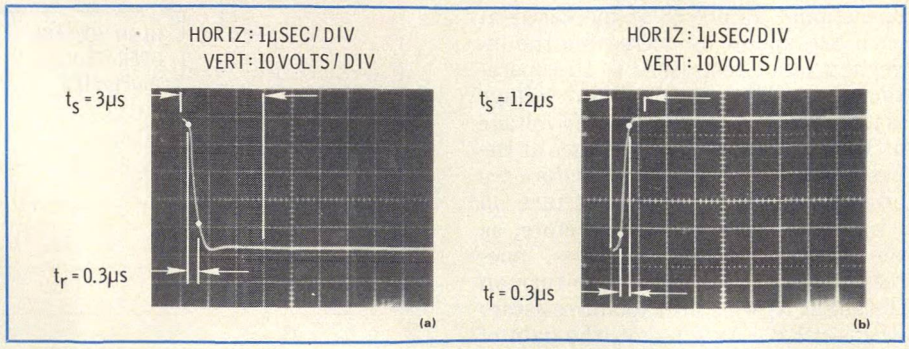

***7. Optimized for a 1-MHz modulation bandwidth,** risetime (a) and falltime (b) are significantly shorter than in Fig. 6.*

imum modulation bandwidth by using different compensation techniques. When the linearizer is optimized for minimum settling time, as shown in Fig. 6, the output RF frequency stabilizes to 1 per cent of the final frequency within 1.5 microseconds after a full band step change in input voltage. The 3-dB modulation bandwidth (full band) is 575 kHz and falls off at 12 dB/octave since the gain of each operational amplifier stage, A1 and A2, falls off at 6 dB octave. In order to prevent oscillation of the operational amplifier, a "zero" is introduced into the linearizer circuit (capacitance C_4 in Fig. 3), which reduces the operational amplifier gain to 6 dB/octave before going through unity gain.

When optimized for modulation bandwidth, the same linearizer achieves a 1.0 MHz bandwidth (full band) which also falls off at 12 dB/octave. The rise and fall times are faster, as shown in Fig. 7. However, note that the 1 per cent settling time is increased to 3 microseconds due to pulse overshoot. Optimum modulation bandwidth is achieved by decreasing the capacitance of C_1—C_3 in the linearizer circuit of Fig. 3.

In many applications, a minimum small signal bandwidth is required. However, for a breakpoint linearizer, this parameter is not constant across the VCO's operating frequency range. As a result of the increase in operational amplifier gain required to match the VCO tuning characteristic, the small-signal bandwidth decreases as the input voltage is increased for a fixed set of compensation capacitors. This is illustrated in Fig. 8, where the bandwith decreases from 2.1 MHz for an input of zero volts, to 750 kHz for an input of 10 volts.

The transient and frequency responses of the linearizer/VCO combination are essentially the same as those for the hybrid linearizer, since the bandwidth of the VCO is at least an order of magnitude greater in this example.

Notes on noise and drift

Once the linearized VCO settles to a given frequency, thermal time constants of critical components cause a shift, or "post-tuning drift" in output frequency as a function of time after a step change in input voltage. In the linearizer, this may be caused by drifts in the operational amplifier itself. However, with an open-loop gain greater than 100,000 and use of resistors having a low temperature coefficient, this is a relatively small factor compared to the shift in breakpoint position due to changes in the base to emitter voltage (V_{BE}) of the breakpoint transistors. When the input is changed from 0 to 10 volts each, breakpoint transistor goes from cutoff to an "on" condition. Heat generated in the transistor junctions causes the base to emitter voltage to decrease at a rate determined by the thermal impedance of the transistors and packaging. The thermal time constant of these devices is typically less than one millisecond. The decrease in V_{BE} causes the point at which the transistors turn on to shift, resulting in a change in the linearizer's output voltage and, therefore, the VCO's output frequency.

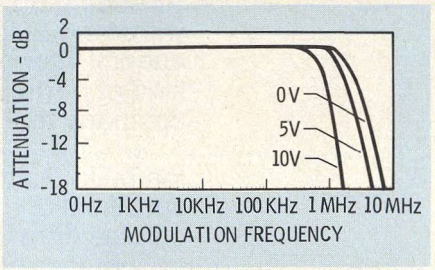

***8. Small signal bandwith** decreases as input voltage is raised.*

Similar effects occur in the VCO itself in which case, both the varactor and active device (transistor or bulk-effect diode) exhibit a change in RF impedance after an input voltage step. The RF impedance change results from a change in junction temperature since the efficiencies of the active devices are frequency sensitive. The thermal time constant associated with the devices in the VCO may be as long as one millisecond.

A comparison of the short-term post-tuning drift of a 4 to 8 GHz VCO with and without a linearizer is shown in Fig. 9. The drift increases from a maximum of 2.6 MHz to 5.1 MHz with the addition of the linearizer.

Noise associated with the VCO output signal is measured in terms of its residual FM. It is expressed as the peak-to-peak deviation at the top of the carrier, or as the sideband level a certain distance from the center of the carrier. The peak-to-peak residual FM of a 4 to 8 GHz VCO is typically 15 kHz.

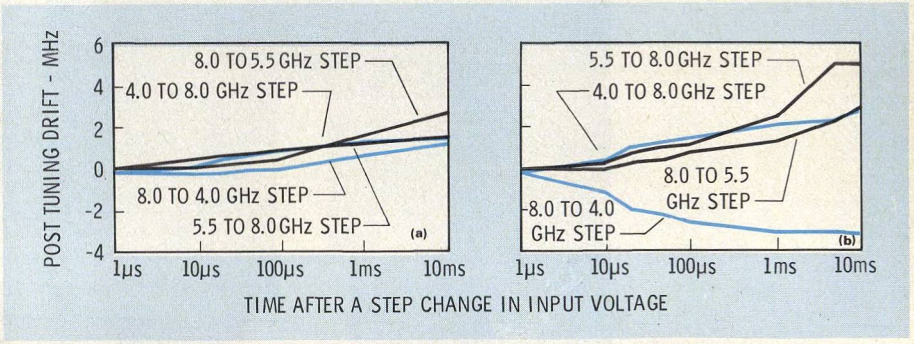

***9. Post-tuning drift** increases with the addition of a linearizer, as shown by this with (b) and without (a) comparison.*

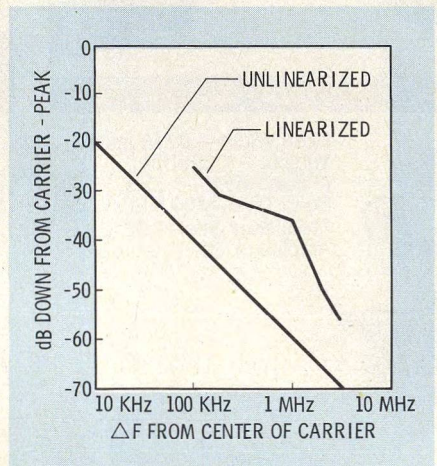

***10. Noise generated in the linearizer** circuit cannot be reduced by the op-amp's open-loop gain.*

The addition of a linearizer causes this to increase to approximately 25 kHz. The sideband level also increases with the linearizer, as shown in Fig. 10. The noise 1 MHz from the carrier in a 10 kHz bandwidth typically increases from −60 to −36 dB. This noise is generated in the linearizer circuit and cannot be reduced by the operational amplifier's open-loop gain because it is relatively low compared to the closed-loop gain at that frequency.

One method to reduce the sideband noise is to place a filter between the linearizer and VCO. For example, a 10 kHz bandwidth filter placed after the linearizer will reduce the VCO's output sideband noise essentially to the same level as for the VCO itself, however, this also limits the linearized VCO modulation bandwidth. ••

Design PIN Modulators With Wide Dynamic Range

A simple resistive model is the key to PIN diode modulator design. Careful approximation of parasitics leads to a series of useful design charts and a step-by-step design process.

THE simulation of radar return signals to test electronic countermeasure techniques and receiver performance requires the precise control of microwave power over a dynamic range of greater than 100 dB. PIN diode modulators provide a low-cost, lightweight and reliable means of achieving these large dynamic ranges at frequencies extending through X-band.

New design techniques have been developed which consider individual diode properties in predicting the behavior of multiple-diode, octave modulators. Specifically, diode resistance, circuit geometry and the relationship between attenuation and frequency have been evaluated using BAMP[1], a circuit analysis program.

The resulting curves and scaling equations demonstrate critical tradeoffs between the maximum attenuation, attenuation slope, bandwidth and current sensitivity of a modulator, and the number of diodes used in the design.

First, consider a resistive model

Although PIN diodes can be used as attenuators in series or shunt circuits, the parallel arrangement is preferred for modulator design as described in, "Diode dynamics." A shunt circuit offers simpler biasing, faster response and better heat dissipation.

The biased diode can initially be considered as a resistive element mounted in a package without parasitic reactances. This model provides solutions which can be analytically manipulated to provide information about multiple diode responses. Since actual diode modulators deviate from the ideal only at the limits of operation, this model is suitable for many applications.

Using matrix techniques, the attenuation of the shunt circuit of the form shown in Fig. 1 can be described by the following set of equations:

$$n = 2 \quad A = 20 \log 1/2(2+2x+x^2) \qquad (1a)$$

$$n = 3 \quad A = 20 \log 1/2(2+3x+2x^2+x^3) \qquad (1b)$$

$$n = 4 \quad A = 20 \log 1/2(2+4x+4x^2+2x^3+x^4) \qquad (1c)$$

where n = number of diodes
$\theta = 90°$
x = real values only

This set of equations is valid for the maximum attenuation of identical elements separated by equal lengths of uniform transmission line with line, source and load impedances assumed to be equal. The variable, X, represents a normalized admittance in shunt, $X = Y/Y_0$, or normalized impedance, $X = Z/Z_0$, in series with a transmission line of impedance $Z_0 = 1/Y_0$. Θ is defined as the ratio of the test frequency to the frequency of maximum attenuation and is normally expressed angularly as $\frac{f}{fo}\left(\frac{\pi}{2}\right)$. Thus, for a quarter wavelength spacing, Θ = 90°.

When X and Θ are allowed to take on all values, it is simpler to first solve for the circuit's transfer function, V_o/V_a. For the cases of two, three and four diode modulators:

$$V_o/V_a = 1/2\,[(2+x)\cos\theta + j(2+2x+x^2)\sin\theta] \qquad n = 2$$

$$V_o/V_a = 1/2\,[(2+3x)\cos^2\theta - (2+3x+2x^2+x^3)\sin^2\theta + j2(2+3x+2x^2)\sin\theta\cos\theta] \qquad n = 3$$

$$V_o/V_a = 1/2\,[2(2x+1)\cos^3\theta - 2(3x^3+5x^2+6x+3)\cos\theta\sin^2\theta + j\{2(5x^2+6x+3)\sin\theta\cos^2\theta - (x^4+2x^3+4x^2+4x+2)\sin^3\theta\}] \qquad n = 4$$

The attenuation across the circuit expressed in dB is:

$$A = 20 \text{ Log} \left| \frac{V_o}{V_a} \right|.$$

By expanding this set of solutions, it becomes evident that the frequency response of a periodic array of resistive

Dr. J.A. Hartman, Group Engineer, Radar Systems, **T.L. Davis,** Aerosystems Engineer, General Dynamics, P.O. Box 748, Fort Worth, TX 76101.

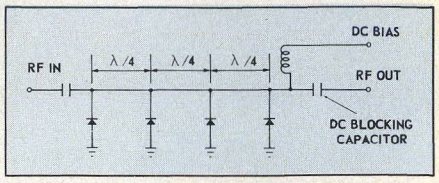

***1. A simple, shunt-diode reflective attenuator** is the basis of more complex absorptive modulator.*

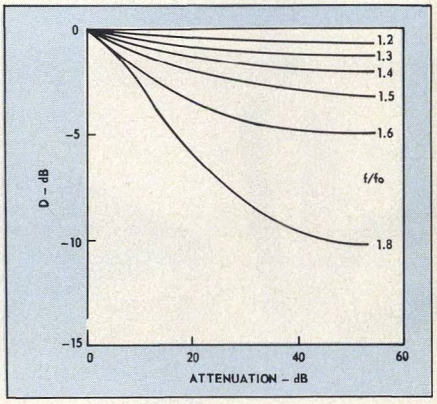

(a)

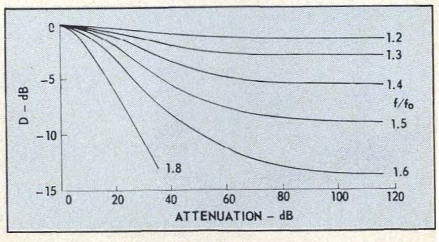

(b)

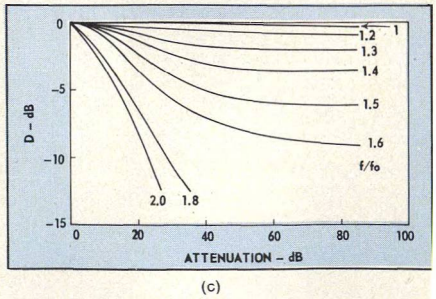

(c)

***2. Deviation curves** illustrate the effect of frequency on attenuation for two, (a) three (b) and four (c) diode modulators.*

elements is symmetrical about the quarter-wavelength frequency of their separation. Like other commensurate length-line microwave circuits, maximum attenuation for resistive elements occurs at odd multiples of the fundamental, while minimum attenuation is found at even multiples.

Now, compensate for inductance

In order to show the effect of frequency on attenuation, let us define the term D as the difference between the maximum (midband) attenuation and the attenuation at some other frequency. This deviation parameter allows all practical values of attenuation to be viewed on a large scale and permits easy evaluation of the maximum attenuation. The deviation for (f/f_0) ratios of 1.2 through 1.8 for two, three and four diodes are plotted in Fig. 2.

It is important to point out that the deviation curves of Fig. 2 are only exact for purely resistive elements. Real diodes have package parasitics such as the wire bond inductances, L_p, which distort the ideal response. In order to use the results of the resistive model, a correction for these inductors is essential. A convenient method is to represent the inductors as a length of transmission line with equivalent impedance. When the electrical length is less than one-eighth wavelength the "correction" length is:[2]

$$\Delta_d = \frac{L_P C_o}{\sqrt{\epsilon_r}\, Z_o} \qquad (2)$$

where C_0 = speed of light

The effective spacing between diodes is increased by twice this length and, therefore, the effective center frequency is:

$$f_o = \frac{C_o}{4\sqrt{\epsilon_r}\,(d + 2\Delta d)} \qquad (3)$$

where d is the distance between diodes.

Using the Eq. 1 and typical diode properties, good predictions of multiple diode modulator performance at midband can be made. In many situations, only the insertion loss and maximum attenuation (i. e., isolation) are of interest and the following approximations can be made:

Isolation:

$$A_n \approx 20 \log \frac{X^n}{2} \qquad (x > 10) \qquad (4)$$

Insertion loss:

$$A_n \approx 20 \log\left(1 + \frac{n}{2}x\right)$$

$$\approx 10\,(\log e)\, n\, x$$

$$\approx 4.34\, n\, x \qquad (x < 1/10) \qquad (5)$$

Using Eq. (4), the relation between two modulators with a different number of diodes (n and m) is:

$$A_n \approx \frac{n}{m} A_m + \left(\frac{n}{m} - 1\right)6 \qquad (x > 10) \qquad (6)$$

It is interesting to see how the number of diodes in a design influences modulation sensitivity. Experimental measurements have shown that the current dependent resistance of a PIN diode is approximately:

$$R = \frac{K}{I^{\beta}} \qquad (7)$$

where the bias current I is given in milliamps. The exponent, β, usually between .8 and .9, is related to the device junction physics and must be determined experimentally. The constant of proportionality, K, is defined as the RF resistance at a bias current of 1.0 mA. Now, substitute Eq. (7) into Eq. (5) and assume $\beta = 1$:

$$A_n \approx 10\,(\log e)\frac{Z_o}{K} I_T \qquad (x < 1/10) \qquad (8)$$

where I_T is the total modulator current. Note that modulator sensivity (A_n as a function I_T) is independent of the number of diodes at low attenuations.

Are circuit inconsistencies critical?

Simulations performed with computer-aided design (CAD) language, employing cascaded two-port s-parameter matrices[1] yield interesting re-

(continued on p. 44)

Diode dynamics

Shunt diodes can be mounted in single or two-port configuration, as shown in Fig. A1. The single-port circuit offers the least insertion loss, but produces a higher impedance in shunt with the line in the "ON" or biased state, thus limiting the maximum attenuation. The two-port arrangement provides more attenuation, hence, greater dynamic range, since wire-bond inductances do not limit the maximum conductance across the transmission line.

Figure A2 is an electrical model of a packaged shunt diode. The series inductors, L_p, represent the inductances of the two wire bonds connecting the chip to the transmission lines, while the inductance L_S results from their mutual coupling. This package offers considerably better attenuation performance than the one-port package because of its smaller series inductance, (L_S).

In addition to the current dependent RF resistance, R, the small signal model of Fig. A2 includes the diode capacitance, C, and a fixed bulk resistance, R_B, The total impedance of L_S and R_B act to limit the maximum attenuation. The wire bond impedances are represented by R_A and L_P.

For small values of R, the attenuation of the model shown in Fig. A2 is:

$$A\,(dB) \approx 10 \log \left\{ \left[1 + \frac{Z}{2\,(R + R_B)}\right]^2 \frac{\left[1 + \left(\frac{\omega}{\omega_O}\right)^2\right]^2}{1 + \left(\frac{\omega}{\omega_P}\right)^2} \right\} \qquad (A1)$$

where $\omega_O = \frac{Z}{L_P}$ $\omega_P = \frac{R + R_B}{L_S}$

When the shunt diode is reversed biased, the major impedances are the capacitance, C, and the lead inductances, L_P. In many instances, one of these reactances will dominate by as much as a factor of 10, allowing the weaker to be ignored. Under these conditions the insertion loss is:

$$A\,(dB) = 10 \log\,[1 + (\omega/\omega_D)^2] \qquad (A2)$$

$$\approx (10 \log e)\,(\omega/\omega_D)^2$$

$$\approx (4.34)\,(\omega/\omega_D)^2$$

where ω_D is equal to Z/L_p or $2/ZC$, whichever is less.

Equations (A1) and (A2) show how the diode and package properties affect the attenuation and insertion loss for the shunt mounted configuration.

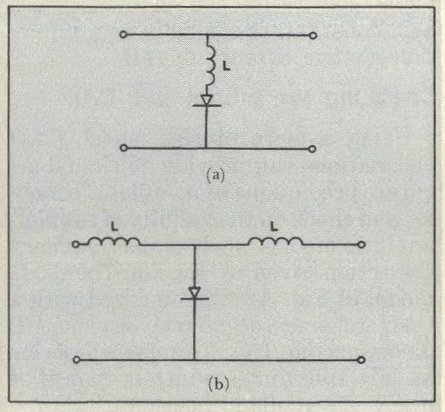

*A1. **Shunt diode mounting** can be fabricated in (a) a single port or (b) a dual port configuration.*

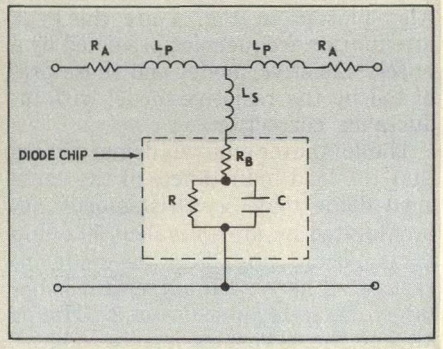

*A2. **This small signal model** represents a two port shunt mounted diode. Typical values are R_A = 0.25 ohm, L_P = 0.25μH, C = 0.1 pF, L_S = 0.025 nH and R_B = 1 ohm.*

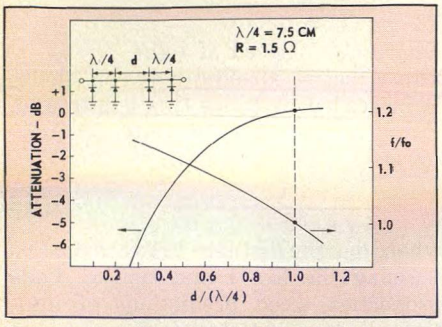

***3. Small differences in diode spacing** only slightly influence modulator performance.*

sults on the effects of varying diode spacing and "on" resistance. Using the reflective modulator shown in Fig. 3, the distance between the second and third diode was varied while the distance between the other diodes was held at one-quarter wavelength spacing. The resultant curves were calculated for the diode modeled with R = 1.5 ohms. As the spacing decreases from 1.13 (λ/4) to 0.26 (λ/4), the 3-dB bandwidth broadens slightly, the maximum attenuation frequency changes from 0.95 f_0 to 1.15 f_0, and the maximum attenuation level decreases approximately 7 dB. This analysis shows that while equally spaced diodes result

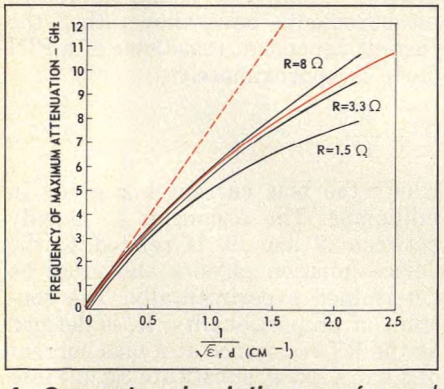

***4. Computer simulations** performed at R = 1.5, 3.3 and 8 ohms show the validity of Eq. (3), the corrected model, represented by solid, color line. Dashed, color line represents the limiting case of a resistive model.*

in optimum modulator performance, small deviations from that spacing will only slightly affect performance.

The effect of diode-to-diode resistance variations can be partially ascertained from Eq. 1. For large values of X (>5), the highest-order term predominates, and it can be shown that each diode contributes equally to this term. Thus, the midband attenuation can be approximated:

$$A_n \approx 20 \log \left(1/2 \prod_{i=1}^{n} X_i \right)$$

High attenuations, therefore, depend largely on the product of the individual diode resistances and little change in attenuation can be expected as long as this product remains constant. To confirm these conclusions, CAD calculations were performed for a four-diode modulator. The individual resistances were varied as much as two-to-one while the resistance products were kept constant, resulting in an attenuation change of only 0.3 dB.

Checking the model with CAD

Using a more precise model, CAD calculations can provide quick and accurate predictions of modulator behavior and check on the validity of simpler, analytic models, such as the frequency correction given by Eq. (3). The diode model of Fig. A2 was analyzed with a CAD routine for quarter-wavelength diode spacing. The parameters describe an HP 3140 diode, which is typical of many shunt diode packages.

The predicted peak attenuation frequency versus diode spacing is plotted in Fig. 4, for R = 1.5, 3.3 and 8 ohms. There is little change in peak attenuation frequency when R exceeds 8 ohms. Also plotted in Fig. 4 are the peak attenuation frequencies predicted by a purely resistive model and those predicted by the resistive model with inductance correction.

The computer analysis demonstrates that the lead inductances of the packaged diode may be satisfactorily approximated by an equivalent 50 - ohm transmission line. For the diode investigated here good agreement is obtained up to frequencies of 8 GHz for all but the lowest resistance values.

Figure 5 (a) is the attenuation versus frequency response for a four diode modulator, calculated using the model of Fig. A2. Since the frequency of maximum attenuation varies with diode resistance (or bias), a convenient normalizing frequency, f_0, was chosen. The somewhat arbitrary, but practical, choice is given by Eq. (3). The data for the resistive model agrees within 0.5 dB at 1 GHz and the two curves essentially conincide on this graph. Curves are also plotted for diode separations of 2.04, 1.25 and 0.45 cm in air (f_0 = 3.2, 4.8 and 10 GHz). At large bias level (R = 1.5 ohms), the inductances cause a decrease in the attainable attenuation; this also causes the peak attenuation to shift to a lower frequency. When the bias is reduced so that R = 3.3 ohms, the curves are within 1 dB of each other for all frequencies and separations.

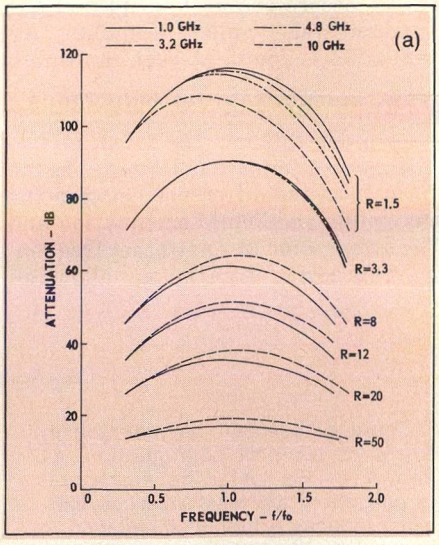

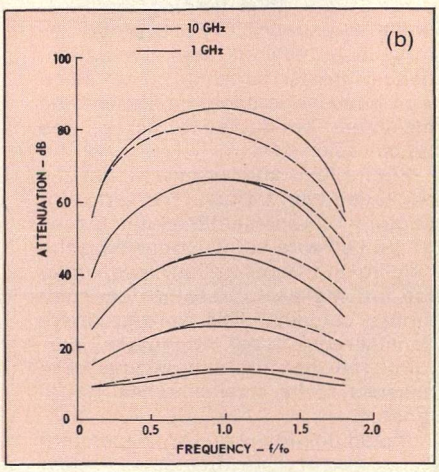

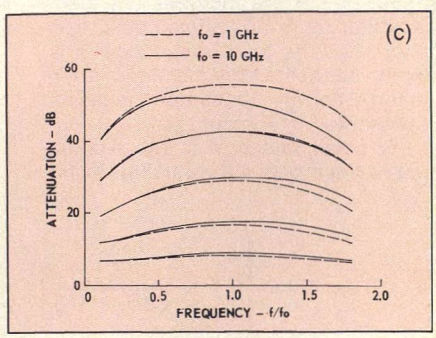

***5. These computer predictions** can be used to estimate flatness for different values of diode resistance. Four (a), three (b) and two (c) diode cases are shown.*

At bias levels causing a diode resistance of 8 ohms or more, the attenuation of the package at 10 GHz causes an increase over the resistive

(continued on p. 46)

model attenuation. The agreement is still within a few dB at 10 GHz and within 1 dB at 5 GHz.

Similar curves for three and two-diode modulators are presented in Figs. 5(b) and 5(c) for center frequencies of both 1.0 GHz and 10 GHz for a variety of arbitrarily chosen resistive values.

In short, the frequency response of the actual PIN modulator compares very well to the theoretical model.

Now, design the modulator

With this in mind, it becomes an easy task to design a reflective modulator using the information presented earlier. After selecting the diode on the basis of speed and power, the remaining steps are:

- Determine from Fig. 2 and the bandwidth requirements how much the maximum attenuation at midband will be.
- Using the maximum required midband attenuation, determine the number of diodes required using Eq. (4).
- Use Fig. 2 to determine the frequency response. Fewer diodes produce a flatter response.
- Alternately, use the results of Fig. 5 if the diode used in that calculation is satisfactory.
- Determine the spacing of the diodes using Eq. (3) or Fig. 4.

An absorptive modulator is essentially two reflective modulators connected by two, 3-dB hybrid couplers (see Fig. 6). Its realization, therefore is a matter of adding circuitry to a dual reflective modulator.

As the power is reflected back through the 90-degree hybrid, the reflected signals add 180 degrees out of phase at the input port to maintain a good VSWR, and combine to be absorbed in the terminated port. The RF filter prevents signals from exiting through the bias port and the video filter inhibits the switching signal on the RF lines.

To demonstrate the design process, consider an application requiring a modulator with a minimum isolation of 100 dB at a center frequency of 1 GHz. Assume that VSWR must never rise above 1.8, and that only 2 dB insertion loss can be tolerated. For manufacturability, choose a three-layer stripline design. Although the three layer design requires a transmission line offset 5.5 mils from the optimum center spacing, the line impedance and the filter performance are not significantly altered. The tight coupling of the 3-dB hybrid is achieved by overlapping the quarter-wavelength

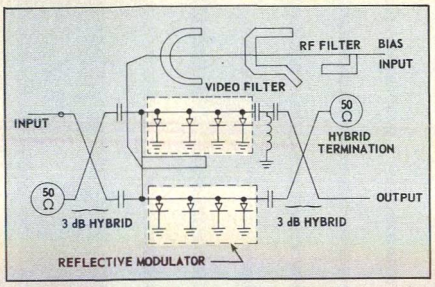

***6. Two reflective attenuators are combined** with 3-dB couplers to form an absorptive modulator.*

center sections.[3] An exact overlap is required so that the two outputs are opposite the input at the same distance. If greater than one octave bandwidth or flatness greater than ± 1 dB is required, multiple section couplers must be designed.[4]

For single quarter-wave sections in materials with dielectric constants of 2.5, the middle layer is 11.6 mils (0.029 cm) thick and the ground plane spacing is 0.130 inches (0.32 cm). Ideally, an electrically variable attenuator would have a control port which had no other effect than to vary the attenuation between the input and output ports. Unfortunately, the controlling and controlled currents must share the same path in a PIN diode modulator. Because of differences in frequencies, the RF and the control or video signals are usually separated by filters.

Filters are often critical

Stringent demands on the filter design of the pulse modulator are often imposed since frequency components of the fast risetime video pulse may extend to RF frequencies. The bias-line filter must be of sufficient bandwidth to pass the video pulse and yet low enough to stop the RF. The reverse is true for the RF filters. It is good practice to design the filters with a guard band so that the RF and bias lines are isolated at all frequencies.

There are two types of filters which can be used depending on the requirements of the design. The lumped element filter in theory has the ideal response but, in practice, will have spurious responses at higher frequencies. Also it is the most expensive and difficult to build. The distributed element equal length line filter is the easiest to design and implement but exhibits repeating responses at odd multiples of the quarter wavelength frequency.

Variations or combinations of these two basic filters may be used in order to suppress unwanted high frequency responses. Included in this category are filters with semi-lumped elements, unequal length distributed elements and both lumped and distributed elements.[5]

The design incorporates a distributed element bandstop filter in the bias line which provides 60 dB isolation across the octave bandwidth of the modulator.

A NASA[6] computer program was used to obtain the line impedances. The input and coupler terminations were isolated with simple series capacitors. The output high-pass filter uses both lumped and semi-lumped elements.

Since the filter/bias line must connect to both reflective modulators the bias line must cross under the transmission line. This is readily achieved because of the three-layer structure. The crossover is made perpendicular to the transmission line to keep the crossover coupling at a minimum. The coupling capacitance of the two lines is 0.05 pF.

For an isolation requirement of greater than 100 dB, attention must be given to a number of critical mounting and packaging details. In general, the output and input lines should be located as far apart as practical. For higher frequency models, additional eyelets and/or grounding screws are placed around the lines and diodes to break up higher-order modes. The diodes are first soldered to both sides of the center board and then are forced into precision cutouts in the ground plane to insure a tight fit between the package and the surrounding dielectric. The entire package is sealed with conductive epoxy to provide EMI shielding and to reduce leakage paths around the package perimeter. Good electrical contact between the launchers and ground planes is insured by painting the mating surfaces with conductive silver. The use of these techniques has resulted in isolations in excess of 125 dB with insertion losses of less than 1.5 dB at bias currents of 100 mA at 1 GHz. ••

References

1. BAMP, Basic Analysis and Mapping Program, Hewlett-Packard Company, Palo Alto, CA.
2. G. L. Matthaei, Leo Young and Emit Jones, *Microwave Filters Impedance Matching Networks and Coupling Structures*, McGraw-Hill, p. 361, (1964).
3. S. B. Cohn, "Characteristic Impedances of Broadside-Coupled Strip Transmission Lines," *IRE Trans. on Microwave Theory and Techniques*, Vol. MTT-8, No. 6, pp. 633-637, (November, 1960).
4. E. G. Cristal and L. Young, "Theory and Tables of Optimum Symmetrical TEM-Mode Coupled-Transmission-Line Directional Coupler," *IEEE Trans. on Microwave Theory and Techniques*, Vol. MTT-13, No. 5, pp. 544-558, (September, 1965).
5. Matthaei, *Op. Cit.*
6. T. C. Cisco, *Design of Microstrip Components by Computer*, NASA Contractor Report, NASA CR-1982, pp. 52-72, (March, 1972).
7. D. Leenov, "The Silicon PIN Diode as a Microwave Radar Protector at Megawatt Levels," *IEEE Trans. on Electron Devices*, Vol. 11, pp. 53-61, (1964).

Check Impedance With An Electronic Slotted Line

Advances in digital technology are revitalizing an old RF idea, the electronic slotted line. Used as an impedance sensing device, the compact component checks the operation of airborne guidance systems.

WITH the advent of stripline and the use of computers on board aircraft and missiles, it now becomes a very practical matter to monitor amplitude and phase of reflections by means of an old idea in impedance measurement: the electronic slotted line.

The prime application of the electronic slotted line as an impedance measuring device (IMD) is to insure that the microwave guidance antenna continues to function properly under conditions of great stress, such as in re-entry. If antenna damage is sensed, the missile can be quickly switched to an alternate form of guidance, such as laser, optical or infra-red, for example. Dual directional couplers are also used in this application, but they are physically larger, cost more and only provide data on the magnitude of reflection. The stripline IMD offers information on phase as well as amplitude.

An electronic slotted line is a passive structure using three loosely coupled probes spaced one-eighth wavelength apart.[1] The theory behind the IMD is simple. A standing wave pattern in a transmission line may be completely specified by three independent values of field strength. Thus, if one can position three fixed probes in the line, the complex load impedance can be determined.

When the probe spacings are equal to one-eighth wavelength, the equations for complex impedance reduce to simple expressions. The insertion length of the IMD is then only slightly more than one-quarter wavelength long. It can be seen that this structure is useful for narrow bandwidths (10 to 15 per cent), which is indeed the case of most missile guidance systems. Furthermore, a stripline structure one-quarter wavelength long will have an RF insertion loss of less than 0.2 dB including connectors, with a VSWR of about 1.10. It will be demonstrated that directivity does not enter into the picture at all.

How does it operate?

In a lossless transmission line of length ℓ and characteristic impedance Z_0, terminated in a complex impedance, $Z_L = R_L + jX_L$, the voltage at a distance y from the termination is given by

$$V_y = V_L \left[\text{Cos } \frac{2\pi y}{\lambda} + \frac{jZ_o}{Z_L} \sin \frac{2\pi y}{\lambda} \right] \quad (1)$$

where V_L in the voltage across the load and λ is the wavelength in the transmission line. Let the values of V_y occurring at points separated by $\lambda/8$ along the line be V_1, V_2 and V_3, with V_0 occurring at the load (see Fig. 1).

Norman Spector, President, Norsal Industries, Inc., 34 Grand Boulevard, Brentwood, NY 11717.

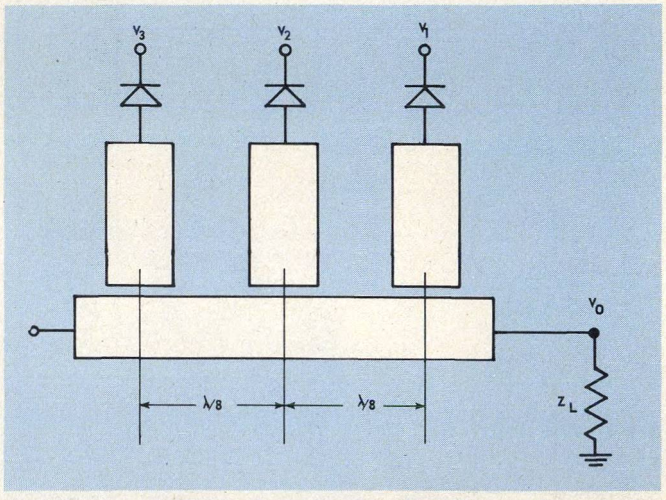

***1. Three probes determine the VSWR** on the central transmission line. In a guidance application, the electronic slotted line is mounted directly behind the antenna.*

To obtain the load impedance, any three consecutive values may be measured and the resistive and reactive parts calculated. It is not practical to place a probe to measure V_0. Therefore, V_1, V_2 and V_3 will be used. The answers, however, determine the impedance at V_0. Commensurate with the requirements of smallest size, the probe measuring V_1 is normally placed as close to the output connector as possible. In order to determine the impedance at some given reference point, the complex impedance can be transformed from the virtual V_0 position to any reference point required.

If V_1, V_2 and V_3 are measured, then

$$X_L' = \frac{V_1^2 - V_3^2}{2V_2^2} \quad (2)$$

and

$$Z_L'^2 = \frac{V_1^2 + V_3^2 - V_2^2}{V_2^2} \quad (3)$$

can be derived from Eq. (1) where X_L' and Z_L' are the normalized reactance and load impedance, respectively. From this, R_L, the normalized load resistance is determined by

$$R_L' = \sqrt{|Z_L'|^2 - |X_L'|^2} \quad (4)$$

The complex impedance at V_0 is

$$Z_L = R_L + jX_L = |Z_L| \epsilon^{j\theta} \quad (5)$$

where θ is defined as

$$\theta = \tan^{-1}\left(\frac{X_L}{R_L}\right) \quad (6)$$

(Continued on p. 50)

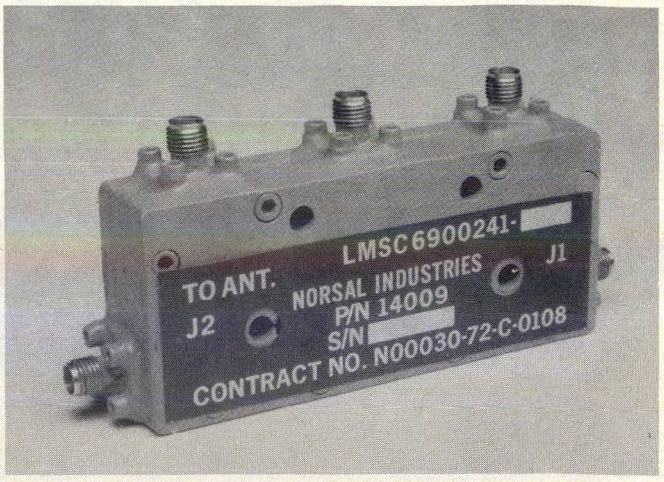

2. Packaged for military environments, *the electronic slotted line measures little more than a quarter-wavelength long at the operating frequency.*

The complex reflection coefficient, Γ, is given by

$$\Gamma = \frac{Z_L - 1}{Z_L + 1} \tag{7}$$

and the standing wave ratio, ρ, is given by

$$\rho = \frac{1 + |\Gamma|}{1 - |\Gamma|} \tag{8}$$

By terminating the impedance measuring device with a matched load, the input power can be determined from V_1, V_2 and V_3 from:

$$P_{in} = \frac{V^2_{max}}{Z_0} \tag{9}$$

where Z_0 is the characteristic impedance of the transmission line. Although the actual voltage cannot be measured, a detector terminating the probes and operating in the square-law region produces a voltage, B_n, such that

$$B_n = \alpha V_n^2 \tag{10}$$

Substituting this in Eqs. (2) and (3) yields

$$X'_L = \frac{B_1 - B_3}{2B_2}$$

$$Z'_L = \frac{B_1 + B_3 - B_2}{B_2} \tag{11}$$

Thus, inputs to a computer can readily be used to determine and print out the load impedance functions.

Designing the IMD

Aside from determining the eighth wavelength spacing, the only other parameter needed to design an IMD is the coupling into the probe lines. The coupling factor is determined by knowing the maximum incident power in the main line and converting it to voltage by

$$V = \frac{P}{Z_0} \tag{12}$$

The peak voltage in the line is assumed to be 2 V since the terminating impedance, Z_L, may be close to an open or short circuit. In either case, the antenna is damaged, but it may only be temporary and to safeguard the diodes, it is best to assume the largest possible voltage on the line.

The coupling factor, K, of the probe line is determined such that the power into the probe will still operate the diode

in the square law region. Since most diodes remain square law up to 100 mW, for an input power of P_0, the coupling factor is determined by

$$K = \sqrt{\frac{4\,P_0}{0.1}} \qquad (13)$$

while the coupling C is given by

$$C = -20 \log K = -10 \log \frac{4P_0}{0.1} \qquad (14)$$

By building a test circuit, the proper probe gap can be determined empirically in a few minutes.

A complete discussion of errors will not be presented here, but only listed to indicate the areas that corrections may have to be made in computer data file.

- Variation of α related to coupling factor of the probes.
- Assumption of 2.0 as law of the crystal.
- Spacing of $(\lambda/8)(1+\delta)$ between probes where δ is the error of placement.
- Error due to probe reflections.

In a normal operation, the first three errors listed above can be held to a minimum by careful manufacturing or calibrated out. Errors due to probe reflections can virtually be neglected if the probe is decoupled by at least 30 dB and care is taken to carefully match the detector. In stripline structures, internal reflections and reradiation can be minimized by use of shorting posts and good matching techniques.

An impedance measuring device such as that described has been built (Fig. 2) and subjected to military qualification testing which it passed. Since the device has no moving parts and is not electrically activated, the reliability of performance is very high and the MTBF approaches that of three microwave detectors.

The major application of the IMD is where size and space is at a premium. The IMD offers a significant advantage over the dual directional coupler (reflectometer) approach in that the complex impedance of the load may be determined rather than just its magnitude. If the load is not at the IMD output but is displaced because of a cable run, the impedance can be rotated back to the actual antenna by means of commonly used transmission line equations. ••

References

1. W. J. Duffin, "Three Probe Method Of Impedance Measurement," *Wireless Engineer*, Vol. 29, pp. 317-320, (December, 1952).

Have You Considered Voltage-Tuned Filters?

Specify voltage-tuned filters at frequencies where YIG-tuning is difficult. Microsecond tuning, compact size and low power consumption are just a few advantages.

FOR years, YIG technology has provided the microwave receiver and instrumentation designer with a convenient source of narrow-bandwidth filters, tunable over a wide range of center frequencies. The VHF and UHF system designer has not been so blessed, however, since YIGs do not offer optimum performance about 500 MHz. Moreover, the bulky driver circuits and high power dissipations required for YIG filters have made them unattractive for many applications where their RF performance is adequate.

The development of high-quality varactor diodes in recent years, stimulated primarily by the need for compact voltage-tuned oscillators, has made possible high-performance voltage-tuned filters (VTFs) and voltage-tuned "supercomponents," such as receiver front ends. Systems designers now have available voltage-tuned filters from HF through low microwave frequencies that have high-performance RF characteristics, compact size and low-power driver requirements.

Voltage-tuned filters have found applications in consumer electronics such as TV sets and high-fidelity tuners and the advent of frequency agile defense electronics has stimulated the use of voltage-tuned filters in military systems. Some examples include the receiver front-end in the ARN-118 Tacan set, the preselector and synthesizer "clean-up" filters in the ARC-143 tactical radio and in surveillance receivers such as the WJ-8940. Novel ECM IF signal processing schemes have also been implemented by using banks of matched VTFs. Considerable size, weight and cost savings have been affected where switched banks of fixed-tuned filters have been replaced by a one cubic-inch VTF.

The voltage-tuned filter is a filter whose center frequency can be varied by the application of a tuning voltage. Simply put, the VTF is a filter, lumped or distributed, in which some or all of the capacitors have been replaced by varactor diodes, as shown in Fig. 1.

What can be achieved with a voltage-tuned filter? Performance characteristics are summarized in simplified form in Table 1. These characteristics primarily relate to wide tuning range filters, and represent moderate performance filters, not the highest state-of-the-art filters possible. For example, microwave VTFs above 2 GHz are feasible, although not in octave tuning ranges. Also, filters of more than four sections are possible, again not in octave ranges. Let's examine some of the more important characteristics individually.

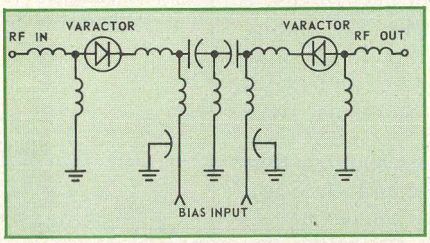

1. Varactors replace capacitors *in a voltage-tuned filter.*

Table 1:
Typical VTF performance

Center Frequencies	10-2000 MHz
Tuning Range:	Up to one octave
Tuning Voltage:	1 to 55 VDC typical
Tuning Current:	<2μA typical
Tuning Speed:	Less than 10μ secs.
Bandwidth:	2% to 10% of center frequency (constant % bandwidth)
Insertion Loss:	2-10 dB
Filter Response:	1-4 section
RF VSWR:	2:1 (50 ohm system)
1 dB Compression Point:	>0 dBm (depends on tuning voltage)

Choose a tuning voltage

Octave tuning ranges are possible in VTFs using abrupt-junction diodes, the diode most commonly used for low-loss, high-frequency VTFs. The diode's reverse breakdown voltage sets the upper tuning voltage limit. The most commonly available diodes are specified for 60, 45 and 30-volt breakdowns. Typical frequency versus voltage plots are shown in Fig. 2 for 25, 40 and 55-volt (curves (a), (b), (c), respectively) maximum tuning voltages. These limits allow a 5-volt guard band below the typical specified breakdown voltages. A 60-volt diode is normally used for octave tuning.

When tuning ranges of less than an octave are required, the system designer has more latitude in selecting a tuning-voltage swing. Curve (d) of Fig. 2 is useful for determining the voltage swing necessary to tune a desired range. For example, if a tuning range of 960 to 1225 MHz (the Tacan range) must be covered, the frequency ratio is 960/1225 = 0.78 and, from Fig. 2, the required voltage ratio is about 25/100 = 0.25. Thus, if a 40-volt supply is

(continued on p. 54)

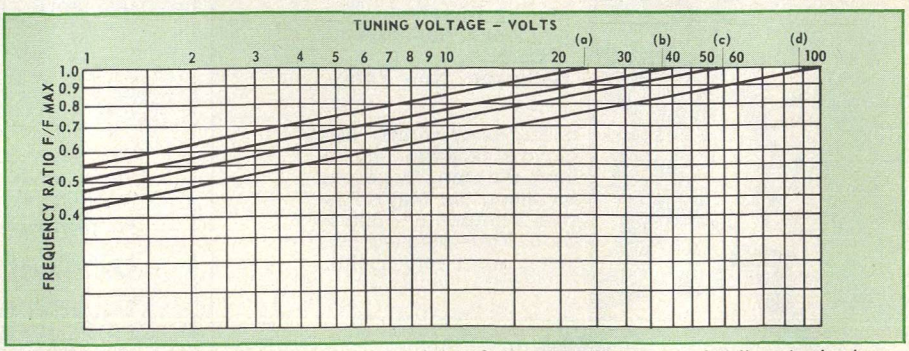

2. Tuning curves *are shown for 25 (a), 40 (b), 55 (c) and 100 (d) volt devices.*

Jim Fuchs, Manager of Solid State Products, Acronetics, 955 Benicia Avenue, Sunnyvale, CA 94086.

available, the voltage swing will be 0.25 (40), or 10 volts to 40 volts.

Keep in mind that intermodulation distortion and loss are better at high tuning voltages. Thus, when these parameters are important, the designer should specify as high a tuning voltage as is possible. Distortion increases as the RF voltage levels within the VTF become comparable to varactor back bias voltage; thus, distortion is greatest at low tuning voltages. The insertion loss of octave bandwidth filters is generally highest at the low end of the tuning range due to reduced varactor Q.

In applications where the available tuning voltage is low, hyper-abrupt diodes can be used to achieve wide tuning ranges with smaller tuning voltage swings. Octave tuning ranges can be achieved with 30-volt tuning voltage swings. Insertion loss and distortion performance are generally poorer in these designs.

It should be noted that the tuning voltage port of the VTF consumes virtually no power. Leakage currents of 2 μA are typical; thus relatively simple driver circuits are adequate. Excessively high driver impedances ($\leq$100kΩ) should be avoided, however. For example, a 100kΩ driver impedance and a 2 μA leakage current will cause a 0.2-volt shift in tuning voltage and noticeable tuning errors at low voltages. Tuning speed is also dependent on driver impedance, as is discussed later.

A look at linearity

The tuning curves shown in Fig. 2 can be used to predict frequency versus voltage variations and determine tuning linearity. Frequency varies with voltage approximately according to

$f = k\,V^{n/2}$ where $k = \dfrac{f_1}{V_1^{\,n/2}}$

$n = 0.374$, typically.

The slope of the curve at any tuning voltage is

$$m = \frac{kn}{2} V^{n/2-1}$$

and the ratio of the slopes at any two tuning voltages is

$$m_1/m_2 = \left(\frac{V_2}{V_1}\right)^{n/2-1}$$

Thus, an octave-tuning VTF tuning between 1.35 volts and 55 volts will show about a 20:1 change in slope across the band. Tuning linearity, as indicated by the frequency deviation from a best-fit straight line, is shown as a function of frequency range in Fig. 3. Tuning linearity for an octave filter is about $\pm$10 per cent and for a "half-octave" filter ($f_1/f_2 = 0.71$), the linearity is about $\pm$4 per cent.

If better tuning linearity is required, linearizers using diode breakpoints can be incorporated into the VTF. This approach can lead to typical linearities of about 2 per cent.

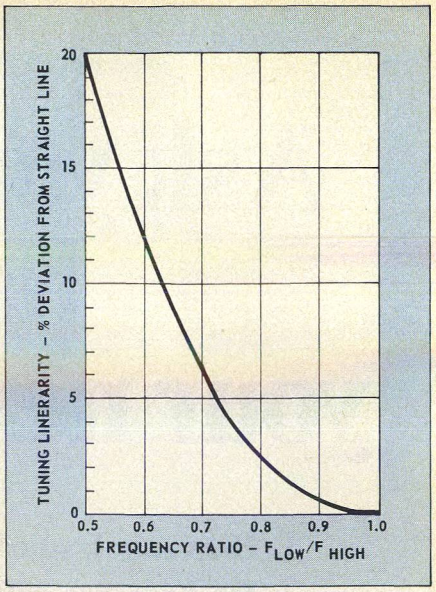

***3. Tuning linearity** can be predicted once bandwidth is known.*

Interestingly, the tuning linearity of a VTF is far less critical than that of a VCO. The major requirement for most VTF applications is that the filter pass the desired signal and its information at a predetermined tuning voltage, and simultaneously reject undesired signals. If the bandwidth of the VTF is adequately wide to pass the desired signals and account for filter frequency drift and tuning nonlinearities, linearization requirements are eased considerably.

When specifying the tuning curve, the desired voltage range should be specified. If a quantity of filters require tuning curve repeatability, specify that the passband and stopband specifications be met by all filters for the same tuning curve. Only as a last resort should the center frequency versus voltage be specified, as the time to align, track and test a quantity of VTFs to a particular curve is extensive. The VTF tuning curve exhibits no noticeable hysteresis, unlike magnetically tuned filters such as YIG filters.

The specifier should also take care not to over-estimate rejection; a multiple-pole filter (three or four sections) is considerably more difficult and expensive to track than a two-pole filter. The basic design prototype used for most VTFs is a maximally flat amplitude response. A typical design uses a coupling technique that results in better rejection on the lower skirts than on the upper skirts. For a two-pole filter, the 30 dB rejection points will fall approximately at f_o [1 – 0.025 (%BW)] and f_o [1 + 0.035 (%BW)]. Some improvement in rejection can be made by special techniques that add rejection points on the high skirt.

What limits tuning speed

VTFs of the type described in this article can be tuned from one frequency to another in a few microseconds. This is a highly desirable feature in many modern frequency agile systems. One constraint on tuning response to a step in tuning voltage is the response time of the VTF bias circuitry, which is partially dependent on the impedance of the runing voltage source. The second and ultimate constraint on tuning speed is the RF bandwidth of the VTF.

Bias circuitry characteristics usually limit tuning speed. Generally, VTFs have bypassing and blocking circuits in the tuning lines to suppress both incoming and outgoing noise on the tuning line. For applications requiring especially fast tuning, the bias circuitry can be designed to maximize tuning speed.

The system designer should be aware that a relatively low impedance driver circuit (e. g., 50 ohms) will be necessary to achieve very fast tuning speeds. For non-critical applications, the designer can assume the tuning line will appear approximately as a 1000 pF load. The tuning speed is then set by the RC time constant of the driver impedance and the 1000 pF load.

The ultimate limit on tuning speed is the VTF's RF bandwidth. The rule of thumb for the rise time response to a tuning voltage step is

$$t_r = \frac{35}{(\%BW)f_o}.$$

Thus, for example, in a 100 MHz VTF with a 5 per cent bandwidth, minimum risetime is 70 nsec. RF time delay, also contributes to total settling time. The delay time for the example just cited would be about 90 nsec; thus the total settling time for the filter described is about 150 nsec minimum.

Phase or time delay characteristics are important in many receiver applications. The phase variations across the filter passband are approximately the same as a comparable fixed tuned Butterworth filter.

For a constant percentage bandwidth VTF, center frequency time delay will vary with center frequency. For two-pole VTFs, the center frequency time delay,

$$t_d = \frac{45}{(\%BW)f_o}.$$

For example, a 5 per cent bandwidth filter at 150 MHz will have a center frequency time delay of about 60 nsec, while at 300 MHz the same filter will have a 30 nsec delay. Delay variations across the 3 dB pass band of two-pole VTF are about 20 per cent of the center frequency delay. ••

Select The Best Diode For Millimeter Mixers

Comparing Schottky-barrier mixer diodes? Consider package parasitics and take a close look at DC parameters. R_s, C_o and η all provide useful clues to a diode's RF performance.

LOW-noise front ends for millimeter-wave systems are in increasing demand for a variety of applications ranging from high data-rate communications terminals to radiometry. Because of a scarcity of high-frequency pump sources, the staple low-noise front end, the parametric amplifier is difficult to apply above 40 GHz. Thus, much effort has been invested in developing low-noise mixers for the millimeter bands.

Results to date have been extremely encouraging, and quite remarkable performance has been achieved even for mixers operating at the upper bands. For instance, room temperature mixers for radio astronomy applications have demonstrated conversion losses as low as 4.6 dB at 85 GHz[1] and 6.5 dB at 140 GHz[2].

The heart of these mixers is the ultra-low capacitance Schottky-barrier diode. Since the tiny dimensions of components at these frequencies generally preclude sophisticated circuit design, it can be said that by and large, mixer performance at millimeter wavelengths is directly dependent on the quality of the semiconductor device. Selecting the best diode for a given mixer design can, however, be a confusing experience for the designer, who is faced with a bewildering array of often ill-defined RF performance data. It is usually extremely difficult to decide which is the best available device for the job at hand.

It is now well established that DC parameters such as spreading resistance (R_s), zero bias capacitance (C_o) and quality factor (η) can be used to give an extremely good indication of the relative quality of the RF performance of various diodes. R_s and C_o are specified in ohms and picofarads, respectively, while η is a dimensionless parameter which appears in the current-voltage relationship:

$$I = I_0 [\exp (qV/\eta kT) - 1]$$

This quality factor, with a magnitude of close to or greater than unity, was originally introduced to explain deviations from an ideal conducting process. Such deviations may arise from the possible presence of a dielectric layer at the interface of the metal and the semiconductor forming the Schottky barrier.

Dr. Gerard T. Wrixon, Director, European Millimeter Diode Laboratory, Department of Electrical Engineering, University College, Cork, Ireland.

Pay close attention to η

For different diodes in the same circuit configurations, conversion loss depends principally on the values of R_s and C_o, while η to a very large extent determines what the diode noise performance is going to be. In practice, except at the highest frequencies, it is usually not too difficult to obtain a diode with a sufficiently high cut-off frequency ($f_c = 1/2\pi R_S C_O$) to ensure reasonably low conversion loss. It is a different story, however, when it comes to η. The small size of low-capacitance millimeter diodes complicates the task of obtaining a metal-semiconductor interface completely free of any contaminating layer. Thus, in many cases, η will be much larger than its ideal value of unity.

The importance of η in determining the noise performance of a diode can be seen when we consider that the main sources of noise in a Schottky diode are shot noise from current flowing across the depletion region and thermal noise from the spreading resistance R_s. For a diode at room temperature, the shot noise contribution is by far the greater. It is possible to model this shot noise by assuming that the diode junction conductance is at an equivalent temperature T_{eq}, such that the resulting thermal noise has the same magnitude as the shot noise. This gives

$$T_{eq} = \eta \frac{T}{2} \qquad (1)$$

where T is the ambient temperature.

Equation (1) shows the physical significance of η in determing the *sensitivity* of the diode. Thus, the quality factor is an important diode parameter and its value should be specified when a particular diode is being described by a manufacturer. In general, its value should be as close to unity as possible; however, as mentioned above, this is difficult to achieve as the diode diameter gets smaller. For diodes operating at millimeter wavelengths (diameter $\leqq 5\ \mu m$), values of $\eta \leqq 1.18$ measured at room temperature are acceptable. The magnitude of η depends heavily on the attention given to semiconductor surface preparation during manufacturing, and a value of greater than 1.2 is evidence that the diode manufacturer does not have his processing technique under full control.

Measure η after bonding

It is a simple matter to measure η and such a measurement should always be carried out to check new diodes. It is also very useful to carry out the measurement after soldering or bonding a diode into a circuit in order to check if the diode has been overheated or damaged in the process, as more often than not, η will be the first diode parameter to degrade due to overheating.

To measure η at room temperature, simply measure the voltage across the diode at forward currents of 10 μA and 100 μA. Then to a good approximation

$$\eta = (V_{100\mu A} - V_{10\mu A})\ 16.82. \qquad (2)$$

If the voltage is also measured at forward currents of 1 mA and 10 mA, then the value of R_s can also be calculated from

$$R_s = 100\ [(V_{10mA} - V_{1mA}) - (V_{100\mu A} - V_{10\mu A})]. \qquad (3)$$

Equation (1) also suggests that if the diode ambient temperature were reduced, then the noise output of the diode would decrease linearly with temperature. Because of the fact that the thermionic emission process is not the correct model for conduction in a Schottky diode at reduced temperatures, it is indeed found that T_{eq}

(continued on p. 58)

SELECT THE BEST DIODE

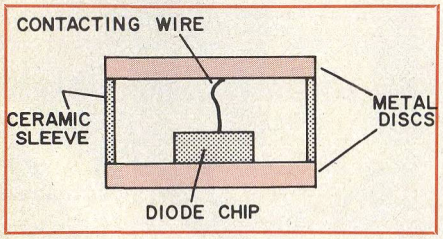

***1. The pill package** is rugged, but presents rather high capacitance.*

decreases with T, but not linearly. Mixers built for radio astronomy at 35 and 115 GHz have shown a reduction in noise temperature of about 2 to 2.5 on being cooled from 290°K to 77°K, while conversion loss remained essentially constant. A room temperature measurement of η is, however, a good qualitive indication of how well a certain diode "cools", in that a low η at room temperature correlates well with a larger cooling factor.

Package capacitance also important

Diode packaging is another important consideration for the mixer designer, since it usually sets a lower limit on the diode's zero bias capacitance, thus effectively limiting cut-off frequency. At millimeter wavelengths, the three most common packages are the pill, beam-lead and Sharpless wafer. Performance of respective mixers built with these types of commercially available diodes is summarized in Table 1.

Of the three, the pill package shown in Fig. 1 is the most rugged. With this packaging method, which is favored by Texas Instruments and Hitachi, the diode chip is soldered on a metal disk and is contacted by an etched wire which is soldered or bonded to a similarly shaped disk. The disks are held together by a cylindrical ceramic sleeve, relieving the contact wire of mechanical strain.

A pill package can be conveniently used in conventional waveguide circuits, but presents two main disad-

Table 1: Mixer performance with commercially available diodes

Diode type and manufacturer	Mixer manufacturer	SSB conversion loss (dB)	Noise ratio (t)	Measured DSB noise figure (dB)	Frequency range (GHz)
Sharpless wafer *Hughes Aircraft*	*Hughes Aircraft*	6.5-7.0 max	—		26.5-70
Sharpless wafer *CDC*	*CDC*	6.0 typ. 7.5 max	1.2 typ. 1.4 max	5.5 dB @ 35 GHz with $N_{i\text{-}f}$ = 1.5 dB	33-60
Pill package *Texas Instruments*	*SpaceKom*	5.0-6.0 typ.	—	4 dB @ 45 GHz 5 dB @ 60 GHz with $N_{i\text{-}f}$ = 2.0 dB	30-60
Beam-lead *AEI Semiconductor*	*Bell Telephone Labs*	4.5	—		60
Beam-lead *AEI Semiconductor*	*AEI Semiconductor*	—	—	90 dB @ 60 GHz with $N_{i\text{-}f}$ = 5.0 dB	60

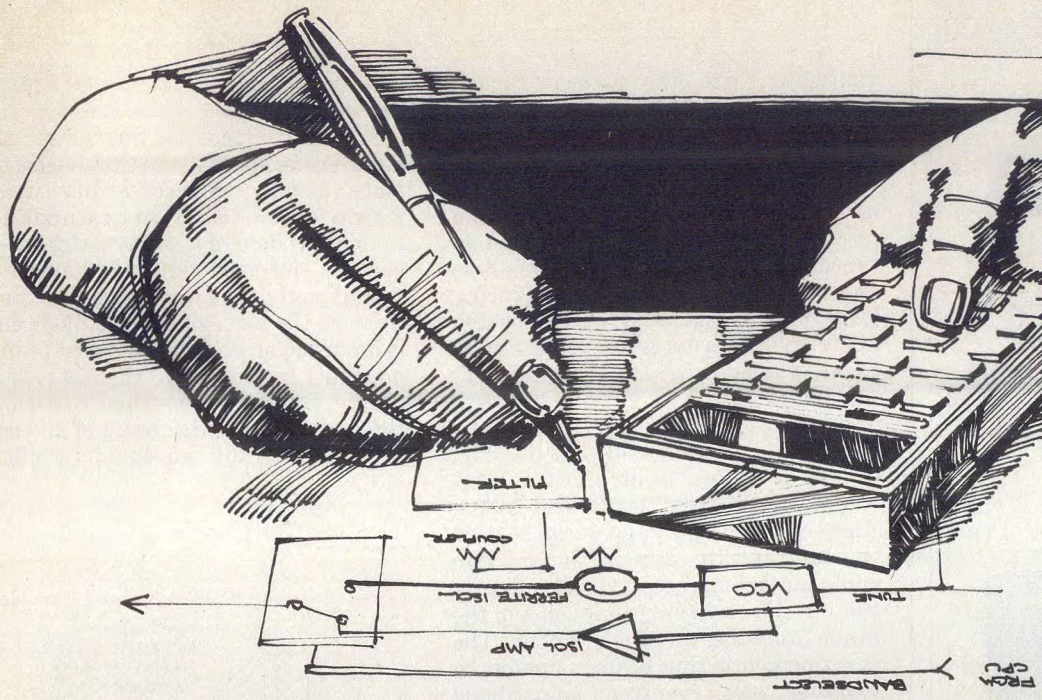

Before you commit to an EW hardware design talk to us.

Here's why.

When it comes to VCO subsystems for ECM and ESM applications, our capabilities extend from sophisticated semiconductors through microwave circuit designs and into the digital/analog and thermal interface. This means that our hardware is not compromised by non-contiguous interfaces, package parasitics and other problems associated with building block designs. We're a total supplier...a single source that understands your needs and can deliver better performance at lower "life cycle" cost.

And we haven't overlooked true reliability, either. Advanced screening techniques, computer aided design and all of the program management techniques that you have wanted, we've got it all. The best way to make sure of getting the optimum energy source for your ECM design is to talk to one of our engineers about it. They speak your language. When you work with Litton, nothing gets lost in the translation of your design to a system that really performs.

The man to talk to here is Al Smith. Write or call him while your design is still in the thinking or talking stage. Electron Tube Division, 960 Industrial Road, San Carlos, CA 94070. (415) 591-8411.

Litton ELECTRON TUBE DIVISION

READER SERVICE NUMBER 59

vantages. First, the package capacitance is quite high, about 0.06 pF, even for the smallest packages. This essentially means that above 50 GHz, conversion loss begins to degrade. Second, as a practical matter, it does not seem possible to make the length (inductance) of the contact wire as small as one would desire. Apart from inducing large back voltages and thereby risking diode failure, a large inductance may make optimum RF matching difficult to achieve.[1].

Beam-lead packaging, as used by AEI Semiconductor and shown in Fig. 2, was developed in an effort to overcome the inherent large lead inductance of the pill package. It can be used in microstrip applications. Two coplanar beams are formed, one contacting the rectifying junction and the other providing an ohmic contact. The junction contacting beam, as might be expected, gives rise to an unavoidable overlay capacitance of 0.02 to 0.05 pF. In an effort to reduce this, diode manufacturers have endeavored to make the area of the device's beam-lead contact smaller and smaller. But this has given rise to mounting problems since the fragile leads may easily break off a diode while it is being bonded into a circuit.

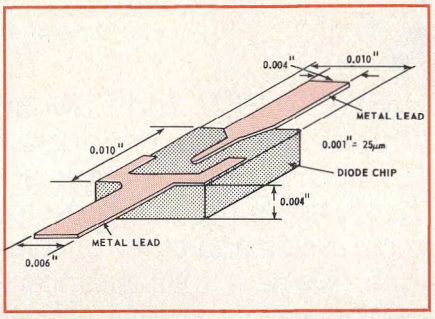

***2. Beam-lead packages** are fragile, since lead contact is made small to minimize capacitance.*

In manufacturing this kind of diode, a thermo-compression bond is used to connect the diode metallizations to the beam lead. Thus, it might be difficult to use this packaging method with diodes where the diameter is less than about 5 μm. However, by that stage, the beam overlay capacitiance would already dominate junction capacitance.

The Sharpless wafer mount shown in Fig. 3 has essentially no parasitic capacitance, hence, its use is favored when good conversion loss performance is required above 60 to 70 GHz. Its main drawback is its lack of ruggedness, due to a tiny spring whisker contact which presses against the diode.

First introduced by Sharpless[3], the mount consists of a waveguide-size (or more usually, *reduced-height* waveguide-size to help impedance matching) hole in a metal wafer which can be inserted into a waveguide mount so that the waveguide hole lines up with the waveguide. The diode chip is mounted on an insulated post (which normally forms part of the low pass IF output filter) so that when fitted into the wafer, the diode on top of the post projects into the waveguide window.

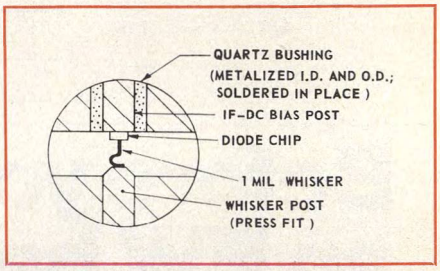

***3. The Sharpless wafer mount** is designed for waveguide circuits. Whisker makes pressure contact.*

The diode is contacted by a means of an etched spring-shaped whisker soldered to another post which projects into the window from the opposite side.

The excess capacitance introduced by this mounting method has been calculated to be about 0.001 pF[4], and thus for all practical purposes, is negligible. The contacting whisker can also be made extremely short with this method, minimizing inductance. In spite of mechanical problems, the wafer mount has offered the best mixer performance to date at millimeter wavelengths, for both cooled and uncooled mixers, and looks to be the most effective in the long run, especially where optimum conversion loss is required above 90 GHz. ••

References

1. A. R. Kerr, "Low-Noice Room Temperature and Cryogenic Mixers For 80-120 GHz," *IEEE Trans. Microwave Theory and Techniques*, Vol. MTT-23, No. 10, pp. 781-787, (October, 1975).
2. G. T. Wrixon, "Low-Noise Diodes and Mixers For The 1-2 Mm Wavelength Region", *IEEE Trans. Microwave Theory and Techniques*, Vol. MTT-22, No. 12, pp. 1159-1165, (December, 1974).
3. W. M. Sharpless, "Wafer-Type Millimeter Wave Rectifiers," *Bell System Technical Journal*, Vol. 35, pp. 1385-1402, (November, 1956).
4. J. Edrich, "A Coolable Degenerate Parametric Amplifier For Millimeter Waves," *IEEE Trans. Microwave Theory and Techniques*, Vol. MTT-22, No. 5, pp. 581-583, (May, 1974).
5. M. V. Schneider—Private Communications.

OCTOBER
1976

MICROWAVES

laser technology

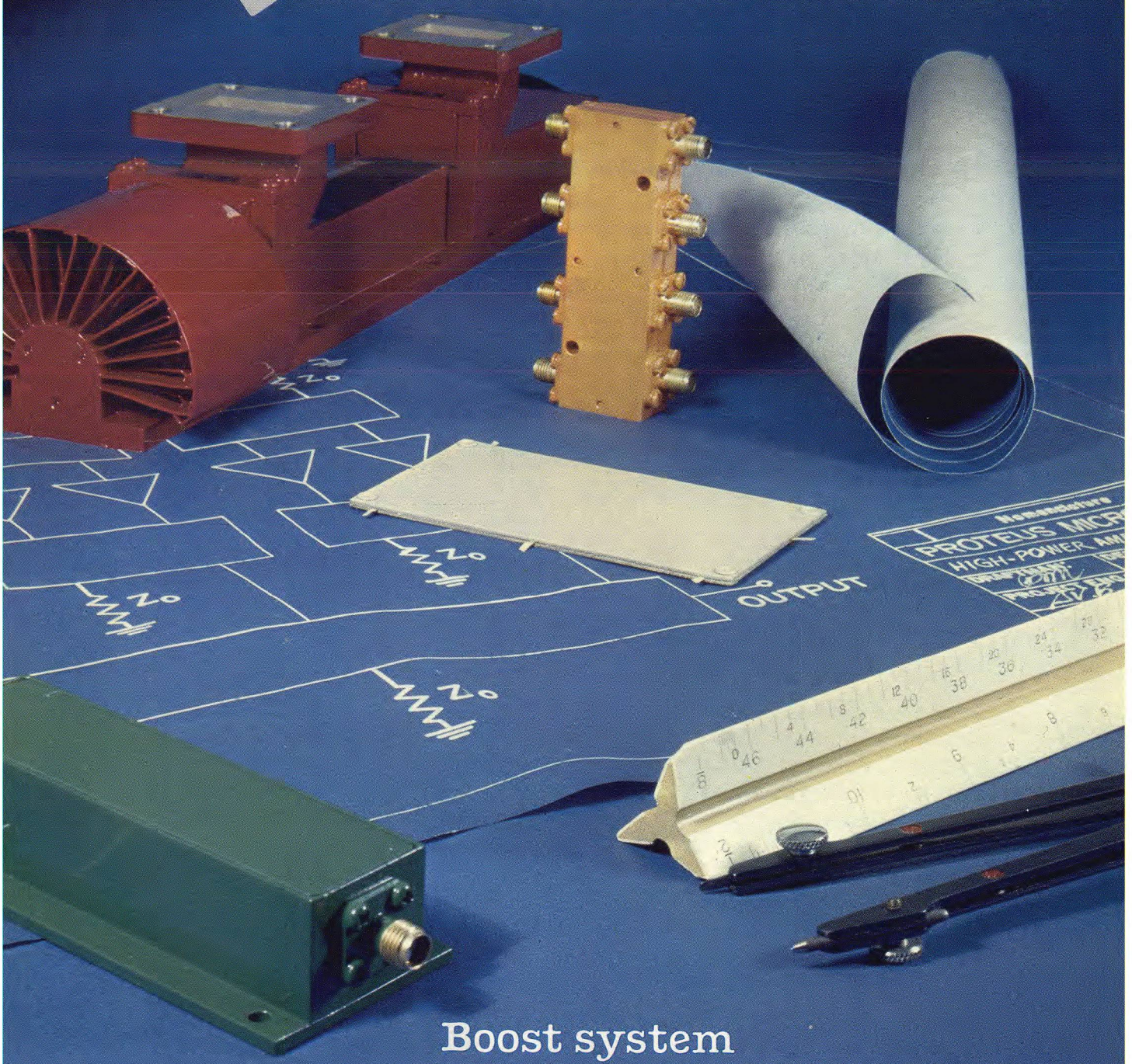

Boost system efficiency and power with amplifier arrays

- MEASURE AND INTERPRET TWT PHASE DATA TO OPTIMIZE POWER
- USE SERIAL FEED ARRAYS FOR GREATER VERSATILITY

O:

IGN HIGH-EFFICIENCY X-BAND AMPS • MICROWAVE HEATING: NEW TOOL FOR CANCER RESEARCHERS

MICROWAVES

October 1976
Vol. 15, No. 9

news

editorial

technical

Amplifiers

departments

About the cover: Whether they are tube or transistor, amplifiers pack a bigger punch when teamed up in an array. Components courtesy of Varian and Merrimac. Photograph by Robert Meehan.

coming next month: International Update

A first-hand look at the underlying currenuts in European microwave technology will highlight the November issue. The detailed report, compiled by Publisher/Editor Howard Bierman, will focus on recent visits to major European firms and on announcements made at September's European Microwave Conference.

Technical articles will include:

Spectrum Conservation Key To North Sea Troposcatter Network. Congested spectrum and wide signal length variations play havoc on the North Sea tropo systems. The article examines the network requirements and design tradeoffs to acheive spectrum economy and optimum reliability.

Realize Dolph-Chebyshev Arrays In Microstrip. Dolph-Chebyshev arrays offer advantages of constant, low sidelobe levels and narrow beamwidths. Realized in microstrip, the arrays can be fabricated on a compact circuit board.

Publisher/Editor
Howard Bierman

Managing Editor
Stacy V. Bearse

Associate Editor
George R. Davis

West Coast Editor
Jose C. De León
Hayden Publishing Co.
744-R Coleman Avenue
Menlo Park, CA 94025
(415) 325-8280

Washington Editor
Paul Harris
Snyder Associates
1050 Potomac St. NW
Washington, DC 20007
(202) 965-3700

Contributing Editor
Harvey J. Hindin

Editorial Assistant
Gail Murphy

Production Editor
Sherry Lynne Karpen

Art Director
Robert Meehan

Production
Dollie S. Viebig, Mgr.
Sandra N. Bowen

Circulation
Barbara Freundlich, Dir.
Trish Edelmann
Sherry Karpen,
Reader Service

Directory Coordinator
Janice Tapp

Editorial Office
50 Essex St.,
Rochelle Park, NJ 07662
Phone (201) 843-0550
TWX 710-990-5071

A Hayden Publication
James S. Mulholland, Jr.,
President

MICROWAVES is sent free to individuals actively engaged in microwave work. Subscription prices for non-qualified copies:

	1 Yr.	2 Yr.	3 Yr.	Single Copy
U.S.	$15	$25	$35	$2.50
FOREIGN	$20	$35	$50	$2.50

Additional Product Data Directory reference issue, $10.00 each (U.S.), $18.00, (Foreign), POSTMASTER, please send Form 3579 to Fulfillment Manager, MicroWaves, P.O. Box 13801, Philadelphia, PA. 19101.

Back Issues of MicroWaves are available on microfilm, microfiche, 16mm or 35mm roll film. They can be ordered from Xerox University Microfilms, 300 North Zeeb Road, Ann Arbor, MI 48106. For immediate information, call (313) 761-4700.

Hayden Publishing Co., Inc., James S. Mulholland, President, printed at Brown Printing Co., Inc., Waseca, MN.

Combining Amplifiers? Try Serial-Feed Arrays

Serial-feed arrays offer a powerful alternative to binary combining schemes. Smaller size, lower cost and the ability to use the minimum number of amplifiers are a few advantages.

SERIAL-feed amplifier arrays are rapidly gaining attention as system designers search for an economical alternative to hybrid-coupled binary arrays. The reason: For small power incrementation over an existing binary design, it is much cheaper to add one or two amplifier stages than to add an entire new binary tier of amplifiers and couplers.

To retain symmetry, a designer must double the number of amplifiers in a binary array system, whenever *any* increase in power is required. Serial-feed systems can combine any number of amplifiers, odd or even. It's easy to see that a strict binary approach is at a distinct economic disadvantage when a power incrementation of less than a factor of two is desired.

For example, a serial array of five amplifiers will produce a 25 per cent increase in power output over a binary array of four amplifiers (see Fig. 1). In a pure binary system, eight amplifiers must be used to gain any additional increase in power over four. Clearly, if only a 10 or 20 per cent power increase over the existing design is required, the addition of four more amplifiers, plus a number of 3-dB couplers, is considerably more expensive than necessary.

In addition to the savings in amplifier and coupler costs, other obvious advantages of serial feed arrays are smaller packaging, power supply and driver requirements. It should be noted that for even greater flexibility, serial feeds of different orders can be combined to suit nearly any power distribution or collection need.

What are serial feeds?

Serial feed systems are no more than a tandem set of series-connected quadrature couplers providing sequential output ports of essentially equal output voltages. The major advantage of this form of arraying lies in its inherent ability to produce non-binary division. Thus, a system of three (consisting of 4.77 and 3-dB couplers) produces an array of three divisions and collections with center frequency differential phases of 0, -90 and −180 degrees. A system of four would add a 6-dB coupler to the input of a system of three, while a system of five would add a 7-dB coupler to the input of a system of four; each additional drop produces an additional −90 degrees of phase length at the center frequency.

Conventional systems consist of a series-connected set of quarter-wavelength couplers, each coupler having a different coupling value, as shown in Fig. 2. The difficulties here are multifold. First, each coupler must have a different coupling value. Thus, the geometry of each coupler must be different, since the even-mode impedance Z_e must change when the coupling changes.

Joseph Cappucci, Vice President, Merrimac Industries, Inc., 41 Fairfield Place, West Caldwell, NJ 07006.

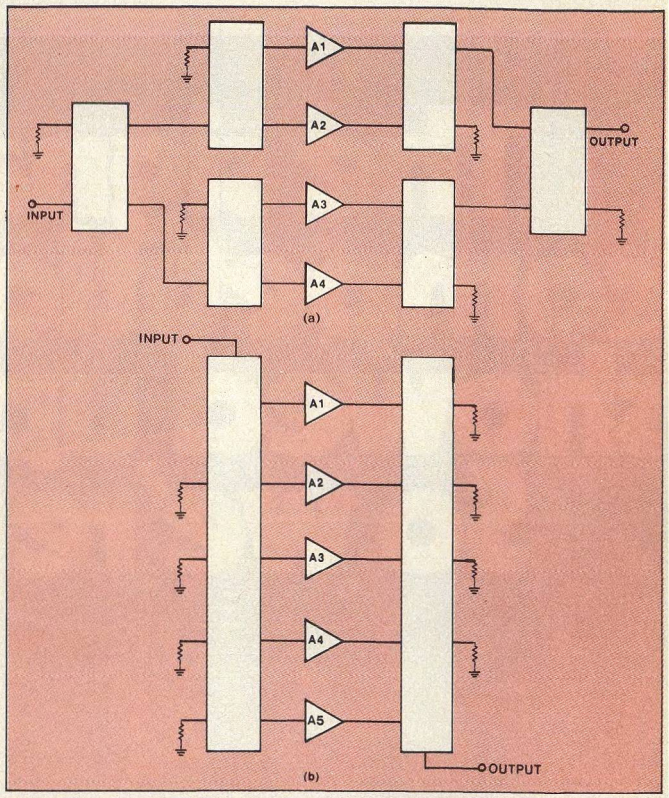

***1. Binary arrays (a)** may only be enlarged by doubling the number of amplifiers. **Serial arrays (b)** can combine any number of amplifiers; the same type of array can be used to divide power by rotating it 180 degrees.*

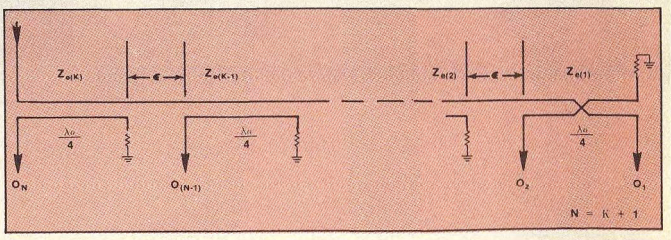

***2. Conventional serial feeds** consist of quarter-wavelength couplers.*

Secondly, there must be some interconnecting length, ϵ, between each coupler which must be added to the output ports to re-equalize the phasing. All of the outputs, except the last 3-dB coupler, must have a length (K-2) (ϵ) added

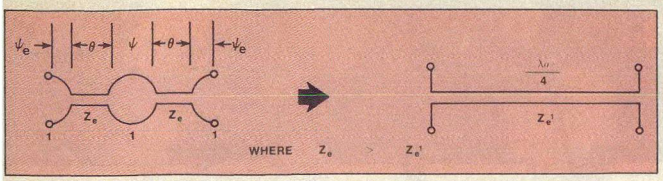

***3. Two-section couplers** respond as quarter-wavelength couplers, yet offer several advantages over the traditional designs.*

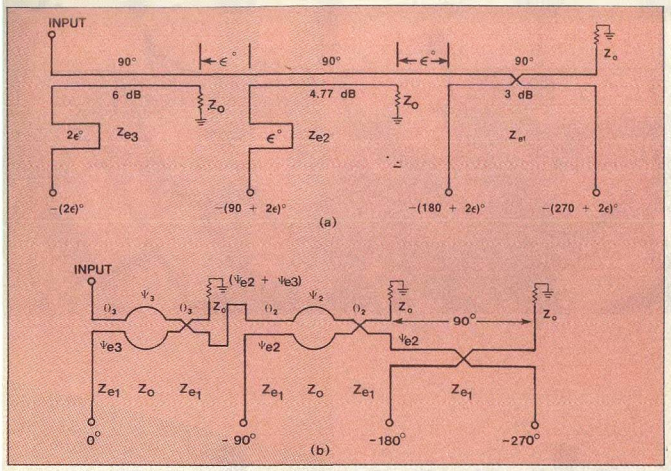

***4. A conventional quarter-wavelength design** to couple four amplifiers (a) requires terminations on both sides of the array. A two-section coupler approach (b) nicely separates amplifiers and loads.*

to the output length to produce the correct phase sequence (K is the serial position of the coupler in the array). These additional lengths produce additional loss which is detrimental to array performance.

Finally, all but one of the idler resistors terminating the couplers are on the output side of the array, usually forcing the interconnecting lengths to be longer than necessary from a geometrical point of view, because room has to be made available for these terminations.

Most of these difficulties can be avoided, however, through the use of two-section couplers.*A two-section coupler simply consists of two sets of coupled lines interconnected by short lengths of uncoupled lines. The amplitude response of a two-section coupler can be made equivalent to that of a quarter-wavelength coupler if the two functions are synthesized to be both stationary and equal-valued at their center frequency. In addition, phase equivalence can be obtained between the two structures by adding short lengths of uncoupled lines to the terminal ports of the coupler. The equivalent structures are shown in Fig. 3.

The use of two-section couplers as coupling elements has the following advantages:

- A common coupled impedance is used throughout the structure, resulting in a single coupled geometry for the entire system.
- Physical crossovers are easily achieved in tightly coupled systems of lines so that all terminations can be placed on the input side of the array.

*The reader is referred to U. S. Patent No. 3,761,843, J. Cappucci, September 25, 1973, for a full discussion of the two-section coupler. The synthesis is discussed in detail in the appendix.

- The interconnecting lengths between couplers can be made equal to the phase compensation needed at the ends of the two-section couplers, so that the excess phase lengths can be minimized.

Quarter-wavelength and two-section coupler serial-feed systems designed to combine four amplifiers are compared in Fig. 4.

Consider some limitations

Serial-feed arrays are not a cure-all; they are restricted by many of the inherent limitations that characterize all systems of couplers. In evaluating some of these difficulties, we will consider the quarter-wavelength type, which is typical and easiest to analyze.

To begin with, serial feeds suffer from amplitude unbalance with frequency, a problem that is characteristic of all quarter-wavelength couplers. But amplitude deviation is no worse, or no better, than a binary array of 3-dB couplers. For example, a three-way serial combiner would have a smaller amplitude deviation than a binary system of four, and a larger deviation than a binary system of two amplifiers.

Secondly, since they are tandem systems, serial-feed insertion losses add as the signal progresses down the array. Coupling must be adjusted to equalize these losses.

The final, and probably most severe problem is the inequality of delay through the couplers. The phase shift, β, through each coupler is given by:

$$\beta\ (\omega) = -\tan^{-1}\left[\left(\frac{Z_e + 1/Z_e}{2}\right)\tan\left(\frac{\pi}{2}\omega\right)\right]$$

At $\omega=1$, the phase shift is always equal to -90 degrees. However, the derivative of $\beta\ (\omega)$ with respect to ω is not a constant:

$$\frac{d\beta\ (\omega)}{d\omega} = \frac{-\pi}{2}$$

$$\left[\frac{1}{\left(\frac{2}{Z_e + 1/Z_e}\right)\cos^2\left(\frac{\pi}{2}\omega\right) + \left(\frac{Z_e + 1/Z_e}{2}\right)\sin^2\left(\frac{\pi}{2}\omega\right)}\right]$$

At $\omega = 1$,

$$\frac{d\beta(1)}{d\omega} = \frac{-\pi}{(Z_e+1/Z_e)}.$$

Since Z_e changes with each coupler, the delay is different for each coupling drop, producing collection errors for bandwidths greater than zero. The largest error is always produced in the last two couplers (3 and 4.77 dB) since they have the greatest change in Z_e .

This collection error is not large for most applications, but it is greater than that encountered in binary arrays. Table 1 shows the calculated performance of serial-feed arrays of three, four and five divisions, and binary-feed arrays of two, four and eight divisions for bandwidths ranging from 10 to 70 per cent. As can be seen from comparing the four-feed case, the major difference between the two schemes lies in the higher collection losses of serial feed systems. There is little difference in the amplitude balance between the two array types.

Another dissimilarity between the binary and serial feed arrays lies in the cancellation of common amplifier reflections. To first order (within the amplitude unbalance), a binary feed system tends to cancel common input reflections due to amplifier mismatch. The same is true for serial feeds, so long as n is an even-ordered division.

(continued on page 40)

Table 1: Calculated performance of binary and serial arrays

Binary array

Bandwidth (%)	N=2 Collection loss (dB)	N=2 Split deviation (dB)	N=4 Collection loss (dB)	N=4 Split deviation (dB)	N=8 Collection loss (dB)	N=8 Split deviation (dB)
10	.00001	±.0067	.00002	±.0134	.00003	±.0201
20	.00017	±.027	.00033	±.054	.0005	±.081
30	.00085	±.061	.0017	±.122	.0026	±.183
40	.0027	±.109	.0055	±.218	.0082	±.327
50	.0068	±.172	.0136	±.344	.0204	±.516
60	.0145	±.251	.0289	±.501	.0434	±.752
70	.0276	±.346	.0551	±.692	.0827	±1.039

Serial array

Bandwidth (%)	N=3 Collection loss (dB)	N=3 Split deviation (dB)	N=4 Collection loss (dB)	N=4 Split deviation (dB)	N=5 Collection loss (dB)	N=5 Split deviation (dB)
10	.0030	±.011	.0045	±.014	.0055	±.016
20	.0122	±.044	.0186	±.056	.0223	±.065
30	.0285	±.101	.0433	±.128	.0519	±.148
40	.0530	±.181	.0805	±.231	.0967	±.268
50	.0879	±.287	.1334	±.368	.1555	±.404
60	.1361	±.420	.2066	±.540	.2498	±.628
70	.2015	±.583	.3065	±.753	.3724	±.876

When the serial-feed array is an odd-ordered division, the input reflection, to first order, becomes (Γ/n) due to incomplete cancellation of the amplifier reflections, Γ being the magnitude of the amplifier reflection, and n the number of divisions in the array.

Compare copper losses

A not-so-obvious advantage of serial feeds is reduced copper losses, due to the smaller coupling value necessary at the array input.

To first order, the loss per coupler is proportional to the power coupling per coupler. Thus, the loss of a 4.77-dB coupler (one-third) is approximately 67 per cent the loss of a 3-dB coupler; the loss of a 6-dB coupler (one-quarter) is approximately 50 per cent the loss of a 3-dB coupler.

Collecting power under these conditions, the copper loss of a four-way serial-feed array is 75 per cent the loss of a four-way binary system. Similarly, when one compares eight-way feeds, the serial feed has 62.5 per cent the loss of an equivalent binary feed.

For example, if we assume 0.2-dB copper loss per 3-dB coupler, then a four-way binary feed would have 0.4-dB loss while a four-way serial feed would have 0.3-dB loss. For eight-way feeds, a binary system would have 0.6-dB loss, while a serial feed system of eight would have 0.375-dB loss.

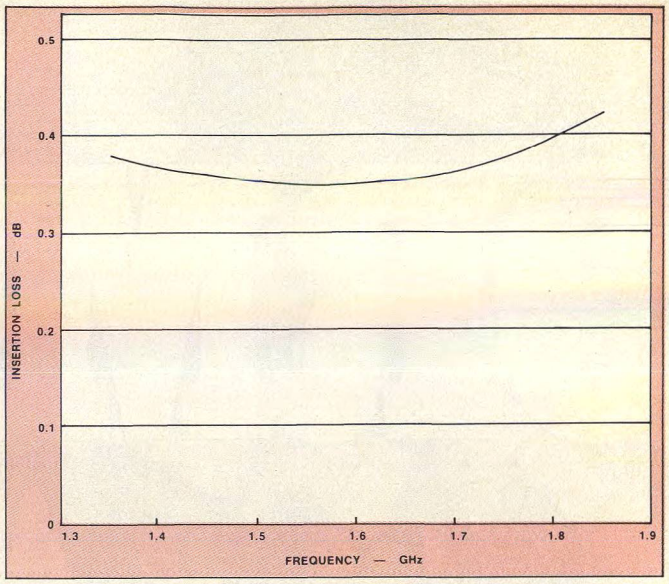

***5. Measured insertion loss** of a commercially available four-way serial feed is typically less than 0.4 dB.*

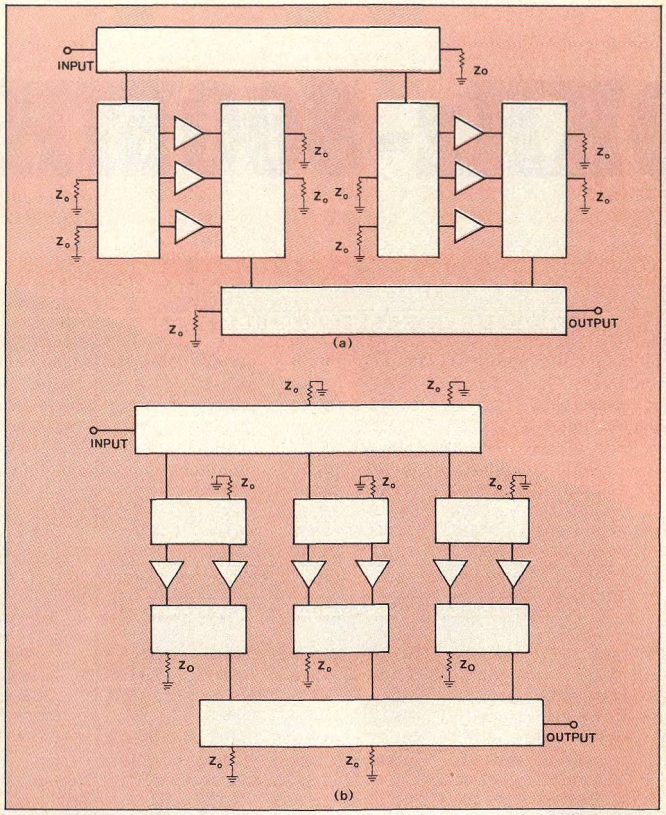

***6. These two schemes for combining six amplifiers** illustrate the versatility of a serial-feed approach.*

This is apparent in the results shown in Fig. 5 where the loss of a pair of four-way serial feeds (distribution and collection) was typically less than 0.4 dB. If this were built as a binary array in these materials a loss of 0.6 dB would have been expected.

Serial-feed systems can be arrayed in binary fashion by using conventional binary distribution or collection at the center tiers and using serial feed systems at the amplifier

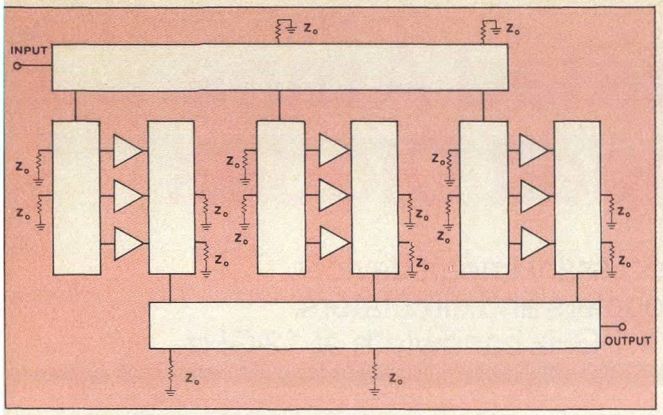

***7. A serial array of nine amplifiers** produces more power than a binary array of eight. The next largest binary array would consist of 16 amplifiers and 30 hybrid couplers.*

face, or by reversing the mode and collecting in serial fashion a non-binary set of binary connected amplifiers. These two options are shown in Fig. 5 for a six-amplifier system. In either case, drivers could be inserted at the input interface between the inner tier couplers and the outer tier dividers.

Alternately, serial feed systems can be used throughout the array. A typical system of nine amplifiers is shown in Fig. 6. Again, driver amplifiers can be inserted either at the input, or at the interface between the input serial feed array and the inner tier dividers.

The devices discussed here are all quarter-wavelength couplers or two-section couplers having quarter-wavelength coupler responses. In this form, systems of the type of Figs. 5 and 6 will tend to provide large amplitude unbalance at the array face since the amplitude balance of a multi-tiered array becomes equal to the sum of the amplitude balance of the parts.

It would be advantageous to consider the techniques described in a previous paper,[1],[2] where the use of multi-section couplers as outer tier elements is discussed. These forms of couplers used as outer tier binary arrays significantly reduce the amplifier drive unbalance. This allows better distribution across the face of the amplifier array and lets maximum power output be achieved since the amplifiers do not have to be derated because of unequal input drive. ••

References

1. J. Cappucci, "Don't Overspecify With Quad Hybrids (Part I)," MicroWaves, Vol. 12, No. 1, pp. 50-54, (January, 1973).
2. J. Cappucci, "Don't Overspecify With Quad Hybrids (Part II)," MicroWaves, Vol. 12, No. 2, pp. 62-64, (February, 1973).

Design Integrated Amps With Hi-Lo Impatt Diodes

First select and characterize the necessary Impatt devices. Then choose the film approach, couplers and circulators, and voilá, a 2.5-W amplifier with a 1.1-GHz bandwidth at 12 GHz.

ALTHOUGH the advantage of GaAs over Si for high-efficiency Impatt diodes was experimentally demonstrated in the early 70's[1-3], the reasons were not completely clear until 1975. At this time, it was determined that the more favorable ionization rates and low parasitic losses due to the high low-field mobility of electrons in GaAs were responsible. In fact, the reported efficiencies of GaAs Impatts, up to 36 per cent, exceeded the maximum value predicted by theoretical calculations. The "hidden" parameter, discovered nearly at the same time by several workers[4-5], was due to the transferred-electron effect leading to differential negative conductivity. Thus, the theoretical analysis of Impatt diodes now can completely explain the gap between GaAs and Si by comparing the dependence on the electric field of two basic parameters: the ionization rates and the electron velocity of these materials.

Table 1. Comparative performance of GaAs Impatt diodes

Profile	Structure	Best Efficiency (C.W. Conditions) Efficiency %	Output Power W	Frequency GHz	Typical Performances (50% Of The Diodes)
Flat	• Sputtered Pt Schottky Barrier	14.1	0.64	13.4	12%/0.5 W X-BAND
	• Diffused P+/N Junction	14.9	0.9	9.6	12%/0.5 W X-BAND
	• Vapor Phase Epitaxial P+/N Junction *	11	0.7	11.3	
HI-LO	• Sputtered Pt Schottky Barrier	24.4	1.55	15	18%/1.5 W X-BAND
		26	1.5	12	"
		28	1.5	10	"
		26.8	1.78	8.6	"
		23	2.1	6.2	"
	• Vapor Phase Epitaxial	25	3	11.8	
LO-HI-LO	• Sputtered Pt Schottky Barrier *	25.8	1	10.7	
	• Vapor Phase Epitaxial P+/N Junction	18.4	4	9.5	

Table 2. Maximum power achieved with CW GaAs Impatts*

Profile	Structure	Best Output Power Output Power W	Efficiency %	Frequency GHz	R_{TH} °C/W
HI-LO	• Sputtered Pt Schottky Barrier	4.8	15	9.35	9.5
	• Vapor Phase Epitaxial P+/N Junction	3	25	11.8	9.1
LO-HI-LO	• Spuuttereed Pt Schottky Barrier	6	20	9.3	7.9
	• Vapor Phase Epitaxial P+/N Junction	4.9	16	9.7	

* PRELIMINARY RESULTS

Impatt fabrication requires control

The hi-lo and lo-hi-lo[2] structures, which offer the high efficiency Read operation, require (1) a very carefully controlled growth process, (2) rapid changes in impurity concentration levels with several orders of magnitude in the doping level, and (3) precise control of the charge density in the n+superficial region (hi-lo) or in the peak (lo-hi-lo)[6]. To eliminate the presence of an interface with defects and compensation at the end of the depleted region, a low resistivity buffer layer, at least 15 μm thick, is required. By using the well-known $AsCl_3$-H_2 method, a technique was developed which satisfies the stringent conditions[7]; this technique was extended with success to the same structures completed by a superficial epitaxial p+ layer, about 1 μm thick, to replace the metallic barrier by a more reliable junction.

Although it would appear that any metal can produce a good Schottky barrier on n-type GaAs, Pt seems to be the only metal which can withstand the high current density (≈1000 A/cm²) and junction temperature (150-200°C) that are often reached in normal operating conditions. However, this barrier is not stable at high temperatures because Pt diffuses into the GaAs and also forms compounds with GaAs which would lead to a gradual consumption of the active layer.[8] This suggests that these two properties are related but there is no experimental evidence for it. In this case, more reliable devices would be expected from p+/n junctions. The fabrication process remains the same for the Schottky-barrier diode and the Pt layer on the heavily doped p+ region (10^{19}

(continued on page 44)

A. Farrayre, Technologist Engineer, **J. Grau*** and **B. Kramer,** Circuit Engineers, **J. Magarshack,** Leader of the Microwave Division, Laboratories d'Electroniquéet de Physique Apliquee, Limeil-Brévannes, France.

*Now with TRT, Le Plessis-Robinson, France

IMPATT AMPLIFIER DESIGN

cm^{-3}) behaves as an ohmic contact. In order to lower the thermal impedance, a quadrimesa structure is currently used. Compared to a monomesa of equal area, it gives a gain of 30 per cent in the thermal resistance.

The Impatt diodes selected were the high-efficiency hi-lo type. Fifty of these diodes were mounted in the standard S4 package for evaluation. In the 11-to-13 GHz range, the mean output power under oscillating conditions was 1.3 watts with 17 per cent efficiency. Although this type of diode is often suspected to be difficult to use because of impedance discontinuities, it was found that, except for very special cases[9], this is not so and the high-efficiency type diode was very practical for amplifier applications.

Characterize the Impatt diodes

Since the Impatt diodes are nonlinear devices, it is necessary to measure the impedance Z_D for different microwave input levels. Z_D is a function of the added power (P_{add}) which is the difference between the output and the input power (P_e). When a network analyzer is used, P_{add} is deduced in a simple manner: $P_{add} = P_e(\rho^2-1)$ where ρ is the voltage reflection coefficient. Figure 2 shows measurements of $(-Z_D)$ as a function of frequency (10.5 to 12 GHz) for different input powers. The solid line represents the behavior at 12 GHz. These measurements were performed on a 50-Ω microstrip line with chip diodes soldered onto a copper block. The thermal compression wire was held in contact with the circuit only by means of an insulating point during the measurements. The chips were mechanically protected by a varnish on the surface of the diodes. Since the high-level reflection co-efficient is very low at 50-Ω, more accurate results were obtained by using a 25-Ω line close to the diode with a wideband taper to join the 50-Ω input line. This measurement is closer to actual working conditions and enables the peak of P_{add} to be reached with less P_e.

The maximum P_{add} observed was similar to that measured on similar chips mounted in S4 packages and measured in coaxial double-slug cavities. Much has been published about the precautions necessary to avoid the subharmonic instabilities that tend to appear with the high-efficiency type Impatt diodes when driven by a large input signal[10-12]. This effect was also found with some of the diodes used in this amplifier but standard procedures with subharmonic absorption traps in the circuit were unsatisfactory; either they did not suppress the unwanted signal sufficiently or they interfered too much at the fundamental frequency. A decision was made to preselect the diodes which had otherwise satisfactory characteristics (power and efficiency). Preselection was found to be quite simple since it appears that the higher the frequency, the less pronounced is the subharmonic instability effects. The diodes can be selected by impedance characterization before connecting them into a circuit either by measuring at the subharmonic frequency with an appropriately high power drive at the fundamental or by observing the smoothness of the impedance trajectory as the power increases at the useful frequency. If there are any jumps present, the diode should be rejected.

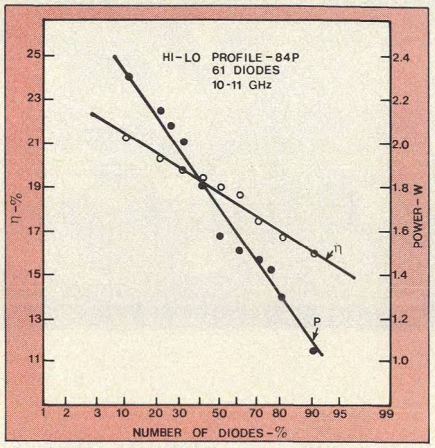

***1. Of 61 hi-low diodes tested** at 10-11 GHz, half displayed efficiencies above 18% and output above 1.7 W.*

Select thin film to reduce losses

To obtain 20-dB gain from a 20-mW input power level, the amplifier was divided into three stages (see Fig. 3):

(continued on page 46)

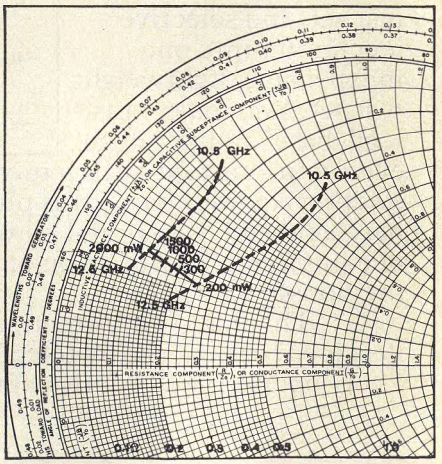

2. Measurement of diode impedance, Z_D, was performed on a 50-ohm microstrip line.

IMPATT AMPLIFIER DESIGN

- The first stage with 10-dB gain, which seems to be a maximum without oscillation problems[13]. There is no problem of power saturation since only 200 mW of added power is necessary (unless one uses specially small diodes).
- The second stage for moderate power levels. If the input power is increased, the maximum gain has to be reduced to 6 dB (800 mW output).
- The third stage, to meet the 2-watt output demand, required a 3-dB coupler with two amplifiers, one on each 3-dB branch. The overall gain is the same as for one high power stage, or about 4 dB. To avoid reactions between stages, isolators were placed between the stages.

Computer simulations were carried out to optimize the amplifier circuits to achieve the high power and wide bandwidth. Due to the requirement of A 500-MHz bandwidth and the relative imprecision of the absolute value of the characteristic resistances, a simple $\lambda/4$ low-impedance transformer (mounted close to the diode) was used followed by a 50-Ω line with an interdigited series blocking capacitor [14]. Since the reactance of the diodes is small, the wire of the diode is directly bonded to the transformer. The value of this transformer impedance is used for high-gain, low-power stages, a higher impedance is desired for average and high power applications. Due to the impedance compression in the diode, the circuit for the two stages is nearly identical. Theoretically[13], P_{add} maximum in amplification is equal to the oscillating power for the same diode. However, for these circuits, differences of about 1.4 dB including the circulator losses were observed.

Since the losses are very important, thin-film evaporated on 99.5 or 96 per cent alumina substrates (0.635-mm thick) and thick-film circuits using gold and copper paste were considered. Thin-film evaporated wafers were found less dispersive with losses of 0.4 dB/inch for a 50-Ω line measured with two SMA connectors or about 0.2 dB/inch at 12 GHz for the microstrip itself. Additional losses of 0.1 dB with Cu thick film and between 0 and 0.2 dB for Au thick film were observed depending on the paste used.

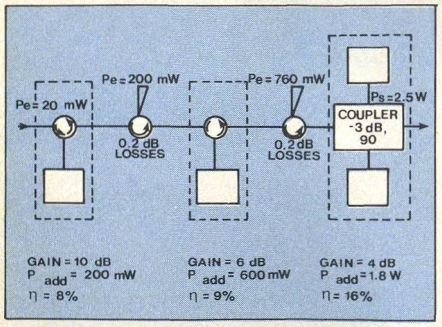

***3. A three-stage Impatt amplifier is** used to provide 20-dB gain with an input level of 20 mw.*

Due to the strong back-biasing effect, it was necessary to use carefully-designed current sources to bias the Impatt diodes. Individual current drivers were constructed with output impedance more than 100 Ω at 100 MHz and output capacitance lower than 50 pF[15]. The current regulators were placed as close as possible to the diodes. On the microstrip circuits, bias filters were used consisting of two $\lambda/4$-cells with high and low impedances. The isolation of such a filter was greater than 35 dB from 8 to 12.4 GHz and the interdigited capacitor had losses lower than 0.1 dB over 1 GHz with a VSWR lower than 1.2.

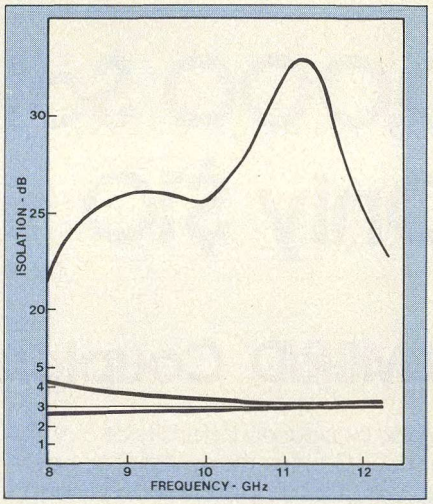

***4. The slot coupler chosen for the amplifier** offers isolation higher than 25 dB from 10.5 to 12 GHz.*

A study of different types of 3-dB couplers was carried out comparing branch, interdigited and slot couplers. The slot coupler [16] was chosen for its better performance. Figure 4 shows these results: isolation greater than 25 dB from 8.5 to 12 GHz, coupling equal to 3 ± 0.2 dB from 10.5 to 12 GHz, phase displacement of 90 ±2 degrees in X-band. The only drawback for this coupler is the need for two well-aligned engravings in both planes of the microstrip.

To achieve complete integration of the amplifier, integrated circulators were studied[17] but commercially-available units were used in the prototype. The best results obtained with the best ferrite type (Y 10) were: losses lower than 0.4 dB, VSWR lower than 1.2 and isolation better than 20 dB over 1 GHz around 12 GHz. This is inferior to that obtained with commercially-available circulators (for instance, Teledyne with 0.2 dB losses over 500 MHz, VSWR lower than 1.2 and isolation over 25 dB), but they are integrated directly on the alumina substrate itself without coaxial connectors.

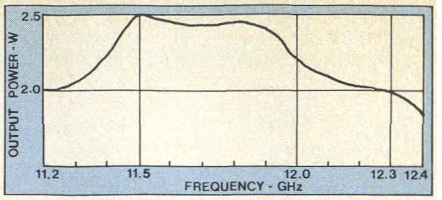

***5. A bandwidth of 1.1 GHz** (from 11.2 to 12.3 GHz) is obtained at −1dB or more than 2 W output.*

Analyze amplifier performance

The maximum output power defined by the amplifier is 2.5 watts at 11.5 GHz with 21 dB gain and 10.5% efficiency. The bandwidths are respectively 600 MHz (11.4 to 12 GHz) at −0.6 dB and 1.1 GHz (11.2 to 12.3 GHz) at −1 dB (more than 2 W output power) as shown in Fig. 5. These results are obtained with a 20-mW input power but are only slightly dependent on this level since the amplifier is working under nearly saturated conditions.

Figure 6 shows the variation of the phase through the amplifier as a function of the input level variation and the frequency. It can be seen that where the output power is maximum (11.5 GHz), the AM/PM conversion is large (5 degree/dB). In fact, from the AM/PM conversion point of view, the amplifier is centered at 12 GHz, instead of 11.5 GHz. Less than 2 degree/dB is obtained from 11.7 to 12.2 GHz (over 500 MHz). This effect has been observed previously and explained theoretically[18].

The third-order intermodulation products are at least 10 dB lower than the fundamental signal and the fifth-order products are about 13 dB down from the fundamental frequency. These results are not surprising since the amplifier works in a saturated region. Lower third-order intermodulation products are obtained with this amplifier by underbiasing the diodes. For instance, third-order can be 22 dB down from the fundamental but output power will decrease to 100 mW.

The variations of the group delay are lower than 0.6 ns over a 500-MHz bandwidth and 0.1 ns over a 20-MHz bandwidth, quite satisfactory for most systems.

The specifications for the radio link systems are met over a 500-MHz bandwidth around 12 GHz with more than 20 dB gain, 2 watts output power, 8 per cent efficiency, less than 2 degree/dB AM/PM conversion, 0.6 ns group delay variations, and IM products lower than 10 dB compared to the fundamental. A transmission of a color TV test pattern was made without any degradation to the picture quality.

The overall size of the original amplifier was rather large (300 x 100

50 mm). But an integrated version, esigned completely on an alumina ıbstrate with integrated circulators, ıeasured only 65 x 35 x 40 mm.

The first test indicated a maximum ıtput power of 2.2 watts at 11.8 GHz ith an efficiency of 9.5 per cent. The ıability to reach the higher power evel can be explained by the fact that he different stages could not be optimized separately, and also by the fact hat spurious signals at subharmonics ccasionally occurred. Indeed, as the irculators have a smaller bandwidth, ubharmonics mismatches could easily ccur and the diodes must be centered ıt a little higher frequency, so as not o have a high negative-impedance at he lower frequencies. The bandwidth

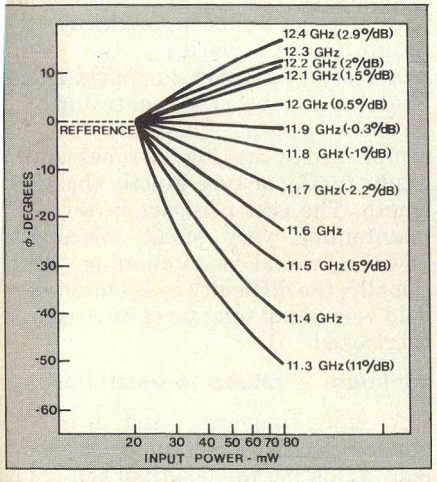

6. At 11.5 GHz, where 2.5W maximum output power is obtained, AM/PM conversion is large (5°/dB).

at −0.6 dB is 700 MHz, better than the previous version. The next step in the program is to use five-watt diodes now available and to construct a similar integrated amplifier delivering 8 watts at 12 GHz with a gain of 20 dB.••

Acknowledgement

This work was partly supported by the DRME (Direction des Recherches et Moyens d'Essais). and the DGRST (Delegation Generale a la Recherche Scientifique et Technique).

References

1. G. Salmer, J. Pribeich, A Farrayre and B. Kramer J.A.P., *44*, 314, (1973).
2. C.K. Kim, W.G. Matthei and R. Steele Proc. of the 4th Biennal Cornell Electrical Eng. Conf. 1973, (Cornell U.P., Ithaca, NY-1973), pp. 299-305.
3. R.E. Goldwasser and F.E. Rosztoczy Appl. Phys. Let., *25*, 1, (1st July 1974)).
4. R.L. Kuvas and W.E. Schroeder IEEE Trans. on ED, *ED-22*, 8, (August 1975).
5. E. Constant, A. Mircea, J. Pribetich, A. Farrayre J.A.P., *46*, 9, (September 1975).
6. A. Farrayre, B. Kramer, A. Mircea Proc. of the 5th Int. Symp. on GaAs (Deauville, France, 1974) (Institute of Physics, London, 1974).
7. L. Hollan, A. Mircea Proc. 4th Int. Symp. on GaAs, Boulder, 1972, 217-223.
8. M.C. Finn, H.Y.P. Hong, W.T. Lindley, R.A. Murphy, E.B. Owens and A. J. Strauss Preparation and properties of electronic materials, conf. paper D1, Las Vegas, 11-1973 (unpublished).
9. B. Kramer, C. Balzano Electr. Letters, *j11*, 21, (Oct. 1975), pp. 509-512.
10. M.E. Hines IEEE, *60*, 12, (Dec. 1972).
11. W.E. Schroeder B.S.T.J., *53*, 7, (Sept. 1974), pp. 1187-1221.
12. S.F. Paik, John, Pallemaerts EMC, Montreux, Sept. 1974, pp. 102-107.
13. C.W. Lee Microwave Journal, *15*, Feb. 72, pp. 29-37.
14. D. Lacombe, J. Cohen MTT, (August 1972), *20*, 8, pp. 555-556.
15. A. Semichon Acta Electronica, *17*, 2, (april 1974).
16. B. Schiek, J. Koeler EMC 1974, Montreux, pp. 536-540.
17. Bosma IEEE on Magnetics, MAG-4, 3, (Sept. 1968), pp. 587-596.
18. B. Carnez 3rd cycle thesis, (Sept. 1975), Lille Univ.

Phase Match TWTs For Reduced Combining Loss

Phase differences in multi-tube TWT arrays can be accurately measured and matched for increased combining efficiency. This simple technique requires only standard laboratory test equipment.

KILOWATT CW power levels over wide bandwidths characterize many of today's microwave communications and military electronic systems. Because of its inherently broad bandwidth and high saturated power levels, system designers continue to rely on the helix-type traveling-wave tube to meet these requirements. Higher output power from a TWT is usually achieved by increasing its beam voltage. However, increasing beam voltages beyond the manufacturers' optimized levels to get that extra few watts often can result in lower overall system efficiencies and shorter tube life.

Paralleling schemes, involving two or more TWTs are therefore necessary when efficiency and high power are both system requirements. In addition to paralleling for power, lobe "steering" required in electronically steerable phased-array systems is most effectively achieved by changing the phase of part of a total array of tubes. Multi-tube parallel configurations with precision phase matching is essential for "steering" the transmitted lobe.

Paralleling: Proceed with caution

Tube paralleling, however, can cause as many problems as it solves if the system designer fails to understand the characteristics of TWT phase measurement and equalization techniques.

In order to combine TWTs for parallel operation, there are several important considerations to take into account. The first is the tube's power level difference. The efficiency of the total system is affected by differences in amplitude of the individual tube outputs. Laboratory measurements show that with power level differences of 10 dB, combining losses will be 1 dB; at a 20 dB power difference, the combining losses climb to 2.6 dB. A second important consideration is component compatibility. Combining devices such as 90° hybrids or magic tees normally exhibit low insertion loss and good VSWR, but even these small losses translate to dollars in a parallel arrangement and hence, combining devices must be carefully chosen.

The third and perhaps most important consideration is the phase difference between tubes. The system designer must understand that phase length differs from tube to tube, *even between two tubes of the same type.* As phase difference is increased, a corresponding increase in the combining loss will result as shown in Fig. 1. This phase difference is due to two factors: individual internal parts tolerances, and vacuum envelope assembling tolerances.

There are several ways that the phase of a tube can be modified. Changing the beam voltage applied to the tube will, of course, change the phase but "defocusing" effects prevent this method from being a serious contender for phase changing except when only very small changes are necessary.

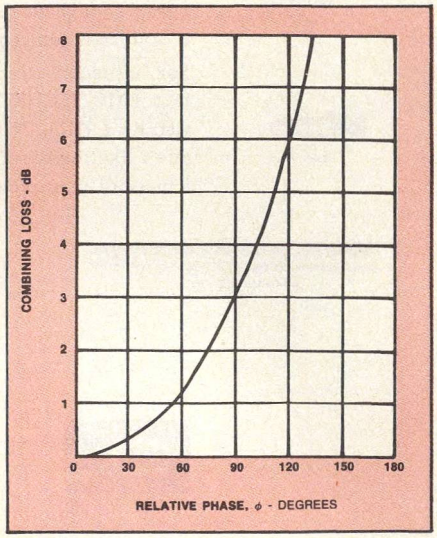

*1. **Efficiency is reduced** as a result of increasing phase difference.*

Also, since system builders normally use a common supply to power the tubes, a constant phase relationship (tube to tube) will be maintained as the beam voltage is varied.

A second approach to changing the phase of a tube is by controlling its physical length. This can be accomplished by making the tubes within a tube family or type exactly the same length. The cost per part involved in maintaining very small tolerances, however, would be astounding. Additionally, the difficulty in assembling to hold very small tolerances must not be overlooked.

Minimum △ phase is essential

A more universal and practical method to control the length of a tube is by adjusting the length of the input or output cable. Of the two, the input cable is usually preferred for adjustment because of the higher power requirements at the tube's output. Any small discontinuity in the adjusted cable would have less effect on the overall tube performance if it were connected to the input. In addition, many power TWTs require waveguide outputs with their inherently higher power capability, and adjusting waveguide for length is prohibitively expensive.

The phase differences of tubes in a system can be held to within ±20 degrees even though traveling wave tubes are typically 10,000 to 20,000 degrees (30 to 60 circuit wavelengths) long. Maintaining these tolerances has several advantages. The efficiency for parallel tube operation, for example, will be increased. Measurements indicate that if the phase between two tubes differs by 25 degrees, a combined power reduction of about 0.2 dB can be expected. And, at a kilowatt level, this loss is appreciable. Another advantage is the minimum system adjustment required when tube replacement becomes necessary. Communications systems, for instance usually include phase shifters with adjustment ranges of only about ±30 degrees.

(continued on p. 50)

Ovlan Fritz, Jr., Senior Test Technician, Varian Associates, 611 Hansen Way, Palo Alto, CA 94303.

PHASE MATCH TWTs

In order to hold close phase tolerances, a tube's physical length must be adjusted. This can be accomplished by using an adjustable length of coax cable to modify the length. What follows is a technique for phase matching TWTs using a short length of coax cable. The tube used in the examination of the technique is a periodic permanent magnet-focused, CW, TWT. The tube's minimum power output is 600 watts over the commercial satellite communications band (5.9-6.4 GHz). Therefore, the input was selected as the adjustable port.

The equipment used for this technique is shown in Fig. 2. If this technique should be applied to a TWT that operates at a frequency that does not fall within the limits of the equipment, some components would have to be changed. The frequency-dependent components of Fig. 2 include Nos. 4, 5, 6, 7, 9, 10 and 13.

Use a coax or TWT standard

The first step is the development of a standard or reference to which the TWTs can be phase matched. A standard could come from two sources: the first tube of a series or a reference coax cable, the length of which is calculated from the internal dimensions of the TWT. The cable length must be electrically equal to the distance from the input to the output of the TWT. The next step is to measure and plot the phase of the reference over the tube's operating bandwidth. Precautions must be taken to use the same procedures for each tube. These precautions will minimize phase changes not due to differences in the tube's length. The TWT's applied voltage must be kept constant to prevent changes in phase. Maintaining a leveled input drive is also essential. Each TWT must be measured at the same output power level and frequency. TWTs from the same tube family exhibit output power differences due to small variations in fabrication. The drive power must be adjusted slightly from tube to tube to produce a constant output level for all the tubes being tested.

Determine the cable length

A convenient frequency used to measure each TWT is the tube's center frequency. Adjust the phase shifter (No. 2, Fig. 2) until the phase of the TWT under test and the phase of the reference are equal. This equality can be observed on the network analyzer (No. 1, Fig. 2) and on the X-Y recorder (No. 12, Fig. 2). The bandwidth of the TWT should now be swept to check the phase balance (equal number of wavelengths) between the reference plot and the present plot. If the phase is not balanced to within a wavelength,

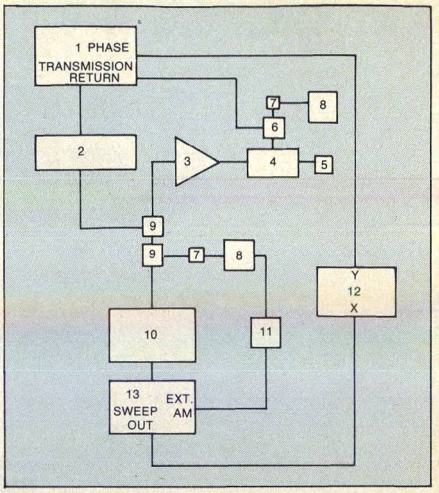

1. HP network analyzer, Model 8410A with reflection-transmission test unit, 2.0 - 12.4 GHz, Model 8743A
2. Precison phase shifter
3. TWT
4. 30-dB w/g coupler
5. High power load
6. 20-dB directional coupler
7. HP thermistor mount, model 478A
8. HP power meter, model 432A
9. 10-dB coaxial directional coupler 4 - 8 GHz
10. TWT amplifier
11. HP leveling amplifier model 8404A
12. X-Y recorder
13. HP sweep oscillator, Model 8690B with plug-in, Model J21-8693B

*2. **This phase-matching test set** can be assembled with equipment on hand in most microwave labs.*

the results will be similar to Fig. 3. If necessary, readjust the phase shifter to balance the TWT and subtract the phase shifter setting (in degrees/GHz) from the setting used for plotting the reference. This will result in a difference in degrees/GHz. Multiply this difference and the center frequency of the TWT (6.15 GHz in this case) and the result is the total phase difference. Experimentally verified calculations have established a phase constant of 0.003 inch/degree at 6 GHz for the coax input cable used with this family of tubes. If the total phase difference is now multiplied by 0.003 inch/degree, the product is the difference in length (inches) of the input cable required to match the TWT under test to the reference. Figure 4 demonstrates the phase

(continued on page 52)

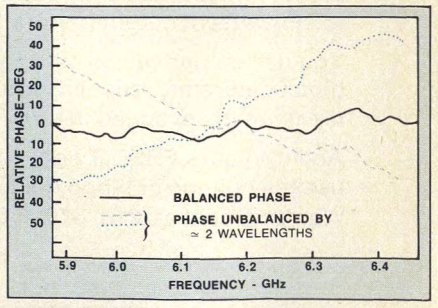

*3. **This X-Y recorder plot** demonstrates the degree of phase error caused by a two wavelength phase differential.*

PHASE MATCH TWTs

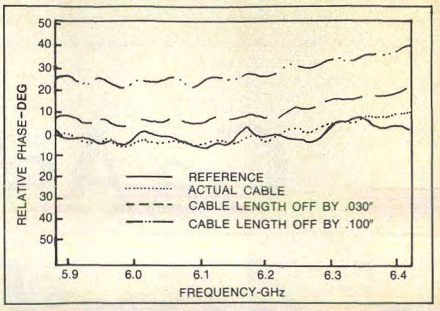

*4. **Cable length must be tightly controlled.** A 0.1-inch error will cause a 30-degree phase imbalance at 6 GHz. Note close agreement between reference standard and properly cut cable.*

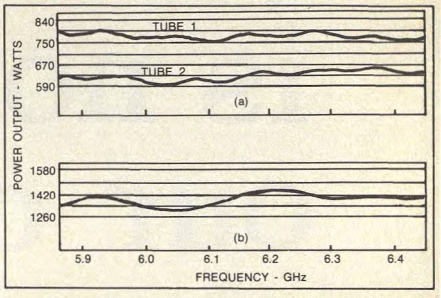

*5. **Combining loss is well illustrated** by comparing the individual outputs of two 600-watt TWTs (a) and their paralleled result (b).*

relationships when the cable length is off by 0.030 and 0.100 of an inch.

Matching increases efficiency

Figure 5 (a) is a plot of the typical saturated output power of two 600-watt TWTs. If the power output at 6.1 GHz of tube 1 is added to the power output at 6.1 GHz of tube 2, the total power will be approximately 1,390 watts (tube 1 = 640 watts and tube 2 = 750 watts). This total output power does not correspond to the power output at 6.1 GHz of the two tubes in parallel as seen in Fig. 5 (b). The difference (1,390 watts – 1,365 watts = 25 watts) is due to the combining losses. At 6.1 GHz, the combining losses equal about 1.8 per cent and are due largely to phase differences between the two tubes.

The advantages of phase matching TWTs can be viewed from several aspects. For example, if TWTs are phase matched, a minimum phase adjustment is necessary at the system level. Additionally, increased output power can be realized from a system because there is less loss due to unmatched phases. The application of the techniques described here have resulted in output powers in excess of 1 KW across wide bandwidths with system efficiencies approaching 30 per cent using two 600-watt traveling wave tubes.••

Cut Oscillator Noise By Careful Mechanical Design

The design of ruggedized Impatt sources demands a rethinking of the traditional design process. Vibrational characteristics influence RF performance and must be considered at the outset.

CW-Doppler radar calls for a microwave source that exhibits very low noise levels, especially during flight-imposed vibration, common to most military systems. These sockets, traditionally filled by klystrons, are rapidly opening up for solid-state sources thanks to the development of the silicon double-drift Impatt diode. When designing ruggedized sources, the traditional approach of first optimizing electrical performance and then installing environmental stopgaps must be abandoned. The oscillator engineer must instead, combine environmental, especially vibrational considerations with microwave performance in the *initial* design scheme.

Although this approach seems alien to the microwave designer, it is nonetheless, the only practical method for "productionizing" a military source design.

The application of this philosophy, in fact, has resulted in the successful design of ruggedized CW Doppler radar sources capable of 1.2-watt outputs at Ku-band with power stabilities of ±10 MHz from −55 to +71°C. In the critical area of FM noise, less than 1.5 kHz peak noise can result from a 10-g vibration. Compare this to an equivalent 250 kHz deviation for a klystron, and you can understand why the Impatt finds wide use in today's Doppler radar applications.

Equivalent circuit leads to design equations

The source design revolves around the diode equivalent circuit. A silicon double-drift diode, developed at HP was utilized for the design. The diode operates at 13.3 GHz and requires a 95-volt input. The Impatt (HP 5082-0660) is a dual mesa device with a single mesh bond. For design purposes, C_j can be assumed equal to 1.0 pF and the negative resistance equal to −1 ohm. Due to the experimentally adjusted output coupling, however, negative resistance is not a critical parameter.

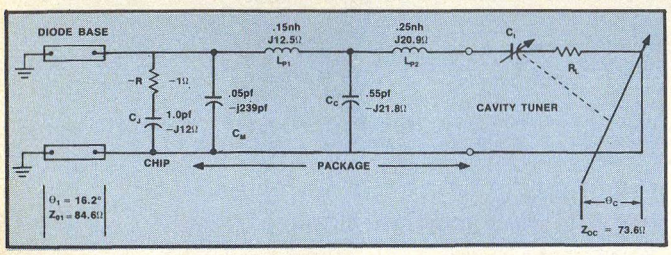

***1. A comprehensive equivalent circuit includes** chip, package and cavity parameters. The gap capacitance increases as the cavity is lengthened.*

Dr. Gerald Schaffner, Manager, Microwave Engineering, Teledyne Ryan Aeronautical, 2701 Harbor Drive, San Diego, CA 92112.

Associated with the chip is a ceramic pill with a prong package. The parasitics of the package are the junction mesh capacitance C_M = 0.05 pF, the mesh inductance L_{P1} = 0.15 nH, the case capacitance C_c = 0.55 pF and the top cap inductance L_{P2} = 0.25 nH. An equivalent circuit of the cavity ocillator is shown in Fig. 1, and the cavity cross-section is detailed in Fig. 2. The diode with an equivalent characteristic impedance, Z_0, of 84.6 ohms and an electrical length Θ_1 of 16.2 degrees (at 13.3 GHz), can be mounted or soldered on the pedestal. Biasing is accomplished by a thin wire (not shown) laid along the diode. The tuning end of the cavity consists of a 0.12-inch diameter tuning screw forming the center conductor of the coax line with a Z_{02} = 73.6 ohms, a length Θ_c and a gap capacitance C_t. As Θ_c is increased, the gap is decreased and hence, C_t is increased according to the relationship of a parallel plate capacitor:

$$C_t = \frac{0.225\ \epsilon_r A''}{t''} \qquad (1)$$

Where C_t is capacitance in pF
ϵ_r = relative dielectric
A'' = plate area = $\pi 0.12^2/4$ = 0.01131 square inches for this example
t'' = gap spacing

Equating to zero the sum of all the reactances seen in both directions from the package terminals (Fig. 1) results in the complete design equation. Neglecting the negative resistance, −R, and the mesh capacitance, C_m, yields:

(continued on p. 56)

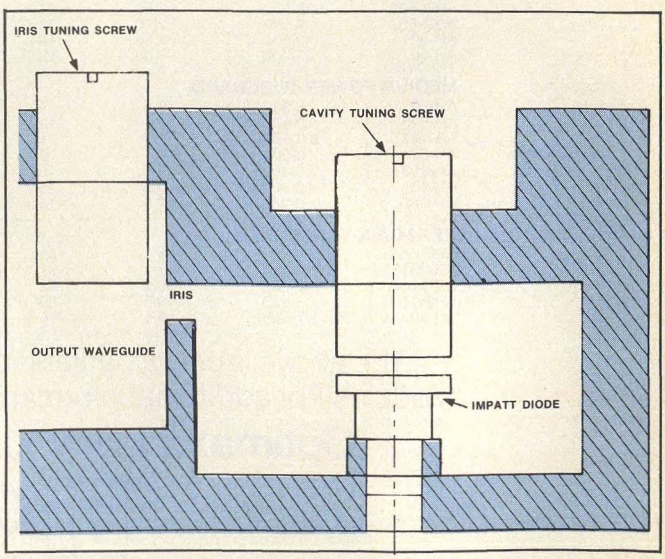

***2. The frequency of this oscillator** can be adjusted by varying the diode gap.*

$$jZ_{01} \tan \Theta_1 + \left[\frac{\left(\frac{1}{j\omega C_j} + j\omega L_{P1} \right) \left(\frac{1}{j\omega C_c} \right)}{j\omega L_{P1} + \frac{1}{j\omega C_c} + \frac{1}{j\omega C_j}} \right] + j\omega L_{PZ} + \frac{1}{j\omega C_t} + jZ_{02} \tan \Theta_c = 0 \quad (2)$$

Substituting the known values:

$$j24.6 + \frac{(-j12+j12.5)\ (-j21.8)}{-j21.3} + j20.9 + \frac{1}{j\omega C_t} + j73.6 \tan \Theta_c = 0$$

choosing a spacing of 0.1 inch from the top of the diode to end of the cavity and assuming a frequency of 13.3 GHz:

$$\Theta_c = (0.1\text{-}t'') \frac{360°}{0.888} = 40.5 - 405t'' \quad (3)$$

Now, substituting Θ_c into Eq. (3) and solving for t″ yields:

$$t'' = 9.94 \times 10^{-3} + 15.7 \times 10^{-3} \tan (40.5 - 405t'') \quad (3)$$

This transcendental equation can now be solved on a scientific calculator by assuming a value of t″, substituting that into Eq. (4), then calculating a new t″ and resubstituting that into Eq. (4). Repeat this process until the assumed and calculated values are sufficiently close. For the source being examined here, t″ = 0.02 and Θ_c = 32.45°. Note that precision is not necessary, because the tuning screw can vary frequency from about 11 to 15 GHz.

Vibration performance must be considered

However, since a movement of 0.1 inches will change the frequency 4 GHz, careful vibration analysis must now be performed. Taking simple ratios, if one wants the deviation frequency to stay within 1 kHz of the center frequency, a movement no greater than $\frac{0.1 \times 1 \times 10^3}{4 \times 10^9} = 0.025 \times 10^{-6}$ inches can occur. The structure, therefore, cannot tolerate a movement greater than 0.025 microinches while vibrating.

Acceptable vibration performance is best obtained by first using a test cavity to determine force, resulting from a frequency change. Weights are placed on the cavity and the resultant frequency change is measured. Using Hook's law, the resultant dimensional changes can then be calculated for a metal cross-section with area A, cavity length L and applied force F:

$$\epsilon = \frac{FL}{AY} \quad (5)$$

Where Y = Young's modules
F = Applied force in pounds
A = Metal cross-section area in square inches
L = Cavity length in inches
ϵ = Dimension change of cavity length in inches

For the cavity in this example:
A = 1.75 inches
L = 0.182 inches
$\epsilon = 0.1 \times 10^{-6}$ inches
Y = 10×10^6 lb/in² for aluminum

Force F, is found from F = Ma where M is the mass on top of the cavity and a is the vibrational acceleration. In this case, F is equal to 10 lb. for a 90-kHz frequency change (in the test oscillator). The use of these equations allows control of vibration response for a given material by varying mass M and cross-section area A. The transmitter must be carefully designed to minimize vibration-induced noise. Particular attention should be paid to the mounting, in order to insure a high enough vibration resonance frequency above the maximum vibration table frequency. An effective vibration analysis, however, can only be carried out after all transmitter components are assembled.

Coupling and regulation are critical

The output coupling must now be considered. In this case, WR 62 Ku-band waveguide was chosen using H-plane iris coupling. The iris slot length and height can be determined experimentally for maximum output power. Beginning with an oversized opening, the length and height dimensions are varied for an optimum window. Using this technique, the slot length was found to be 0.335 inches and the height was optimized to 0.047 inches. Matching of the cavity and output coupler can now be performed using a single tuning screw.

An isolator and cross-guide coupler follow the oscillator in the transmitter system as shown in Fig. 3. The Moreno-type[1,2,3] coupler, in this case, provides local oscillator power in the range of +16 to +18 dBm, a requirement of this Doppler socket.

The current regulator has several design constraints. It must, of course, provide a constant current and voltage to the Impatt diode, while at the same time reducing input current ripple to the microamp region with an applied ripple voltage of several volts. This is best accomplished by a combination of a capacitive input filter and a feedback circuit referencing the DC output voltage to a zener diode. The regulator also must provide a high output impedance over a very broad bandwidth to prevent bias oscillations.[4] In addition, short circuit protection is required. If the series-pass transistor fails in the short condition, the Impatt diode will be destroyed. A transistor designed to supply full current with the total line voltage across the device should be used to provide short circuit operation. Figure 4 is a block diagram of a regulator suitable for this application.

Frequency stability, always an important consideration for military sockets, is achieved by using the known temperature characteristics of the Impatt diope and the surrounding cavity.[5,6] Careful selection of different metals in the cavity and tuning mechanism is essential to achieve the desired frequency stability. As temperature increases, the diode junction capacitance, C_j of Fig. 1, decreases due to the increase of operating voltage caused by the varactor action. This tends to increase frequency. The linear expansion of the mesh inductance LP_1 and the cavity trans-

(continued on p. 58)

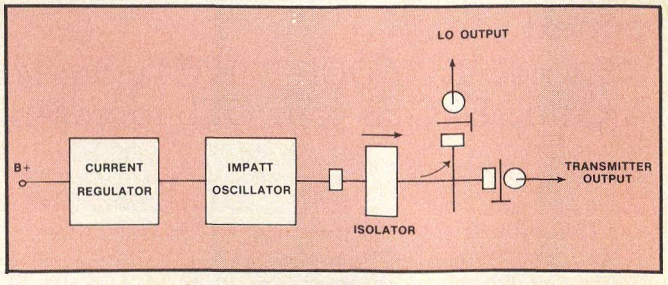

***3. The transmitter assembly** includes a Moreno-type coupler to supply LO power.*

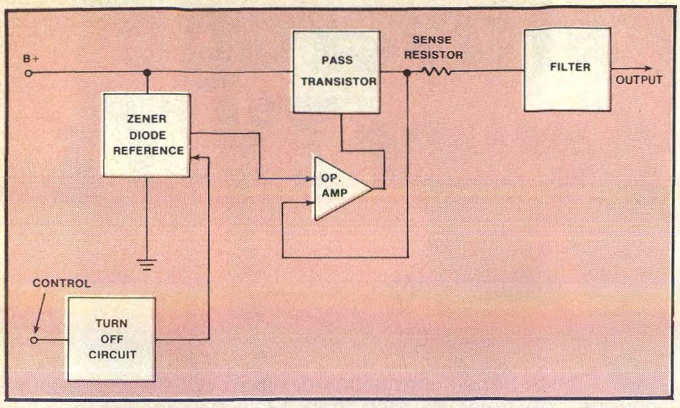

***4. This current regulator design** is ideal for Impatt oscillator applications.*

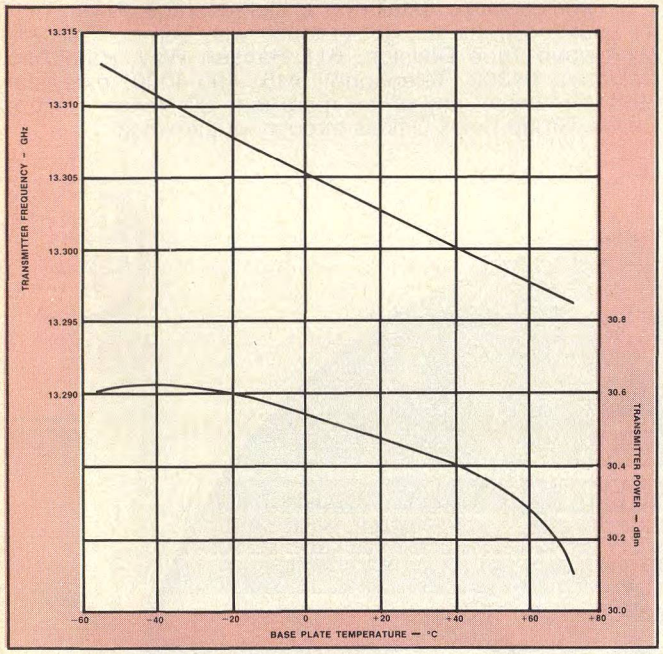

***5. The Impatt oscillator's performance** exhibits a frequency drift (top curve) of −16 MHz and a power drift of 0.5 dB from −55 to +71°C.*

mission lines Θ and Θ_c offsets the junction capacitance decrease. These factors, as well as an increase of C_c with temperature due to the nature of the alumina ceramic, cause a net decrease of frequency with increasing temperature. For the design described here, compensation can be obtained by use of an invar tuning screw to form C_t. As the aluminum cavity expands with temperature, the end of the invar screw moves away from the diode, decreasing C_t and increases frequency. Careful control of the tuning screw length will provide excellent frequency compensation. Shore's thesis gives a more quantative analysis of this compensation technique.[6] Figure 5 details the oscillator's power and frequency as a function of temperature. Interestingly, an important advantage of Impatt diodes over power Gunn diodes is this constancy of power with temperature. The extremely flat result is made possible by the slight increase of the regulator current at the lower temperatures.

Noise measurements require precision testing

AM and FM noise under vibration is perhaps the biggest design challenge of all. Noise during vibration is a function of the cavity's dimensional stability. Particularly critical areas are the stress/strain relationship distorting the cavity as given by Eq. (3), the tuning screw threads and the bias circuit. A cavity with a large cross section and a small mass pressing on the tuning screw is essential for low noise. The tuning screw should fit the cavity threads closely. The bias circuit is also a particularly critical element. Compression mounting with a low-pass filter for the bias is not enough to insure success. Such a circuit tends to move slightly, causing noise. A completely soldered diode and bonded bias wire arrangement was used in this design to insure low noise operation. The thin wires sufficiently decouple the cavity from the bias circuit.

Measurement techniques for AM and FM noise during vibration is a challenge in itself. Figure 6 is the block diagrams of the AM and FM measurement test sets. For the AM test (Fig. 6(a)), the output from the transmitter (SSX) is sent to a zero IF or homodyne receiver where it is converted to an audio signal. In such a receiver, the SSX output signal acts as an LO mixing with its own noise. After amplification, it is sent through a bandpass filter tracked to the vibration input frequency. For the FM measurement, the interconnect system of Fig. 6(b) is used. The signal is converted to the FM band by the frequency counter where it is amplified and converted to AM by the FM receiver.

(continued on p. 60)

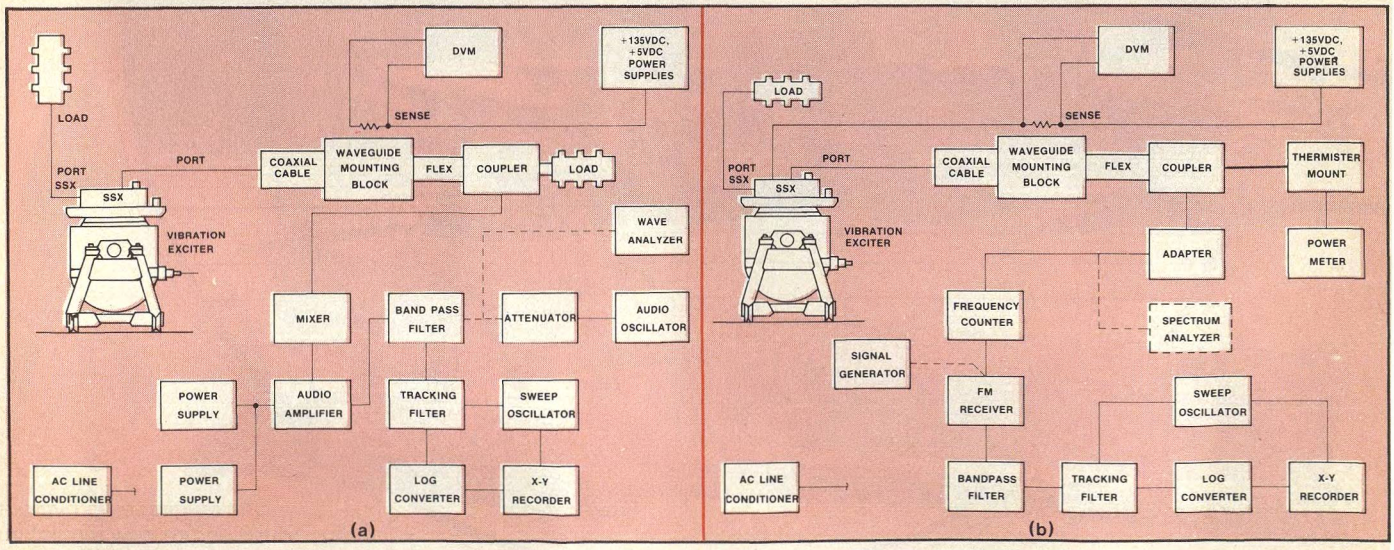

***6. This interconnect scheme** can be used to measure AM (a) and FM (b) noise characteristics during vibration testing*

CUT OSCILLATOR NOISE

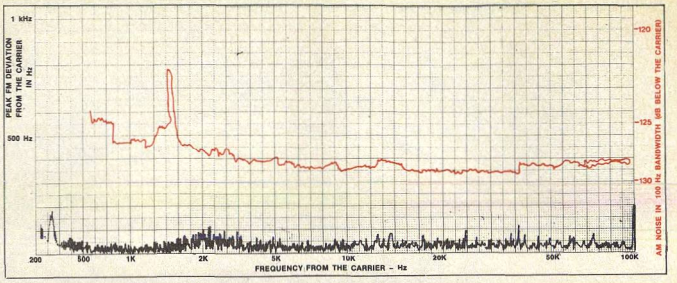

***7. The baseline standard for determining AM and FM** noise magnitude was determined by measuring the noise in a nonvibrated mode. The AM standard is represented by the colored line.*

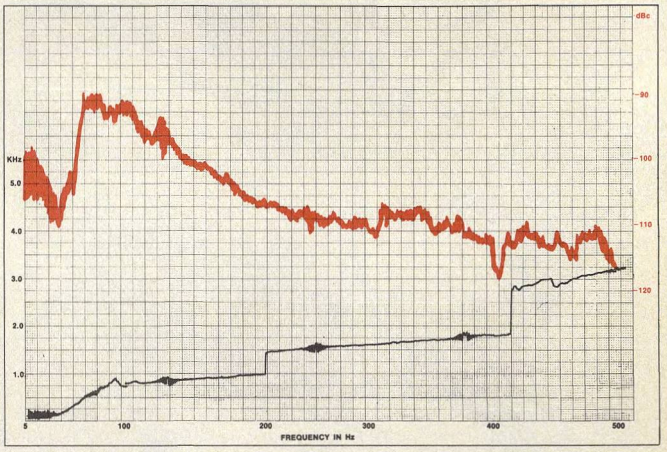

***8. Actual AM and FM noise measured on the X-axis** can be referenced to Fig. 7. The AM noise is shown by the colored plot.*

Again, a bandpass filter is used which is tracked to the vibration frequency. FM calibration is provided by modulating the FM signal generator feeding the FM receiver at varying audio rates, subsequent frequency levels are then marked along the X axis of the noise plot. The noise standard for these measurements is the quiescent (non-vibrated) base line noise of the transmitter. Figure 7 is the AM and FM standards for the transmitter.

Measured data during vibration is shown in Fig. 8. For the critical FM noise, the measurements show about a 100 Hz/g level of peak deviation.••

References

1. T. Moreno, Report No. 5224-1088, Engineering Division, Sperry Gyroscope Company, Inc., Great Neck, NY, (1947).
2. T. N. Anderson, "Directional Coupler Design Nomogram," *The Microwave Journal*, Vol. 2, No. 5, pp. 34-38, (May, 1959).
3. W. A. Geoffrey Voss, "Optimized Crossed Slot Directional Coupler," *The Microwave Journal*, Vol. 6, No. 5, pp. 83-87, (May, 1968).
4. C. A. Brackett, "The Elimination of Tuning Induced Burnout and Bias Circuit Oscillations In Impatt Oscillators," *Bell Systems Technical Journal*, pps. 271-306, (March, 1973).
5. G. Schaffner, "Space Applications Complicate Microwave Design," *Micro Waves*, Vol. 12, No. 7, pps 54-57, (July, 1973).
6. D. Shores, "Frequency Stability of An Impatt Oscillator," Master's Thesis in Electrical Engineering, San Diego State University, (June, 1972).

Acknowledgements

The author would like to acknowledge the efforts of H. Otzen in the microwave design area, R. Hout in the directing the regulator design, D. C. Wells in directing the mechanical design and most of all B. Kipp in personally bringing this transmitter through all development phases.

Modeling The Bipolar Transistor

Ian Getreu

It has almost become a cliché to comment on the rapid growth of the computer as a tool in circuit design. The use of computer-aided design (CAD) techniques allows engineers to perform tasks not possible with other methods. CAD however, can be a jungle in itself. In circuit designs incorporating a bipolar transistor, for example, the engineer is confronted with a bewildering array of choices. Not only must he select a bipolar model, he must also choose from a selection of available CAD programs, each with different formats, rules and notations.

Getreu's work is aimed at reducing this confusion by taking a systematic approach to bipolar transistor modeling. The subject is presented from two perspectives—device physics and measurements. Emphasis is on the large-signal model used in nonlinear DC and transient analysis, since this according to the author, is where most problems are encountered.

The book ties together recent developments in BJT modeling in a way that the reader can use most, if not all of the circuit analysis programs available. It should be noted, however, that the models presented are oriented toward three computer programs, SLIC, SINC and SPICE, readily available from the University of California at Berkely. The use of these programs does not seriously restrict the value of Getreu's book, as the parameters can normally be transformed for other programs. These programs, written in FORTRAN IV for CDC 6000 series computers, are available in other formats for other computers, Getreu points out.

In both sections, the text begins with the fundamental and gradually builds to the more complex. The publication does a commendable job of avoiding tedious mathematical derivations wherever possible to clarify the message. (255 pp; $8.00). **Tektronix, Inc., PO Box 500, Beaverton, OR 97077.**

feedback

A note on radiometric noise

To the editor:

In his article, "How Noisy Is That Load?" (MicroWaves, p. 54, January, 1976), Dr. Viggh makes a timely comment concerning noise measurements at millimeter wavelengths, even though it is questionable whether "precision radiometry" is relevant at frequencies and temperatures where the Rayleigh-Jeans approximation is no longer valid, as is clear from the graph of radiometric temperature ($\equiv \frac{P}{k \bullet \Delta f}$) against physical temperature (see figure).

Millimeter-wave noise temperatures are usually measured using 77°K and 295°K calibration terminations; since the noise temperatures themselves are normally in excess of 77°K, below 1 THz the deviation from Rayleigh-Jeans is simply a constant depression of the radiometric temperature, independent of physical temperature. Hence , all such noise temperature measurements will result in an apparent increase in system noise temperature, equal to the reduction in the apparent (radiometric) temperature of the calibration terminations. The designation of a system noise temperature is therefore, still useful, even though the radiometric temperature is no longer equal to the physical temperature.

The situation changes when the physical temperature drops appreciably below 5°K, since the radiometric temperature scale experiences compression, in addition to the constant offset. For the purposes of comparison, at 230 GHz, a physical temperature

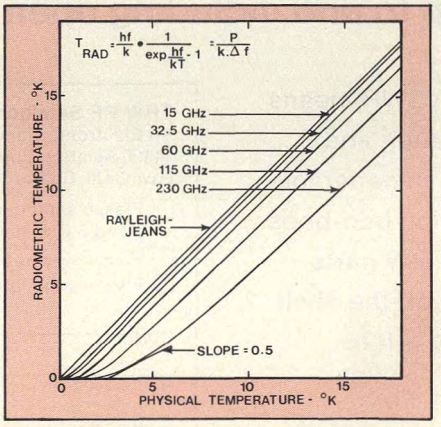

of 15°K results in a radiometric temperature of 10°K, and the slope, $\partial T_{RAD} / \partial T_{PHYS} = 1$. However, at 4.2°K, the radiometric temperature is 0.8°K, and the slope, $\partial T_{RAD} / \partial T_{PHYS} = 0.5$—in marked contradiction to the concept of a radiometric temperature scale.

Nigel J. Keen
Millimeter Technology Division
Max-Planck-Institut für Radioastronomie
Auf dem Hugel 69
D-5300 Bonn
West Germany

VEMBER
1976

MICROWAVES

EUROPEAN UPDATE

"Old World" Technology? Don't Believe It!

European firms continue to steadily advance the state-of-the-art on many fronts. In semiconductor materials, most of the attention is turning to indium phosphide. The challenge: To turn a "black magic" material into a manufacturable device. In device technology, production engineers are hustling to improve the GaAs FET, while co-workers in the laboratory are just beginning to learn of the FET's capability as a microwave power amplifier. Radar applications are demanding refinements in Trapatt and Baritt technologies — and European firms are gearing up to meet the challenge.

Sophisticated solid-state devices are finding their way into MIC designs at an ever-accelerating pace, for commercial as well as military applications. European firms are turning out marketable systems, such as a 30-GHz. . .(continued on p. 35)

Also in this issue:

MICROWAVES

November 1976
Vol. 15, No. 11

news

editorial

technical

International

departments

About the cover: Look west, young man, and east and north and south as well. The international marketplace is where it's all happening. For a closer look at what's going on in Europe, turn to page 35. (Cover composition by Art Director Robert Meehan).

coming next month...Supercomponents

First, waveguide evolved into coax. Then, coax gave way to MIC technology. Today, MICs are expanding into supercomponents—highly integrated, multi-function mini-systems that signal a new stage of maturity for microwave circuit technology. December's staff report examines the strategy behind the super-component philosophy, and what the trend means to device, component and system designers.

How Much Power Can That Coax *Really* Handle? Authors from Westinghouse caution that the maximum power ratings on cable data sheets may not always be reliable. Using a simple equation, however, it's easy to double-check the specification.

The Navy Develops A New Sub-Millimeter Power Source. Researchers at NRL have produced more than 1 MW at 750 GHz by bouncing a 15 GHz signal off a relativistic electron beam. An interview with the developer reveals some surprising applications.

Publisher/Editor
Howard Bierman

Managing Editor
Stacy V. Bearse

Associate Editor
George R. Davis

West Coast Editor
Jose C. de León
Hayden Publishing Co.
744-R Coleman Avenue
Menlo Park, CA 94025
(415) 325-8280

Washington Editor
Paul Harris
Snyder Associates
1050 Potomac St. NW
Washington, DC 20007
(202) 965-3700

Contributing Editor
Harvey J. Hindin

Editorial Assistant
Gail Murphy

Production Editor
Sherry Lynne Karpen

Art Director
Robert Meehan

Production
Dollie S. Viebig, Mgr.
Sandra N. Bowen

Circulation
Barbara Freundlich, Dir.
Trish Edelmann
Sherry Karpen,
Reader Service

Directory Coordinator
Janice Tapp

Editorial Office
50 Essex St.,
Rochelle Park, NJ 07662
Phone (201) 843-0550
TWX 710-990-5071

A Hayden Publication
James S. Mulholland, Jr.,
President

MICROWAVES is sent free to individuals actively engaged in microwave work. Prices for non-qualified subscribers:

	1 Yr.	2 Yr.	3 Yr.	Single Copy
U.S.	$15	$25	$35	$2.50
FOREIGN	$20	$35	$50	$2.50

Additional Product Data Directory reference issue, $10.00 each (U.S.), $18.00, (Foreign). POSTMASTER, please send Form 3579 to Fulfillment Manager, MicroWaves, P.O. Box 13801, Philadelphia, PA. 19101.

Back Issues of MicroWaves are available on microfilm, microfiche, 16mm or 35mm roll film. They can be ordered from Xerox University Microfilms, 300 North Zeeb Road, Ann Arbor, MI 48106. For immediate information, call (313) 761-4700.

Hayden Publishing Co., Inc., James S. Mulholland, President, printed at Brown Printing Co., Inc., Waseca, MN.

Spectrum Efficiency Key To North Sea Tropo Network

Congested spectrum and wide signal length variations play havoc on the North Sea tropo systems. Requiring virtually zero downtime, careful design and proven hardware are the order of the day.

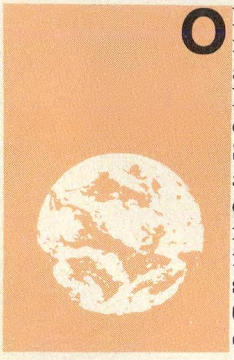

OIL and gas recovery operations in the British sector of the North Sea are being aided significantly by a rapidly growing tropospheric scatter (troposcatter) communications network. The inauguration of a British Post Office (BPO) network has brought the number of commissioned links to four, while an additional ten links are currently being installed. Contracts for three more links will be let this year.

Wide signal variations experienced in the North Sea area, together with the congested spectrum impose severe constraints on the system and equipment designer. Careful subsystem designs have not only overcome these environmental stumbling blocks but have also resulted in a network of communication systems truly exhibiting spectrum efficiency.

B. S. Skingley, Group Leader, Tropospheric Scatter Modems Development, Marconi Communications Systems Ltd., Chelmsford, Essex, England.

Troposcatter systems employ diffraction in the troposphere (the lower atmosphere) to achieve reliable wideband communication at distances considerably beyond the horizon. The path losses depend upon the efficiency of this diffraction, as shown in Fig. 1. The diffraction, in turn, is dependent upon the refractive index (n)−, or more customarily, the refractivity (N_S), where $N_S = (n-1) \times 10^6$.[1]

Variations in the received signal have two major components: long term changes, dependent upon variations in N_S and other climatic factors, and short term (within the minute) fading caused by movement of individual scatterers. The former obeys a log-normal distribution with a standard deviation varying between 6 and 20 dB, depending upon climate and range. The latter follows a Rayleigh distribution[2], as depicted in Fig. 2.

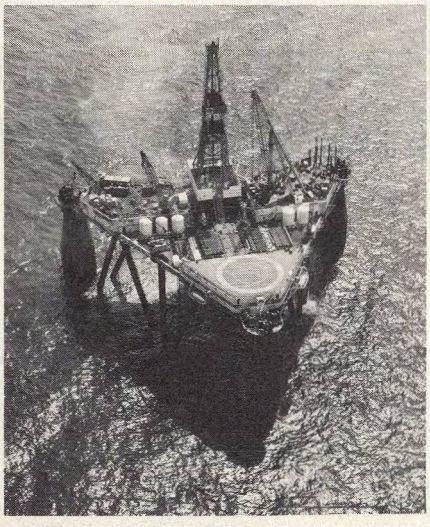

To overcome long-term variations, which for typical North Sea paths approach 120 dB between 0.02- and 99.98-per cent levels[3], high power amplifiers and large antennas are employed together with low-noise receivers. Level-control systems help to maximize spectrum utilization.

Fast Rayleigh fading is controlled by use of uncorrelated diversity channels and combining techniques[2, 7] as discussed below and illustrated in Fig. 2.

Spectrum conservation: A priority

There are currently more than 20 tropo stations operating in and around the North Sea, each with substantial transmitter power and multi-channel communications requirements. This number of high-power radiators, packed into a relatively small area (see, "The crowded North Sea tropo network"), leaves the door open for a variety of interference problems. With only a limited bandwidth to work with, system designers are attempting to minimize the number of carrier frequencies required, reduce the spacing between carriers, and minimize the

(continued on p. 50)

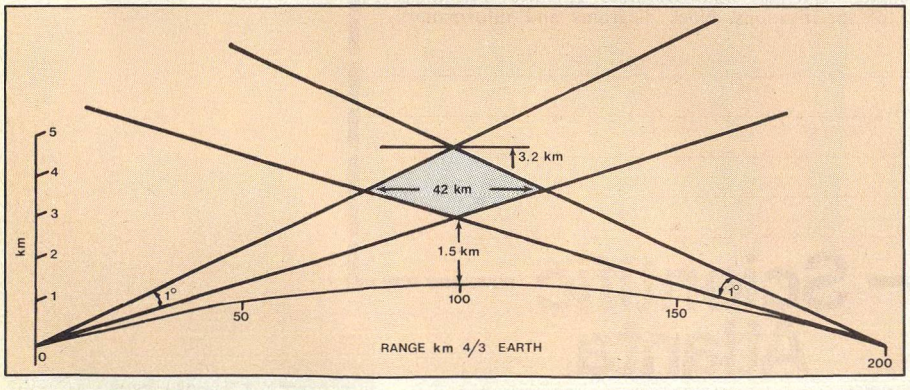

***1. This typical path geometry** curve shows the effect of diffraction efficiency on range. Scatter volume is the diamond-shaped area measuring 42 x 3.2 km.*

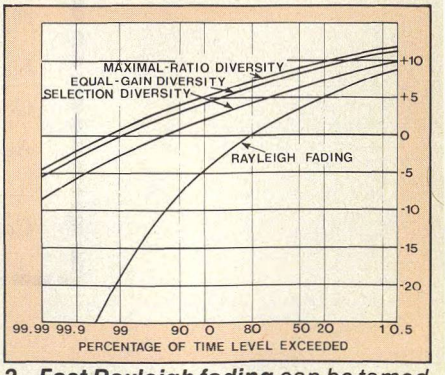

***2. Fast Rayleigh fading** can be tamed via uncorrelated diversity channels and combining techniques.*

coordination distance between systems in order to use the allocated spectrum most efficiently.

The first objective is achieved by the use of quadruple space diversity with polarization selection together with frequency re-use on tandem routes and alternately working between adjacent platforms. This also considerably improves the system availability. Frequency re-use is used on the Ekofisk-Emden system operated by Phillips while alternate route working is used on both the BP private network as well as throughout the BPO network.

Reduction of carrier spacing is complicated by anomalous propagation conditions which enable the coexistance of carrier-to-interference (C/I) ratios as high as −10 dB and signal levels up to −15 dBW for 0.2 per cent of the year. Conventional IF selectivity is not sufficient, due to the high-level intermodulation products (IP) created in the receiver front end. Also, achievement of sufficient selectivity at 2 GHz has been proven to be impractical. The filter response would have to provide greater than 20 dB rejection at ±2.4 MHz while providing less than 100 pwp distortion to a 72 channel carrier with 200 kHz rms test tone deviation and an insertion loss lower than 2.0 dB.

It has been found necessary to implement a receive level-control system to reduce the input level to the receiver, and thus minimize intermod products during these infrequent, yet devastating periods of anomalous propagation. The required selectivity is then obtained with a combination of RF and IF filters. This enables a 3-MHz spacing between the 72-channel carriers to be employed in the BPO network. Coordination distances have been minimized via transmit level-control systems which reduce the transmitter power during periods of anomalous propagation.

Uncorrelated signals over a trans-horizon path can be provided by transmitting the signal over paths separated by space, frequency, time or angle of arrival.

For space diversity, the necessary antenna spacing has been shown to be[4] $\frac{1.6\lambda}{\theta}$ where λ is the free-space wavelength and θ is the scatter angle in radians. Efficient frequency diversity can be obtained with frequency spacings as low as 1 per cent for path lengths greater than 200 km.[4]

Angle diversity has been demonstrated in two separate experiments[5],

The crowded North Sea tropo network

The British Petroleum (BP) network uses alternate routes, working from one shore station to two platforms. There is a link between them to enable platform-to-platform and shore-to-platform communication. In the event of failure of the tropo equipment on one of the platforms, communication would still be maintained with the shore.

The Phillips Petroleum system is the largest private-user communications network in the North Sea. A major complication of this system lies in the distribution of the network across four national areas of the sea. The main terminal is at Ekofisk in Norwegian waters, the oil pipeline terminates at Teesside in England, while the gas pipeline terminates at Emden, Germany, crossing Danish waters on the way. Tropospheric scatter links are being installed along each pipeline with communications to each pump and compressor station.

The complex consists of seven troposcatter links of widely differing ranges. Channel capacities range from 12 to 96. The differing link requirements are satisfied by employing power amplifiers varying between 2 W and 1 kW and low-noise amplifiers to achieve system noise figures between 3 and 10 dB with a standard quadruple-diversity drive and receiver.

Additional requirements are placed on the link to Germany to minimize overshoot into an already heavily congested spectrum in North Europe. Short, 50-W maximum links are used together with a transmit level control. Additionally, only two frequencies are allocated for all three links.

The link to Teesside is direct from Ekofisk with a 1-kW link. The pump stations (PS1 and PS2 on map) receive a sample of the transmitted signals from Teesside and Ekofisk and use only 12 channels of the baseband. Each return path is accomplished with a separate 12-channel unidirectional link so that only

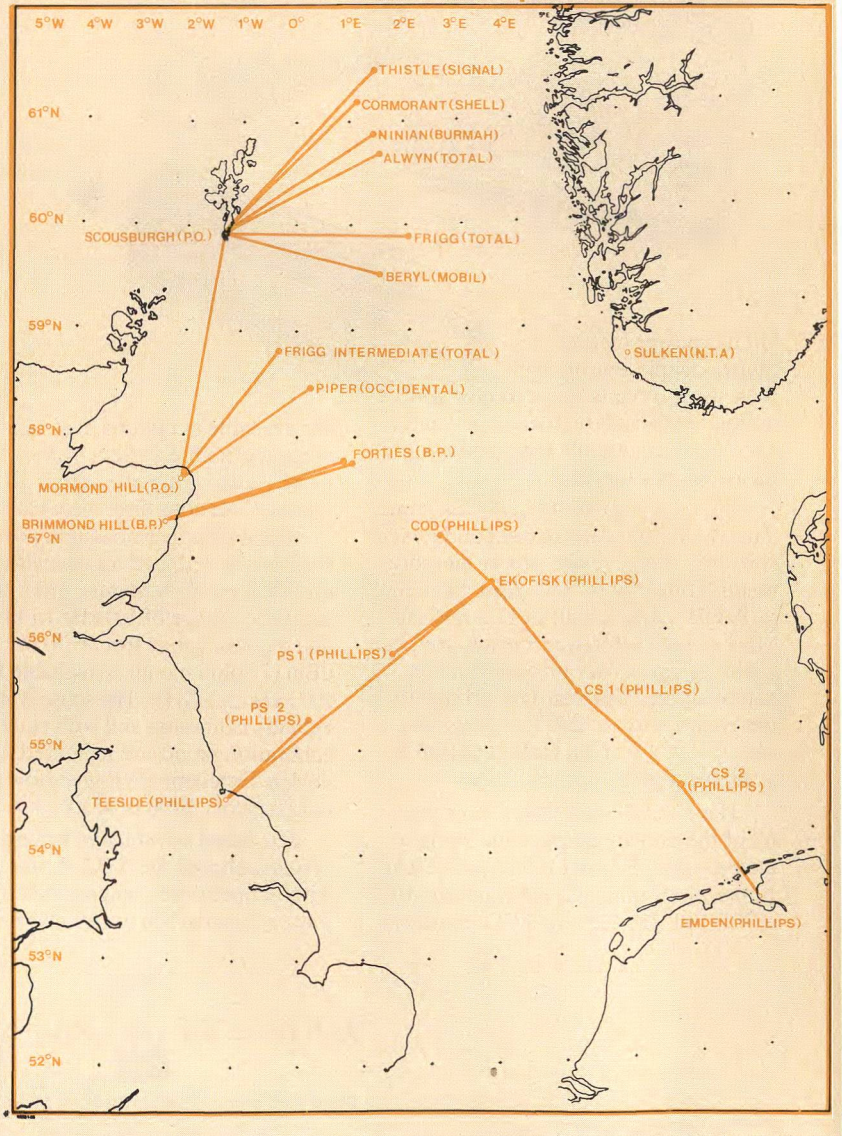

When completed, the North Sea tropo network will include over 20 stations.

our frequencies are required for three separate tropospheric scatter links. To keep this in context, most existing troposcatter links use four frequency hops to achieve quadruple space frequency diversity.

Oil and gas wells in the North Sea are linked to shore-based control and communications center by three major troposcatter networks (see map). The first operational North Sea tropo link, built for the British Post Office (BPO) by Marconi, radiates from two shore stations located at Mormond Hill, in northeast Scotland, and at Scousborough, in the Shetland Isles. From these sites, the system covers all likely production areas in the northern sector of the Sea.

The BPO links operate in the 1.9-to-2.6 GHz range, and are designed to provide a 2400-baud bit error rate of 1 in 10^5 for 99.98 per cent of the worst month. The other two North Sea systems, privately operated by British Petroleum (BP) and Phillips Petroleum, are designed with a slightly lower availability target of 99.90 per cent.

Maximum frequency use in the BPO network is obtained by alternately working adjacent host platforms. Each transhorizon link has a capacity of either 72 or 132 channels. Switching of the alternate system is performed manually, on a time-sharing basis, or by automatic means in the event of a tropo system failure. All current and predicted requirements will be met by 1-kW power amplifiers and paramps yielding a system noise figure, including filters, of 3 dB.

Range variations are accommodated by varying antenna sizes and including threshold-extension demodulators where required. Antennas in the North Sea network vary from 5-meter paraboloids on the production platforms to 19-meter, double-offset billboards at the shore stations. ••

used to verify Gough's theoretical work.[6] These experiments provided firm evidence for additional gain due to long-term decorrelation between the beams—a unique advantage for angle diversity.

Quadruple diversity systems are the most prevalent and cost effective, providing 19, 26 and 34 dB improvements at 99, 99.9 and 99.99 per cent levels. They are historically implemented by a combination of space and frequency diversity. Modern systems like those used in the North Sea, however, make use of quadruple space diversity with polarization selection, enabling links to be implemented with half the number of frequencies previously required.

Predetection combiner chosen

Combining of the diversity signals can be carried out before (predetection) or after (post detection) demodulation. The former requires additional phase control circuits, but results in a significant improvement in availability due to a 6 dB threshold improvement. The post-detection combiner offers the advantage of enabling the combiner to be controlled by total baseband noise, thus enabling full account to be taken of selective fading.

All but one of the current North Sea systems are being implemented with predetection combining systems with the consequent advantages of availability and performance.

The Marconi predetection combiner, implemented at 70 MHz, enables full IF and RF loop testing. Unlike previous combiners, the phase correction does not rely on a wideband phase detector with its own threshold causing errors. The combiner, instead, operates in the maximal ratio mode achieved by shaping the transfer characteristic of the phase corrector to follow the square law. This yields a ratio-squared maximal combiner.

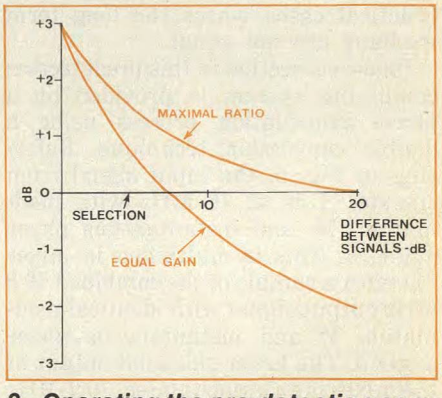

***3. Operating the pre-detection combiners in a maximal mode** results in a significant static improvement.*

The signal-to-noise ratio (S/N) improvement formula for a dual diversity maximal ratio combiner is:

$$\frac{S}{N_{op}} = \frac{S}{N_1}\left(\frac{1 + C^4 - C^2 \cos\phi}{1 + C^2}\right)^{1/2} \quad (1)$$

where $\frac{S}{N^1}$ is the best channel signal/noise ratio

C is the ratio between signal voltages

and ϕ is the phase difference between the signals

The case of zero phase difference yields the static improvement curve drawn in Fig. 3. Figure 4 shows the combining errors due to phase and amplitude differences between the two channels.

While there would appear to be little advantage in implementing the more complex maximal ratio combiner, it

(continued on p. 52)

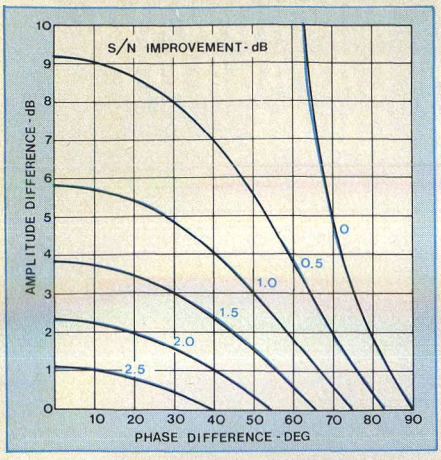

***4. Incorrect relative scanner amplitudes and phases** cause poor combinational performance.*

offers considerable advantages for practical cases where the long term medians are not equal.

Phase correction in this predetection combining system is provided by a phase cancellation process using a double conversion technique. Referring to Fig. 5, the input signal from channel A is at 70 MHz with modulation, M, and instantaneous phase angle, α. This is multiplied in mixer ① with a sample of the combined 59.3 MHz output signal with identical modulation M and instantaneous phase angle β. The lower sideband output of the mixer is an unmodulated, 10.7-MHz signal, with an instantaneous phase angle of $(\alpha-\beta)$.

This is filtered in filter ②, and applied to mixer ③, which also has a portion of the input signal applied to it. The lower sideband output of mixer three is then fed to filter ④. The resultant output frequency of 59.3 MHz, contains the original modulation and a phase angle equal to the difference between the phase angle of the signals applied to the mixer. The foregoing is better expressed:

$$\alpha - (\alpha - \beta) = \beta \qquad (2)$$

from $\cos A \cos B = \frac{1}{2}\left(\cos (A+B) + \cos (A - B)\right)$

taking $A = \omega_1 t\ (\alpha)\ B = \omega_2 t + B$

the difference component $= \cos\left((\omega_1 = \omega_2)\ t + (\alpha-\beta)\right)$

Thus the output of the phase corrector, which is applied to the passive combiner, ⑤ is a perfect replica—in frequency, modulation and phase—of the signal fed from the combiner on lead ⑥.

Figure 6 shows the combination of two channels A and B with instantaneous phase angle α and γ. In both cases, the resultant phase angle is β, thus enabling correct voltage addition of the signals from each path.

Phase-locked loop not mature

Two types of threshold-extension demodulators are currently employed on the Marconi trans-horizon system. Frequency modulation feedback (FMFB) demodulators[8] were used initially on higher channel capacities (72, 96 and 132) with tracking filter AFC. The primary alternative, the phase-locked loop (PLL), was at the time considered a doubtful contender, since sufficiently wideband components were not generally available, and little practical experience was available on its recovery from loss of lock, interference susceptibility and linearity.

The FMFB demodulator is a traditional design with the addition of a tunable single-pole filter to enable the center frequencies of the incoming carrier and the filter to be matched to insure a clean carrier and minimize threshold "pull back". The error voltage is produced by sweeping the filter at 70 Hz which produces AM components at 70 and 140 Hz. The 70-Hz components are zero when the filter and incoming carrier are coincident. An error in either direction produces a rapid increase of the 70-Hz component with opposite phase in each direction. The AM component is detected and its phase compared with the original 70-Hz waveform to produce the error voltage.••

References

1. P. L. Rice and A. G. Longley, "Transmission Loss Predictions For Tropospheric Communication Circuits," National Bureau of Standards Technical Note 101.

2. D. G. Brennan, "Linear Diversity Combining Techniques," *Proceedings Of The IRE*, (June, 1959).

3. Private communication, United Kingdom Home Office, Directorate of Radio Technology.

4. M. Hirai, et al, "Correlation Between Amplitude Of Radio Waves Of Different Frequencies In UHF Beyond The Horizon Propagation," *Journal Radio Research Laboratories*, Japan, (September, 1960).

5. M. W. Gough and G. R. Rider, "Angle Diversity In Troposcatter Communication," *Proc. IEE*, No. 7, Vol. 122, (July, 1975).

6. M. W. Gough, "Angle Diversity Applied To Tropospheric Scatter Systems," *AGARD Conference Proceedings*, No. 70, Dusseldorf, (September, 1970).

7. J. R. Sharmon, "Pre-detection Combing Point-To-Point Communication," Vol. 17, No. 3, (September, 1973).

8. L. M. Enloe, "Decreasing The Threshold In FM By Frequency Feedback," *Proc. IRE*, 50, 18, (1962).

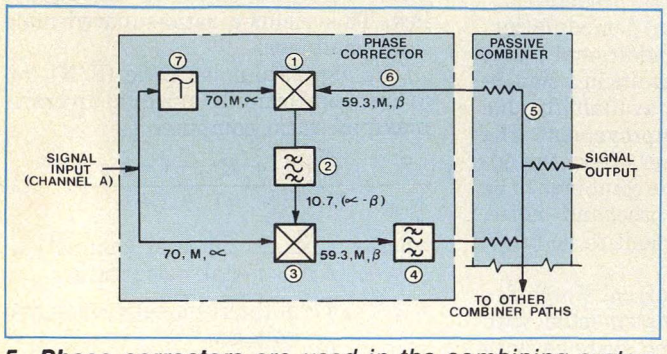

***5. Phase correctors** are used in the combining system to offset any phase, frequency or modulation difference.*

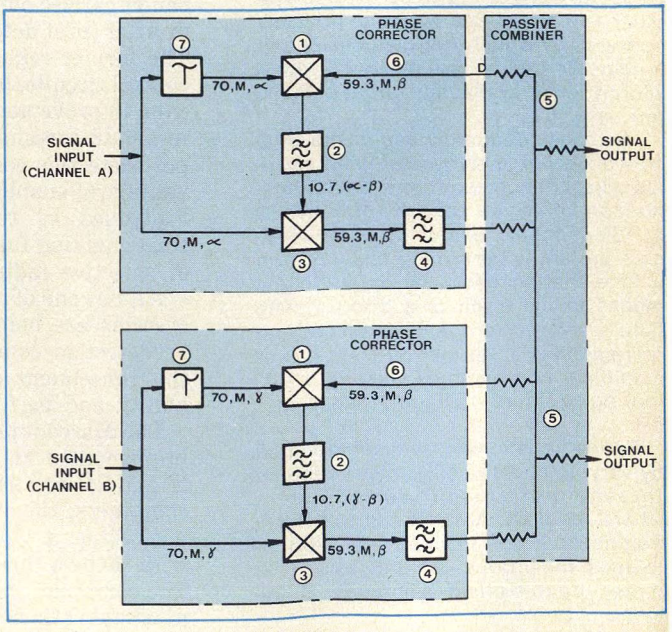

***6. Combiner schemes** ensure zero phase angle differential.*

Build An Integrated Dolph-Chebyshev Array

This developmental note describes a six-element Dolph-Chebyshev array built on a single board. Sidelobe levels of −28 dB and a half-power beamwidth of 24.7° are achieved.

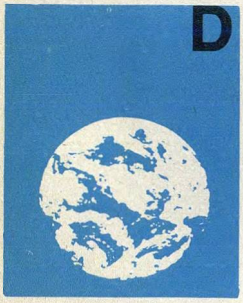

DOLPH-Chebyshev antenna arrays offer the advantages of very low, constant sidelobe levels along with narrow beamwidth. Although theoretical calculations are readily available for systems with sidelobe levels as low as −45 dB and with as many as 24 elements, realization of such a unit in practice involves many technological obstacles.

Most of the difficulties arise when realizing the array in a printed-line form, such as microstrip. Although this type of fabrication results in a compact antenna, the effect of mutual coupling makes it difficult to properly match the radiating system, resulting in a sidelobe level above the theoretical value. The transmission medium itself poses further problems. For example, if sidelobe levels as low as −40 dB are required with a modest number of radiators, the outer pairs of power dividers (see Fig. 1) require high-impedance lines so thin that they will be quite difficult to realize with present printing technology.

This article reports the development procedure and experimental results of a six-element Dolph-Chebyshev antenna array system with −30 dB theoretical sidelobe levels. An experimental model, built in microstrip form on a Texolite substrate, demonstrates −28 dB sidelobe levels and a half-power beamwidth of 24.7 degrees.

The S-band design uses simple, monopole radiators—rigid lengths of rod with specified length and length-to-diameter ratio that results in a nearly resistive, 50-ohm input impedance. In actuality, the impedance is complex and varies with frequency so that the system is somewhat frequency sensitive. Helical radiators with constant, high-resistive impedance over a wide range of frequency, could also be employed but would require impedance transformers.

A summary of Dolph-Chebyshev design steps

In order to design the particular branch-line couplers necessary for the Dolph-Chebyshev energy distribution, one must first define an element factor (Z_o) based on the total number of radiating elements (2n) and the desired ratio of mainlobe-to-sidelobe (r):[1]

$$Z_o = \cosh\left[\frac{1}{2n}\left[\cosh^{-1}\frac{1}{r}\right]\right] \qquad (1)$$

The spacing between radiators, d, can be adjusted to achieve desired half-power beamwidth, which can be expressed as:[1]

$$\sin\phi_{hp} = \frac{\lambda}{\pi d}\cos^{-1}\left[\frac{1}{Z_o}\cosh\left[\frac{1}{2n-1}\cosh^{-1}\left(\frac{r}{\sqrt{2}}\right)\right]\right] \qquad (2)$$

The distance between the radiators must remain in the vicinity of $\lambda_o/2$. If it is decreased, the beamwidth increases for a given number of elements. If it is approached, a second main lobe appears. Too large a distance will make the mutual coupling between the radiators weaker, but the unit will be unnecessarily large; closer spacing will make the mutual coupling stronger and different for individual radiator pairs. For the given case, d is equal to $0.55\lambda_o$.

For a six-element array with two symmetrical sides, the amplitude of the current in the radiating elements, starting from the outer radiator pair, can be expressed as:[1]

$$I_1 = Z_o^5 \qquad (3a)$$

$$I_2 = 5I_1 - 5Z_o^3 \qquad (3b)$$

$$I_3 = 3I_2 - 5I_1 \pm 5Z_o \qquad (3c)$$

(continued on p. 56)

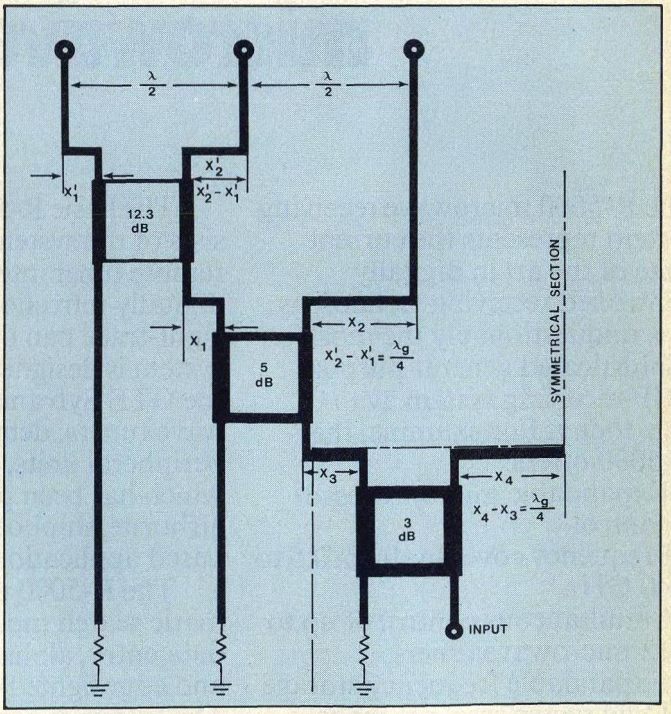

***1. Dolph-Chebyshev power distribution** is achieved with branch-line couplers.*

Dr. Chinmoy Das Gupta, Assistant Professor, Indian Institute of Technology, Department of Electrical Engineering, Kanpur, U. P., India, and **Professor Paul Delogne,** Head, Dept. ElHy, U.C.L, Belgium.

DOLPH-CHEBYSHEV ARRAYS

The ratio of power distribution among the elements can be determined by squaring the ratio of current distribution provided all the radiators have identical input impedance. Although the self-impedance of the radiators can be kept constant for all six elements, the total input impedance is modified due to differences in mutual coupling. The influence of mutual coupling on impedance can be roughly estimated theoretically,[2] but experimental verification of its magnitude in conjunction with other uncertainties, such as fringing field effects, phase descrepancies and partial mismatch of the radiators, is extremely difficult. One means for this study is to put tunable and calibrated plungers on the connecting lines at a distance of half the guided wavelength from the radiators. But to the author's knowledge, such tedious experimental work has not been done so far.

The self-impedance of the monopole radiator can be experimentally decided with the help of a half-wavelength ground plane. The length and length-to-diameter ratio of a matched radiator can first be estimated using Reference 3. The total impedance of the radiator considering the effect of mutual coupling, can be estimated using:[2]

$$Z_{in_1} = \frac{V_1}{I_1} = Z_{11} + Z_{12}\left(\frac{I_2}{I_1}\right) + Z_{13}\left(\frac{I_3}{I_1}\right) + Z_{14}\left(\frac{I_3}{I_1}\right) + Z_{15}\left(\frac{I_2}{I_1}\right) + Z_{16}. \quad (4)$$

where:

Z_{in1} is the net input impedance of the outer pair of the radiators.

Z_{11} is the self impedance of the radiators.

For the different current ratios (I_2) and (I_3) mutual impedances $Z_{in\ n=2...6}$ can be theoretically estimated from Reference 2.

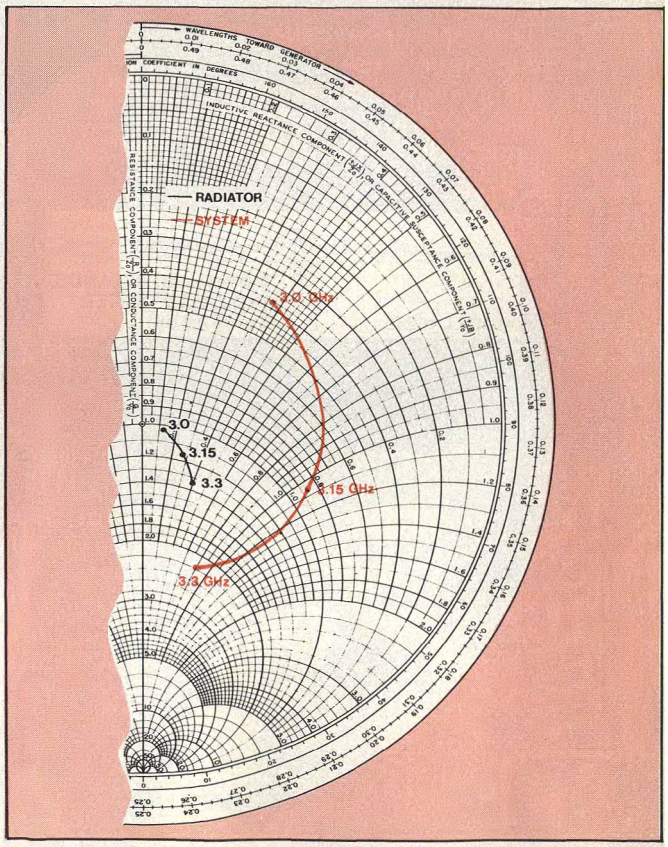

***2. System and radiator impedances** must be matched for optimum performance.*

n analogous manner, the input impedance of the other radiator pairs can be represented as:

$$Z_{in_2} = Z_{21}\left(\frac{I_1}{I_2}\right) + Z_{22} + Z_{23}\left(\frac{I_3}{I_2}\right) + Z_{24}\left(\frac{I_3}{I_2}\right) + Z_{25} + Z_{26}\left(\frac{I_3}{I_2}\right) \quad (5)$$

$$Z_{in_3} = Z_{31}\left(\frac{I_1}{I_3}\right) + Z_{32}\left(\frac{I_2}{I_3}\right) + Z_{33} + Z_{34} + Z_{35}\left(\frac{I_2}{I_3}\right) + Z_{36}\left(\frac{I_1}{I_3}\right) \quad (6)$$

Using these equations, the input impedance of a monopole radiator, 2-mm in diameter and 22.5-mm in length, was estimated to be 54 + j 20 ohms. The impedance of the radiator is compared with the input impedance of the distribution system in Fig. 2. The wider mismatch of the system is due to the central pair of radiators after mutual coupling.

Once the current distribution is known and the effects of mutual coupling are accounted for, the coupling values of the branch-line couplers can be simply calculated using familiar methods.[4,5] For example, a six-element Dolph-Chebychev antenna array system with a theoretical sidelobe level of −30 dB and half-power beamwidth of 22 degrees would require 3, 5 and 12.3 dB couplers, as shown in Fig. 1. From a developmental point of view, it is quite essential that the individual couplers be designed, fabricated and tested separately before they are put in the final system. Otherwise, it will be extremely difficult to localize any fault in the system. Having realized the individual couplers as per requirement, they can be duplicated in the ultimate system and verified with the initial designs.

Experimental model exhibits −28-dB sidelobes

Subsequent design, fabrication and testing in the experimental six-element branch-line coupler's array showed that couplers with coupling factor of 3 dB and 5 dB could be successfully realized on Texolite, according to the theoretical specification. But the 12.3-dB coupler showed a coupling value of 9 dB, due to widening of the high-impedance line by diffusion of light during formation of photo-reduced mask; the width of this high-impedance line for the particular substrate was to be of the order of 0.1 mm. Although edge-coupled lines are easier to design and fabricate for such a coupling factor, their phase characteristic is more difficult to adjust.[6] On the other hand, branch-line couplers can be realized more precisely.

To compensate for the inability to realize a 12.3-dB coupler, an additional branch-line coupler of coupling factor 4 dB was incorporated in the system. This bypassed the extra amount of power from the outer radiators in order to satisfy the power division more according to the Dolph-Chebyshev distribution. Schematic representation of the final layout is shown in Fig. 3; the right section of the layout is symmetrical with respect to the input of 5 dB coupler.

Although the division of power according to the Dolph-Chebyshev distribution can be realized in this manner, it must be noted that the additional 4-dB coupler wastes power, particularly in the case of weak signal detection, and increases noise level.

An alternate approach would be to fabricate the 12.3-dB coupler on a thicker substrate. The ratio of line thickness to substrate thickness remaining constant, the wider, high-impedance lines can be realized with less technological difficulties. Polyguide substrates, for example, have almost the same dielectric constant as Texolite, but are available in 3-mm thickness, which is nearly four times that of Texolite. But the wider lines necessary with techniques also bring increased insertion losses and, higher noise levels.

(continued on p. 58)

DOLPH-CHEBYSHEV ARRAYS

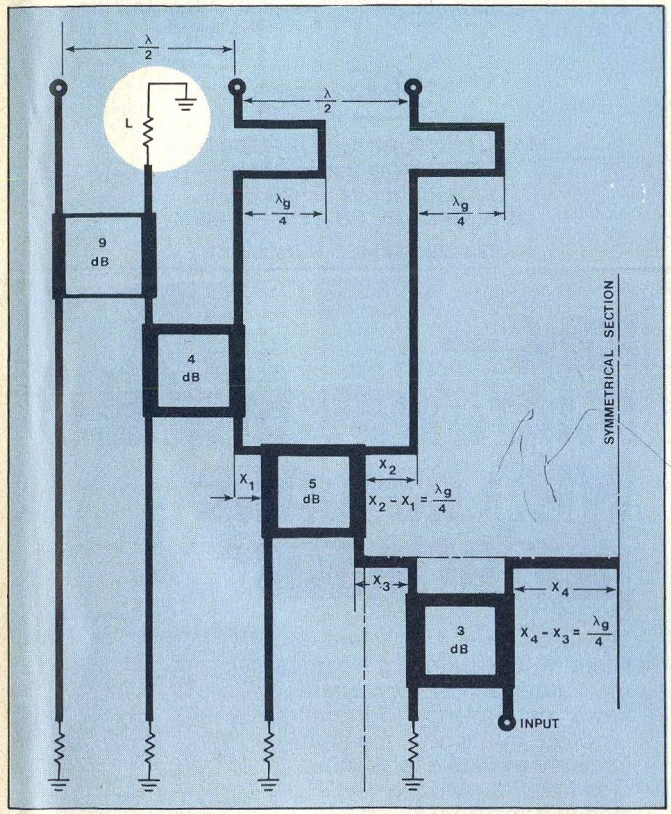

***3. Nine and 4-dB couplers** substitute for the hard to realize 12.3-dB geometry. Power is wasted in load L.*

When terminating the couplers on the final layout, care should be taken so that the lengths of the connecting lines are such that the radiators are excited at identical phases. Realization of shorter and identical terminating lines will make the system less frequency sensitive.

If the system can be made less frequency sensitive both for the feeder system and the radiators, preferably with constant resistive impedance over a wide frequency range, the same unit will fulfill the requirement of different customers. Thereby its commercial demand will be much higher than that of the present one. This work is in progress.

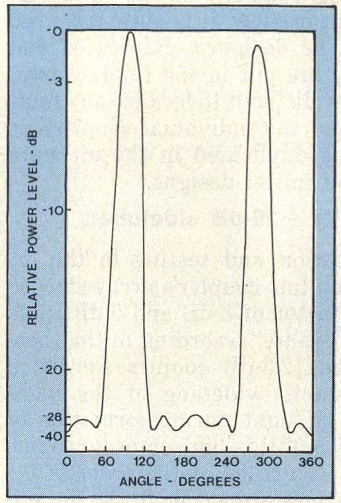

***4. Measurements** of the six-element prototype confirm −28 dB sidelobe levels.*

A radiation pattern plot of the unit as a receiving antenna is shown in Fig. 4. The sidelobes are −28 dB below the main lobes. The back lobe for the present adjustment is 1 dB below the forward main lobe. Higher value of sidelobe level by 2 dB from the theoretical value can be attributed to the mismatch of the radiating system and the phase descrepancy of the radiators.

Half-power beamwidth of the system is 24.7 degrees, which agrees quite well with the theoretical calculated value of 22 degrees.

Better agreement for the sidelobe level can be achieved by proper matching of the radiating system, which is at present, a tedious task due to the effect of mutual coupling. Helical radiators with circular polarization can be made linearly polarized by putting one clockwise and the other clockwise in series. These radiators show constant and high resistive impedance over a wide range of frequency. However, these radiators must be matched to 50-ohm lines through stripline impedance matchinng trransformers.••

Acknowledgement

Author expresses thanks to Mr. J. C. Louis from the Electronics Laboratory of the Institute of Nuclear Physics, Louvain-la-Neuve, Belgium, for fabricating the unit, to Mr. A. Sevrin and the staff members of the Unite El-Hy for helping in the experimental part of the work.

References

1. C. L. Dolph, "A Current Distribution For Broad Side Arrays Which Optimizes The Relationship Between Beamwidth and Sidelobe Level," *Proc. I. R. E.*, Vol. 34, pp. 335-348, (June, 1946).
2. W. L. Weeks, *Antenna Engineering*, McGraw Hill Electronics Science Series, New York, NY.
3. H. Jasik, *Antenna Engineering Handbook*, McGraw Hill Book Company, New York, NY.
4. G. L. Mathei, L. Young and E. M. T. Jones, *"Microwave Filters, Impedance Matching Networks and Coupling Structures*, McGraw Hill Book Company, New York, NY.
5. Burke and Gelnovatch, "Characteristics For Microstrip Transmission Lines According To A. H. Wheeler," *Microwave Journal*, Vol. , No. , pp. 65-66, (February, 1969).
6. L. S. Napoli and J. J. Hughes, "Characteristics Of Coupled Microstrip Lines," *RCA Review*, (September, 1970).

DECEMBER
1976

MICROWAVES

laser technology

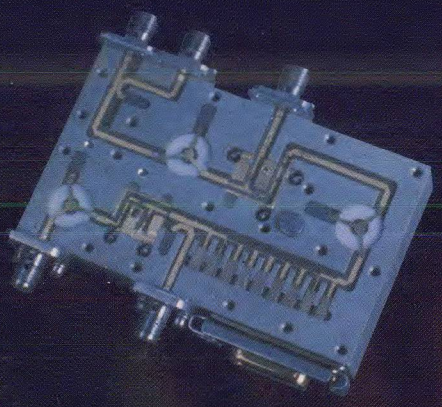

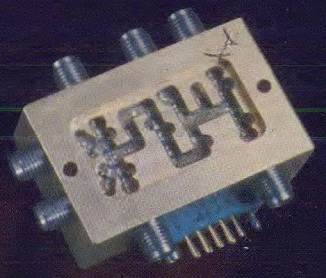

SUPER COMPONENTS COME OF AGE

A SPECIAL REPORT

Also: Coax cable - Are power ratings accurate? · Maser developments spur radio astronomy

MICROWAVES

December 1976
Vol. 15, No. 12

news

editorial

technical

departments

About the cover: Although most designers are hard-pressed to define the term supercomponent, the word seems to jump at you wherever you go. Components courtesy of Omni-Spectra, Merrimac, NH and Raytheon Special Microwave Devices Operation, Waltham, MA. See story on p. 36 for details. Cover composition and photography by Art Director Robert Meehan.

coming next month...Communications

Trends in Earth Station Design: In a comprehensive staff-written report, MicroWaves examines the technological challenges created by the exploding, world-wide demand for small, simple, inexpensive earth stations for satellite communications. Higher frequency usage, advances in low-noise amplifier design, improved antennas and a new generation of satellites are putting satcom within the reach of a wide spectrum of new users, ranging from developing countries to independent cable TV operators.

Upgrade Coax Switches For High Power Transfer. Dr. Robert Winch of Teledyne Microwave shows how to modify coax switches to meet the rigors of power transfer between satellite antennas.

Publisher/Editor
Howard Bierman

Managing Editor
Stacy V. Bearse

Associate Editor
George R. Davis

West Coast Editor
Jose C. de León
Hayden Publishing Co.
744-R Coleman Avenue
Menlo Park, CA 94025
(415) 325-8280

Washington Editor
Paul Harris
Snyder Associates
1050 Potomac St. NW
Washington, DC 20007
(202) 965-3700

Editorial Assistant
Gail Murphy

Production Editor
Sherry Lynne Karpen

Art Director
Robert Meehan

Production
Dollie S. Viebig, Mgr.
Sandra N. Bowen

Circulation
Barbara Freundlich, Dir.
Trish Edelmann
Sherry Karpen,
Reader Service

Directory Coordinator
Janice Tapp

Editorial Office
50 Essex St.,
Rochelle Park, NJ 07662
Phone (201) 843-0550
TWX 710-990-5071

A Hayden Publication
James S. Mulholland, Jr.,
President

MICROWAVES is sent free to individuals actively engaged in microwave work. Prices for non-qualified subscribers:

	1 Yr.	2 Yr.	3 Yr.	Single Copy
U.S.	$15	$25	$35	$2.50
FOREIGN	$20	$35	$50	$2.50

Additional Product Data Directory reference issue, $10.00 each (U.S.), $18.00, (Foreign). POSTMASTER, please send Form 3579 to Fulfillment Manager, MicroWaves, P.O. Box 13801, Philadelphia, PA. 19101.

Back Issues of MicroWaves are available on microfilm, microfiche, 16mm or 35mm roll film. They can be ordered from Xerox University Microfilms, 300 North Zeeb Road, Ann Arbor, MI 48106. For immediate information, call (313) 761-4700.

Hayden Publishing Co., Inc., James S. Mulholland, President, printed at Brown Printing Co., Inc., Waseca, MN.

Electronically tunable filters isolate high-power transmitters

As a result of an Air Force requirement for high-power electronically tuned filters, Stanford Research Center, Menlo Park, CA, with the support of the Rome Air Development Center, Air Force Systems Command, has developed a design approach which leads to UHF filters capable of CW operation at 1 kW. The filter, inserted between a frequency agile transmitter and its antenna, prevents spurious wideband energy from reaching the antenna and also isolates collocated transmitters. According to Dr. Arthur Karp, senior research engineer in SRI's Radio Physics Laboratory, "The Air Force requirement pertains to ground/air/satellite communications systems which transmit and receive information over a number of constantly-changing frequency channels. The bandpass filter must therefore be able to change frequency at high speed in step with the change in transmitted channels."

As reported in the September, 1976 issue of *MicroWaves* (pp. 52-55), the state of the art in commercial electronically-tuned bandpass filters is well advanced—at RF power ratings of the level of milliwatts. At power levels of tens, hundreds and thousands of watts, however, the SRI designers rely on discrete-step electronic switching since the mechanically-tuned high-power filters of the past cannot track their transmitters at microsecond speeds. "The types of switches usually used are PIN diodes," explains Dr. Karp, "because they are available with very high breakdown voltages and because the electrical characteristics of a good switch can be closely approached. The SRI filters tune in quantized steps, the particular application dictating the size of the steps."

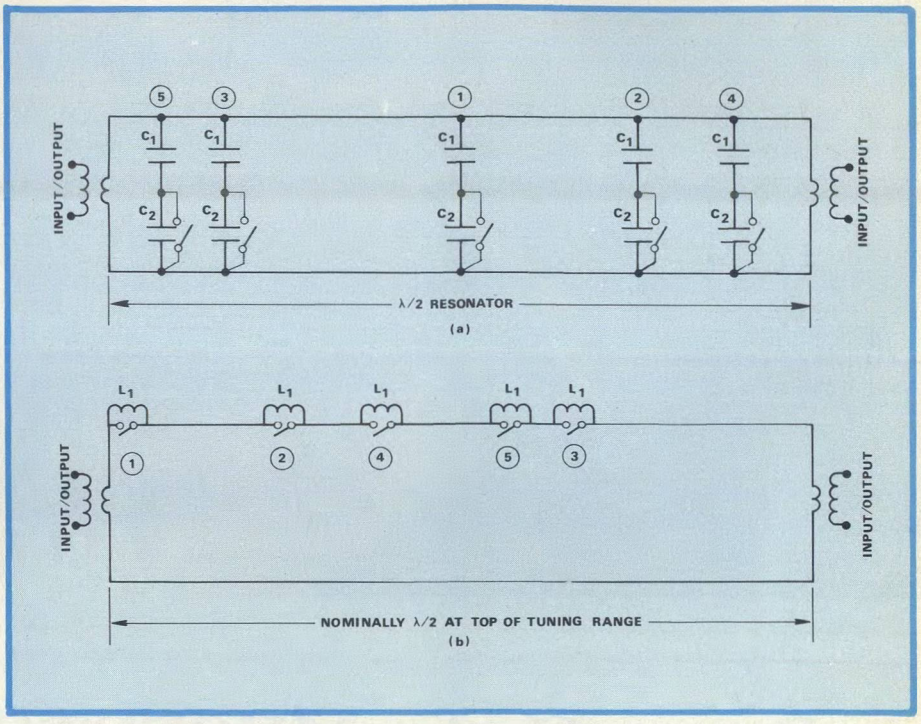

***1. Basic filter resonators** with independent C-type (a) and L-type (b) tuning reactances provide a series of binary-scaled tuning increments. Each switch symbol indicates a suitable grouping of PIN diodes.*

Filter tunes like flute

In the initial stages of the R&D program, the electronically-tuned filters were developed to track a frequency-agile, solid-state aircraft transmitter operating at a CW output level in the order of 100 W. "To date," states Dr. Karp, "the UHF band (225 to 400 MHz) has been the primary area of interest, but since the heart of each filter is a half-wave transmission-line resonator, distributively loaded either with shunt-capacitive irises or series-inductive stubs, it is clear that microwave techniques are being used. These "Flauto" type filter designs should be extendable to the GHz frequency range, and not only to transmitter systems but to receiver systems in locations where the interfering signals may be so strong that varactor or YIG tuning is precluded."

The term "Flauto" has been chosen because the nature of the filter resonator is rather analogous to that of a flute, recorder or other woodwind. These musical instruments (unlike the slide trombone or multiresonator organ, for example) have a single, fixed-length resonator that can have a large gamut of resonances made possible by a small number of independent, spatially distributed, two-valued reactive perturbations—the open or closed state of the finger holes.

The concept on which SRI's Flauto filters are based employs the simplest mode of resonance in an essentially coaxial-line resonator, distributively loaded with several identical but independent reactive elements each containing switches that enable its effective reactance to be two-valued.

"The resonator configuration initially studied used a shunt-capacitive iris for each reactive element and we completed a second-order (two cascaded resonators) filter with a CW rating of 100 W," Dr. Karp reports. "More recently, a series-inductive radial-line stub has been investigated as the filter's reactive element, and a feasibility model was produced to handle at least one kilowatt, CW. In either case, the use of PIN diodes as the switches associated with each independent reactive element enables high-speed channel tuning and hence agility with switching speed presently limited by the bias-driver circuitry to a few tens of microseconds. In addition, since the diodes are used as two-state devices, devices with a continuously variable parameter such as varactors are avoided and intermodulation distortion is minimized."

The unloaded Q of the filter resonator can be quite high. SRI researchers have reported values of at least 1000 in the C-type designs developed to date (see Fig. 1(a)), while an unloaded Q of 2000 is typical for the current L-type feasibility model (see Fig. (1b)). (A

(continued on p. 17)

Jose C. de Léon, West Coast Editor

Power GaAs MESFETS from TI... 1 Watt output at 8 GHz!

That's one big reason to specify Texas Instruments microwave products.

State-of-the-art MSX801 Series Power GaAs MESFETS more than meet your toughest requirements for high performance, high reliability oscillators and amplifiers. You get substantial outputs at X-band frequency...*what* you need, *where* you need it. Typical power-added efficiency of the MSX801 Series is 30%. Available in low-parasitic chip carriers. These new devices are perfect for such applications as radar, telemetry and communications.

MS450 Bipolar Transistors

A new 1.0 micron bipolar transistor has been added to TI's innovative microwave product line. The MS450, now moving into volume production, operates in the 4.0 to 8.0 GHz band as a YIG tuned oscillator. It's available in a nonmagnetic Y package or in chip form.

MS350 S-Band Transistor

The new MS350 from TI is an S-band medium power amplifier transistor with outputs of 0.5W at 2.0 GHz and 0.25 at 4.0 GHz. Volume quantities available now.

Device Type	MSX801	MSX802	MSX803
Min Power Output (W)	0.25	0.50	1.00
Min Gain (dB)	4	4	4
Cont Device Diss (W)	1.33	2.13	4.00
Max Junction Temp (°C)	185	185	185
Price (1-9)	$250	$500	$1000

Beam Leads

Of course you can choose from such familiar TI beam-lead products as: PIN switching diodes; step recovery diodes; Schottky mixer diodes; capacitors and chip capacitors. All parts are designed manufactured and tested to hi-rel specifications and standards.

TI microwave products are available now from your authorized TI distributor or directly from TI. For more information, write to: Texas Instruments Incorporated, P. O. Box 5012, M/S 308, Dallas, Texas 75222. Or call us at (214) 238-3186.

TEXAS INSTRUMENTS
INCORPORATED

READER SERVICE NUMBER 12

63090

ELECTRONICALLY TUNABLE FILTERS *(continued from p. 15)*

filter insertion loss of only 0.5 dB is therefore obtained here when the loaded 3-dB bandwidth is around 1 per cent). Since the RF power rating depends on the reverse breakdown voltage of the PIN diodes as well as on the resonator configuration, diodes with voltage breakdown ratings in the 1000 to 2000 V region are most attractive.

Binary logic drives tuning

The filter resonators are tuned by binary logic, which requires that the tuning increments resulting from the switching of each member of the series of two-valued reactances be related very nearly by the ratios ½, ¼, ⅛, . . ., $\frac{1}{2^N}$ where N is the total number of reactances added to the resonator. (As reported in the July 1969 issue of *MicroWaves*, California Microwave Inc., Sunnyvale, CA, was successful in using a binary-logic digital-tuning scheme employing switched capacitors in a low-power microwave oscillator cavity). In the SRI configurations, the several reactances are actually equal, but the binary progression of tuning increments is a result of the distinctive spatial distribution pattern followed in installing the reactive elements. Dr. Karp points out that while the tuning effect of a shunt capacitive element is weakened by moving it closer to a short-circuited end of the resonator, the tuning effect of a series-inductive element is strengthened.

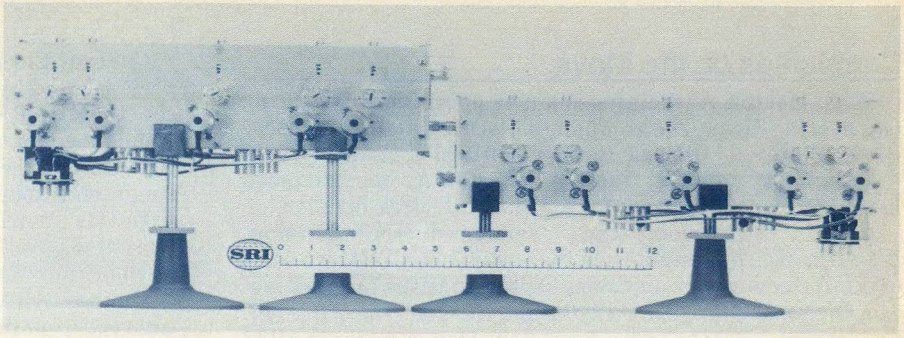

***2. Two cascaded resonators** with electronic tuning provide a second-order UHF bandpass filter rated at 100 W, CW.*

Figures 1(a) (C-type) and 1(b) (L-type) show the essentials of SRI's filter resonator configurations. The switch symbol actually represents a parallel or series-parallel grouping of PIN-diodes chosen to have suitable characteristics. For simplicity, only five tuning elements are illustrated. In Fig 1(a), C_1 represents the capacitance provided by a transverse iris that is spaced from the outer conductor of the coaxial line by the diodes, whose collective residual capacitance under reverse bias is C_2. In Fig 1(b), L_1 represents an inductance provided by a short-circuited radial line joined onto the main resonator, but capable of being shorted out by a group of diodes.

While the electronically-tuned 1kW filter for the 350 to 400 MHz region is still in the "feasibility model" stage, a second-order bandpass filter capable of handling 100 W CW has been built (Fig. 2). Each resonator has seven binary-scaled tuning reactances so that 2^7 or 128 tuning channels are available. SRI achieved a maximum tuning increment of 550 kHz, and the tracking error between the two resonators never exceeds 120 kHz, with the bias-driving commands to each resonator consisting of the same seven-bit binary word. Each channel of this filter has 3-dB and 40-dB bandwidths of about 2 and 22 MHz, respectively and a total channel-center insertion loss of about 2.5 dB.••

SUBMILLIMETER-WAVE POWER SOURCE *(continued from p. 12)*

incident electromagnetic wave excites plasma oscillations in the electron beam. In effect, it density bunches the beam, as seen in Fig. 1(b). The incident wave required for this bunching is larger than in the front-edge method. Incident waves of hundreds of megawatts at 2-centimeter wavelengths (15 GHz) have been used. The output observed during these experiments included coherent signals with 400-micron wavelengths at 1 megawatt power levels. The pulse width, however, is limited only by the time the current pulse is in the tube.

Useful source in 3 to 5 years

The new generator, although still in the basic research phase is already being discussed as a means of heating controlled plasmas for nuclear reactions. Radar and communications applications seem practical also. While millimeter waves are absorbed by the earth's atmosphere, they do propagate efficiently in space. In view of the frequency and power levels possible, radar and communication systems capable of extremely long ranges must be considered as real applications of this unique generator. Although further development of the system depends as always on funding, Granatstein says, "If pursued with vigor, we could have a polished useable device in three to five years." Initial cost estimates are also promising. The most expensive item in the present system is the relativistic electron beam accelerator developed at NRL at a cost of $100,000. The researchers feel that with continuing technology that might represent the finished product cost.

The scientists are, in fact, presently addressing themselves to the cost/efficiency factors. A recent development is the inclusion of a magnetic resonator to enhance the pump effect. Placing the resonator between the pump and the cyclotron has strengthened the pump effect on the beam. The electron beam now requires a one kilogauss magnetic field, but a field/power tradeoff may be possible. In addition, practical pump sources may soon become available. NRL is particularly excited about a new 1.7-gigawatt magnetron developed by Professor Bekefi at MIT. The 3-GHz maggie is presently being evaluated by the Navy researchers to determine its reliability. Other efficiency studies are underway to reduce beam power. The current device uses a beam current of 50 kiloamps to 1 megaamp for scattering.

A super TWT amplifier?

The generator, detailed in Fig. 2, is primarily considered a millimeter and sub-millimeter power source, but the growing wave phenomena also indicates amplification possibilities. By coupling sub-millimeter energy into one end of the device, an effective traveling-wave amplifier could be realized. The energy would essentially increase as it travels through the tube due to the free-growing nature of the reflected power. Conceptually, it is the same process employed by a traveling-wave tube. The output would be extracted in the same manner as in the generator case—through a waveguide window. The dotted view in Fig. 2 represents an input laser irradiating a mirror in the drift tube. Energy could reflect off the mirror and enter the active region of the tube. The extracted output would thus be an amplified sub-millimeter signal.••

Companies on the Move

M.C. Horton Associates is a new microwave consulting engineering firm. The company is located at 19916 Roscoe Blvd., Suite 16, Canoga Park, CA 91306 (213) 998-0368.

Crown Microwave, Inc., Billerica, MA, has expanded manufacturing facilities for its diode devices division.

Alpha Industries, Inc., semiconductor division, Woburn, MA, has announced the opening of a Western sales office for customers and sales representatives in Washington, Oregon, California, Arizona and Nevada. The office will be located at 3031 Tisch Way, San Jose, CA 95128 (408) 247-6876.

Contracts and Financial News

RCA, Moorestown, NJ, a $1.6-million contract from the **Army** to provide them with two EQUATE Automatic Test Systems. EQUATE (Electronic Quality Assurance Test Equipment), is a computer-controlled automatic test system for diagnostic, fault-isolation and performance testing of all types of military electronics, including communications, radar and avionic equipment. **RCA,** Moorestown, NJ, a $159.2 million contract from the **Navy** to develop a shipboard combat system using the RCA-designed AEGIS fleet air defense system as its nucleus.

RHG Electronics Laboratory, Inc., Deer Park, NY, a $158,000 contract from the **Air Force,** Eglin AFB, FL, for a quantity of all-weather microwave relay links for use at various Air Force test ranges.

Cutler-Hammer's AIL division, Melville, NY, a contract from the **National Aeronautics and Space Administration,** Johnson Space Center, Houston, TX, for a Ku-band parametric amplifier/downconverter for experimental use associated with the Space Shuttle.

Fujitsu Limited, Tokyo, Japan, a ¥ 1,200-million order from the **Bangladesh Telegraph and Telephone Board (BTTB)** for three separate microwave systems to be installed in different regions of the country.

Raytheon Company's Equipment division, Wayland, MD, a $28-million contract from the **Air Force,** to build the new submarine-launched ballistic missile (SLBM) warning system PAVE PAWS at Beale Air Force Base, CA.

LogiMetrics, Inc., Plainview, NY, a $400,000 contract from the **Department of the Army** for three high power travelling-wave tube amplifiers covering the frequency range of 200 MHz to 1 GHz.

Scientific-Atlanta, Inc., Atlanta, GA, an order from **WBEN,** Buffalo, NY, to furnish and install a transmitting and receiving video satellite earth station.

American Electronic Laboratories, Inc., Colmar, PA, a $364,075.00 contract from **NASA-Ames Research Center,** Moffett Field, CA, for the design, development, integration and testing of a low cost airborne microwave landing system receiver.

Delta Microwave, Inc., Westlake Village, CA, a $750,000 contract from **Datron Systems, Inc.,** Chatsworth, CA to provide UHF diplexers as part of their Navy Satellite Communications Systems program.

Marconi Communication Systems Limited, Chelmsford, England, £ 1 million contract from the **British Post Office** for trophospheric scatter equipment for use in the communications network serving oil production platforms in the North Sea.

Applied Devices Corp., Hauppauge, NY, a $737,742 contract from the **Air Force Systems Command, Electronic Systems Division,** Hanscom Air Force Base, MA.

General Electric Cosmos Group, Valley Forge, PA, has been selected by the **AEROSAT** partnership, composed of the **COMSAT General Corp. of the US,** the **European Space Agency** and the **Government of Canada,** to build AEROSAT, the international experimental transoceanic communications satellite for commercial aircraft.

Harris Satellite Communications' Operation, Melbourne, FL, a $29-million contract from the **Government of Sudan** for a domestic satellite communications system.

Hughes Aircraft Co., Culver City, CA, a $15-million contract from the **Federal Republic of Germany Ministry of Defense** for REMUS electronic test systems.

GTE Sylvania, Inc. Mountain View, CA, a $1.4-million contract from the **Army** for installation of an electronic system that provides computer-controlled processing, data storage and retrieval.

RCA's Government & Commercial Systems , Moorestown, NJ, a $5,356,000 modification from the **Naval Sea Systems Command** for development of the Aegis weapon system.

Narda Microwave Corp., Plainview, NY, announced a quarterly cash dividend of $.05 per share to stockholders of record October 29, 1976 payable on November 15, 1976. The company also reported a loss of $.04 per share on sales of $2,052,000 for the three months ended September 30, 1976, as compared with earnings of $.10 per share on sales of $2,223,000 for the same period ended September 30, 1975.

Comtech Laboratories, Inc., Smithtown, NY, announced record operating results for the fiscal year ended July 31, 1976. Net sales for 1976 were $23,128,055 as compared to $16,563,517, earnings per share in 1976 were $1.44 as compared to $.94 for the previous year.

People on the Move

A reorganization has formed the **Consolidated Instruments Operation** at the Santa Clara Division of **Hewlett-Packard. Jack Leiberman** has been named general manager and **Ned Barnholt** has been named marketing manager of the operation while **Duncan MacVicar** has been promoted to product marketing manager for frequency counter product lines.

James L. Godbout has been appointed operations manager for **GHz Devices, Inc.,** Chelmsford, MA.

Lawrence F. Miller has been named vice president-engineering for **EIP, Inc.,** Santa Clara, CA.

William G. Parzybok Jr. has been appointed general manager of **Hewlett-Packard Company's Loveland instrument division,** Loveland, CO.

James E. Duggan has been named manager of engineering for the **solid state products division, Addington Laboratories, Inc.,** Sunnyvale, CA. **Paul A. Bittner** has been appointed to the position of quality assurance manager for the solid state products division. **Gerald K. Zimmerman** has joined **Addington Labs** as quality assurance test engineer and **Richard Mason** has been named mechanical engineer for the division's USMC diplexer project.

Allan P. Steiner has been elected vice president-finance for **Wavecom Industries,** Palo Alto, CA.

Mr. D.J. Humphries has been named regional manager for **Marconi Communication Systems Limited,** England. He will be responsible for the oil industry communication systems.

Danny E. Cornett has been appointed account representative, cable communications products for **Scientific-Atlanta, Inc.,** Atlanta, GA. —*S.L.K.*

parable impedance ranges, Houdart points out that these media present disadvantages in other areas.

"Suspended stripline has the disadvantage that unwanted transmission modes are likely to limit the operating bandwidth, while slot-line has the drawback of being difficult to excite when designed for broadband applications," he cautions. "Furthermore, slot-line circuits have a tendency to radiate energy which poses additional problems."

Houdart's work findings point up the fact that propagation parameters of coplanar waveguide are relatively insensitive to changes in the thickness of the ceramic dielectric. Houdart also reports that the characteristic impedance of the transmission line can be accurately controlled by varying the ratio of line width to ground plane separation.

While a broad range of impedances is certainly useful, the main advantage of coplanar waveguide in most applications is the ease with which circuit elements such as semiconductors and capacitors can be mounted. Since the conductor and ground plane are both located on the same surface, there's no need to drill through the substrate or use edge plating to find ground. For narrowband components, this isn't much of an advantage, since in a microstrip circuit, one need only to add an open-circuited, low-impedance, quarter-wavelength line to find ground on the conductor side of the substrate. But for broadband microstrip circuits, this type of grounding scheme falls apart, and expensive drilling is usually required.

Coplanar line, enclosed in a channel has been successfully used at frequencies as high as 60 GHz. The ability to realize high impedance lines that are wide relative to microstrip widths makes it a natural for GaAs FET circuits. Perhaps the major drawback to coplanar line is the requirement that all ground planes be held at exactly the same potential. This usually requires bond wires bridging the conductor.

With many strong advantages, one would naturally think that coplanar waveguide would have gained the same acceptance as microstrip and stripline in the seven years since its inception. However, most of the production-oriented component manufacturers polled by *Micro Waves* had a common response: Although promising, coplanar line is still just a bit too exotic for everyday use.

Wanted: A set of standardized mil-specs

Finally, a word should be said about military specifications. Although all of the companies contacted by *Micro-Waves* said that they had no problems meeting existing mil-specs with multi-function components, there is some desire in the industry for a standard specification exclusively for hybrid integrated circuits.

"Since more and more people are going toward the multi-function approach, and since virtually all the really high-order integration approaches require the use of hybrid circuits, the problem of specification and controlling reliability really comes to the surface," claims Raytheon's Thomas Rose. "Depending on whether it's an Army, Navy or Air Force Program, there are different specs that must be applied."

Many designers integrating diverse circuits together find that MIL-STD-883, written for small, discrete semiconductors, can just not be applied. "Most customers say, 'use paragraphs so and so of MIL-STD-883 with the following changes'," charges one designer. "What happens is that since nobody standardizes, you end up using virtually different design approaches for different customers even where the functions are identical. This just goes against the grain of the entire supercomponent approach."••

How Much Power Can That Coax Cable *Really* Handle?

Data sheets for coaxial cable do not always provide reliable power ratings. But armed with physical constants, insertion losses and ambient temperature, it's simple to check the spec.

SYSTEM and sub-system designers employing RF coax cable have often discovered discrepancies between published and actual RF cable power ratings. A little detective work into vendors' methods of obtaining cable power ratings yields some surprising results.

- Cable vendors do not always test all sizes of a cable they supply, but instead, rely on a test of a single size and project power capabilities for the remaining sizes.
- Power ratings are often a result of interpolation of the maximum capability of other cable types—even though these are not always similar.
- Some vendors actually *depend on their competitor's catalog* to determine ratings of cable in their own inventory.

While it is acknowledged that it is uneconomical for a vendor to test all cable types and sizes they stock, the question remains—"How can a designer be confident of a vendor's cable rating?"

The problem has one obvious though impractical solution: mandatory incoming test of all supplied cable. Calculating cable power rating, unfortunately, is usually a long-winded rigorous process that designers can normally ill afford.

With this in mind, a technique was developed to determine coax cable power ratings, using a simple series of calculations based on the cable insertion loss and environmental temperature. Using this technique several published power rating errors were discovered.

The method is designed to give quick estimates of power capability using a minimum of calculations. It is not theoretically rigorous, but an empirical approach that has proven successful for all RF cables.

The attractiveness of this simple technique is that it can be used to calculate cable power handling regardless of cable type, size, dielectric material, or operating temperature.

What factors control maximum cable power?

The limiting parameter controlling the power capability of a coaxial cable is heat. Most of the heat is generated by the center conductor resistance. More precisely, it is the dielectric's ability to withstand the temperatures generated, and its effectiveness to transfer heat to the outer jacket that limits the power handling capability of the coaxial cable. In the case of the most widely used dielectric, Teflon, a maximum operating temperature of 200 to 250°C is the upper allowable limit. That is, the operating temperature of the center conductor must be limited to a maximum of 250°C.

What then, are the parameters that affect the operating temperature of the cable? There are four:

- **attenuation,** defined as the combined conductor and dielectric losses at the operating frequency,
- **ambient temperature** defined as temperature of the cooling medium,
- **heat transfer characteristic** of the dielectric and finally,
- **surface area** of the outer conductor.

Since the center conductor is the major contributor of heat, let us consider it as a heat source and the outer cable conductor as a sink. Assuming the conductor is operating at its maximum temperature and knowing the thermal resistance of the sink, one can calculate the thermal dissipation of the coaxial cable:

$$\frac{T_c - T_a}{\theta} = S \qquad (1)$$

where T_c = center conductor temperature, °C
T_a = ambient temperature of cooling medium, °C
θ = temperature resistance, °C/watt/ft.
S = thermal dissipation, watts/ft.

(continued on p. 46)

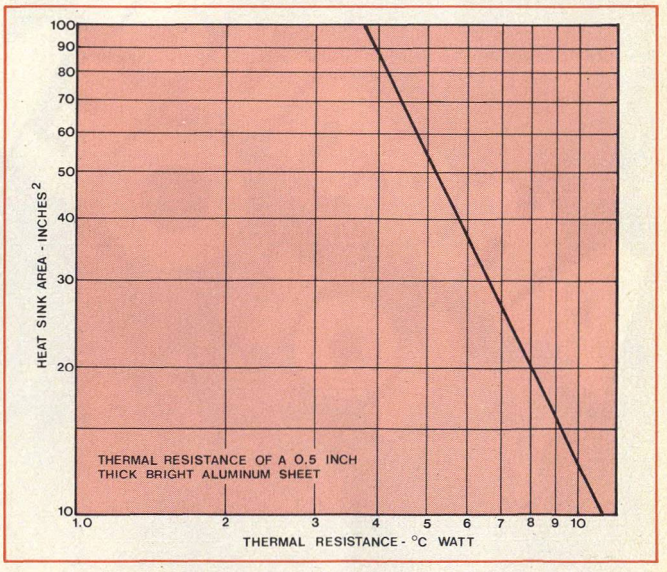

1. Use a thermal resistance curve, *such as this one for aluminum and a few simple calculations to determine RF coax cable power rating. Figure courtesy of Motorola.*

S. R. Goodman, Senior Engineer, and **R. F. Porter,** Senior Engineer, Westinghouse Electric Corp, Defense and Electronic Systems Center, Baltimore MD 21203.

CABLE POWER CAPABILITY

The effectiveness of a surface's ability to dissipate heat can be described by its temperature resistance. Temperature resistance curves for most useable materials can be found in a number of engineering handbooks. A temperature resistance curve[1] showing the ability of aluminum to dissipate heat to the environment is shown in Fig. 1.

Use a step-by-step approach to find power rating

To relate thermal dissipation, S, to power loss, first calculate the fraction of the power dissipated in the cable by the common expression:

$$\alpha = -10 \log P \quad (2)$$

where,

α = attenuation in dB/ft.
$P = 1-\Gamma^2$ fraction of power transmitted
Γ^2 = fraction of power dissipated in cable per unit length
Γ = reflection coefficient

Power rating in watts (P_R) can than be calculated from:

$$P_R = \frac{S}{\Gamma^2} \quad (3)$$

A typical problem might involve a 0.5-inch, aluminum-jacketed cable with an attenuation of 14.5 dB/100 ft. This cable's power ratings can be calculated in a simple five-step approach.

Step 1

A 0.5-inch diameter cable would provide a heat sink surface area of,

$$(\pi D) = \pi\ (0.5)\ 12 = 18.85\ \text{in}^2/\text{ft}$$

Step 2

From Fig. 1, a heat sink area of 18.85 inches^2 provides a thermal resistance, (θ), of 8.3°C/watt/ft.

Step 3

$$\begin{aligned} \alpha &= -10 \log P \\ -0.145 &= -10 \log P \\ 1.03395 &= P \\ 1 - \Gamma^2 &= P \\ \Gamma^2 &= 0.03395 \end{aligned}$$

Step 4

$$\frac{T_c - T_a}{\theta} = S$$

$$S = \frac{250°C - 25°C}{8.3°C/\text{watt/ft}} = 27.11\ \text{watts/ft}$$

Step 5

$$P_R = \frac{S}{\Gamma^2} = \frac{27.11}{0.03395} = 798\ \text{watts}$$

The power rating for the 0.5-inch diameter cable with a Teflon dielectric is 798 watts.

Compare with a detailed analysis

At first glance, the foregoing may seem a bit too empirical to be accurate. A more detailed analysis, however, proves the validity of this simple technique. A thorough inspection of Fig. 1, for example, indicates that the parameters used in the cable power calculations are not as stringent as those encountered in a real cable.

The figure represents a square plate held vertically in still air. This resistance is much larger than the convective thermal resistance of a coaxial cable. If this effect is

(continued on p. 48)

accounted for, it would significantly increase the power handling capability of the cable. There is, however, a counterbalancing resistance which is not included in the empirical method. Since the heat is generated in the center conductor, it must dissipate through the dielectric to be rejected to the air at the outer surface. This additional resistance causes the calculated power handling capability of the coax to be approximately equivalent to the empirical estimate.

To demonstrate the similarity between the power estimates obtained by the two methods, a more rigorous method may be used to solve the sample problem detailed earlier. Steps 1 through 3 remain unchanged.

Step 4

Taking into account individual thermal effects, first calculate the thermal resistance through the dielectric:

$$\theta_1 = \frac{\ln (D_0/D_1)\ (1.89)}{2\pi kt}$$

where D_0 = Outer diameter of the dielectric (0.46 inch)
D_i = Inner diameter of the dielectric (0.137 inch)
k = Thermal conductivity of the dielectric material (for Teflon k = 0.14 Btu/hr°F ft)
t = 1 foot

$$\theta_1 = \frac{\text{In}(.46/0.137)(1.89)}{2\pi(0.14)\ 1} = 2.6$$

Step 5

Now, calculate the convective thermal resistance from the outer case to the air:

$$\theta_2 = 3.7\ (D_0/\Delta T)^{0.25}\ (1.89)/\text{Area}$$

where: D_0 is in feet
T is in degrees Fahrenheit
Area is in feet^2

$$\theta_2 = 3.7\ (0.5/12(250\text{-}251)1.8)^{0.25}\ 1.89\ (144)/18.85$$
$$\theta_2 = 5.38$$

Step 6

$$\frac{T_c - T_a}{\theta_1 + \theta_2} = S$$

$$S = \frac{250 - 25}{2.6 + 5.38} = 28.2$$

Step 7

$$P_R = \frac{S}{\Gamma_2} = \frac{28.2}{0.03395} = 830 \text{ watts}$$

The resulting power rating is obviously very close to that obtained with the empirical method—within 5 per cent.

It is essential to point out that this analysis is still not completely rigorous, since 100 per cent of the power is not dissipated in the center conductor, and there are interface thermal resistances which were not included. However, these effects are small and again tend to be self-compensating. Including the interface resistances tends to decrease the power handling capability of the cable, whereas including effects of some power dissipation in the dielectric tends to increase the power handling capabilities.

The net result of a very thorough analysis is that the end result is very close to that obtained by the simplified method.••

References

1. *Motorola Power Transistor Handbook*, Motorola, Inc., First Edition, p. 25, (1961).

A Hybrid Ring You Can Build Yourself

It's easy to build a crossover hybrid ring for applications as a power splitter, linear mixer or RF isolator. All you need are simple hand tools, cable scraps and four inexpensive connectors.

A hybrid ring is a bilateral electric network which may be used to add or subtract two RF signals without causing frequency "pulling" or other adverse interaction between the signal sources. This article describes a unique type of "crossover" hybrid ring that is generally not commercially available. The design has been simplified so anyone with ordinary hand tools and scrap materials may try a "do-it-yourself" design, construction and test project.

Described herein are the theory of operation, design equations and performance characteristics of a crossover-type coaxial hybrid ring designed for wideband (2:1) operation in the 500 to 1000 megahertz frequency range.

Hybrid ring used as linear mixer

The application of a hybrid ring as a linear mixer is illustrated in Fig. 1. Note that this particular diagram shows the hybrid ring as a symmetrical, four-port device. Any of the ports may be used as an input, because all input ports have the same impedance, as will be shown in subsequent discussion.

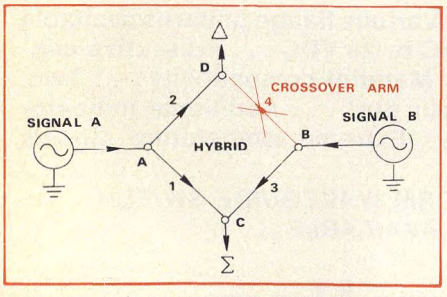

***1. The hybrid ring** operates as a linear mixer.*

Antonio N. Paolantonio, P. E., Registered Electrical Engineer, Radio and Communications Consultant, 17806 Elkwood Street, Reseda, CA 91335.

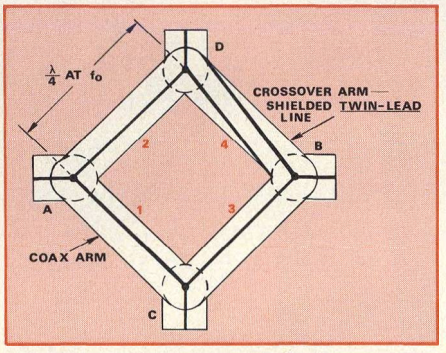

***2. The crossover arm** of the coaxial hybrid ring provides a phase shift of 270 degrees.*

In this example, signal A is fed to port A, where the power is split equally into arms one and two of the hybrid. Similarly, signal B is fed to port B, where the power is split equally into arms three and four. The crossover arm of the hybrid causes a phase shift of 270 degrees, while the phase shift in each of the remaining three arms is 90 degrees; hence, phase cancellation and reinforcement occur in the two sides of the figure. Output signals at ports C and D become, respectively, the sum and the difference of signals A and B. In addition, a high order of isolation is inherently maintained between A and B.

Crossover resembles twin-lead line

A schematic diagram of the crossover type coaxial hybrid ring is shown in Fig. 2. All arms of the hybrid are of equal length; i.e., a quarter wavelength at the center of the frequency band (f_0). However, it can be seen that the internal construction of the crossover arm is quite different from that of the other three arms. While arms one, two and three are constructed in the familiar, coaxial TEM mode, arm four resembles a parallel-wire, twin-lead transmission line inside an outer shield.

The crossover technique allows a three-quarter wavelength electrical phase shift to take place in the space of a quarter wave due to the combined effect of the transformer action of the parallel line and its actual physical length. The parallel line, acting as a transformer, provides a 180-degree phase shift, which when combined with the physical quarter wavelength of the line, provides a 270-degree phase shift.

A cross-sectional view at any point along arms, one, two and three may be represented as shown in Fig. 3. The equation for the characteristic impedance of the coaxial transmission line is given by:

$$Z_{oc} = \frac{138}{\sqrt{\epsilon}} \log_{10}\left(\frac{D}{d}\right) \quad (1)$$

(continued on p. 54)

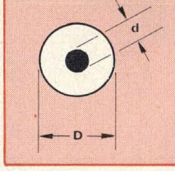

***3. A cross-sectional view** at any point along arms one, two and three shows that they operate in the coaxial TEM mode.*

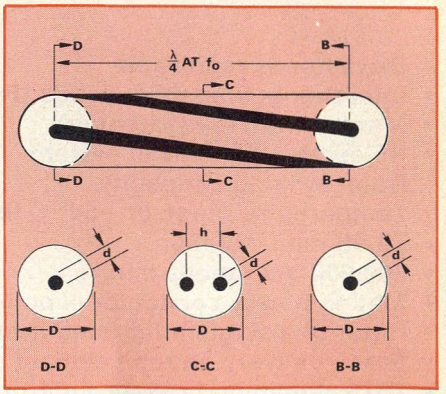

***4. The crossover arm** is a parallel-wire, twin-lead transmission line with an outer shield, but has a coaxial configuration from either end and becomes a shielded twin-lead transmission line at the center.*

HYBRID RING

The crossover section, arm four, is a parallel-wire, twin-lead transmission line with an outer shield, as shown in Fig. 4. Looking into either end of the crossover arm, the transmission line is coaxial. At the center of this arm, however, it becomes a shielded twin-lead transmission line. To provide a smooth transition from the coaxial to twin-lead configuration along this arm, it may be seen that:

$$h \ll \left(\frac{\lambda}{4} \text{ at } f_o \right) \gg D \qquad (2)$$

Where:

$$f_o = \sqrt{f_1 f_2} \qquad (3)$$

f_1 = upper band limit
f_2 = lower band limit

The equation for the characteristic impedance of a twin-lead transmission line where ϵ is the dielectric constant of the insulating material inside the transmission lines.

Step-by-step design

With all equations on hand, a sample design of a practical hybrid ring will be carried out. To begin the design procedure, convenient connectors for the four ports must be selected and the diameter of the inner conductors and outer shields determined. To complete the procedure, the length of the arms must be computed and the gap spacing between the two lines in the twin-lead transmission line for arm four calculated. The completed hybrid ring can then be assembled and tested.

In following the design procedure as outlined above, the following calculations must be made:

- *Connector selection:* In this sample design, a type N connector was selected both for convenience and because it is a rugged unit. But the calculations herein apply to other types of connectors as well.
- *Center conductor size:* To reduce junction discontinuities, the center conductors were made equal in size to the connector pin; i. e., 0.16-inch in diameter. Using Eq. (7) to compute the inside diameter of the shield:

$$\frac{D}{d} = 3.51; \text{ hence, } D = 3.51 \times 0.16$$

$$\therefore D = 0.562 \text{ inch}$$

The example given here uses an "air-loaded" line; hence, $\epsilon = 1.00$.

- *Length of arms:* The design center frequency is computed with the aid of Eq. (3). Assuming the band limits are from 500 to 1000 MHz:

$$f_o = \sqrt{f_1 f_2} = \sqrt{500 \times 1000}$$

$$\therefore f_o = 707 \text{ MHz}$$

(continued on p. 56)

DO-IT-YOURSELF HYBRID RING

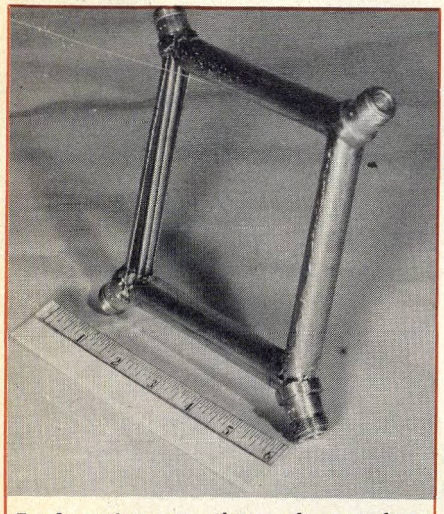

***5. A cut-away view of arm four** shows the crossover construction.*

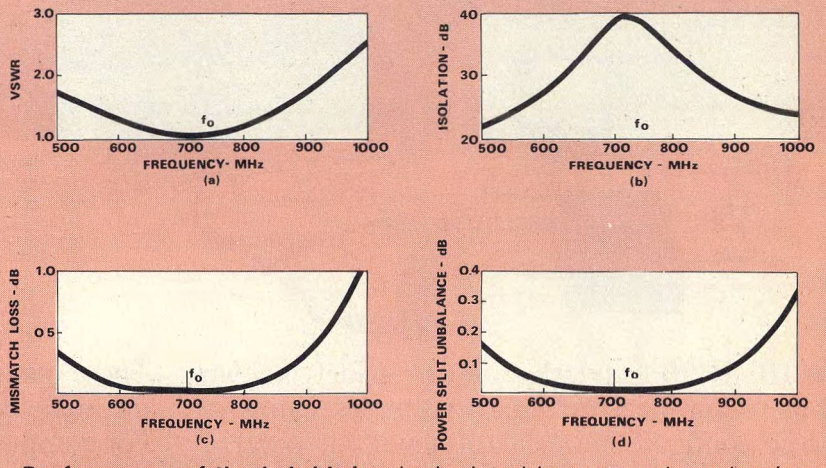

***6. Performance of the hybrid ring** is depicted in curves showning input VSWR (a), isolation (b), input mismatch (c) and power split unbalance (d).*

Each arm is a quarter-wavelength long at this frequency, therefore:

$$L = \frac{\lambda}{4} = \frac{300}{f_o}\left(\frac{1}{4}\right)$$

$\therefore$ L = 10.6 cm. (4.20 inches).

- *Conductor spacing:* Use Eq. (8) to compute spacing of twin-lead bars in arm four.

$$h = 1.125d = 1.125 \times 0.16$$

$\therefore$ h = 0.18 inch (between centers)

The design is now complete. A summary of parameters is given below.

Frequency band:	500 to 1000 MHz
Length of each arm:	4.20 inches
ID of shield:	0.562
OD of inner conductors:	0.16 inch
Twin-lead spacing:	0.18 inch
Connectors:	Type N

The completed crossover-type coaxial hybrid ring is shown in Fig. 5 with half of the shield removed from the crossover arm to show internal construction.

The proof of the design lies in the actual test results, shown in Fig. 6. Relevant measurements include input standing-wave ratio, isolation between opposed ports, mismatch loss and power split unbalance. All signal source and external terminating impedances were 50 ohms for these measurements.••

Thank you!

Several months ago we asked for your comments on our editorial coverage. The response has been overwhelming! We've been congratulated for our successes, blasted for our shortcomings and educated on new topics of interest. The result: A more interesting magazine that is better tailored to your needs.

Thanks again for your response, but don't stop now! Please take a few minutes to jot your thoughts on this month's Reader-Service card. We're waiting to hear from you!

1976 ANNUAL INDEX

Abbreviations: (TA) - Technical Article, (N) - News, (CF) - Cover Feature, (PF) - Product Feature, (SR) - Staff Report.

(continued on p. 62)

Annual Index

■ *Upcoming DOD Budget: $110-B Plus Expected,* (N), Feb, p. 20.

Electronic Warfare

■ *Campaign Rhetoric Focuses On Navy,* (N), July, p. 22.

■ *Congress Stalls On B-1 Bomber,* (N), July, p. 21.

■ *DOD Says "NO" To Condor Missile,* (N), Jan, p. 20.

■ *ECM Development Scored At Pentagon,* (N), Jan, p. 21.

■ *Eleven More Tridents Ordered By Pentagon,* (N), Apr, p. 19.

■ *General Dynamics Lands Cruise Missile Contract,* (N), May, p. 22.

■ *MiG 25 Avionics: "Relatively Crude,"* (N), Dec, p. 24.

■ *Navy Is Troubled By F-14 En[illegible] Woes,* (N), Apr, p. 20.

■ *Senate Has Strict Arms Sale Measure,* (N), Jan, p. 20.

Filters

■ *Dielectric Filter Key To X and K-Band Antenna Feed,* (N), May, p. 24.

■ *Electronically Tunable Filters Isolate High-Power Transmitters,* (N), Dec, p. 14.

■ *Have You Considered Voltage-Tuned Filters?,* (TA), Sept, p. 52.

■ *MTS Filter Exploits Charge Transfer Techniques,* (N), Apr, p. 24.

Front Ends

■ *Fused Silica: A Better Substrate For Mixers?,* (TA), Jan, p. 34.

■ *Hybrid Paramp/Downconverters Cover 2.2 to 35 GHz,* (PF), Jan, p. 63.

■ *What's New With Receiver [illegible]otectors?,* (TA), Jan, p. 44.

Instrumentation and Measurement

■ *Computer-Controlled IR Scanner Quickly Pinpoints Thermal Problems,* (N), Jan, p. 14.

■ *$4000 Buys A Complete Swept Measurement System,* (PF), May, p. 66.

■ *French Scope Features 4-GHz Bandwidth,* (N), July, p. 24.

■ *Frequency Counter Automates Pulsed RF Measurements To 18 GHz,* (CF), Apr, p. 82.

■ *How Accurate Is Your Spectrum Analyzer?,* (TA), June, p. 36.

■ *How Noisy Is That Load?,* (TA), Jan, p. 54.

■ *Measure and Interpret Short-Term Stability,* (TA), July, p. 34.

■ *Measure Group Delay Fast and Accurately,* (TA), June, p. 60.

■ *Millimeter Thermistor Mounts Don't Drift,* (PF), Mar, p. 70.

■ *Program Updates Test System For Swept Non-Linear Measurements,* (PF), Jan, p. 64.

■ *$6850 Buys Coverage To 18 GHz With Tight, 1-Hz CW Resolution,* (PF), Oct, p. 62.

■ *$6200 Frequency Counter Extends Automatic Measurements To 24 GHz,* (PF), Feb, p. 70.

■ *Synthesizer Purity and AM/FM Combined in 2-18 GHz Generator,* (CF), Mar, p. 68.

■ *$3700 Buys 6.5 GHz Capability With 40 dB Dynamic Range,* (PF), Oct, p. 62.

■ *Use Electrical Tests For Thermal Measurements,* (TA), June, p. 48.

Lasers and Integrated Optics

■ *Hang-On Transducers Modulate Optical Fibers,* (N), Feb, p. 22.

■ *Improved Semiconductor Laser Developed For IOCs,* (N), Jan, p. 13.

■ *Japanese Modulate Semiconductor Lasers At 500 Mb/s Rate,* (N), Mar, p. 22.

■ *OTP To Study Fiber Optics,* (N), June, p. 21.

■ *Optical Fiber Exhibits Lowest Loss Yet Reported,* (N), Aug, p. 22.

Materials

■ *Fused Silica: A Better Substrate For Mixers?,* (TA), Jan, p. 34.

Millimeter Waves

■ *Balanced Mixer-Preamp-LO Assembly Opens New Opportunities At 94 GHz,* (PF), Oct, p. 62.

■ *British Plant Promises Lowest Cost MM-Waveguide,* (N), Oct, p. 24.

■ *Design Space Qualified Millimeter-Wave Doublers,* (TA), July, p. 46.

■ *Dielectric Waveguide: A Low-Cost Option For ICs,* (TA), Mar, p. 56.

■ *Downconverter Design Slashes Pump Frequency Requirements,* (N), Oct, p. 12.

■ *GaAs Or Si: What Makes A Better Mixer Diode?,* (TA), Mar, p. 46.

■ *Low-Loss Waveguide Key To Bell's Millimeter-Wave System,* (N), July, p. 10.

■ *MM Wave Field Tests Successful For British P. O.,* (N), Mar, p. 22.

■ *Millimeter-Waves: Controversy Brews Over Transmission Media,* (SR), Mar, p. 32.

■ *Navy Researchers Develop New Sub-Millimeter-Wave Power Source,* (N), Dec, p. 12.

■ *300-GHz Radio Telescope Nears Completion,* (N), Sept, p. 14.

Miscellaneous

■ *A Carter Administration? It's Wait and See,* (N), Dec, p. 21.

■ *Can Science Prevent Future World Ills?,* (N), Dec, p. 21.

■ *Congress Tackles Patent Reform,* (N), June, p. 22.

■ *Final Countdown For Science Advisor,* (N), Mar, p. 20.

■ *Ford Names Seven To National Science Board,* (N), Nov, p. 21.

■ *Ford Signs "Sunshine Bill,"* (N), Nov, p. 22.

■ *Ford Taps NSF Head As Science Advisor,* (N), Sept, p. 21.

■ *House Will Tackle Patent Reform In 1977,* (N), Nov, p. 21.

■ *Microwave Monitors Measure Australian Gas Flow,* (N), Oct, p. 24.

■ *More Flak On Danger From Moscow's Microwaves,* (N), Oct, p. 21.

■ *Patent Reform Fails In Congress,* (N), Sept, p. 21.

■ *Pentagon Greases Skids For New Missile,* (N), Dec, p. 21.

■ *Soviet Jamming Prompts New Health Questions,* (N), Apr, p. 19.

■ *Women Scientists Gain In College Teaching Posts,* (N), Nov, p. 22.

Packaging

■ *Try Impact Extrusion For Low-Cost MIC Packaging,* (TA), June, p. 62.

R&D

■ *Accurate Measurements Key To Forecasting Earthquakes,* (N), May, p. 10.

■ *Attention Turns To Rome As New Devices and Circuits Debut,* (N), Aug, p. 16.

■ *Congress Is Set For Science Advisor,* (N), Jan, p. 19.

■ *Impatts and Trapatts Star In New Circuits,* (N), June, p. 9.

■ *Microwaves Score TKO In Fight Against Cancer,* (N), Oct, p. 14.

■ *OTP Study Updates Radiation Hazards,* (N), Aug, p. 19.

■ *"Old World" Technology? Don't Believe It!,* (SR), Nov, p. 35.

■ *R&D Funding Predicted To Increase 11% In '76,* (N), Feb, p. 14.

■ *Science Gains Higher Presidential Priority,* (N), May, p. 22.

Radar

■ *Airborne Radar Market Seen At $3.3 Billion Over Next Five Years,* (N), Sept, p. 12.

■ *Coherent Radar Relies On Five Gunn Sources,* (N), May, p. 24.

■ *Constant Product Improvement Key To European Radar Success,* (N), July, p. 9.

■ *Dutch Defense Radars Use SAW Pulse Compression,* (N), Apr, p. 24.

■ *14.5 GHz Transponder Developed For Airport Surface Detection Radar,* (N), Feb, p. 10.

■ *France Extends Lead In W. Europe's Communications and Radar Markets,* (N), Feb, p. 9.

■ *Helicopter Rotor Blade Doubles As Radar Antenna,* (N), July, p. 24.

■ *Improved Radar Designs Outwit Complex Threats,* (TA), Apr, p. 54.

■ *Keep Track Of That Low-Flying Attack,* (TA), Apr, p. 36.

■ *MTI Filter Exploits Charge Transfer Techniques,* (N), Apr, p. 24.

■ *Marine Radar Ordered For Heavy Vessels,* (N), Aug, p. 20.

■ *Metal-Detecting Radar Rejects Clutter Naturally,* (N), Aug, p. 12.

■ *Overall Radar Market Looks Flat, But Funding Shifts Are Detected,* (N), Apr, p. 13.

■ *Planetary Radar Blazes A Path For Deep-Space Probes,* (N), Nov, p. 14.

■ *Simulator Checks Radar System ECCM,* (N), Sept, p. 24.

Satellite Communications

■ *Arabs Plan Domsat System. China Next?,* (N), June, p. 26.

■ *Biologists Track A Bear By Satellite,* (N), Sept, p. 14.

■ *Comsat Pacts With IBM, Aetna,* (N), Feb, p. 20.

■ *Congressional Attention Turns To Solar Satellites,* (N), May, p. 20.

■ *FCC Orders Comsat To Lower Rates,* (N), Jan, p. 19.

■ *Foreign Earth Station Needs Will Pace Satcom Growth,* (N), Aug, p. 9.

■ *Intelsat V Satellite Contracts Are Readied,* (N), Nov, p. 22.

■ *Intelsat Shake Up: Taiwan Out, Red China In,* (N), Dec, p. 24.

■ *Justice Wants Hearing On IBM Satellite Venture,* (N), July, p. 22.

■ *Maritime Satellite Off To Rocky Start,* (N), Apr, p. 20.

■ *Orbital Test Satellite Forerunner Of Future Vehicles,* (N), Jan, p. 22.

■ *OTP Asks For U. S. Voice In Mobile Satellite Forums,* (N), Apr, p. 20.

■ *RCA Satellite Gets FCC Nod,* (N), Jan, p. 20.

■ *Telecasting To Provide 2 TV Channels To Europe,* (N), Jan, p. 22.

■ *Tide Is Turning For Small Earth Stations,* (N), Aug, p. 19.

Semiconductors and MICs

■ *Dielectric Waveguide: A Low-Cost Option For ICs,* (TA), Mar, p. 56.

■ *Flatpack, TO-8 Modules Offer High-Rel Hybrid Construction,* (PF), Jan, p. 62.

■ *GaAs FETs: Device Designers Solving Reliability Problems,* (SR), Feb, p. 32.

■ *Gigabit Logic: Real-Time Response For Tommorrow's Threats,* (N), Sept, p. 9.

■ *Improved Devices Debut At Solid-State Conference,* (N), Apr, p. 9.

■ *Low-Noise FET Offers Power For Wide Dynamic Range,* (PF), Aug, p. 62.

■ *New Transistor Provides Powerful UHF Performance,* (N), Aug, p. 22.

■ *SOS Switch Could Reduce Phased Array Prime Power Needs,* (N), Jan, p. 16.

■ *Varactor Doubler Boasts 80% Efficiency,* (N), Apr, p. 17.

Sources

■ *Behind The Design Of VCO Linearizers,* (TA), Sept, p. 36.

■ *Coherent Radar Relies On Five Gunn Sources,* (N), May, p. 24.

■ *Combat Turn-On Problems In Gunn-Effect Sources,* (TA), Aug, p. 56.

■ *Cross The Barrier Of Varactor Drift,* (TA), Aug, p. 36.

■ *Cut Oscillator Noise By Careful Mechanical Design,* (TA), Oct, p. 54.

■ *For Broadband, Tunable Sources Combine Varactor Control With Dielectric Tuning,* (TA), Aug, p. 50.

■ *Specifying Isolation To Limit Frequency Pulling,* (TA), May, p. 55.

■ *Think Group Delay For A New Look At Source Stablity,* (TA), Aug, p. 42.

■ *Trapatt Source Aimed At TWT Radar Sockets,* (N), July, p. 24.

Systems

■ *Dead-Stick Landings Demand Foolproof Guidance,* (N), Oct, p. 9.

■ *FAA Pens Rules For ISMLS Converters,* (N), Feb, p. 19.

■ *International MLS: Will Approval Come Too Late?,* (N), Nov, p. 9.

■ *Microwave Monitor Keeps An Eye On The Road,* (N), June, p. 14.

■ *NRL Develops Microwave Imaging System,* (N), Mar, p. 19.

■ *New Products Unveiled at Naval Research Labs,* (N), Sept, p. 22.

■ *Scanning-Beam MLS Wins Soviet Endorsement,* (N), June, p. 26.

■ *U. K. To Participate In French MLS System Program,* (N), Feb, p. 22.

Tubes

■ *High Gain UHF Tetrode Eliminates Driver Tubes,*(N), Sept, p. 24.

■ *Industrial Klystron Produces 50 kW,* (N), May, p. 24.

■ *Multipacting Key To Electronically-Tuned Maggie,*(N), June, p. 26.

■ *Phase Match TWTs For Reduced Combining Loss,* (TA), Oct., p. 48.

■ *What's New With Receiver Protectors?* (TA), Jan, p. 44.

Sweeper and signal generator features combined in one package

The melody of this microwave source system is versatility thanks to an entire orchestra of options. These options convert the SG-811 from a 1.9 to 18-GHz sweeper to a fully shielded signal generator. As a sweep oscillator, the basic unit puts out 7 milliwatts and power options boost the output to 15 or 400 mW. The sweeper features a unique removable, remotable RF assembly and a flicker free sweep.

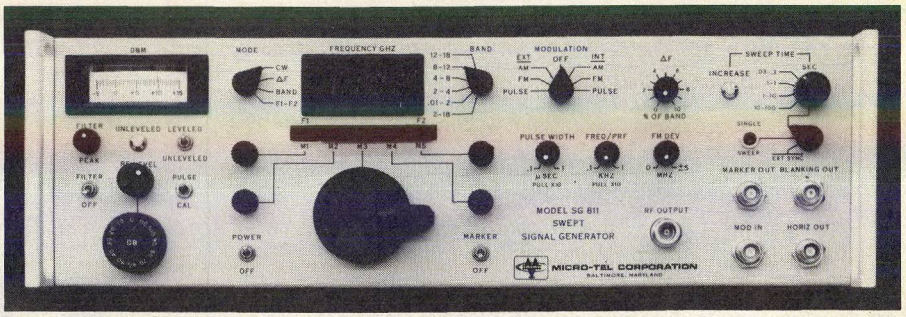

As a signal generator, the fully shielded package promises a 20 dB maximum harmonic output and the addition of a filtered-output option pushes the harmonic content down to 60 dB. Other possibilities include coverage to 10 MHz, 130 dB output attenuation, RF sampling, internal pulsing with a 65 dB on-off ratio and digital frequency control.

The 5.25 x 17 x 18 inch (13.3 x 43.2 x 45.7 cm) unit can be teamed up with the FCS-811 counter-synthesizer to perform as a synthesized signal generator with less than 400 Hz residual FM. The task of examining filtered devices can be eased using the pulse generator option thanks to a 65 dB pulse on-off ratio with pulse widths from 0.1 to 10 μseconds and PRF from 100 Hz to 10 kHz.

The remotable RF section allows operation from as far as 300 feet away (further on special order). The assembly is independently shielded and fits easily into the mainframe for local control.

The addition of an RF sample option provides a nominal -20 dBm signal sample useful for operations with counters, synthesizer or stabilizers. Either 1.9 or 0.01 to 18 GHz samplers are available. The calibrated output attenuators, adding 70 or 110 dB more attenuation, are adjustable in 1 dB steps and can be controlled manually or digitally.

Internal and external modulation can be performed via three methods. In addition to the available pulse modulation scheme, the 40 lb unit (18.2kg) can be AM modulated with a 100 to 10,000 Hz square wave or FM modulated with a 100 to 10,000 Hz signal with 0 to 5 MHz deviation. P&A: from $19,000 (basic model SG-811A); 60 days. **Micro-Tel Corporation, 6310 Blair Hill Lane, Baltimore, MD 21209 (301) 823-6227.** **CIRCLE NO. 109**

Bandpass multiplexers now cover 9:1 bandwidths

Refinements in synthesis techniques have enabled designers at Acronetics to extend the bandwidth of bandpass-type multiplexers to 9:1 within the 1 to 18 GHz range.

The traditional design approach to broadband multiplexers for EW or ECM applications calls for a combination of low-pass and high-pass filters to achieve the high degree of selectivity required for each band. The Acronetics' design uses a single bandpass filter for each channel. These combline filters are tied together at a common junction at the input of the multiplexer. Advantages of this approach are said to include higher reliability, smaller size and lighter weight.

According to Acronetics, traditional high-pass/low-pass multiplexers may have 75 to 100 discrete parts linked by 40 to 50 solder joints. Equivalent combline filter designs reduce the parts count by about half, and the number of solder joints to roughly 10. A typical three-channel component, shown in the figure, measures 3.5 x 2.5 x 0.5 inches.

The multiplexers may be specified with contiguous bands, passbands

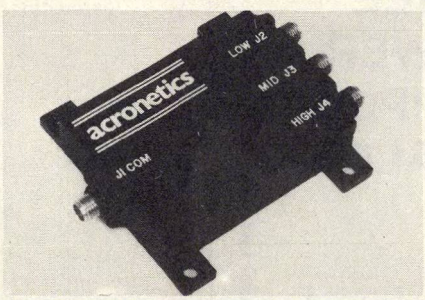

separated by guard bands or in hybrid designs. Sets matched in terms of phase and amplitude are available, and amplitude tracking is maintained into the crossover regions. Drift of the crossover frequency is specified as ±0.1 per cent from -55 to +125°C.

Rejection of over 60 dB can be achieved only 10 per cent from crossover, as well as from upper and lower band edges. Typical insertion loss is 0.7 dB in-band and 4.5 dB at the crossovers.

Price and availability depend on customer specifications, since the multiplexers are tailored to order. Two to eight output channels may be specified. **Acronetics, 955 Benicia Avenue, Sunnyvale, CA 94086 (408) 245-8000.** **CIRCLE NO. 110**

AMPLIFIERS

Transistor amplifier aims at Marisat market

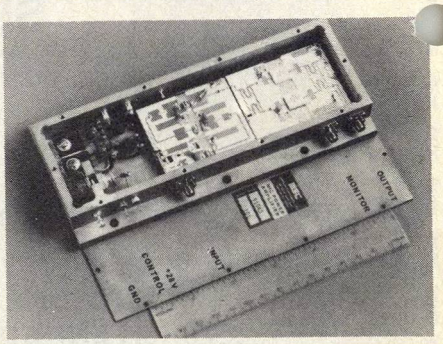

Model MSC 91045 is a solid-state amp designed for Marisat shipboard telecommunications terminals. A nominal input power of 125 mW produces a 45-W output (1.62 to 1.66 GHz) with an overall efficiency of 35 per cent. Worse-case specs include 0.1 dB/MHz gain slope, 2:1 input VSWR, 8°/dB AM-to-PM conversion and −20 dBc harmonic level. The 7.5 x 3.4 x 1 inch (19 x 8.6 x 2.54 cm) amplifier requires a +28 VDC bias. **Microwave Semiconductor Corporation, 100 School House Road, Somerset, NJ 08873 (201) 469-3311.** **CIRCLE NO. 111**